



**HAL**  
open science

# Recycling of metals from NiMH batteries: development of liquid-liquid selective extractions based on ionic liquids

Matthieu Gras

► **To cite this version:**

Matthieu Gras. Recycling of metals from NiMH batteries: development of liquid-liquid selective extractions based on ionic liquids. Material chemistry. Université Grenoble Alpes, 2018. English. NNT: 2018GREAI053 . tel-01913113

**HAL Id: tel-01913113**

**<https://theses.hal.science/tel-01913113v1>**

Submitted on 6 Nov 2018

**HAL** is a multi-disciplinary open access archive for the deposit and dissemination of scientific research documents, whether they are published or not. The documents may come from teaching and research institutions in France or abroad, or from public or private research centers.

L'archive ouverte pluridisciplinaire **HAL**, est destinée au dépôt et à la diffusion de documents scientifiques de niveau recherche, publiés ou non, émanant des établissements d'enseignement et de recherche français ou étrangers, des laboratoires publics ou privés.

## THÈSE

Pour obtenir le grade de

### **DOCTEUR DE LA COMMUNAUTE UNIVERSITE GRENOBLE ALPES**

Spécialité: 2MGE: Matériaux, Mécanique, Génie civil, Electrochimie

Arrêté ministériel : 25 mai 2016

Présentée par

### **Matthieu GRAS**

Thèse dirigée par **Eric Chainet**, Directeur de recherche, CNRS, Grenoble et codirigée par **Farouk Tedjar**, Collaborateur industriel, Grenoble INP

Préparée au sein du **Laboratoire d'Electrochimie et de Physico-Chimie des Matériaux et des Interfaces** dans l'**École Doctorale I-MEP2 – Ingénierie – Matériaux, Mécanique, Environnement, Energétique, Procédés, Production**

### **Recyclage de métaux venant d'accumulateurs NiMH: développement d'extractions liquide-liquide sélectives à partir de liquides ioniques**

### **Recycling of metals from NiMH batteries: development of liquid-liquid selective extractions based on ionic liquids**

Thèse soutenue publiquement le **12 Octobre 2018**, devant le jury composé de :

#### **Dr François LAPICQUE**

Directeur de Recherche, CNRS, Nancy, Rapporteur

#### **Dr Corinne LAGROST**

Chargée de Recherche, CNRS, Rennes, Rapporteur

#### **Pr Maria FORSYTH**

Professeur, Université de Deakin, Examineur

#### **Pr João Manuel Costa Araújo Pereira COUTINHO**

Professeur, Université d'Aveiro, Examineur

#### **Dr Eric CHAINET**

Directeur de Recherche, CNRS, Grenoble, Directeur de thèse

#### **Dr Farouk TEDJAR**

Collaborateur industriel, Grenoble INP, Co-directeur de thèse

#### **Dr Nicolas PAPAICONOMOU**

Maître de Conférences, Université Savoie Mont Blanc, Examineur

#### **Dr Isabelle BILLARD**

Directrice de Recherche, CNRS, Grenoble, Présidente du jury





## Acknowledgment

During my studies, I've read a couple of thesis, let's be honest, rarely entirely but I always had an emotional eye on the acknowledgment part. Since that time, I've imagined writing them a thousand times. However today, my keyboard remains silent as I am now aware of the difficulty of finding the right word to show my gratitude to all the scientists, friends and members of my family who have contributed to the success of this project.<sup>1</sup>

First of all, I'd like to thank my thesis supervisors. Eric, it was not always easy to find some time together but I think we found a way of working efficiently. I will remember your expertise and your humour and I thank you for putting your trust in me. Nicolas, it has also been a challenge to find you in Grenoble during these three years but our discussions always lead to great ideas. Your scientific imagination guided remarkably my work and I hope that we will still find time for some beers. Isabelle, you are not officially supervising my work but I can say that you highly contributed to this PhD thesis. I am extremely grateful for your numerous advices and your constant kindness. I think that I have improved both, my chemical and chess skills thanks to you. Finally, I would like to acknowledge F.Tedjar for providing NiMH batteries from Recupyl<sup>®</sup>.

I thank François Lopicque and Corinne Lagrost for accepting to review my work. I am grateful to João Coutinho, firstly for being member of the jury but more importantly, for welcoming me warmly in his laboratory. My stay in Aveiro had an important influence on this project. I would also like to express my gratitude to Maria Forsyth for being member of the jury. My first academic experience took place more than three years ago at the IFM in your team, what a nice symbol to conclude my studies with you being present at my PhD defence!

I would like to emphasize on the technical help I received from numerous scientists. To Sarah Bureau and Richard Bressoux for giving me a special access to ICP and AAS analysis respectively and to Karine and Muriel for letting me enter in the building at unlikely hours, a warm thank you. My thoughts also go to Francine,

Joëlle, Rachel and Frederic, the microscope team for their training and numerous advices in the quest of the perfect image. I'd also like to acknowledge Malaurie and Marie, two fantastic interns who contributed to this work with a perpetual good mood.

A special thank you to Yasmine and Claire, the administrative staff, my trips in Europe were driving you crazy but you did a great job. Those responsible for that are Isabelle Schuster and Chistine Dominjon, from the EIT KIC InnoEnergy that I sincerely thank for granting my application to the PhD school. To all PhD candidates I met during the program in Barcelona, Amsterdam, Kraków, Paris and Grenoble, especially Juan, Amr, Anthony... I'd like to express my gratitude for the exchanges we had.

During my PhD, I had the opportunity to meet amazing people. They allowed me to spend three wonderful years in and outside the lab that I shall never forget. I'd like to thank the captain of the LEPMI football team, the impassable defender Fred,<sup>ii</sup> for all the good memories and the trophies we won as well as D.Deschamps for the second star! Thanks to the former PhD students of the team, Vincent,<sup>iv</sup> Rémi,<sup>v</sup> Raph,<sup>iii</sup> Fanny<sup>vi</sup>, I was the only student to arrive in the EIP-third floor team in 2015 and after a few weeks this place already sounded like family. I have a special thought for Céline<sup>vii</sup> with whom I have shared so much deception and joy doing electrochemistry in the "recycling lab". I'd also like to thank Tristan<sup>viii</sup> for his support and his sincere friendship even at 8800 km from here. My acknowledgement of course goes to the new LEPMI-EIP members, this is to say, Guillaume,<sup>ix</sup> Eris,<sup>x</sup> Jérôme,<sup>xi</sup> Fabien,<sup>xii</sup> Marion,<sup>xiii</sup> Marine<sup>xiv</sup> and Clémence,<sup>xv</sup> many researchers are working on energy storage but none of them are spreading positive-energy in a team as you do. Finally, it is important for me to thank Vijetha, UPIIL member, who shared my office during one year. Now, Let's cross the Pyrenees to land in Aveiro, Portugal where I was more than welcomed. Helena,<sup>xvi</sup> thanks a lot for your time and your kindness, it was a real honour to learn more about ABS by your side. Nicolas,<sup>xvii</sup> I really appreciated working with you, thanks for all the time we spent extracting metals, reducing them and drinking *uma caneca por favor*. Of course, I would like to thank all the Path members, Mónia, Chica, Carlos and the others for your friendship and our meetings in convívio.

We shall now step out of the labs. I'd like to thank Gabau<sup>xviii</sup> and Gaël<sup>xix</sup> for their unchanging friendship since the beginning of my studies where we met. At that time, we were very far from imagining doing a PhD, and here we are, good luck to both of you for the end of your thesis! Thanks to the ones I have pleasure to see when I go back home, even if some of you are, like me still suffering from “economic delocalisation” in the north, Johan, Guilhèm, Anaïs, Got, DellaNora, Guadza, Benêt, Natacha, Clément, Guibbert, Barre, Lucas, Calu and the others, *on ne s'arrêtera pas à Moularès*.<sup>xx</sup>

A sincere thank you to my family, more precisely to my parents, my sister Capucine and my brothers Elliot and Gabin for their love and support. To my grandmother without whom nothing would have been possible, thank you. Special mention to my mother, as I am currently writing the acknowledgement part of my thesis she just prepared some chocolate muffins and a home-made vanilla milkshake to have an additional sentence in the thesis, so thanks for that, this is delicious! :)

I will conclude my acknowledgments with you Maureen,<sup>xxi</sup> my princess since many years. I abandoned you 6 months in Australia, 4 months in Portugal and 3 years in Grenoble to complete my studies however all this would have been meaningless without your support. I thank you for your patience and your affection and I am now looking forward to going to the next step of our life together.

*“La rota, la rota, lo grand viatge  
Lo quintran, l’envam, lei viratges  
La mar, l’ocean e sei rivatges  
La rota, bota desamarratge!”*

M.F.D 

“À ma grand-mère”

# Table of content

<b>INTRODUCTION.....</b>	<b>20</b>
<b>I. CHAPTER I STATE OF THE ART .....</b>	<b>24</b>
I.1 PRESENTATION OF THE NiMH BATTERY .....	25
I.1.1 <i>A historical overview of the energy sector.....</i>	25
I.1.2 <i>The battery devices, from performance to market.....</i>	27
I.1.3 <i>The NiMH technology.....</i>	30
I.2 MINING AND RECYCLING OF METALS .....	37
I.2.1 <i>Raw materials criticality.....</i>	37
I.2.2 <i>Challenges for transition metals: the case of cobalt.....</i>	39
I.2.3 <i>Rare Earth Elements as highly critical raw materials.....</i>	42
I.3 IONIC LIQUIDS AS GREENER SOLVENTS .....	52
I.3.1 <i>Definition.....</i>	52
I.3.2 <i>Structure.....</i>	53
I.3.3 <i>Properties and application.....</i>	54
I.4 RECYCLING NiMH BATTERIES .....	57
I.4.1 <i>Overview.....</i>	57
I.4.2 <i>Leaching and precipitation.....</i>	61
I.4.3 <i>IL-based Liquid-liquid extraction.....</i>	65
I.4.4 <i>IL-based Aqueous Biphasic Systems (ABS).....</i>	71
I.4.5 <i>Electrodeposition in ionic liquids.....</i>	76
I.5 SPECIFICATION OF THE STUDY .....	81
<b>II. CHAPTER II SEPARATION OF TRANSITION METALS FROM RARE EARTH ELEMENTS.....</b>	<b>84</b>
II.1 INTRODUCTION.....	85
II.2 PREPARATION AND MECHANICAL TREATMENT OF NiMH BATTERIES .....	86
II.2.1 <i>Laboratory scale black mass production.....</i>	86
II.2.2 <i>Industrial scale black mass production.....</i>	92
II.3 LEACHING.....	96
II.3.1 <i>Preliminary tests with an ideal black mass.....</i>	96
II.3.2 <i>Leaching NiMH black mass produced at Recupyl®.....</i>	105
II.3.3 <i>Possibilities and limitations of using hydrophilic ILs in leaching process.....</i>	118
II.4 SELECTIVE PRECIPITATION .....	121
II.5 CONCLUSION.....	129
<b>III. CHAPTER III SEPARATION OF CERIUM, LANTHANUM, NEODYMIUM AND PRASEODYMIUM.....</b>	<b>132</b>
III.1 INTRODUCTION.....	133



III.2	SEPARATION OF CERIUM FROM LANTHANUM, NEODYMIUM AND PRASEODYMIUM SULPHATE SALTS .....	134
III.2.1	<i>Introduction</i> .....	134
III.2.2	<i>Oxidation of Ce(III) in alkaline conditions</i> .....	135
III.2.3	<i>Liquid-Liquid extraction of Ce(IV) by ILs</i> .....	141
III.2.4	<i>Conclusion</i> .....	153
III.3	RECOVERY OF CERIUM FROM SPENT NiMH BATTERIES.....	154
III.3.1	<i>Extraction of cerium in spent NiMH batteries</i> .....	154
III.3.2	<i>Electrodeposition of cerium in an ionic liquid: an alternative recovery strategy</i> 158	
III.4	TOWARDS THE SEPARATION OF NEODYMIUM FROM LANTHANUM .....	166
III.5	CONCLUSION .....	172
<b>IV.</b>	<b>CHAPTER IV SEPARATION OF COBALT, NICKEL, MANGANESE AND IRON.....</b>	<b>174</b>
IV.1	INTRODUCTION .....	175
IV.2	DICYANAMIDE IONS AS COMPLEXING AGENT OF COBALT: FROM WEAK LIGANDS IN WATER TO STRONG ONE IN IONIC LIQUIDS .....	176
IV.2.1	<i>Introduction</i> .....	176
IV.2.2	<i>Construction and fitting of a complexation model</i> .....	179
IV.2.3	<i>Co-DCA complexes in water</i> .....	181
IV.2.4	<i>Co-DCA complexes in ionic liquids</i> .....	187
IV.2.5	<i>Cobalt extraction by dicyanamide-based ionic liquids</i> .....	198
IV.2.6	<i>Conclusion</i> .....	201
IV.3	NOVEL IONIC LIQUID-BASED ACIDIC AQUEOUS BIPHASIC SYSTEMS (ACABS): FROM FUNDAMENTALS TO METAL EXTRACTION .....	203
IV.3.1	<i>Introduction</i> .....	203
IV.3.2	<i>Fundamentals of Acidic Aqueous Biphasic System</i> .....	206
IV.3.3	<i>Acidic Aqueous Biphasic systems for metal extraction</i> .....	215
IV.3.4	<i>Recovery of cobalt by electrodeposition in ABS-AcABS</i> .....	221
IV.3.5	<i>Conclusion</i> .....	233
IV.4	SEPARATION OF TRANSITION METALS FROM SPENT NiMH BATTERIES .....	235
IV.4.1	<i>Introduction</i> .....	235
IV.4.2	<i>Inducing an AcABS from leachate solutions: A versatile process</i> .....	235
IV.4.3	<i>Conclusion</i> .....	243
IV.5	CONCLUSION .....	245
<b>V.</b>	<b>CONCLUSION AND PERSPECTIVES.....</b>	<b>248</b>
<b>VI.</b>	<b>REFERENCES .....</b>	<b>256</b>
<b>VII.</b>	<b>ANNEX.....</b>	<b>286</b>

---

---

## List of Publications in this Manuscript

### *Scientific publications*

- (1) Gras.M, Papaiconomou.N, Chainet.E, Tedjar.F, Billard.I, Separation of cerium(III) from lanthanum(III), neodymium(III) and praseodymium(III) by oxidation and liquid-liquid extraction using ionic liquids, *Separation and Purification Technologies* **178** (2017) 169-177
- (2) Gras.M, Papaiconomou.N, Schaeffer.N, Chainet.E, Tedjar.F, Coutinho.J.A.P, Billard.I, Ionic-Liquid-Based Acidic Aqueous Biphasic Systems for Simultaneous Leaching and Extraction of Metallic Ions, *Angewandte*, **57** (2018) 1563-1566
- (3) Schaeffer.N, Passos.H, Gras.M, Mogilireddy.V, Leal.J, Perez-Sanchez.G, Gomez.J.R.B, Billard.I, Papaiconomou.N, Coutinho.J.A.P, Mechanism of ionic liquid-based acidic aqueous biphasic systems formation, *Physical Chemistry Chemical Physics*, **20** (2018) 9839-9846
- (4) Mogilireddy.V, Gras.M, Schaeffer.N, Passos.H, Svecova.L, Papaiconomou.N, Coutinho. J.A.P and Billard.I, Understanding the fundamentals of Acid-Induced Ionic Liquid-based Aqueous Biphasic System, *Physical Chemistry Chemical Physics*, (2018)
- (5) Dicyanamide ions as complexing agents of Co(II): From weak ligands in water to strong ones in an ionic liquid, Solvent extraction and ion exchange (2018), *accepted article in a special issue*

### *Patent*

- (1) Papaiconomou.N, Gras.M, Coutinho.J.A.P, Billard.I, Ionic liquid acid aqueous two phase system, FR3058735A1, 2016

---



---

## List of Figures

<b>Figure I.1.</b> World energy consumption of fossil fuels from 1800 to 2000. <sup>6</sup> .....	26
<b>Figure I.2.</b> Production of electricity by renewable energies in the world. <sup>8</sup> .....	27
<b>Figure I.3.</b> Evolution of the worldwide market of rechargeable batteries in volume from 1995 to 2016. <sup>18</sup> .....	29
<b>Figure I.4.</b> Share of NiMH batteries sold for HEV application worldwide in value from 2000 to 2015. <sup>18</sup> .....	30
<b>Figure I.5.</b> Schematic view of the NiMH battery.....	31
<b>Figure I.6.</b> The main geometries for NiMH batteries. <b>A:</b> Prismatic cell. <b>B:</b> Cylindrical cell. <b>C:</b> Button cell. <sup>22</sup> .....	32
<b>Figure I.7.</b> $AB_5$ crystal structure. 1 large grey atom: A in position (0, 0, 0). 2 small white atoms B in position (1/3, 2/3, 0). 3 small black atoms B in position (1/2, 0, 1/2). <sup>27</sup> .....	34
<b>Figure I.8.</b> Frequencies of criticality designations from seven studies. Some metals were treated as minerals or metal groups. Regarding rare earth elements, g: as element. h: as compound of REE group. <sup>35</sup> .....	38
<b>Figure I.9.</b> Price of transition metals contained in NiMH battery electrodes from 2014 to 2018 expressed in US dollars per kilogram (USD/kg). The red and green curves express the decreasing or increasing price respectively within 4 years. A: manganese. B: Nickel. C: Aluminum. D: Cobalt. ....	40
<b>Figure I.10.</b> Evolution of the use of cobalt in tons per year for Electric Vehicles (EV), Hybrid Electric Vehicles (HEV) and portable batteries in 2010 and 2020. ....	41
<b>Figure I.11.</b> Characteristics of the main light REE ores. <sup>53,56</sup> Pie charts are expressed in weight percentages of the average ores concentration. ....	44
<b>Figure I.12.</b> Applications of light REE contained in NiMH batteries. Percentages are expressed in terms of weight production. <sup>59</sup> .....	45
<b>Figure I.13.</b> Worldwide production of REE in tons from 1950 to 2017. <sup>62,63</sup> .....	47
<b>Figure I.14.</b> Evolution of REE oxide prices from 2009 to 2017. <sup>41,62</sup> .....	48
<b>Figure I.15.</b> Flow sheet of the extraction of light REE from Baotou mines in China. <sup>64</sup> .....	49
<b>Figure I.16.</b> Evolution of the interest of ionic liquids in scientific papers from 1990 to 2018. <sup>86</sup> ..	52
<b>Figure I.17.</b> Popular structures of cations and anions forming ionic liquids.....	53
<b>Figure I.18.</b> Circular economy defined by ERAMIN project. <sup>137</sup> .....	57
<b>Figure I.19.</b> Primary and secondary battery recycling centers in France. ....	58
<b>Figure I.20.</b> General flowsheet for the recycling of metals from NiMH batteries. ....	59
<b>Figure I.21.</b> Efficient cations for the leaching of metals $[\text{Hbet}]^+$ and $[\text{N}_{22}\text{HSO}_3\text{H}]^+$ .....	65
<b>Figure I.22.</b> Macroscopic view of an IL-based liquid-liquid extraction of metal. Ce(IV) in nitric acid and $[\text{C}_1\text{C}_4\text{Pyrr}][\text{NTf}_2]$ are used for the aqueous and ionic liquid phases respectively. ....	67

<b>Figure I.23. A:</b> Typical phase diagram of an ABS. Binodal curve in blue. Tie lines in red. <b>B:</b> Thermomorphic behaviour of an ABS. Red and blue lines, binodal curves for LCST and UCST systems respectively. ....	73
<b>Figure I.24.</b> IL-based electrodeposition, as part of a recycling process. ....	78
<b>Figure II.1.</b> Characteristics and snapshot of the commercial NiMH batteries from SUPPO® .....	86
<b>Figure II.2.</b> Snapshots of a NiMH commercial battery with sawed extremities. A: The battery is sawed. B: Positive terminal. C: Negative terminal. ....	87
<b>Figure II.3.</b> View of a NiMH battery after isolating electrodes and separators. ....	87
<b>Figure II.4.</b> SEM images of different NiMH battery components using BSE. A: Positive electrode (magnification $\times 200$ ). B: grid (magnification $\times 30$ ). C: Negative electrode (magnification $\times 400$ ). ....	88
<b>Figure II.5.</b> X-ray diffractogram of the washed negative electrode. Circles are used to identify the anode intermetallic material, namely hexagonal LaCeNdPrNiCoMn, while triangles define lanthanum hydroxide hexagonal peaks. ....	91
<b>Figure II.6.</b> Process for the production of NiMH black mass from the recycler Recupyl® .....	93
<b>Figure II.7.</b> SEM images of washed BM produced at Recupyl® (magnification $\times 29$ ) performed with BSE. Purple A: Positive electrode. Blue B: grid. Green C: Negative electrode. Red D: Other components. ....	94
<b>Figure II.8.</b> EDS spectra of solid residue after leaching A: $2 \text{ mol.L}^{-1} \text{ H}_2\text{SO}_4$ at $80 \text{ }^\circ\text{C}$ during 3 hours. Leaching B $1 \text{ mol.L}^{-1} \text{ H}_2\text{SO}_4$ at $20 \text{ }^\circ\text{C}$ during 3 hours. ....	97
<b>Figure II.9.</b> Snapshots of several leachates .....	101
<b>Figure II.10.</b> Investigation on the influence of temperature, sulfuric acid concentration and reaction time on the leaching of NiMH negative electrodes. ....	101
<b>Figure II.11.</b> XRD analysis of the solid residue after leaching a NiMH ideal black mass produced at a laboratory scale with $\text{H}_2\text{SO}_4 2 \text{ mol.L}^{-1}$ at $25 \text{ }^\circ\text{C}$ . Circles and triangles are used to identify nickel cubic and hydrated nickel sulphate monoclinic peaks respectively. ....	102
<b>Figure II.12.</b> Exothermicity of the leaching reaction .....	104
<b>Figure II.13.</b> Snapshots of the two different BM granulometries from the Recupyl® process. A: particle size between 1 and 10 mm. B: particle size lower than 1 mm. ....	106
<b>Figure II.14.</b> Leaching of NiMH black mass containing particles below 1 mm in full line and with coarse particles between 1 and 10 mm in dotted line. Experiments were undertaken at 25, 50 and $75 \text{ }^\circ\text{C}$ in green, blue and red respectively. A: The leachate is an aqueous solution containing sulfuric acid. B: The leachate is an aqueous solution containing hydrochloric acid. ....	108
<b>Figure II.15.</b> Leaching NiMH black mass produced at Recupyl® with particle size below 1 mm. Leachate composed of an aqueous solution containing between $0.5$ and $10 \text{ mol.L}^{-1} \text{ H}_2\text{SO}_4$ or HCl. Temperatures were set at 25, 50 and $75 \text{ }^\circ\text{C}$ in green, blue and red respectively. <b>A:</b> composition of metals in the leachate after filtration for experiments at 1, 2, 4 and $8 \text{ mol.L}^{-1} \text{ H}_2\text{SO}_4$ or HCl. <b>B:</b> Leaching yield ( $Y_L$ ) for sulfuric and hydrochloric acid in circles and squares respectively. ....	109
<b>Figure II.16.</b> EDS spectra of the precipitate obtained after leaching a NiMH black mass with $10 \text{ mol.L}^{-1} \text{ H}_2\text{SO}_4$ at $75 \text{ }^\circ\text{C}$ . ....	111

<b>Figure II.17.</b> Solid residue analysed by SEM (magnification $\times 100$ ) after leaching 1 g of BM produced at Recupyl <sup>®</sup> with $\text{H}_2\text{SO}_4$ 2 mol.L <sup>-1</sup> at 25 °C during 1 hour. A: Imaging using secondary electrons (SE). B Imaging using Back Scattered Electrons (BSE). .....	115
<b>Figure II.18.</b> Leaching of NiMH black mass containing particles below 1 mm with sulfuric acid and/or [P <sub>44414</sub> ][Cl] IL in an aqueous phase. Experiments were undertaken at 25, 50 and 75 °C in green, blue and red respectively. Leachates were composed of 60, 30 and 0 vol. % of $\text{H}_2\text{SO}_4$ in full color, light color and striped line respectively. All experiments were carried out at 0, 2 and 4 mol.L <sup>-1</sup> of acid. ....	119
<b>Figure II.19.</b> Snapshot of the precipitate obtained while the pH is comprised between 1 and 2 by addition of $\text{Na}_2\text{CO}_3$ 1.5 mol.L <sup>-1</sup> to the leachate. ....	122
<b>Figure II.20.</b> Evolution of the concentration of metals in the leachate while increasing the pH from -0.25 to 8. ....	123
<b>Figure II.21.</b> Concentration of metals in the aqueous solution. In green, after leaching at pH -0.25 and in blue after precipitation at pH 1.7. Concentration of La, Ce, Nd and Pr was multiplied by 20 for graphical reason. ....	125
<b>Figure II.22.</b> SEM analysis of the precipitate obtained at pH 1.7. A: SE image (magnification $\times 100$ ). B: BSE image (magnification $\times 2270$ ). C: Elemental analysis by EDS. ....	126
<b>Figure II.23.</b> XRD analysis of the precipitate obtained at pH 1.7. ....	127
<b>Figure II.24.</b> Flowsheet corresponding to the separation of transition metals from rare earth elements. ....	131
<b>Figure III.1.</b> Molar extinction coefficients for <b>A:</b> Ce(IV) in orange and Ce(III) in grey lines in 8.0 mol.L <sup>-1</sup> $\text{H}_2\text{SO}_4$ and <b>B:</b> Nd(III) in purple, La(III) in grey and Pr(III) in green lines in 8.0 mol.L <sup>-1</sup> $\text{H}_2\text{SO}_4$ .....	137
<b>Figure III.2.</b> Oxidation yield of cerium for several concentrations of sodium hydroxide. At 30°C: blue triangle, at 50°C: red square. ....	139
<b>Figure III.3.</b> Updated E-pH diagram of Ce-H <sub>2</sub> O system. Reedited from: Hayes et al. The phase stability of cerium species in aqueous systems, <i>J. Electrochem. Soc.</i> , <b>149</b> (12) C623-C630 (2002). <sup>250</sup> .....	140
<b>Figure III.4.</b> Snapshots of cerium(IV) extractions by [P <sub>66614</sub> ][NTf <sub>2</sub> ] at various concentrations of $\text{HNO}_3$ .....	143
<b>Figure III.5.</b> Distribution coefficients for lanthanides ( $[\text{Ln}] = 2.0 \times 10^{-2}$ mol.L <sup>-1</sup> ) extracted separately towards [C <sub>1</sub> C <sub>4</sub> Pyrr][NTf <sub>2</sub> ] at various concentrations of $\text{HNO}_3$ . <b>A:</b> Cerium(IV) in orange diamond and cerium(III) in black dotted line. <b>B:</b> lanthanum(III) in grey square, neodymium(III) in purple diamond, cerium(III) in black dotted line and praseodymium(III) in green triangle. ....	144
<b>Figure III.6.</b> Distribution coefficients of lanthanides ( $[\text{Ln}] = 2.0 \times 10^{-2}$ mol.L <sup>-1</sup> ) after single liquid-liquid extractions by [P <sub>66614</sub> ][NTf <sub>2</sub> ] at various concentrations of $\text{HNO}_3$ . <b>A:</b> Cerium(IV) in orange diamond and cerium(III) in black dotted line. <b>B:</b> lanthanum(III) in grey square, neodymium(III) in purple diamond, cerium(III) in black dotted line and praseodymium(III) in green triangle. ....	145

<b>Figure III.7.</b> Distribution coefficients for cerium(IV) extracted towards $[C_1C_4Pyrr][NTf_2]$ at various concentrations of $[Ce(IV)]_0$ for two different nitric acid concentrations. $2.44 \text{ mol.L}^{-1} \text{ HNO}_3$ : blue diamond, $3.45 \text{ mol.L}^{-1} \text{ HNO}_3$ : red square.....	147
<b>Figure III.8.</b> Consecutive extraction steps of cerium(IV) obtained by ten extractions-stripping cycles of $[Ce(IV)]_0 = 1.0 \times 10^{-2} \text{ mol.L}^{-1}$ in $[HNO_3] = 3.45 \text{ mol.L}^{-1}$ by $[C_1C_4Pyrr][NTf_2]$ . .....	150
<b>Figure III.9.</b> Flow sheet for the recovery of pure cerium hydroxide starting from $NaREE(SO_4)_2$ produced from spent NiMH batteries. ....	155
<b>Figure III.10.</b> SEM analysis of the recycled cerium obtained from spent NiMH batteries. A: SE image (magnification $\times 500$ ). B: Elemental analysis by EDS. ....	157
<b>Figure III.11.</b> Recycling yield for cerium after each leaching, precipitation, oxidation, extraction, stripping and precipitation steps on the overall recycling process of spent NiMH batteries. ....	157
<b>Figure III.12.</b> Cyclic voltammetry experiments recorded at a scan rate of $0.05 \text{ V.s}^{-1}$ . The temperature is set to $25^\circ\text{C}$ and the rotating speed is 500 rpm. Grey curve: neat $[C_1C_4Pyrr][NTf_2]$ . Yellow curve: $[C_1C_4Pyrr][NTf_2]$ loaded with Ce(IV) after extraction in a nitric acid media.....	160
<b>Figure III.13.</b> Chronoamperometry experiments for $[C_1C_4Pyrr][NTf_2]$ loaded in Ce(IV) after extraction in a nitric acid media. A gold rotating electrode and a potential of $-2.00 \text{ V vs. Fc/Fc}^+$ during 2 hours is used. ....	162
<b>Figure III.14.</b> SEM images of the gold electrode after chronoamperometric experiment at $-2.00 \text{ V vs. Fc/Fc}^+$ during 2 hours in $[C_1C_4Pyrr][NTf_2]$ loaded in Ce(IV) after extraction in a nitric acid media. A and B: Secondary electron (SE) images at a magnification of 25 and 2000 respectively. C and D: Back scattered electron (BSE) images at a magnification of 1000 and 8000 respectively. ....	163
<b>Figure III.15.</b> Process for the consecutive extraction and electrodeposition of cerium in $[C_1C_4Pyrr][NTf_2]$ .....	165
<b>Figure III.16.</b> Chemical structures of efficient REE extractants: <b>A:</b> di-(2-ethylhexyl) phosphoric acid (DEHPA). <b>B:</b> tributyl phosphate (TBP). <b>C:</b> Cyanex 572 <sup>®</sup> <b>D:</b> 1-octyl-1methylpyrrolidinium octylphosphite ( $[C_1C_8PYR][C_8PO_3H]$ ). ....	166
<b>Figure III.17.</b> Synthesis flow sheet of $[C_1C_8PYR][C_8PO_3H]$ .....	168
<b>Figure III.18.</b> Distribution coefficients of lanthanides ( $[Ln] = 2.0 \times 10^{-2} \text{ mol.L}^{-1}$ ) after single liquid-liquid extractions by $[C_1C_8PYR][C_8PO_3H]$ in sulfuric acid and water at pH 1 and 2.....	170
<b>Figure III.19.</b> Flowsheet corresponding to the separation of cerium from lanthanum, neodymium and praseodymium.....	173
<b>Figure IV.1.</b> Molar extinction coefficient of $CoSO_4$ in water as function of the wavelength.....	182
<b>Figure IV.2.</b> Molar extinction coefficient for various $[DCA^-]/[Co(II)]$ ratios (0 to 200) in water versus the wavelength.....	183
<b>Figure IV.3.</b> Experimental and calculated absorbance at 509 nm versus the $R$ ratio (0 to 200) in water. Diamond: experimental points. Solid line: calculated data according to our model assuming one complex.....	184
<b>Figure IV.4.</b> Chemical speciation for $[Co(H_2O)_6]^{2+} (X_0)$ and $[Co(H_2O)_5(DCA)]^+ (X_1)$ for each $R$ ratio in an aqueous solution. Triangle: $(X_0)$ concentration. Square: $(X_1)$ concentration.....	185

<b>Figure IV.5.</b> Molar extinction coefficient of $\text{Co}(\text{NTf}_2)$ in $[\text{C}_1\text{C}_4\text{Pyrr}][\text{NTf}_2]$ versus the wavelength. ....	188
<b>Figure IV.6.</b> Molar extinction coefficient of the solution for various $[\text{DCA}^-]/[\text{Co}(\text{II})]$ ratios ( $R = 0$ to 5040) in $[\text{C}_1\text{C}_4\text{Pyrr}][\text{NTf}_2]$ versus the wavelength. ....	189
<b>Figure IV.7.</b> Experimental and calculated absorbance at 614 nm versus the $R$ ratio (0 to 5040) in $[\text{C}_1\text{C}_4\text{Pyrr}][\text{NTf}_2]$ . Diamond: experimental points. Dashed line: calculated value according to our model assuming three complexes. Solid line: Calculated value according to our model assuming four complexes. ....	191
<b>Figure IV.8.</b> Chemical speciation for $[\text{Co}(\text{NTf}_2)_3]^+$ ( $X_0$ ), $[\text{Co}(\text{NTf}_2)_{(3-x)}(\text{DCA})]^{(x-2)}$ ( $X_1$ ), $[\text{Co}(\text{NTf}_2)_{(3-x)}(\text{DCA})_2]^{(x-3)}$ ( $X_2$ ), $[\text{Co}(\text{NTf}_2)_{(3-x)}(\text{DCA})_3]^{(x-4)}$ ( $X_3$ ) and $[\text{Co}(\text{NTf}_2)_{(3-x)}(\text{DCA})_4]^{(x-5)}$ ( $X_4$ ) for each $R$ ratio in the ionic liquid. Dashed line: ( $X_0$ ) concentration. Diamond: ( $X_1$ ) concentration. Triangle: ( $X_2$ ) concentration. Square: ( $X_3$ ) concentration. Full line: ( $X_4$ ) concentration. ....	196
<b>Figure IV.9.</b> Chemical speciation for $[\text{Co}(\text{NTf}_2)_3]^+$ ( $X_0$ ), $[\text{Co}(\text{NTf}_2)_{(3-x)}(\text{DCA})]^{(x-2)}$ ( $X_1$ ), $[\text{Co}(\text{NTf}_2)_{(3-x)}(\text{DCA})_2]^{(x-3)}$ ( $X_2$ ), $[\text{Co}(\text{NTf}_2)_{(3-x)}(\text{DCA})_3]^{(x-4)}$ ( $X_3$ ) and $[\text{Co}(\text{NTf}_2)_{(3-x)}(\text{DCA})_4]^{(x-5)}$ ( $X_4$ ) function of pDCA in the ionic liquid. Dashed line: ( $X_0$ ) concentration. Diamond: ( $X_1$ ) concentration. Triangle: ( $X_2$ ) concentration. Square: ( $X_3$ ) concentration. Full line: ( $X_4$ ) concentration. ....	197
<b>Figure IV.10.</b> Extraction of cobalt $5 \cdot 10^{-3} \text{ mol.L}^{-1}$ in water with $[\text{P}_{66614}][\text{DCA}]$ from an aqueous phase containing $[\text{DCA}]/[\text{Co}]$ ratios of 1, 3, 10, 20, 50, 100, 150 and 200. Snapshots of extraction at ratios of 0, 3, 10, 50, 100 are presented. Ionic liquid phase is on top. ....	199
<b>Figure IV.11.</b> Extraction of cobalt $5 \cdot 10^{-3} \text{ mol.L}^{-1}$ in water and $1 \text{ mol.L}^{-1}$ of sodium dicyanamide by $[\text{P}_{66614}][\text{DCA}]-[\text{P}_{66614}][\text{NTf}_2]$ mixtures. Weight percentages of $[\text{P}_{66614}][\text{DCA}]$ are of 0, 25, 50 and 100 wt %. Snapshots of all extractions are presented. 0 and 25 wt % of $[\text{P}_{66614}][\text{DCA}]$ : Aqueous phase is on top. 50, 75 and 100% of $[\text{P}_{66614}][\text{DCA}]$ , ionic liquid phase is on top. ....	200
<b>Figure IV.12.</b> Scheme for the point titration technique. ....	206
<b>Figure IV.13.</b> Binodal curves for various $[\text{P}_{44414}][\text{Cl}] / \text{Acid} / \text{H}_2\text{O}$ AcABS at $24^\circ\text{C}$ . Blue diamond: $\text{HCl}$ , red square: $\text{H}_2\text{SO}_4$ , green triangle $\text{HNO}_3$ and purple circle $\text{H}_2\text{SO}_3$ . ....	208
<b>Figure IV.14.</b> Binodal curves for $[\text{P}_{44414}][\text{Cl}] / \text{HCl} / \text{H}_2\text{O}$ AcABS. Blue square: $25^\circ\text{C}$ , red diamond: $36^\circ\text{C}$ , green triangle: $45^\circ\text{C}$ , orange circle: $50^\circ\text{C}$ , Purple square: $56^\circ$ . Mixture points from A to E are represented in large yellow squares. Points $[\text{IL}] > 30 \text{ wt. \%}$ were measured by V.Mogilireddy during her post-doctoral position. ....	210
<b>Figure IV.15.</b> 3D phase diagram of $[\text{P}_{44414}][\text{Cl}] / \text{HCl} / \text{H}_2\text{O}$ from 25 to $56^\circ\text{C}$ . ....	211
<b>Figure IV.16.</b> The effect of $\text{NaCl}$ concentration on the binodal curve of $[\text{P}_{44414}]\text{Cl-HCl-H}_2\text{O}$ system at $24^\circ\text{C}$ . All binodal points containing $\text{NaCl}$ were measured by N.Schaeffer during his post-doctoral position. ....	212
<b>Figure IV.17.</b> Snapshots of $[\text{P}_{44414}][\text{Cl}] / \text{HCl} / \text{H}_2\text{O}$ AcABS with $\text{Fe}(\text{III})$ and $\text{Co}(\text{II})$ from 24 to $50^\circ\text{C}$ . Metals are only present to provide coloring of both phases. ....	213
<b>Figure IV.18.</b> Influence of the temperature on the phase splitting. The $\text{HCl}$ -rich phase is assumed to be completely depleted in ionic liquid. Metals are only present to provide coloring of both phases. ....	215

<b>Figure IV.19.</b> Extraction efficiency of single ion solution of 0.1 mol.L <sup>-1</sup> Co(II), Ni(II) or Mn(II) chloride in [P <sub>44414</sub> ]Cl-HCl-H <sub>2</sub> O AcABS using 30 wt.% [P <sub>44414</sub> ]Cl as a function of HCl concentration at 24 °C. ....	218
<b>Figure IV.20. (A)</b> CV experiments at a 0.01 V.s <sup>-1</sup> scan rate of various solutions containing 0.1 mol.L <sup>-1</sup> of Co(II) and concentration of [P <sub>44414</sub> ][Cl] ranging between 0 (black dotted line) and 20 wt. % (light to dark blue colours). <b>(B)</b> Evolution of the inset peak corresponding to the reduction of Co(II) to Co(0) as a function of the concentration of [P <sub>44414</sub> ][Cl]. ....	224
<b>Figure IV.21.</b> CV of various systems after extraction of cobalt in an aqueous solution containing 0.1 mol.L <sup>-1</sup> Co(II). Scanning rate: 0.01 V.s <sup>-1</sup> . Current densities (J) are multiplied by 25 for the ABS, AcABS and ABS-AcABS. ....	226
<b>Figure IV.22.</b> SEM-SE images (magnification × 1000) of working electrodes after 1 hour of electrodeposition at -2.00 V vs. Ag/AgCl. ....	227
<b>Figure IV.23.</b> Chronoamperometry experiments using a potential of -2.00 V vs. Ag/AgCl for 1 hour. Current densities (J) are multiplied by 25 for ABS and ABS-AcABS systems. ....	229
<b>Figure IV.24.</b> XRD diffractograms of deposits obtained after extraction of metals from a mixed solution containing 0.1 mol.L <sup>-1</sup> Co(II), Ni(II) and Mn(II) and electrodeposition at a potential of -2.00 V vs. Ag/AgCl during 1 hour. ....	232
<b>Figure IV.25.</b> Extraction yields of iron, cobalt, manganese and nickel for leachates using 6, 8 and 10 mol.L <sup>-1</sup> HCl after addition of approximatively 30 wt. % of [P <sub>44414</sub> ][Cl] at 50 °C. ....	238
<b>Figure IV.26.</b> Extraction yields of iron, cobalt, manganese and nickel for leachates using 2 mol.L <sup>-1</sup> H <sub>2</sub> SO <sub>4</sub> after a precipitation step at pH 1.7. 1, 2 or 3 mol.L <sup>-1</sup> NaCl was added to the solution before extraction with approximatively 30 wt. % of [P <sub>44414</sub> ][Cl] at 50 °C. ....	239
<b>Figure IV.27.</b> Flow sheet for the separation of transition metals from spent NiMH batteries by ABS-AcABS. ....	240
<b>Figure IV.28.</b> Chronoamperometry measurements, the potential applied is of -0.5 V vs. Ag/AgCl during 160 seconds in the IL-rich phase. ....	242
<b>Figure IV.29.</b> SEM analysis of the deposit obtained on a copper electrode after electroplating nickel at -0.5 V vs. Ag/AgCl during 160 sec A: SE image (magnification × 1000). B: SE image (magnification × 5000). ....	243
<b>Figure IV.30.</b> Flowsheet corresponding to the separation of cobalt, nickel, manganese and iron. ....	247
<b>Figure V.1.</b> Flowsheet for the recycling of metals from NiMH batteries. ....	250
<b>Figure V.2.</b> Ce(III) 0.02 mol.L <sup>-1</sup> in 4 mol.L <sup>-1</sup> HNO <sub>3</sub> after 10 hours bubbling of 2.6 mol.h <sup>-1</sup> O <sub>3</sub> . ...	251
<b>Figure V.3.</b> Modelling the impact of the anion, the cation and waste during the synthesis of [C <sub>1</sub> C <sub>4</sub> Pyrr][NTf <sub>2</sub> ]. Method used: ILCD 2011 Midpoint + V1.05. Data are provided by Florence Betmont from G-Scop laboratory. ....	252
<b>Figure V.4.</b> Recycling process of platinum from spent PEMFC currently developed. ....	254



---



---

## List of Tables

<b>Table I.1.</b> Characteristics of various batteries technologies. ....	28
<b>Table I.2.</b> Families of intermetallic compounds in NiMH batteries. <sup>25</sup> .....	34
<b>Table I.3.</b> List of critical raw materials from the EU level 2010. Platinum Group Metals: platinum, palladium, iridium, rhodium, ruthenium and osmium. Rare Earth Elements: yttrium, scandium, lanthanum, cerium, praseodymium, neodymium, promethium, samarium, europium, gadolinium, terbium, dysprosium, holmium, erbium, thulium, ytterbium and lutetium. ....	38
<b>Table I.4.</b> Generalities of REE used in NiMH batteries. ....	43
<b>Table I.5.</b> Applications and production of Light REE contained in NiMH batteries. <sup>56,58</sup> .....	46
<b>Table I.6.</b> Experimental conditions for leaching and precipitation REE from NiMH batteries. ....	63
<b>Table I.7.</b> Striking examples of pure hydrophobic ILs used in extraction of metals. ....	69
<b>Table I.8.</b> IL-based ABS used for the extraction of metals found in NiMH batteries. ....	75
<b>Table I.9.</b> Striking examples of pure ILs used for electrodeposition of metals. ....	79
<b>Table II.1.</b> Elemental analysis of different NiMH battery components using EDS. ....	89
<b>Table II.2.</b> Elemental analysis of the washed negative electrode using EDS. ....	90
<b>Table II.3.</b> Elemental analysis of washed BM produced at Recupyl <sup>®</sup> using EDS. ....	94
<b>Table II.4.</b> Elemental analysis of the solid residue after Leaching <i>A</i> and <i>B</i> by EDS. Only metallic species, namely TM and REE are quantified. Leachate composition analysed by ICP. Leaching yield ( $Y_L$ ) calculated by weighing the solid residue. ....	98
<b>Table II.5.</b> Elemental analysis of the precipitate obtained after leaching a NiMH black mass with 10 mol.L <sup>-1</sup> H <sub>2</sub> SO <sub>4</sub> at 75 °C by EDS. ....	111
<b>Table II.6.</b> Data collected in the literature for complexation constants <sup>236</sup> of TM and REE and solubility <sup>235</sup> of Ni, Co, Mn and Fe sulphate salts. All solubility data are given at 20 °C in pure water for (TM)SO <sub>4</sub> salts. ....	113
<b>Table II.7.</b> Comparison of the Ni/REE ratio between an ideal BM and BM produced at an industrial scale. ....	114
<b>Table II.8.</b> Leachate composition after leaching 1 g of BM produced at Recupyl <sup>®</sup> with H <sub>2</sub> SO <sub>4</sub> 2 mol.L <sup>-1</sup> at 25 °C during 1 hour. ....	115
<b>Table II.9.</b> Elemental analysis of the solid residue obtained after leaching a NiMH black mass produced at Recupyl <sup>®</sup> with 2 mol.L <sup>-1</sup> H <sub>2</sub> SO <sub>4</sub> at 25 °C by EDS. ....	116
<b>Table II.10.</b> Evolution of the concentration of metals in the leachate while increasing the pH from -0.25 to 1, 1.5, 1.7 and 2. ....	124
<b>Table II.11.</b> Elemental analysis of the precipitate obtained at pH 1.7 by SEM-EDS. ....	126
<b>Table III.1.</b> Molar extinction coefficient for Ce(IV), Ce(III), La(III), Nd(III) and Pr(III) at 212, 242 and 315 nm. ....	137
<b>Table III.2.</b> Distribution coefficients for lanthanides ( $[Ln] = 0.02 \text{ mol.L}^{-1}$ ) extracted separately towards [C <sub>1</sub> C <sub>4</sub> Pyrr][NTf <sub>2</sub> ] and [P <sub>66614</sub> ][NTf <sub>2</sub> ] at various concentrations of HNO <sub>3</sub> and their related separation factors of cerium(IV) from lanthanides(III) at 4.00 mol.L <sup>-1</sup> HNO <sub>3</sub> . ....	146

<b>Table III.3.</b> Distribution coefficient for cerium(IV) using $[C_1C_4Pyrr][NTf_2]$ at various concentrations of $[Ce(IV)]_0$ for two different nitric acid concentrations. ....	148
<b>Table III.4.</b> Distribution coefficients for lanthanides and separation factors of cerium(IV) from lanthanides(III) extracted towards $[C_1C_4Pyrr][NTf_2]$ , subsequently to an oxidation step using NaOH. Extraction carried out using $3.45 \text{ mol.L}^{-1} \text{ HNO}_3$ and $1 \times 10^{-2} \text{ mol.L}^{-1}$ lanthanide ions. ....	148
<b>Table III.5.</b> Mass balance for oxidation, extraction, stripping and precipitation steps in the overall process of cerium separation from lanthanum, neodymium and praseodymium. ....	156
<b>Table III.6.</b> Elemental analysis of the cerium deposit by SEM-EDS .....	163
<b>Table III.7.</b> Data for distribution coefficients and separation factors of Ln(III) and Nd/La respectively. Concentrations of REE(III) are of $0.02$ and $0.13 \text{ mol.L}^{-1}$ for pure $[C_1C_8PYR][C_8PO_3H]$ and Cyanex 572 <sup>®</sup> $1.0 \text{ mol.L}^{-1}$ diluted in an aliphatic solvent respectively. data for Cyanex 572 <sup>®</sup> were collected from Cytec-Solvay. <sup>69,272</sup> .....	169
<b>Table IV.1.</b> Calculated parameters for cobalt complexation by dicyanamide in an aqueous solution (Model assuming one complex). ....	186
<b>Table IV.2.</b> Calculated parameters for cobalt complexation by dicyanamide in an aqueous solution (Model assuming one complex) and in $[C_1C_4Pyrr][NTf_2]$ (Model assuming three and four complexes). ....	194
<b>Table IV.3.</b> Composition of mixtures A to E of the corresponding $[P_{44414}][Cl] / HCl / H_2O$ AcABS formed. ....	207
<b>Table IV.4.</b> Behaviour of both phases in terms of volumes, water content of the IL-rich phase and HCl content of the acid-rich phase at $24$ and $50 \text{ }^\circ\text{C}$ . ....	214
<b>Table IV.5.</b> Extraction yields (%E), distribution coefficients (D), separation factors ( $\beta_{CoUp}$ ) and mole fractions of cobalt in the upper phase ( $x_{CoLow}$ ) and of nickel in the lower phase ( $x_{NiLow}$ ) using $[P_{44414}][Cl] / HCl / H_2O$ ([IL] = 30 wt. %) at $24$ and $50 \text{ }^\circ\text{C}$ . Initial concentrations for all metals were $0.1 \text{ mol L}^{-1}$ . ....	220
<b>Table IV.6.</b> Composition of the ABS, AcABS and ABS-AcABS systems studied and their related extraction yields at $50 \text{ }^\circ\text{C}$ . ....	222
<b>Table IV.7.</b> Elemental analysis of the electrodeposited deposits obtained in ABS, AcABS and ABS-AcABS (undiluted and diluted) systems after extraction from solution containing $0.1 \text{ mol.L}^{-1} \text{ Co(II)}$ . ....	227
<b>Table IV.8.</b> ICP analysis performed for ABS, ABS-AcABS and ABS-AcABS diluted systems. The composition of deposits and Faraday efficiencies ( $E_F$ ) are given for all systems. ....	230
<b>Table IV.9.</b> Reminder of aqueous solutions compositions after leaching using $8 \text{ mol.L}^{-1} \text{ HCl}$ and leaching using $\text{H}_2\text{SO}_4$ followed by a precipitation step at a pH of 1.7. Data are given for the treatment of 1 g of black mass. ....	236
<b>Table IV.10.</b> AcABS and ABS-AcABS systems formed using $[P_{44414}][Cl] / HCl / H_2O$ and $[P_{44414}][Cl] / H_2SO_4 / NaCl / H_2O$ systems respectively. ....	237
<b>Table IV.11.</b> Concentration of Fe, Co, Mn and Ni in both IL and Acid-rich phases during extraction 1 and 2 by ABS-AcABS. ....	241

**Table IV.12.** Elemental analysis of the deposit obtained on a copper electrode after electroplating nickel at -0.5 V vs. Ag/AgCl during 160 sec. Transition metals, except from copper are considered. .... 243

---

---

## List of Abbreviations

**IAEA:** International atomic energy agency

**NiMH:** Nickel-metal hydride

**REE:** Rare earth element

**TM:** Transition metals

**IL:** Ionic liquid

**VOC:** Volatile organic solvent

**EU:** European Union

**IUPAC:** International union of pure applied chemistry

**EV:** Electric vehicle

**HEV:** Hybrid electric vehicle

**BM:** Black mass

**LLE:** liquid-liquid extraction

**ABS:** Aqueous biphasic system

**AcABS:** Acidic aqueous biphasic system

**LCST:** Lower critical solution temperature

**UCST:** Upper critical solution temperature

**WE:** working electrode

**RE:** reference electrode

**CE:** counter electrode

**GC:** Glassy carbon electrode

**NHE:** Normal hydrogen electrode

**ICP-OES:** Inductively coupled plasma-optical emission spectroscopy

**AAS:** Atomic absorption spectroscopy

**NMR:** Nuclear magnetic resonance

**SEM:** Scanning electron microscopy

**SE:** Secondary electron

**BSE:** Backscattered electron

**EDS:** Energy dispersive X-ray spectroscopy

**XRD:** X-ray diffraction

**KF:** Karl Fischer titration



---

---

# Introduction

In 2015, the United Nations Climate Change Conference in Paris (COP21) committed 195 countries to stabilize global warming under 2 °C by 2100. To reach this ambitious objective, Nicolas Hulot, the French minister of the ecological transition, presented in 2017 a “climate plan” to define a trajectory with the aim of reducing greenhouse gas emissions. One of the major policies aimed to eliminate the sale of oil and diesel cars in 2040. Battery-driven vehicles are thus widely investigated to fit greener emissions requirements and to reduce the environmental impact of vehicles. Among them electric vehicles (EVs) but also hybrid electric vehicles (HEVs) powered by Li-ion or Nickel-metal hydride (NiMH) batteries are developed. Since their first commercialisation in a HEV in 1997 thanks to the Toyota Prius car model, the production of NiMH has taken an important part in the battery market with 1 billion devices sold in 2016. However, sustainable and disruptive technologies are demanding increasing amounts of strategic metals whose impacts on the economy, geopolitics and environment are largely underestimated. It is worth noticing that the French mathematician and deputy Cedric Villani, winner in 2010 of the Fields medal, identified in a report from 2017 on artificial intelligence (AI) that one of the biggest threats in the development of AI technologies was linked to the availability of critical metals.

NiMH batteries are composed of large amounts of valuable metals. Nickel is mainly present at the positive electrode under the form of a hydroxide compound. An intermetallic alloy can be found at the negative electrode where a mixture of transition metals (nickel, cobalt, manganese) and rare earth elements (lanthanum, cerium, neodymium and praseodymium) allows hydrogen storage during the charge. However, according to a very recent report from the European Union on critical materials, cobalt is the transition metal presenting the highest criticality rate. Its price has been multiplied by 3 from 2014 to 2017 due to (i) its low concentration in ores (ii) the domination of the production in DR Congo (60 % of the world production) (iii) the increasing demand mainly due to battery technologies in EVs and HEVs. Most alarmingly, rare earth elements (REE) were

commonly identified as critical raw materials by the EU and the U.S geological survey. More than 97 % of the production has been delocalized to China and 40 % of the extracted REE is done so illegally. Mining processes have dramatic impacts on the environment and on public health because of the use of toxic compounds. Furthermore, because lanthanides are always mixed in ores with actinides, a large amount of radioactive wastes is produced during the extraction of REEs. Therein lies a huge paradox at the centre of green technologies. Such growing technologies as NiMH batteries and wind turbines are labelled ‘green’ despite requiring large amounts of REE, resulting in a final product which is more harmful than the technologies they aim to replace. To tackle this issue, numerous potential solutions are under investigation: the reuse of devices, to substitute polluting elements by more sustainable ones and their recycling. The latter solution will be considered in this work.

All industrial extraction processes of transition metals and rare earth elements are based on the dissolution/dilution of an extractant in a volatile organic compound (VOC). Evolution of European policies towards chemical processes initiated by the REACH regulation (Registration, Evaluation, Authorization and Restriction of Chemicals) is strongly aimed at limiting the use of VOCs. Greener solvents thus need to be developed for extraction and recycling processes. Among them, Ionic liquids (ILs) were described as promising solvents. ILs are salts liquid at temperatures lower than 100 °C and present highly tuneable properties. ILs can act both as the extractant and solvent for metal separation. Furthermore, because they also exhibit good ionic conductivities and electrochemical stabilities they are studied as electrolytes for the recovery of metals by electrodeposition.

To face the emerging environmental and economic challenges presented, the recycling company Recupyl<sup>®</sup> and the academic laboratory LEPMI elaborated a project to develop a recycling process of metals from NiMH batteries with ILs. Recupyl<sup>®</sup> will lead the mechanical treatment steps of real spent NiMH batteries in order to produce a concentrated powder in strategic metals named black mass (BM). Starting from the BM, hydrometallurgical and electrochemical steps will be performed in LEPMI aiming the separation and recovery of strategic metals.

To make a sense of this work and fully understand the key issues of the project, **chapter I** will be devoted to a summary of the state of the art. In **chapter II**, mechanical treatment of end-of-life batteries and characterization of the material obtained will firstly be investigated. In a second part the leaching step, this is to say the dissolution of the battery will be carried out in various solutions using acid, water and/or IL. Finally, transition metals and REEs will be separated by a precipitation method. A process for the separation of cerium from lanthanum, neodymium and praseodymium will be proposed in **chapter III** by oxidation and liquid-liquid extraction. The recovery of Ce will then be investigated by precipitation and electrodeposition. **Chapter IV** will be devoted to the separation of transition metals. The first part will study the speciation of cobalt during liquid-liquid extractions by dicyanamide-based ILs. The second part will highlight novel extraction solutions by the development of acidic aqueous biphasic systems for both extraction and electrodeposition of metals. Based on the results obtained from the previous chapters, a flowsheet will be proposed for the recycling of metals from NiMH batteries.

This work is a partnership between the academic laboratory LEPMI from INP Grenoble and the company Recupyl<sup>®</sup> and has been supported by:

- Labex CEMAM
- ERAMIN program
- EIT KIC InnoEnergy





---

---

# CHAPTER I

## State of the Art



*Apparatus for fractionated distillation. Abu Musa Jabir VIII<sup>th</sup> century. Reedited from *Philosophi ac Alchimistae Maximi* by Johannes Greininger, Strasbourg, 1531.*

# I.1 Presentation of the NiMH battery

---

## I.1.1 A historical overview of the energy sector

Very recently, the French paleoanthropologist, Jean Jacques Hublin brought the proof that *homo sapiens* emerged more than 300 000 years ago thanks to the discovery of new fossils from the site of Jebel Irhoud in Morocco (*Hublin et al. Nature, 2017*).<sup>1</sup> Since this period, the human being has never ceased to try to increase his comfort by the development of new technologies. It rapidly appeared that the utilization and the production of energy was a key point to reach higher standards of living. Energy can be defined as the ability to do a work leading to the production of movement, heat or electromagnetic radiation.<sup>2</sup> The first evidence of production of energy dates back to 1 million years ago, where the combustion of several light plants, leaves and grass was highlighted in South African caves.<sup>3</sup> Later on, during the middle age, water mills were commonly used to grind cereals, quickly followed by the wind mills. The complexity of these technologies increased constantly over the centuries allowing humans to produce higher amounts of energy. The end of the XVIII<sup>th</sup> century was strongly marked by the industrial revolution. In 1775, the patented *James Watt's Fire Engines*<sup>4</sup> allows the use of power steam engines for transportation and industry. At this time, coal started to be extensively extracted and was used as the main fuel during more than 100 years. **Figure I.1** shows the world energy consumption of various fossil fuels plotted from 1800 to year 2000. Energy consumption is expressed in mega tons equivalent petroleum (Mtep). 1 tep represents the calorific value released after burning 1 ton of oil which represents more than 11.6 kW.h. An exponential increase in the world energy consumption started during the XX<sup>th</sup> century with the discovery of oil and natural gas resources corresponding to a second energy revolution. Finally, in the 70's, nuclear plants started to be used commercially, firstly in the USSR, then in the USA and in Europe. According to the International Atomic Energy Agency (IAEA), more than 440 nuclear reactors are currently producing electricity in the world.<sup>5</sup>

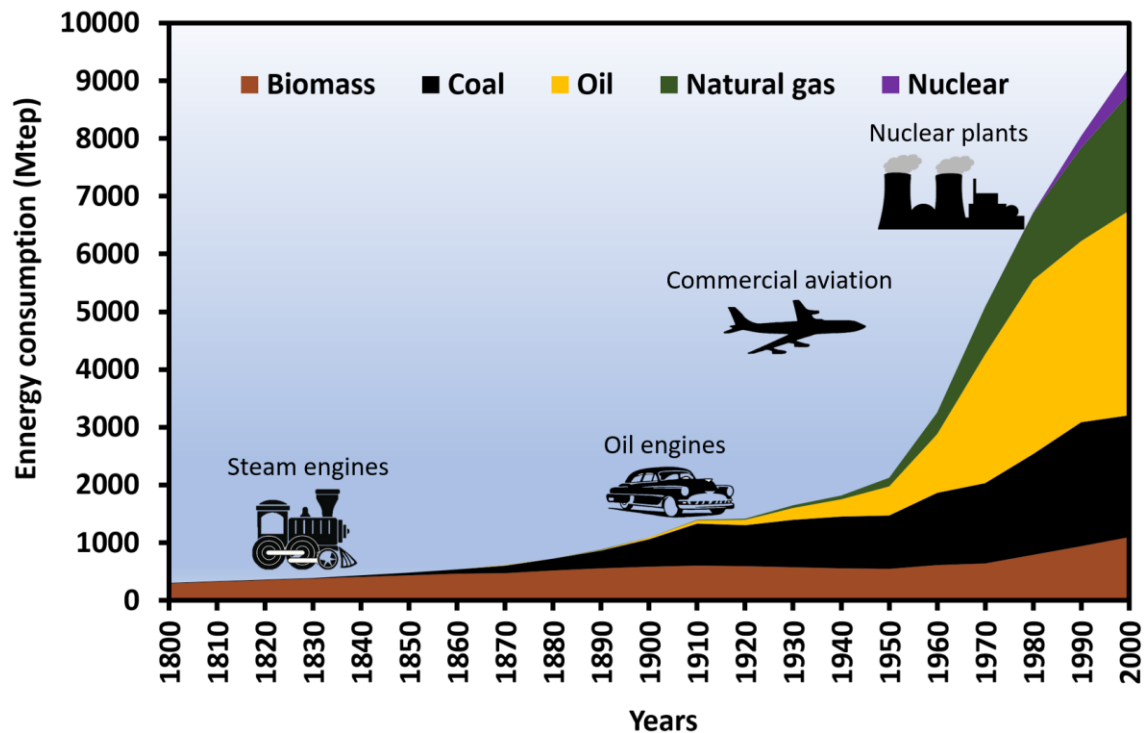


**Figure I.1.** World energy consumption of fossil fuels from 1800 to 2000.<sup>6</sup>

Since the beginning of the XXI<sup>st</sup> century, mankind, worried about climate changes due to the production of energy from fossil fuels, started to develop renewable energies. The latter have the reputation to not produce any carbon dioxide emissions or radioactive wastes during their utilization. However, the manufacture of devices or plants required to produce such renewable energy does not follow these criteria.<sup>7</sup> Nevertheless, according to the *Renewable Energy Policy Network REN21, annual report 2016*,<sup>8</sup> renewable energies represent in 2015 19 % of the world energy consumption and over 23 % of the electricity production. **Figure I.2** highlights the fact that the predominant renewable energy is by far hydropower, followed by wind power. Solar power from photovoltaic panels represents only 1.2 % of the global electricity production. This new way of producing energy has already been described as the third energetic revolution by the American economist Jeremy Rifkin.<sup>9</sup>

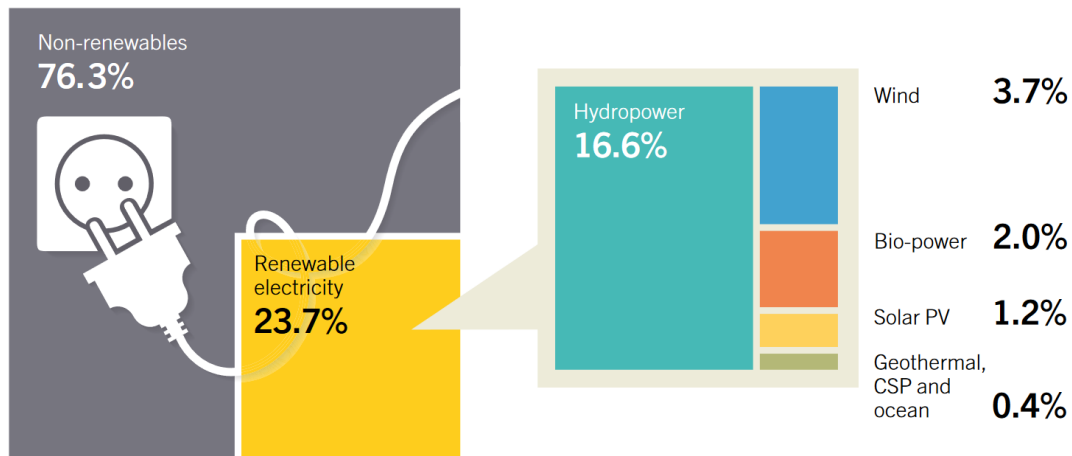


**Figure I.2.** Production of electricity by renewable energies in the world.<sup>8</sup>

However, production through wind turbines, solar panels and even hydroelectric power plants is highly dependent on the meteorological conditions. This is why the increasing energy demand combined to the uncertainty of a continuous production forces us to find some energy storage solutions. Electrochemical accumulators such as batteries are one answer to this issue. Furthermore, every new generation of portable communication systems (mobile phones, tablets, laptop computers...) requires advanced battery technology supporting the device performance needs. Likewise, the progressive increase in battery-driven transportation is expected to ensure the replacement of the oil engine. Recently, the Swiss aviator Bertrand Piccard (*Solar Impulse project*)<sup>10</sup> was able to travel 40000 km during a world tour in a plane powered by batteries charged thanks to photovoltaic panels. This success echoes the tremendous energetic transition that we are facing by the development of new energy production and storage solutions.

### **I.1.2 The battery devices, from performance to market**

A battery is an energy storage/conversion device that converts the energy of chemical reactions into electric energy. A battery is basically a galvanic cell which consists of two electrodes electrically separated by an insulating separator and ionically connected by an ion conductive electrolyte. The latter can be an aqueous or organic salt solution, a molten salt or a solid containing mobile ions.<sup>11</sup>

The Voltaic Pile was the first electrical battery that could continuously provide an electrical current. It was invented by Alessandro Volta in 1799 and published in 1800 (*On the electricity excited by the mere contact of conducting Substances of different kinds*).<sup>12</sup> It consisted of a stack of zinc and copper disk electrodes separated with a cloth soaked in a salt solution. Since the beginning of the XIX<sup>th</sup> century, many different electrochemical storage technologies were developed, among them, secondary batteries are defined as rechargeable cells. The most popular and efficient ones are depicted in **Table I.1** according to several studies.<sup>13,14</sup>

Battery Technology	Negative electrode	Positive electrode	Reaction during discharge	electromotive force	Theoretical capacity (Ah/kg)	Specific theoretical energy (Wh/kg)	Cost (€/kWh)
Acid-Pb	Pb	PbO <sub>2</sub>	$\text{Pb} + \text{PbO}_2 + \text{H}_2\text{SO}_4 \rightarrow 2\text{PbSO}_4 + 2\text{H}_2\text{O}$	2.1	120	252	50-150
NiCd	Cd	NiO(OH)	$\text{Cd} + 2\text{NiOOH} + 2\text{H}_2\text{O} \rightarrow 2\text{Ni(OH)}_2 + \text{Cd(OH)}_2$	1.35	181	244	250-400
NiMH	MH	NiO(OH)	$\text{MH} + \text{NiOOH} \rightarrow \text{M} + \text{Ni(OH)}_2$	1.35	178	240	300-700
Li-ion	Li <sub>x</sub> C <sub>6</sub>	Li <sub>1-x</sub> CoO <sub>2</sub>	$\text{Li}_x\text{C}_6 + \text{Li}_{1-x}\text{CoO}_2 \rightarrow \text{LiCoO}_2 + \text{C}_6$	4.1	100	410	700-2000
LiS	Li	Sn <sup>2-</sup>	$\text{Li}_x + \text{S} \rightarrow \text{SLi}_x + \text{Li}_{1-x}$	1.7-2.5	1870	550	-
Li-air	Li	O <sub>2</sub>	$2\text{Li} + \text{O}_2 \rightarrow \text{Li}_2\text{O}_2$	2.96	3840	11400	-

**Table I.1.** Characteristics of various batteries technologies.

Acid-Pb batteries were the first electrochemical storage devices produced at large scale after their invention in 1859 by Gaston Planté.<sup>15</sup> The second half of the XX<sup>th</sup> century saw the commercialization of NiCd batteries thanks to the invention of Waldemar Jungner in 1899.<sup>13</sup> Much more robust and lighter than the acid-lead batteries, the cadmium technology was widely used for portable application. The active materials are composed of cadmium and nickel oxide hydroxide at the negative and the positive electrode respectively. The well-known toxicity of cadmium forced the European Union to forbid the use of this technology in most applications through the European directive 2006/66/CE published in September 2006 in the official journal of the European Commission.<sup>16</sup> NiCd rechargeable batteries can still be found in specific applications such as medical tools or aeronautic technology. The next major battery technology was the NiMH battery. Following a collaboration between two automotive industries, namely Volkswagen and Daimler-Benz (now Mercedes-Benz), a US patent entitled ‘*Accumulator electrode with capacity for storing hydrogen and method of manufacturing said electrode*’ was granted in June 1972.<sup>17</sup> Similarly to the NiCd technology, the positive electrode is composed with the couple NiO(OH)/Ni(OH)<sub>2</sub>. The negative

electrode is made of a metallic hydride able to store hydrogen during charge and to release it during discharge. Commercialized in 1990, NiMH batteries were mainly used in portable devices such as computers, cell phones and lightweight tools replacing NiCd devices. One year later, Sony started the commercialization of a disruptive electrochemical device: the Li-ion battery.<sup>14</sup> Presenting a specific theoretical energy nearly twice as high as that of NiMH batteries, the Li-ion technology rapidly dominated the market and allowed portable systems to reach much higher autonomy. The evolution of the worldwide rechargeable battery market from 1995 to 2016 is represented in **Figure I.3**.

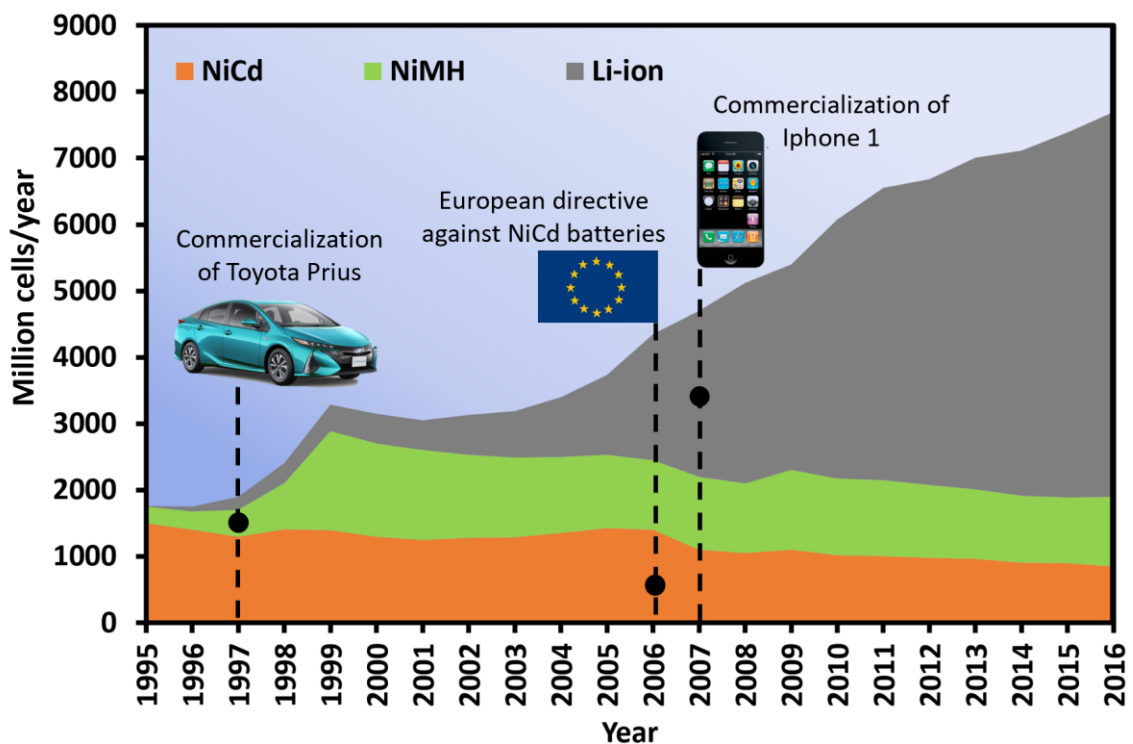


**Figure I.3.** Evolution of the worldwide market of rechargeable batteries in volume from 1995 to 2016.<sup>18</sup>

New battery technologies threatening the Li-ion domination such as LiS<sup>19</sup> and Li-air batteries<sup>20</sup> presenting incredibly high specific theoretical energies of 550 and 11400 Wh.kg<sup>-1</sup> respectively are under the scope of many research and industrial groups. However, the NiMH battery remains a resilient technology on the market and presents a constant production of 1 billion cells per year within the last ten years.<sup>18</sup> This is linked to the application of NiMH batteries in Hybrid Electric Vehicles (HEV) combining a combustion engine as well as an electrical propulsion. Toyota, the actual leader in the HEV market, commercialized its first

hybrid car in 1997 using a NiMH battery thanks to the Prius car model. Since then, the metal-hydride technology was mainly used for HEVs while it has been progressively replaced by Li-ion batteries for numeric applications such as laptops and cell phones. **Figure I.4** highlights the evolution of the market of NiMH batteries (in value) during the beginning of the XXI<sup>st</sup> century.

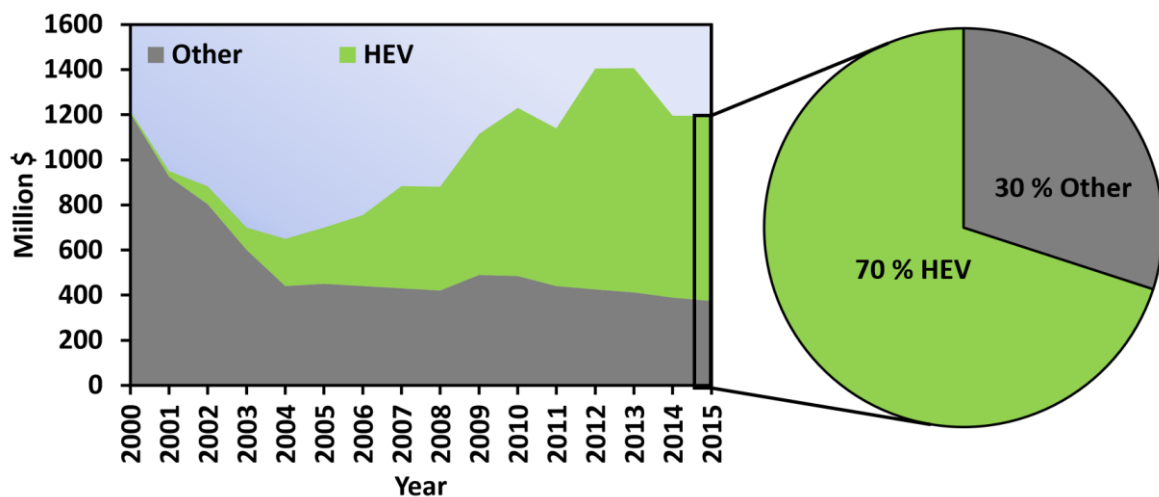


**Figure I.4.** Share of NiMH batteries sold for HEV application worldwide in value from 2000 to 2015.<sup>18</sup>

To conclude, even if the NiMH market is diluted by the tremendous success of Li-ion technology, these electrochemical storage devices are far from being abandoned. Thanks to their high power and increased safety, combined with their low price, they represent 1.45 Billion \$ sales each year with a major application in a growing and promising transportation solution: the hybrid electric vehicles.<sup>18</sup>

### I.1.3 The NiMH technology

#### a. Generalities

A schematic view of an operating NiMH battery is given in **Figure I.5**. Briefly, nickel hydroxide is used at the positive electrode. A hydride intermetallic alloy can be found at the negative terminal. They are electrically isolated by an electrolyte separator reducing the distance between the active materials. It is made of polyolefin, usually a non-woven polypropylene.<sup>21</sup> The latter is soaked in a concentrated potassium hydroxide solution which plays the role of the electrolyte.



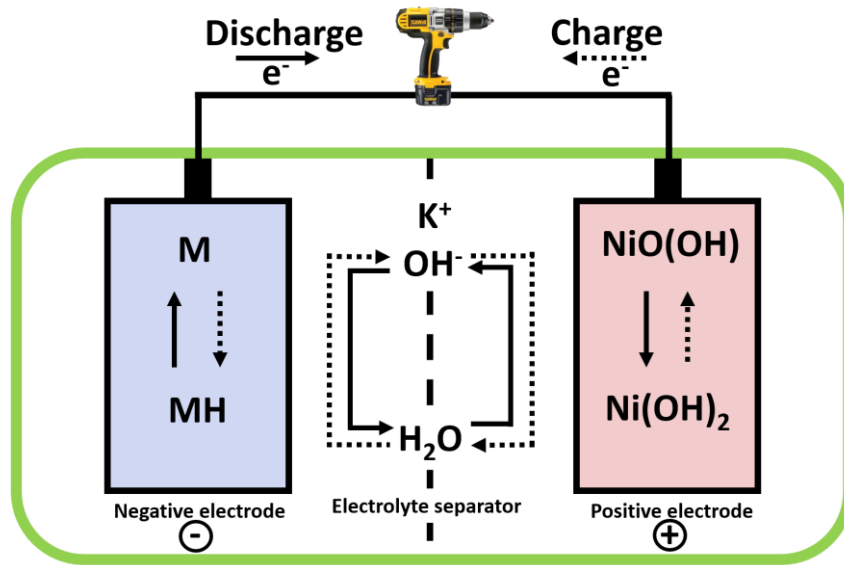


**Figure I.5.** Schematic view of the NiMH battery.

Spontaneous redox reactions are ruled by the electromotive force. The latter is due to a potential difference between two electrode materials. Potential is function of the redox couple of materials, concentration of the species and temperature and is described by the Nernst law:

$$E = E^0 + \frac{RT}{nF} \ln \frac{a_{Ox}}{a_{Red}} \quad (1)$$

$E$  = Potential of one electrode

$E^0$  = Standard potential of one redox couple

$n$  = Number of exchanged electrons

$R$  = Constant of the ideal gas law =  $8.314 \text{ Jmol}^{-1}\text{K}^{-1}$

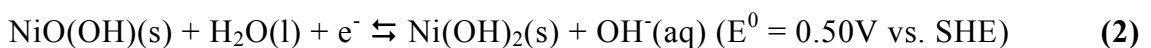
$F$  = Faraday's constant =  $96500 \text{ C}$

$T$  = Temperature in Kelvin (K)

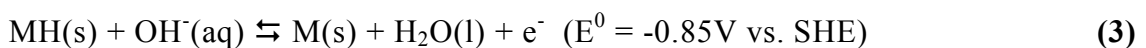
$a_{Ox}$  and  $a_{Red}$  = Chemical activity of species

During discharge, the chemical reaction described below takes place<sup>21</sup>:

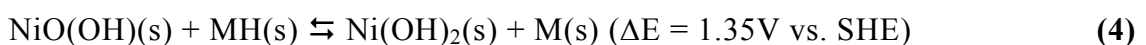
*Positive electrode:*



*Negative electrode:*



*Global reaction:*



During charge, the exact opposite reactions occur.

NiMH secondary batteries can be found under three main geometric configurations: button, cylindrical cell and prismatic cell.

In button cells, active materials are compressed under a disk shape. It is the simplest configuration of a battery but also the less efficient. It is mainly used for low regime applications such as memory backup. Within the cylindrical geometry, electrodes and separator are under the form of thin rectangular layers. They are rolled together until reaching a distance electrode-electrode of 120 to 180  $\mu\text{m}$ . These systems are mainly used in portable tools such as drilling and sanding machines. Finally, the prismatic cells present stacks of positive electrode / separator / negative electrode. As more active material can be used for the same volume, this geometry is the most efficient for large battery design and is widely used in HEV.<sup>22</sup> Their price is, however, slightly higher than that of cylindrical cells as they are more complex to manufacture.

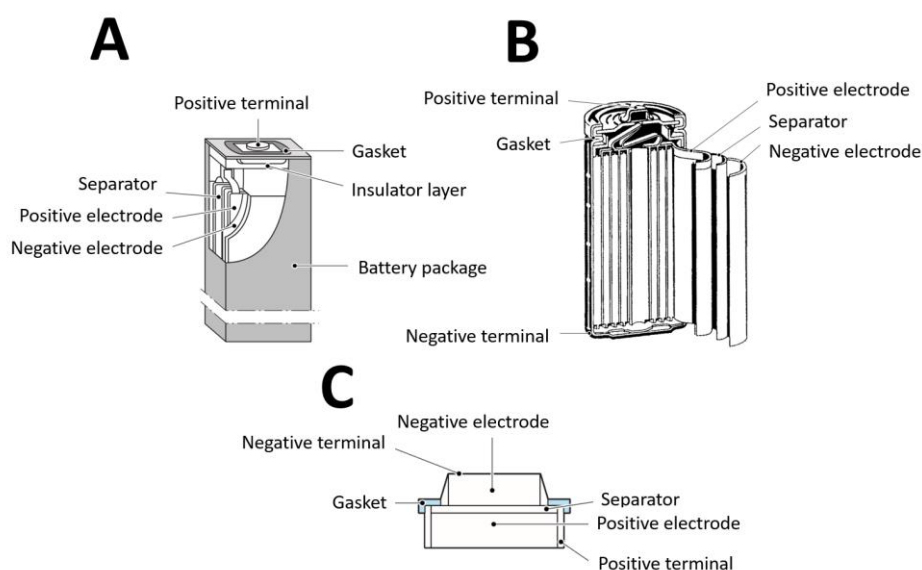


**Figure I.6.** The main geometries for NiMH batteries. **A:** Prismatic cell. **B:** Cylindrical cell. **C:** Button cell.<sup>22</sup>

#### b. Electrolyte

It has been widely accepted that the optimal concentration of KOH in the aqueous electrolyte should be around 30 wt.% ( $\approx 6 \text{ mol.L}^{-1}$ ) in industrial batteries. The

latter value was chosen because potassium hydroxide reaches a maximum specific conductivity in this concentration range.<sup>23</sup> Small amounts of LiOH can however be added to the solution in order to increase the charge acceptance (ability to accept energy) at the positive electrode. The amount of electrolyte in these systems is very low, typically under 2 mL.Ah<sup>-1</sup>. Considering a 1.2 V classical cylindrical battery with a capacity of 3 Ah, the volume will be of 6 mL maximum in 40 g which justifies their qualification of “dry batteries”.<sup>22</sup> The electrolyte has a great influence on the charge and discharge potential of the electrodes. Furthermore, it is responsible of the degradation of the nickel hydroxide positive electrode into  $\gamma$ -NiOOH. Some papers such as the work from *Wang, Forsyth et al.* have thus focussed on the development of solid electrolyte to tackle this issue.<sup>24</sup>

### c. The positive electrode

Nickel hydroxide in the active material presents a theoretical capacity of 289 mA.g<sup>-1</sup>. In order to increase the properties of the electrode regarding conductivity, stability or even oxygen over voltage, nickel is often substituted by cobalt in the ratio Ni<sub>97</sub>Co<sub>3</sub>.

Two main techniques are known for the preparation of Ni(OH)<sub>2</sub>:

#### *Ni(OH)<sub>2</sub> precipitation in a nickel sintered support*

This was the first strategy used to prepare all positive electrodes since the development of the NiCd batteries. Nickel sulphate (NiSO<sub>4</sub>) is precipitated out from an aqueous solution within a porous metallic nickel structure obtained by sintering by increasing the aqueous pH using sodium hydroxide (NaOH). Several precipitation cycles are performed. This is probably the most robust process to produce positive electrodes which brings high cyclability to NiMH batteries. However, this material presents only 35 % of active material. This is a strong limitation to produce high performance portable storage solutions.<sup>22</sup>

#### *Ni(OH)<sub>2</sub> precipitation in a nickel foam*

This strategy was firstly developed by Matsushita (now Panasonic) at the end the 80s and is currently the dominating method for the preparation of NiMH positive electrodes. Starting from a polyurethane foam, a thin coating of metallic nickel is

added by Chemical Vapor Deposition (CVD) to increase the conductivity of the material. Similarly to the sintered method,  $\text{Ni}(\text{OH})_2$  is then obtained after precipitation in alkaline media. Finally, polyurethane is degraded by thermic treatment leading to a particle size of  $10 \mu\text{m}$  of  $\text{Ni}(\text{OH})_2$ . The active material now represents 60 % of the electrode.<sup>21</sup>

d. The  $AB_5$  negative electrode

The negative electrode is made of a metal hydride metal and usually presents a theoretical capacity of  $289 \text{ mA}\cdot\text{g}^{-1}$ . The metal is composed of binary alloys. Andreas Züttel et al.<sup>25</sup> reviewed six main types of alloys for hydrogen storage. They are displayed in **Table I.2**. However, the  $AB_5$  intermetallic compound represents the huge majority of batteries in the market and will be the only one recycled in this work.<sup>26</sup>

Intermetallic compound	Composition	Hydride	Structure
$AB_2$	ZrMn <sub>2</sub> / ZrV <sub>2</sub>	ZrMn <sub>2</sub> H <sub>5.5</sub>	Hexagonal/Cubic
$A_2B_7$	Y <sub>2</sub> Ni <sub>7</sub>	Y <sub>2</sub> Ni <sub>7</sub> H <sub>3</sub>	Hexagonal
$AB_5$	LaNi <sub>5</sub>	LaNi <sub>5</sub> H <sub>6</sub>	Hexagonal
$AB_3$	CeNi <sub>3</sub> / YFe <sub>3</sub>	CeNi <sub>3</sub> H <sub>4</sub>	Hexagonal
$AB$	TiFe / ZrNi	TiFe	Cubic
$A_2B$	Mg <sub>2</sub> Ni / Ti <sub>2</sub> Ni	Mg <sub>2</sub> NiH <sub>4</sub>	Cubic

**Table I.2.** Families of intermetallic compounds in NiMH batteries.<sup>25</sup>

$AB_5$  alloys crystallize in an hexagonal type  $\text{CaCu}_5$  structure.<sup>27</sup> The crystal structure is given in **Figure I.7**.

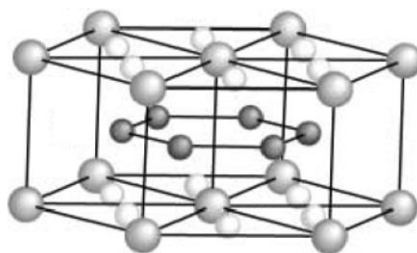


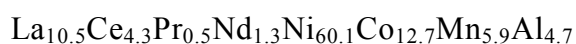
**Figure I.7.**  $AB_5$  crystal structure. 1 large grey atom: A in position (0, 0, 0). 2 small white atoms B in position (1/3, 2/3, 0). 3 small black atoms B in position (1/2, 0, 1/2).<sup>27</sup>

Hydride properties of  $\text{LaNi}_5$  material were first reported by Van Vucht.<sup>28</sup> During charge, the crystal lattice is able to expand of 25 % allowing hydrogen to be stored in tetrahedral sites.<sup>29</sup> However, to reduce the overall price of the battery, electrodes are manufactured starting from mixture of metals related to the nature of ores. The latter alloy is commonly designed as a mischmetal. As a result, nickel is mixed with cobalt and manganese while lanthanum is substituted with cerium, neodymium and small amounts of praseodymium. The influence of REE composition modifications compared to the  $\text{LaNi}_5$  on thermodynamic properties and corrosion resistance was studied and brought the proof that neodymium and praseodymium doping could increase the ability to store hydrogen.<sup>30</sup> One main technique was used for the formulation of such electrodes:

*the plasticized technology*

The active material is mixed with a conductive paste containing a thickener and a binder. It is then deposited on a nickel-steel perforated plate. A thin nickel coating can also be added to the electrode.<sup>22</sup>

In order to develop an efficient recycling process, we need to have a very precise idea of the metals that will be present in the active materials. The formulation of the mischmetal is thus a key point in the realization of this work. The intermetallic compound present in the  $AB_5$  alloy was reported to have 2 main compositions:<sup>21</sup>



e. Metals in NiMH batteries

NiMH batteries are widely used to store energy in Hybrid Electric Vehicles. The active materials found in both electrodes originate from complex matrices where eight main elements form intermetallic compounds. These metals can be divided in two main categories: Transition Metals (TM) including nickel, cobalt, manganese and aluminum, and Rare Earth Elements (REE) including lanthanum, cerium, neodymium and small amounts of praseodymium. The latter category of metals is present in the negative electrode (elements are given in each category from the most concentrated to the less concentrated). Large amounts of valuable metals are

needed to manufacture such storage devices. The question of the extraction and recycling of such metallic elements is thus a key point in the development of low environmental impact technologies.

## I.2 Mining and recycling of metals

---

### I.2.1 Raw materials criticality

In his very recent study, Guillaume Pitron alarms us that the world will have to double the production of rare metals every 15 years to support the change in our energetic model. This will imply the extraction of more ores during the next 30 years than during the past 70 000 years.<sup>7</sup> Furthermore, the variety of metals used in technologies is highly increasing. While only seven metals were used between ancient history and Renaissance (Au, Cu, Pb, Ag, Sn, Hg and Fe), about 20 were extracted during the XX<sup>th</sup> century. Nowadays, the entire 84 primordial elements of the Mendeleïev table are part of the manufacture of modern technologies.<sup>7,31</sup>

Similarly to most of all natural resources, the tremendous increase in the production of metals already creates some geopolitical conflicts.<sup>32</sup> In order to identify the risks many countries were facing regarding specific pivotal systems using metals (e.g. energy supply, defense, communication...), the notion of criticality was introduced. Several methodologies<sup>33,34</sup> were used to calculate the criticality of metals. They have been nicely reviewed by Erdmann and Graedel.<sup>35</sup> According to seven academic papers on the subject, they were able to define the criticality rate as the number of criticality designation on the number of studies. This diagram is displayed in **Figure I.8**.

On the eight different metals used in NiMH battery electrodes (Ni, Mn, Co, Al, La, Ce, Pr, Nd), all of them have been described at least once as a critical element. Furthermore, cobalt and rare earth elements are described by 50 and 100 % of the studies respectively as being critical metals.

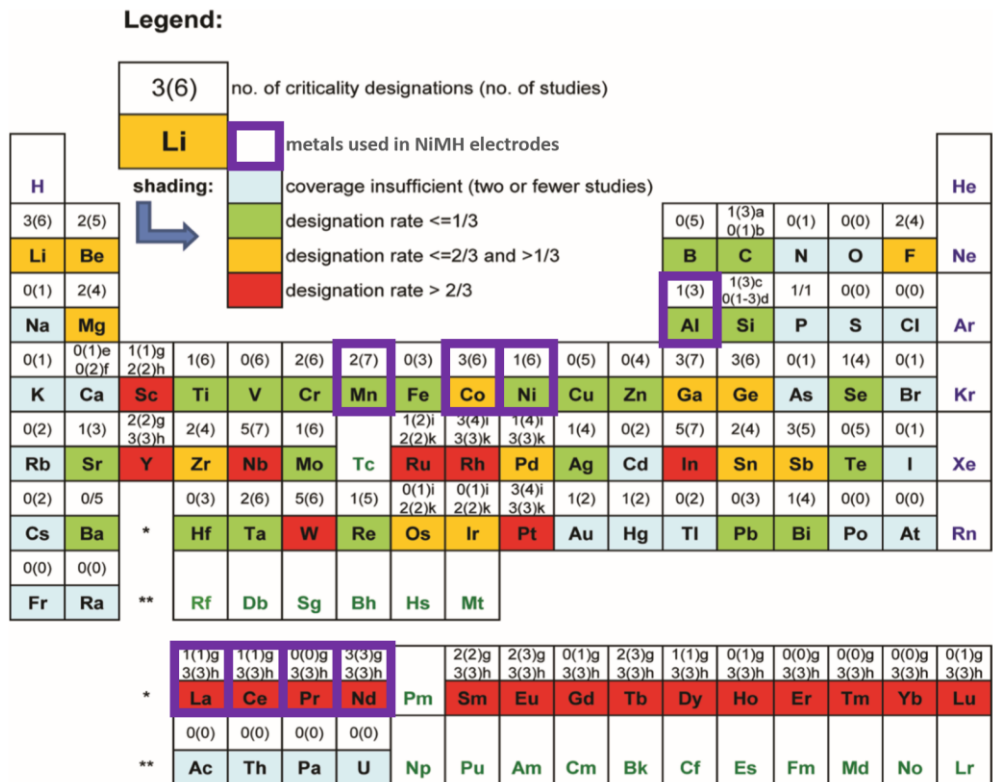


**Figure I.8.** Frequencies of criticality designations from seven studies. Some metals were treated as minerals or metal groups. Regarding rare earth elements, g: as element. h: as compound of REE group.<sup>35</sup>

In 2010, the European Commission identified that the availability of metals was under pressure and asked a college of experts to build a report on “Critical raw materials for the EU”.<sup>36</sup> This report stands as a warning towards European governments and a manifest for the need to build strong policies to tackle this issue. Depending on the economic importance and the supply risk of each element, they pointed out a list of 14 so-called critical raw materials:

List of critical raw materials	
Antimony	Platinum Group Metals
Indium	Gallium
Beryllium	Rare Earth Elements
Magnesium	Germanium
Cobalt	Tantalum
Niobium	Graphite
Fluorspar	Tungsten

**Table I.3.** List of critical raw materials from the EU level 2010. Platinum Group Metals: platinum, palladium, iridium, rhodium, ruthenium and osmium. Rare Earth Elements: yttrium, scandium, lanthanum, cerium, praseodymium, neodymium, promethium, samarium, europium, gadolinium, terbium, dysprosium, holmium, erbium, thulium, ytterbium and lutetium.



Following this work, the European experts expressed eight recommendations. The first one was to have an update of those data every five years maximum. A report was thus published in 2014<sup>37</sup> excluding tantalum and adding borates, coking coal, chromium, magnesite, phosphate rock and silicon metal to the list. Very recently, in 2017 the last updated report from the EU<sup>38</sup> added bismuth, hafnium, scandium and vanadium to the list.

## I.2.2 Challenges for transition metals: the case of cobalt

### a. Generalities

Transition metals were defined by IUPAC as: “*an element whose atom has an incomplete d sub-shell, or which can give rise to cations with an incomplete d sub-shell.*”<sup>39</sup> They actually include most elements from group 3 to 11 of the Mendeleïev table excluding lanthanides and actinides.

Manganese is the third most abundant transition metal after iron and titanium. Around 17 million tons of metal are extracted from the grounds of South Africa, China and Australia mainly. This element exists under several oxidation numbers, mainly (II), (IV) and (VII). The vast majority of manganese is used in alloys such as steel.<sup>40,41</sup>

Aluminum is widely used for its anti-corrosion and mechanical properties in transport manufacture, packaging, construction material, electronics... It is the third most abundant element in the earth’s crust. It can be oxidized to its third oxidation state. More than 50 % of the extraction of aluminum takes place in China.<sup>40,41</sup>

Nickel is used for a wide range of applications such as anticorrosion material, catalyst, coins, battery electrodes and in various alloys. The production is now over 2 million tons per year. The main producers are Philippines and Russia. It is however interesting to notice that France extracts about 7 wt. % of the nickel production thanks to its mines in New Caledonia.<sup>36,40,41</sup> It mainly exists under the oxidation state (II).

Cobalt exhibits chemical properties similar to nickel. It exists under two main oxidation states, (II) and (III). Cobalt is a byproduct of the mining of nickel and copper. Extraction takes place at more than 60 % in the Democratic Republic of Congo. The world production is estimated to be close to 120 000 tons per year.<sup>40–42</sup>

According to data collected in Info Mine<sup>41</sup> the price evolution within 4 years of these 4 transition metals is expressed in **Figure I.9**.

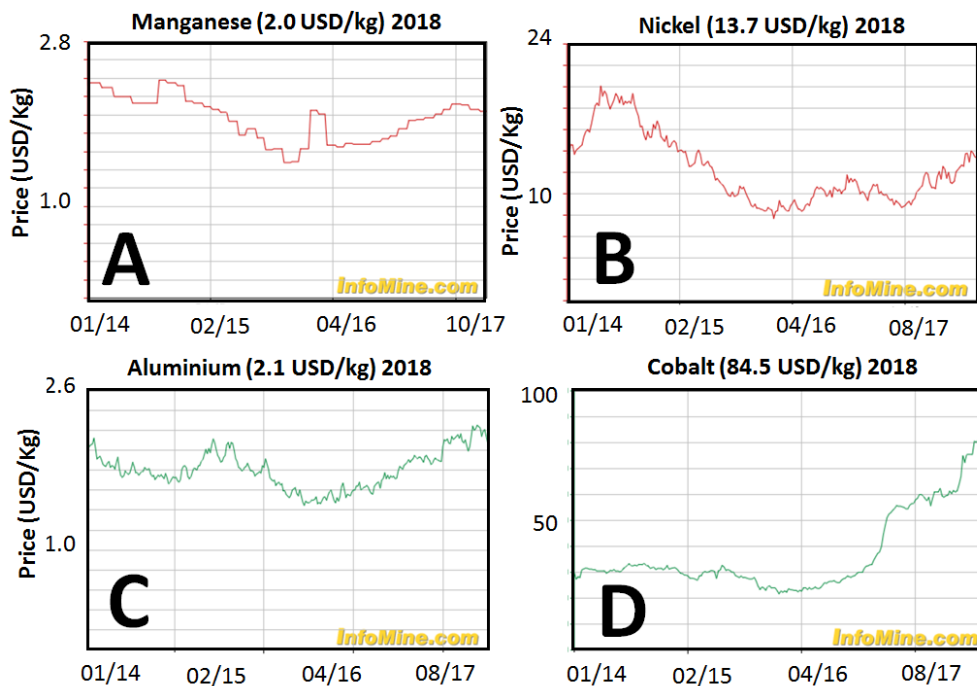


**Figure I.9.** Price of transition metals contained in NiMH battery electrodes from 2014 to 2018 expressed in US dollars per kilogram (USD/kg). The red and green curves express the decreasing or increasing price respectively within 4 years. A: manganese. B: Nickel. C: Aluminium. D: Cobalt.

Manganese and aluminum are sold at prices 7 times lower than that of nickel and over 40 times lower than that of cobalt. Furthermore, the amount of Mn and Al in a NiMH battery is very low which makes them less interesting to recycle. Nickel being the major element in NiMH battery, it needs to be recovered, but no tension is to be seen on the market as its price seems stable within 4 years. This is not the case of cobalt which price has more than tripled from 2014 to 2018.

#### b. Extraction process of cobalt

Extraction techniques of cobalt depend on the nature of the ores processed. Co can be found under the form of arsenide (Morocco), oxide (New Caledonia) or more frequently sulphide in RD Congo. According to several books and reviews from *Hannis et al.*<sup>43</sup> and *Crundwell et al.*<sup>44</sup> the extraction procedure is performed in five main steps. (i) Ores are mined and crushed before being treated (ii) Leaching step is performed using concentrated sulphuric acid at high pressure (4.4 Million Pa)

and temperature (250 °C). (iii) A washing and decanting step leads to metal concentration in the liquid phase. (iv) Copper and iron are precipitated out from the sulfuric medium with ammonia. (v) Nickel and cobalt are finally separated using solvent extraction techniques or electrowinning.

c. Tension towards cobalt mining

Defined as a critical material by the scientific community<sup>35-38</sup>, identified as having a very volatile price,<sup>41</sup> cobalt is the center of numerous geopolitical tensions. Several parameters can explain this phenomenon.

First of all cobalt is used in many battery technologies, including NiMH electrodes and Li-ion cathodes<sup>21</sup>. The needs of cobalt for energy storage are thus dramatically increasing as expressed by the following figure.

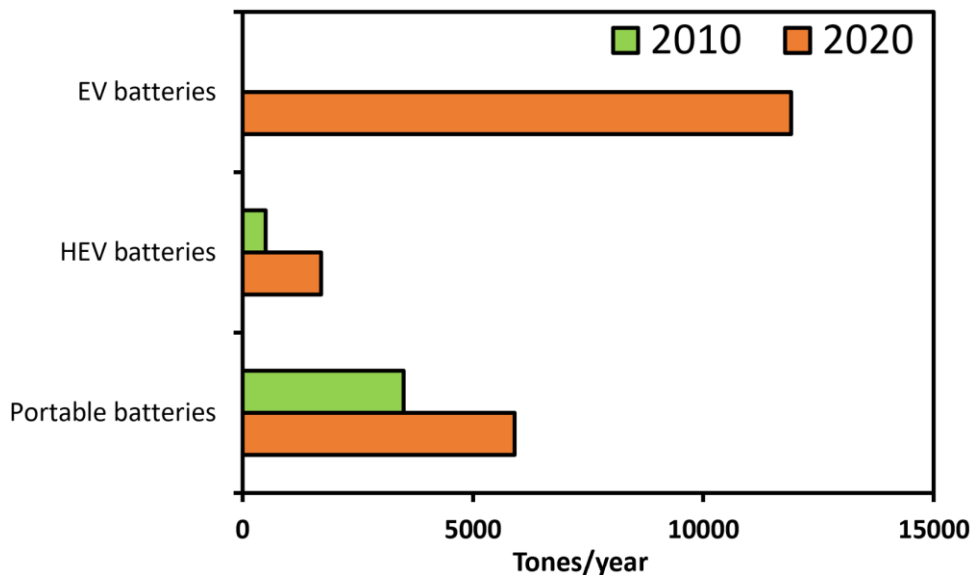


**Figure I.10.** Evolution of the use of cobalt in tons per year for Electric Vehicles (EV), Hybrid Electric Vehicles (HEV) and portable batteries in 2010 and 2020.

As an example, the Li-ion battery developed by the famous brand Tesla weighs 544 kg (data for Model S).<sup>45</sup> This represents 25 wt. % of the car and about 80 kg of cobalt to get 500 km of autonomy.<sup>7</sup> Furthermore, Elon Musk, the CEO from Tesla recently announced to the American channel CNBC that he will be able to reach an autonomy of 800 km with his new battery design (*Millions of Teslas, 500-miles range coming*) by consuming more raw materials.<sup>46</sup> Recently, Nicolas Hulot, the French Minister of the ecological transition declared that he was aiming at the end

of the diesel and oil cars on the market by 2040.<sup>47</sup> Since more than 39 Million cars are used in France,<sup>48</sup> the amount of cobalt needed to power these vehicles is already beyond comprehension.

Second, the mining industry is concentrated in one country. RD Congo is the center of many conflicts and the potential of war in the region strongly affects the supply chain of cobalt *et vice versa*<sup>42</sup> As a result companies are stockpiling huge amounts of metal replacing the *zero stock* and *just in time* strategies by safer and more expensive economic models.<sup>49,50</sup> Furthermore, even if RD Congo is the main country exploiting cobalt, more than 80 % of this metal is refined by China. Indeed, Chinese companies are strongly present in the eastern part of the country creating a new monopoly. As an answer, the Congolese government recently signed a new law in order to increase its mining royalties.<sup>51</sup>

Consequences of such policies lead to a strong volatility on the cobalt price and are already destabilizing the battery industry.

Despite the situation with cobalt, as described by the European commission in 2010,<sup>36</sup> 2014<sup>37</sup> and 2017<sup>38</sup> the most critical metals found in NiMH batteries are the Rare Earth Elements (REE).

### **I.2.3 Rare Earth Elements as highly critical raw materials**

#### **a. Hidden twins**

Rare Earth Elements are defined by IUPAC<sup>39</sup> as the 15 lanthanides elements (lanthanum to lutetium) as well as scandium and yttrium. They can be divided in two main categories: light REE (lanthanum to samarium) and heavy REE (europium to lutetium plus yttrium and scandium).<sup>52</sup> The distinction between light and heavy REE varies from one review to another as no official definition exists. As far as we are concerned, our focus will be on the light Rare Earth Elements lanthanum, cerium, neodymium and praseodymium, present in NiMH batteries. Their names are either linked to the mythology (cerium was named from Ceres, the Roman Goddess of agriculture) or from their discovery. The origin of lanthanum is linked to the Greek etymology of the word “*hidden*” because La was considered to be cerium oxide for a long time. This confusion also existed with Pr/Nd. While

praseodymium stands for the “*the green twin*” because it exhibits a green color in a large range of salts, neodymium can be translated in “*the new twin*” because Pr/Nd were undifferentiated for years.

b. Generalities

These designations are perfectly accurate to define light REE. They are present in relatively high concentrations in the earth crust. Cerium is for example as abundant as copper ranging in a concentration of 48ppm.<sup>53</sup> However, due to their close physicochemical properties, they are extremely difficult to extract and overall to isolate which justifies the denomination *rare* or *hidden*. All of them can be found under the third oxidation state except from cerium that can also be stable after oxidation in the fourth oxidation state. The coordination number for lanthanum(III), cerium(III), praseodymium(III) and neodymium(III) is similar between most light REE and reaches a value of 9 in water.<sup>54</sup> A decrease of the ionic radius of elements from lanthanum to lutetium can be observed. This phenomenon is known as the lanthanide contraction. REE can be characterized by 4f electrons who present a small shielding effect of the nuclear charge. This shielding effect is decreasing within the following series:  $s > p > d > f$ . As a result, the higher the nuclear charge, the higher the attracting effect on electrons and the lower the ionic radius.<sup>55</sup> However the difference in the ionic radius between the larger and the smaller cation, lanthanum and neodymium respectively is of 0.06 Å. This small difference can thus hardly be used for the separation of light REE and justifies the denomination of *twins*. Properties of La, Ce, Nd and Pr are described in **Table I.4**.

Lanthanide (Z)	Electronic configuration	Main oxydation states	Coordination number in water	atomic radius of Ln(III) (pm)
La(57)	[Xe]5d <sup>1</sup> 6s <sup>2</sup>	3	9	103.2
Ce(58)	[Xe]5d <sup>1</sup> 6s <sup>2</sup> 4f <sup>1</sup>	3;4	9	101.0
Pr(59)	[Xe]5d <sup>0</sup> 6s <sup>2</sup> 4f <sup>3</sup>	3	9	99.0
Nd(60)	[Xe]5d <sup>0</sup> 6s <sup>2</sup> 4f <sup>4</sup>	3	9	98.3

**Table I.4.** Generalities of REE used in NiMH batteries.

c. Nature of the ores

The nature and concentration of the main Light REE ores are depicted in

**Figure I.11.** Three main ores can be found for the mining of light REE. Metals are extracted under phosphate, oxide or carbonate salts in monazite, loparite and bastnaesite respectively. Of all three ores, monazite exhibits the highest concentration of REE. It is however composed of yttrium which represents 40 wt. % of the total REE amount. The presence of actinides in monazite is a further huge issue as high amounts of radioactive wastes are produced during the ore processing. This is also the case for loparite. This ore is however lucrative because of the presence of niobium, another critical metal. Bastnaesite contains lower but non-negligible amounts of thorium and uranium.

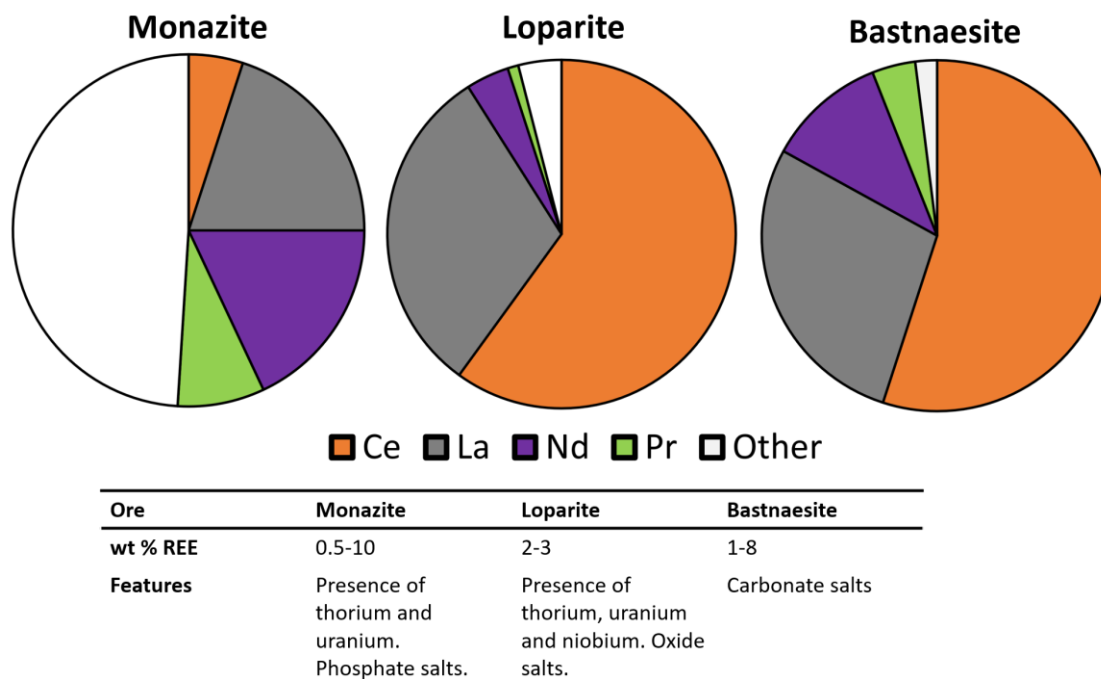


**Figure I.11.** Characteristics of the main light REE ores.<sup>53,56</sup> Pie charts are expressed in weight percentages of the average ores concentration.

Generally, 1 ton of ore only produces between 10 and 80 kg of REE while it is consuming 200 m<sup>3</sup> of water.<sup>7</sup> It is important to point out that the variety of ores is large and some of them can be more concentrated in La, Ce or even Nd. For example, monazite-(Nd) is known to contain 30 wt. % of neodymium.

d. Applications of REE: the balance problem

Close to 30 kg of light REE can be found in a NiMH battery coming from a Toyota Prius HEV.<sup>56</sup> 26 wt. % of the production of lanthanum is devoted to the latter energy storage device. However, La is also used for catalytic converters (44 wt. % of the production) and in specific optical glasses<sup>57</sup> found in microscopes or telescopes. This is not the case for praseodymium and neodymium which are mainly used for magnet production. 53 % in value of the whole REE industry is dedicated to magnets.<sup>56</sup> They can be used to produce energy in wind turbines, to power cars in electric engines or even to store data in hard drives.<sup>58</sup> They can also be found in highly strategic applications such as guided missiles.<sup>7</sup>

Applications and production of light REE found in NiMH batteries are depicted in **Figure I.12** and **Table I.5** respectively.

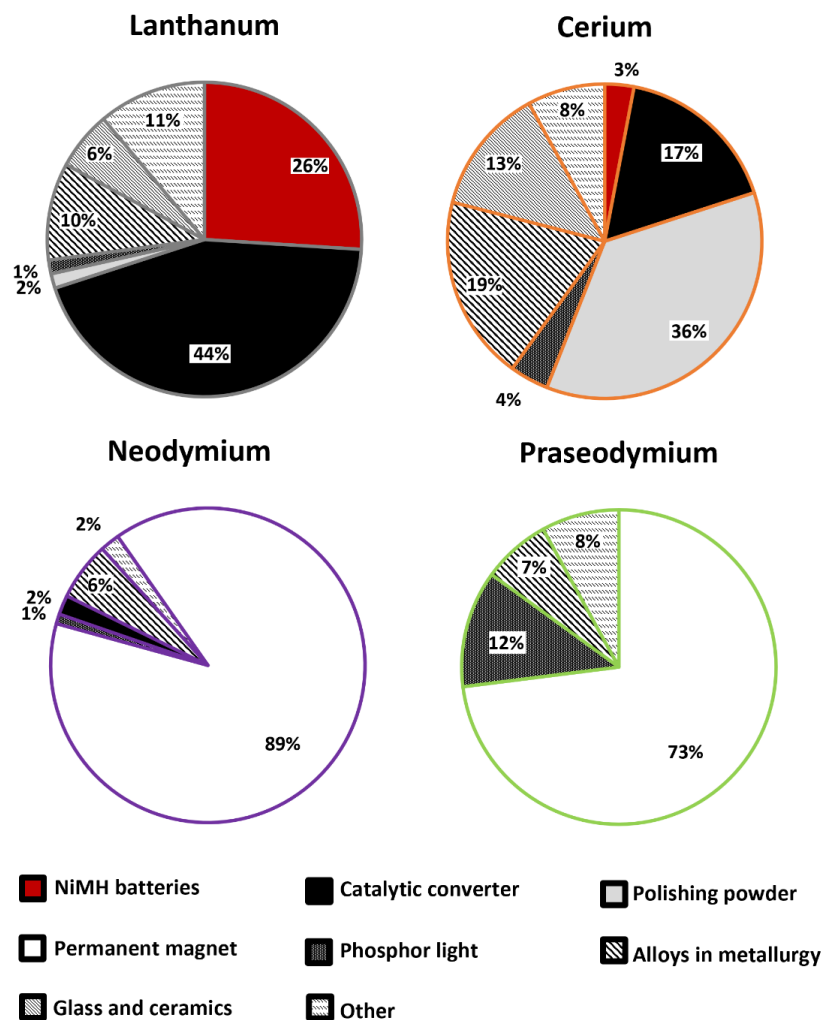


**Figure I.12.** Applications of light REE contained in NiMH batteries. Percentages are expressed in terms of weight production.<sup>59</sup>

Light REE	Mass in a NiMH batteries (kg)	Production 2010-2014 (tones/year)
Lanthanum	10 -15	35 146
Cerium	5 - 10	51 430
Praseodymium	1 - 2	6 500
Neodymium	4 - 7	22 391

**Table I.5.** Applications and production of Light REE contained in NiMH batteries.<sup>56,58</sup>

Cerium is mainly used as a polishing compound as Cerium(IV) oxide ( $\text{CeO}_2$ ).<sup>60</sup> It is the most produced Light REE in mass with more than 51 000 tons of metal extracted each year.

However, this important production of cerium is not only linked to the demand but also to the concentration of this metal in ores. Similarly to cobalt produced as a byproduct from nickel ores, neodymium is extracted in ores containing high amounts of cerium. Briefly, the more neodymium is needed, the more cerium needs to be produced. This creates an oversupply in cerium. This phenomenon was firstly described as the balance problem by *Falconnet* from the Rhone Poulenc industry in 1985 in his review.<sup>61</sup> It was updated in 2018 by *Binnemans et al.*<sup>56</sup>

China owns about 50 % of the known resources of REE. It is followed by Russia (17 %). USA and Australia possess 4 and 3 % respectively of these critical metals. However, significant reserves still need to be discovered. A Japanese research group reported (*Kato, Iwamori et al., Nature geoscience 2011*) that concentrated Rare Earth ores were present in the deep-sea Pacific Ocean.

Despite this discovery, the production is nowadays the result of a huge monopoly.

#### e. Tension surrounding the REE production

From 1965 until the end of the XX<sup>th</sup> century, REE were mainly extracted from Bastnaesite in the USA. This extraction took place in the Mountain Pass mine (California) exploited by the company Molycorp. The mining process was creating significant quantities of acidic waters, carbon dioxide emissions, chemical pollution and overall radioactive wastes. In the 90s, after releasing its wastes in the



desert and according to new environmental laws, Molycorp had to pay 1.4 Million \$ fine and to adjust its process. As a result, it increased the cost of extraction of REE. At the same time, the Chinese government opened new mining sites, mainly in Baotou (Inner Mongolia).<sup>7</sup> According to permissive regulations, they started to extract as much REE as the USA in 1993. Ten years later, the production in China tripled with cheaper extracting techniques. As a consequence, the Mountain pass mine closed. From the beginning of the XXI<sup>th</sup> century until now, China is dominating the market of lanthanides. Baotou is now considered as the capital of REE in the world.

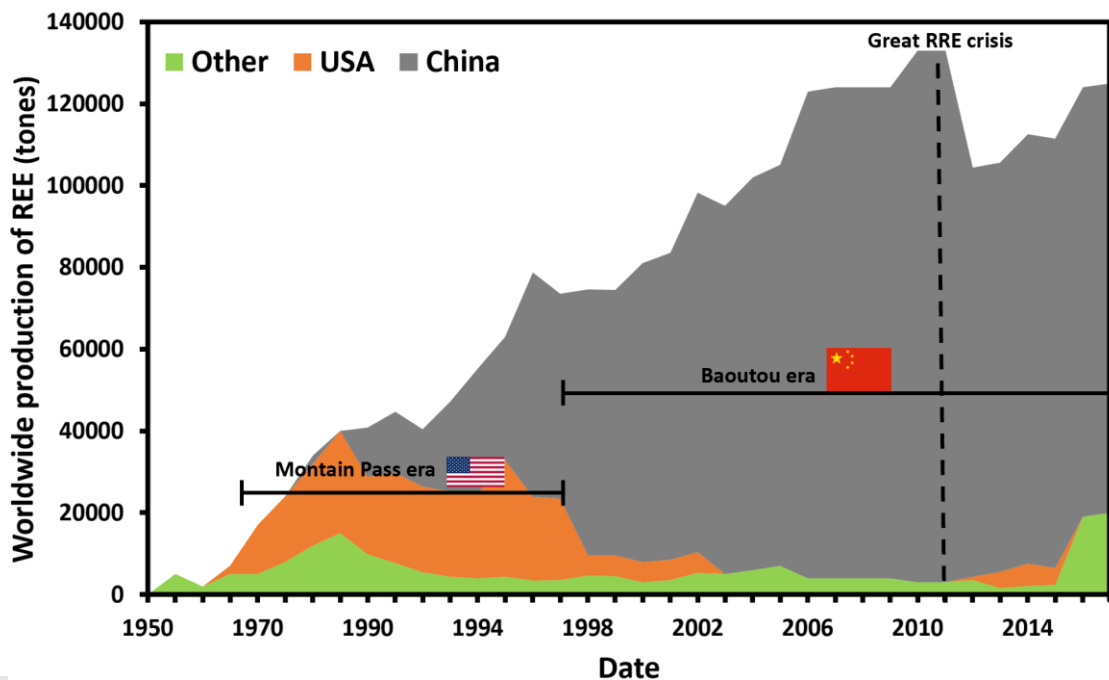


**Figure I.13.** Worldwide production of REE in tons from 1950 to 2017.<sup>62,63</sup> The production of such Chinese REE was close to 98 % of the total production in 2011. All data regarding their production are available in the United States Geological Survey (USGS) data sheets.<sup>62</sup>

In 2011, following a geopolitical conflict between China and Japan, exportation of REE was highly limited. As all developed countries are fully dependent of the Middle Kingdom production, the prices of all REE started to drastically increase. From one day to another, Europe, USA Japan and Russia understood that China had a tremendous power on the manufacturing of numerous strategical application.

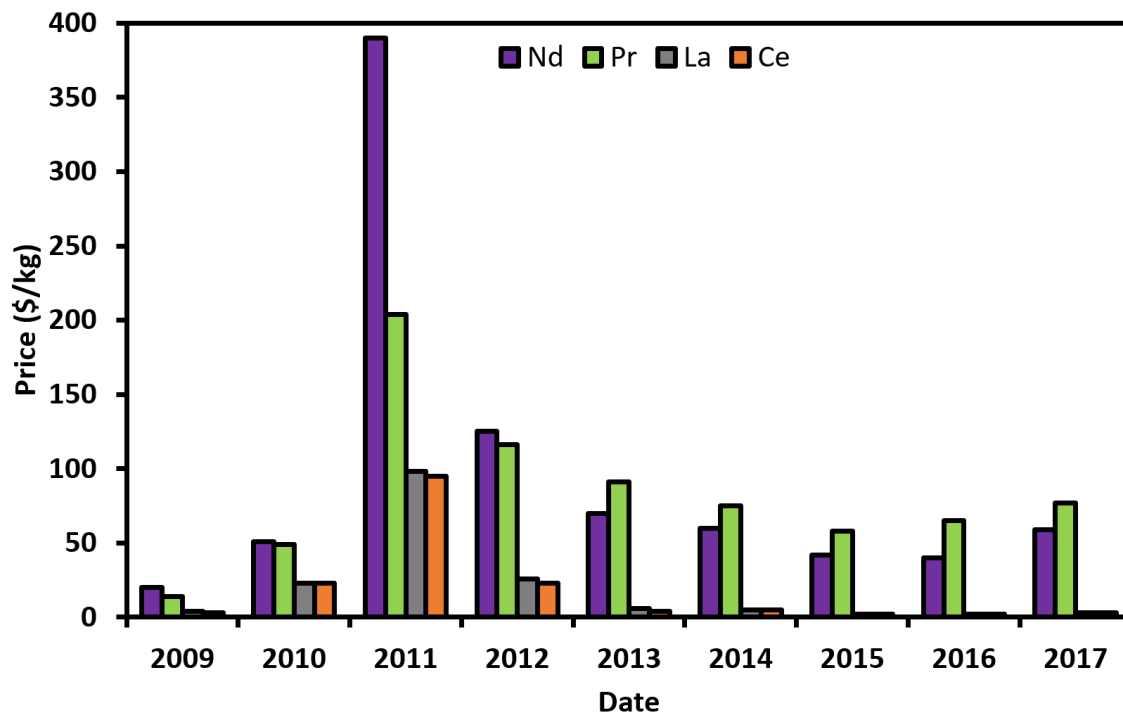


**Figure I.14.** Evolution of REE oxide prices from 2009 to 2017.<sup>41,62</sup>

As a result, USA re-opened the Mountain Pass mine in 2012. Quickly, the price of REE decreased and Molycorp had to close it again two years later. Only Russia and Australia are nowadays considering large scale REE mining.<sup>7</sup> In 2017, the prices of the two major REE found in NiMH batteries namely lanthanum and cerium were close to 3 \$/kg and are similar to the prices of manganese and aluminum. Even if neodymium and praseodymium are found in lower amounts in  $AB_3$  negative electrodes, they exhibit prices of 59 and 77 \$/kg respectively.

f. A polluting extraction process

Details on mining process for REE in China is difficult to obtain. Nevertheless an approximate flow sheet of the extraction of bastnaesite in Baotou was given by *Simoni et al.*<sup>64</sup>

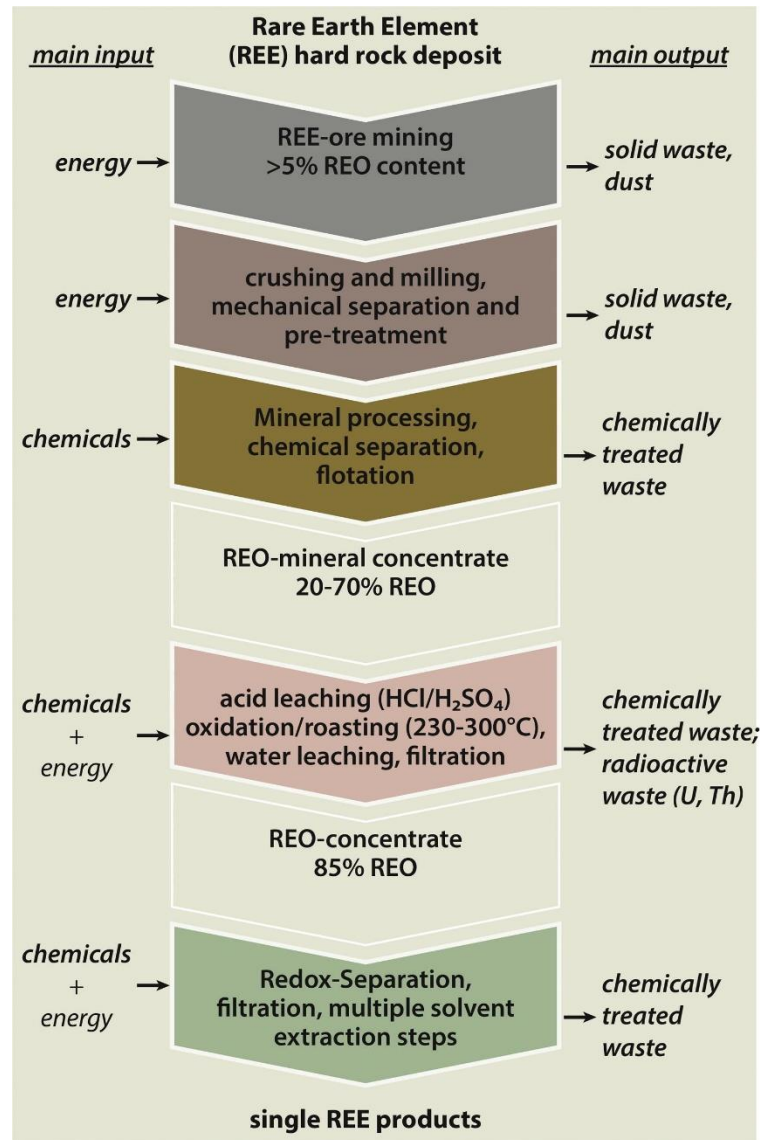


**Figure I.15.** Flow sheet of the extraction of light REE from Baotou mines in China.<sup>64</sup>

The ores are firstly crushed and grinded in order to obtain a powder. Some minor transition metals and minerals are separated by flotation and chemical treatment.<sup>65</sup> A concentrated REE powder is then obtained. In order to remove actinides, REE are leached in concentrated sulfuric acid and roasted at temperature in the range 230 to 300 °C to produce lanthanide sulphates.<sup>66,67</sup> The latter are leached in HCl and converted to lanthanide chlorides.<sup>64</sup> The last step consists in several extraction steps using solvent extraction. This step isolates all REE under the form of pure oxides. A common extractant is di-(2-ethylhexyl) phosphoric acid (HDEHP) also named (HA) dissolved in kerosene.<sup>68</sup> The extraction mechanism is linked to a cation exchange and is depicted in the following equation:



A large range of phosphorus based chelating agents named Cyanex<sup>69</sup> has also been developed by Cytec (Solvay). After dissolution in an organic solvent, these extracting systems were shown to isolate several REE. Many research groups have been focusing on extraction of REE by Cyanex 272,<sup>70</sup> 301,<sup>71-73</sup> 302,<sup>73,74</sup> 921<sup>75</sup> and 923<sup>71</sup> diluted in kerosene,<sup>75</sup> toluene,<sup>70</sup> xylene<sup>71</sup> and heptane.<sup>50,72,74,75</sup>

After this liquid-liquid extraction step, REE are calcined to obtain pure oxides. If needed, lanthanides can be reduced to the metallic state by various reducing agents or by electrowinning.<sup>68</sup>

An accurate methodology to measure the environmental impact of the extraction of REE is the Life Cycle Assessment (LCA) methodology. Several LCA studies were performed regarding the present flow sheet.<sup>65-67,76</sup>

It has been shown that for each ton of REE extracted, 2 tons of acid should be used.<sup>68</sup> Acid roasting has thus been described by *Vahidi et al.* as the most adverse step of the process regarding pollution and healthcare.<sup>67</sup> The leaching step is thus commonly designed as the most polluting in metal LCA analysis.<sup>65,77,78</sup>

However, it has been reported that a very low waste treatment policy was applied in Inner Mongolia. Retention ponds containing high amounts of uranium, thorium, acid, extractant and organic solvent can be found near numerous villages. Many cases of cancers were spotted.<sup>7,79</sup> A 2018 LCA analysis (*Arshi, Zhao et al. ACS Sustainable Chemistry*)<sup>65</sup> studied the impact of the extraction of cerium, lanthanum, neodymium and praseodymium on environment but also on human health. They reported that the more concentrated a metal in the ore, the lower the impact. Focusing on neodymium, 1 kg of Nd could be responsible of  $4.4 \cdot 10^{-6}$  cancers. Considering the production of Nd in Baotou, this represents more than 100 cancers per year for the mining of one metal. Yet, this value is most probably under estimated, because of the little access scientists have on the facilities and waste management protocols.<sup>65</sup> They also reported the production of 89 kg equivalent of CO<sub>2</sub> regarding global warming per kilogram of extracted neodymium.

The offshore company Adwen, gives precise data on the characteristic of its offshore windturbines.<sup>80</sup> 350 kg of REE and 150 kg of neodymium can be found in its 8MW model. A Toyota Prius model can contain up to 1.5 kg of REE.<sup>52</sup> However they are considered as highly sustainable devices to produce and store energy respectively. After studying the mining of REE, we can assess that carbon dioxide emissions, radioactive wastes and various pollutions are not at all suppressed with those devices. We are simply facing a delocalization of the pollution from developed country to China. Guillaume Pitron, French journalist and expert in rare metals, described this phenomenon as the “*largest green washing operation in history*”.<sup>7</sup>

Since the great REE crisis in 2011, finding solutions towards greener and safer process regarding the Rare Earth Industry has become the focus of many research groups and governments worldwide. While the recycling rate of light REE was below 1 % in 2010,<sup>36,52</sup> this value has now been upgraded to 3 % (European Commission report on critical raw materials, 2017).<sup>38</sup>

Recycling processes must be designed in a more sustainable manner. Furthermore, because liquid-liquid extraction highly impacts the toxicity of the procedure due to VOCs, toxic and flammable organic solvents need to be replaced by safer and greener molecules.

## I.3 Ionic Liquids as greener solvents

### I.3.1 Definition

In 1996, *Anastas et al.* described green chemistry as the ability to reduce human and environmental risks during chemical processes.<sup>81</sup> Later on, 12 principles were presented to fulfill this goal.<sup>82</sup> Among them, using catalysis, reducing wastes, energy consumption and hazardous compounds. Designing safer solvents was also described as a priority to reach sustainable and environmental friendly chemical processes. Ionic Liquids (ILs) have been presented as promising candidates for the replacement of hazardous solvents, both in academic and industrial activities.<sup>83</sup>

ILs can be defined as salts that melt below 100 °C forming liquid phases composed only with cations and anions. Some ILs are liquid under 25 °C and are called room temperature ionic liquids (RTILs).

Historically, the field of ionic liquids started after Paul Walden's observations of ethylammonium nitrate in 1914.<sup>84</sup> This salt presents a melting point of 11 °C and was investigated to be a substitute to nitroglycerin in explosives.<sup>85</sup> Moving away from these hazardous applications, ionic liquids started becoming popular in the late 90s. Ever since, the study and use of ILs in a large range of applications has grown tremendously.

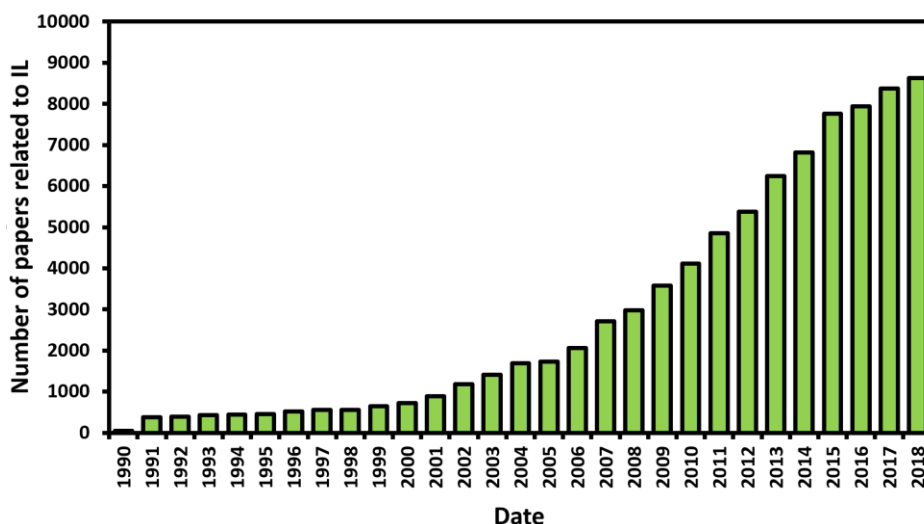


**Figure I.16.** Evolution of the interest of ionic liquids in scientific papers from 1990 to 2018.<sup>86</sup>

### I.3.2 Structure

Contrary to molten salts, ionic liquids present a low charge density and an asymmetric geometry. These characteristics are responsible for the decrease in their melting point compared to molten salts.<sup>87</sup> The cation is usually an organic compound. It can be a cyclic molecule based on nitrogen, namely, imidazolium  $[C_nC_nIM]^+$ , pyrrolidinium  $[C_nC_nPyrr]^+$ , pyridinium  $[C_nC_nPYR]^+$  or a non-cyclic one based on quaternary nitrogen or phosphorus with ammonium  $[N_{nnnn}]^+$ , phosphonium  $[P_{nnnn}]^+$  and sulfonium  $[S_{nnn}]^+$  cations respectively. The subscript “n” represents the number of carbons, i.e. the length of the alkyl chain.

The anion can be a simple inorganic ion such as chloride  $[Cl]^-$ , bromide  $[Br]^-$ , nitrate  $[NO_3]^-$ , hydrogenosulfate  $[HSO_4]^-$  or even dicyanamide  $[DCA]^-$ . Perfluorinated anions such as tetrafluoroborate  $[BF_4]^-$  and hexafluorophosphate  $[PF_6]^-$  have widely been studied for their remarkable hydrophobic properties. Due to some chemical stability issues related to the possible formation of HF when contacted with water<sup>88</sup> they are now often replaced by more stable organic ions such as bis(trifluoromethylsulfonyl)imide  $[NTf_2]^-$ .

The most popular ionic liquid structures are depicted in **Figure I.17**.

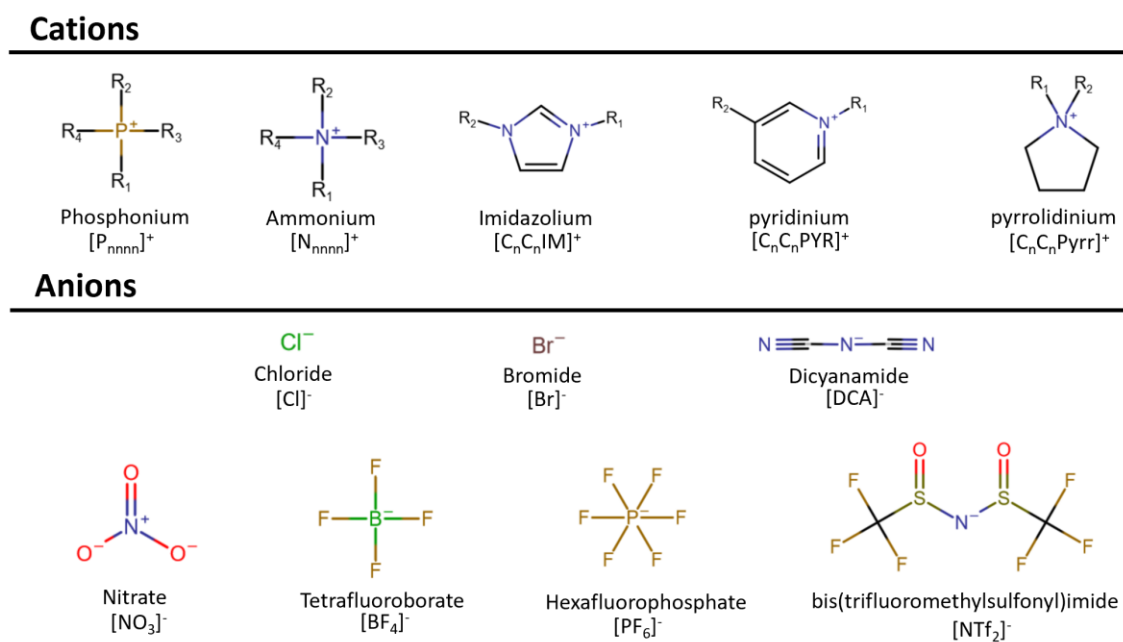


**Figure I.17.** Popular structures of cations and anions forming ionic liquids.

The ability to easily change the alkyl length of cations as well as the possibility to combine various kinds of ions together allow researchers to synthesize and study a nearly unlimited combination of new solvents. Each IL will then have the ability to present unique physicochemical characteristics in order to be used for a large range of specific applications. This high tuneability of ILs allows them to be presented as “designer solvents”.<sup>89</sup>

### I.3.3 Properties and application

Ionic liquids usually appear as colorless or slightly yellow liquids. Their viscosity generally ranges from 30 to 2000 mPa.s.<sup>90</sup> For comparison, viscosity of water is of 1 mPa.s at 20 °C while honey presents a viscosity between 5000 and 10000 mPa.s. This higher viscosity compared to organic solvent is mainly due to the presence of electrostatic and Van der Waals interactions. However, this can be overcome by decreasing the length of alkyl chain, by increasing the temperature or by mixing IL with molecular solvents. They are defined in the literature as green solvents thanks to their potential to replace volatile organic solvents (VOCs). They usually present a low flammability compared to VOCs and are mostly non-volatile.

#### a. Non-hazardous and safe solvents?

Toxicity of ILs has been characterized and reviewed in numerous articles recently.<sup>91–93</sup> Most of them report a high ability of fluorinated anions such as  $[\text{BF}_4]^-$  and  $[\text{PF}_6]^-$  to suffer from hydrolysis leading to the formation of hazardous hydrofluoric acid.<sup>88</sup> This issue has now been overcome thanks to the synthesis of bis(trifluoromethylsulfonyl)imide  $[\text{NTf}_2]^-$ . This fluorinated anion is known to exhibit strong and stable carbon-fluoride bonds.<sup>94</sup> The cation can also have a toxicological hazard potential. It has been shown that toxicity was increasing with the length of the alkyl chain.<sup>93</sup> However, this chain length effect could be decreased by adding polar functional groups.<sup>92</sup>

Ionic liquids were also described as non-flammable and non-volatile for over a decade. However, some papers highlighted that ILs could be evaporated before degradation.<sup>95,96</sup> Even if their volatility is far lower from those observed in VOCs, they should now be defined as solvents with low vapor pressure. In the same manner, most of those solvents are excellent flame retardant. Most of them are



stable until 300 °C where they usually degrade (deteriorate).<sup>95</sup> However some ILs can be used as combustible.<sup>97</sup> *Zhang et al.* even reviewed ILs as potential fuel for rockets.<sup>98</sup> In a nutshell, risks for environment and humans are generally decreased using ILs compared to VOCs. However, those properties can be very different from one structure to another.

#### b. Price

The question of the price of ILs is a strong issue as they can be 5 to 20 times more expensive than molecular solvents.<sup>83</sup> One should take into account though that they are still produced in small batch reactors. *Chen and co-workers (2014)*<sup>99</sup> highlighted that a large industrial scale synthesis could bring the price of [C<sub>1</sub>C<sub>1</sub>im][HSO<sub>4</sub>] to less than 5.88 \$.kg<sup>-1</sup>. Moreover, several papers showed that ionic liquids could be recycled and reused in several steps which would highly decrease the overall cost and environmental impact of the process.<sup>83,100</sup> In a nutshell, large scaled production of more efficient ionic liquids could easily bring these promising solvents to viable industrial process. This statement is supported by the wide range of applications in which ILs are involved.

#### c. A large range of applications

By definition, an ionic liquid is only composed of ions and thus presents a good ion conductivity.<sup>94</sup> It has been reported that ILs could also form large ion neutral pairs through aggregates.<sup>101</sup> This phenomenon can be responsible for the decrease in conductivity since not all the ions are available for charge transportation. Thanks to the Walden rule reported in 1900<sup>84</sup>, the ability of a salt to form clusters can be analysed empirically with the following equation:

$$\Lambda \times \eta = \text{constant} \quad (6)$$

where  $\eta$  represents the viscosity of the system and  $\Lambda$  stands for the molar conductivity of a compound.  $\Lambda = \sigma M \rho^{-1}$  where,  $\sigma$  is the conductivity,  $M$  is the molecular weight and  $\rho$  represents the density.

The ability to conduct ions combined with a good electrochemical stability<sup>94</sup> make ILs suitable to be applied in electrochemical devices as demonstrated by several reviews.<sup>94,102,103</sup> It has been shown that ILs could be used as electrolytes to

transport electroactive ions from one electrode to another during charge and discharge in Li-ion<sup>104,105</sup> and more recently Na-ion batteries.<sup>101,106</sup> Furthermore, those liquid salts were also used as gel or liquid electrolytes in a large range of electrochemical devices converting energy into electricity such as fuel cells<sup>107</sup> (conversion of hydrogen), solar cells<sup>108,109</sup> (conversion of UV-light) or thermocells<sup>110</sup> (conversion of a difference of temperature).

Molten salts were mainly used as an electroplating electrolyte thanks to their high thermal and electrochemical stability as well as for their high conductivity.<sup>111,112</sup> Because Room Temperature Ionic Liquids present similar characteristics, and because they avoid the experimenter to heat a system to several hundred degrees, they are of great interest for the electrodeposition of metals. Condensed a few years ago in a review, (*Abbott et al, Annu Rev Matter Res, 2013*),<sup>113</sup> and in a book (*Endres et al. Electrodeposition from ionic liquids, 2008*)<sup>114</sup> electroplating of transition metals<sup>115</sup> and more recently of REE<sup>88,116–118</sup> was thus highlighted in the literature.

Catalysis was one of the first application of ionic liquids and was early reviewed (*Welton et al, Coord Chem Rev, 2004*).<sup>119</sup> The tuneability of these solvents is a strong asset in the optimization of many parameters influencing chemical synthesis and catalysis such as polarity and miscibility with molecular solvents and gases. Drastic changes in the IL properties were reported in mixed IL/Molecular systems. As a result, many research groups reported great solvent properties for IL used in additions,<sup>120</sup> substitutions<sup>121</sup> and acid/base catalyzed reactions.<sup>122</sup>

Finally, one of the main applications of ionic liquids is related to extraction and separation processes. The tuneability of the polarity and of the functional groups in ILs is creating remarkable interactions with water and with the compound that needs to be extracted respectively. Furthermore, ILs are recognized as performant solubilization solvents and are thus efficient to dissolve inorganic extractants.<sup>123</sup> As a result, ionic liquids were widely studied for the separation of gases,<sup>124,125</sup> organic acids, cyclic molecules and alcohols,<sup>123,126,127</sup> proteins and various biomolecules<sup>128–132</sup> and metals.<sup>133–136</sup> The latter represents the main interest of this work as it will be studied for the recycling of metals present in NiMH batteries.

## I.4 Recycling NiMH batteries

### I.4.1 Overview

#### a. Circular economy

In order to reduce the environmental impact of NiMH batteries several strategies can be applied: Reuse, substitute and recycle. These methods are part of the circular economy model and are briefly detailed below:

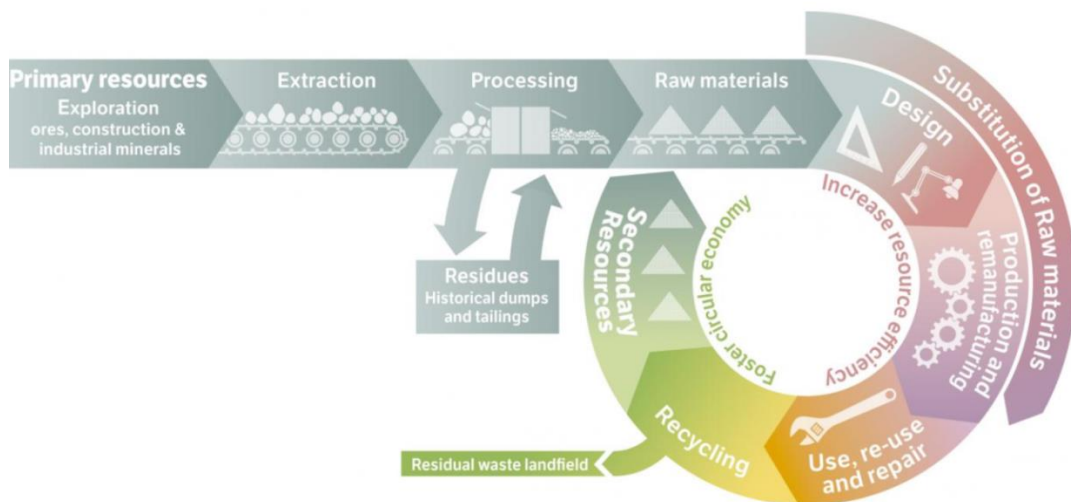


**Figure I.18.** Circular economy defined by ERAMIN project.<sup>137</sup>

- Reuse of batteries

The aim of this technique is to build a methodology to characterize batteries after their first utilization. In a second step, function of the performance of the degraded batteries, suitable new applications are investigated. This concept has been applied to Li-ion batteries from EV cars<sup>138</sup> but also to NiMH secondary batteries used in their end of life for stationary applications.<sup>139,140</sup> The main advantage of this strategy is that no chemicals are used and no wastes are generated.

- Substitution of polluting metals by more sustainable elements

Some research groups have been focusing on the replacement of REE for hydrogen storage by other less rare and valuable metals. Numerous papers converge towards magnesium-based alloys because of their high hydrogen storage potential.<sup>14</sup> Promising results have been reported for Mg-Ni alloys<sup>141,142</sup> as well as Mg-Ti

alloys.<sup>143</sup> However the strong stability of the hydride bonding hinders the electrode to provide a capacity higher than 8mAh/g.<sup>144</sup>

- Recycling of metals

Recycling can be defined as the reprocessing of valuable materials from wastes reinjecting them in a manufacture process or in a supply chain.<sup>145</sup> In the case of NiMH batteries, it is a process allowing the recovery of plastics, the external cage but mainly of valuable metals from the electrodes. Taking into account the amount of elements, the price and the environmental impact of metals in NiMH electrodes, cobalt, nickel and REE need to be recovered from wastes. With the increasing amount of end of life devices, electronic wastes are now considered as secondary resources. This denomination is motivated by the concentration of rare metals present in these wastes that is as high or even higher than those found in natural ores.<sup>56,145</sup> This strategy will be the main concern of the present work and will be detailed in the following section.

a. French recycling industries

The recycling industry is already a mature technology regarding primary batteries and acid-Pb secondary devices.

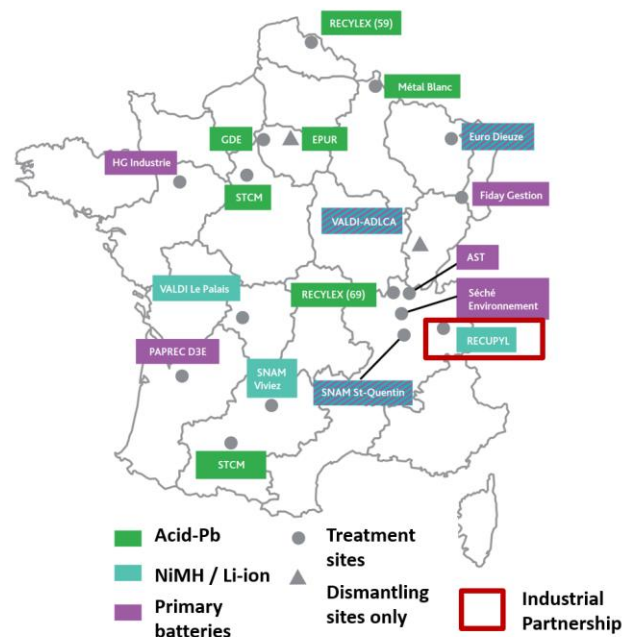


**Figure I.19.** Primary and secondary battery recycling centers in France.

However, NiMH and Li-ion are recent wastes on an industrial scale and need innovative processes. Few companies are starting to recover metals from devices mainly lithium, nickel, cobalt and REE. On the national level, France possesses a dozen of recycling centers spread all over the territory.<sup>146</sup>

To the best of our knowledge, the largest NiMH recycling center is led by SNAM. In 2010 it passed an agreement with Toyota to recycle batteries from the Prius model. More recently, the car manufacturer PSA Peugeot Citroën signed a contract with SNAM for the recycling of metals from NiMH batteries powering the Peugeot 3008 HY4 model.<sup>147</sup> Recupyl<sup>®</sup> is a company located near Grenoble in the Auvergne-Rhone-Alpes region, France. It is currently dismantling and recycling Li-ion batteries by recovering nickel, cobalt and lithium salts. This recycler was, at the beginning of the project, interested in the recovery of valuable metal from NiMH batteries.

b. Flow sheet

The following flowsheet highlights different steps followed by the industry to recover valuable metals from NiMH batteries.

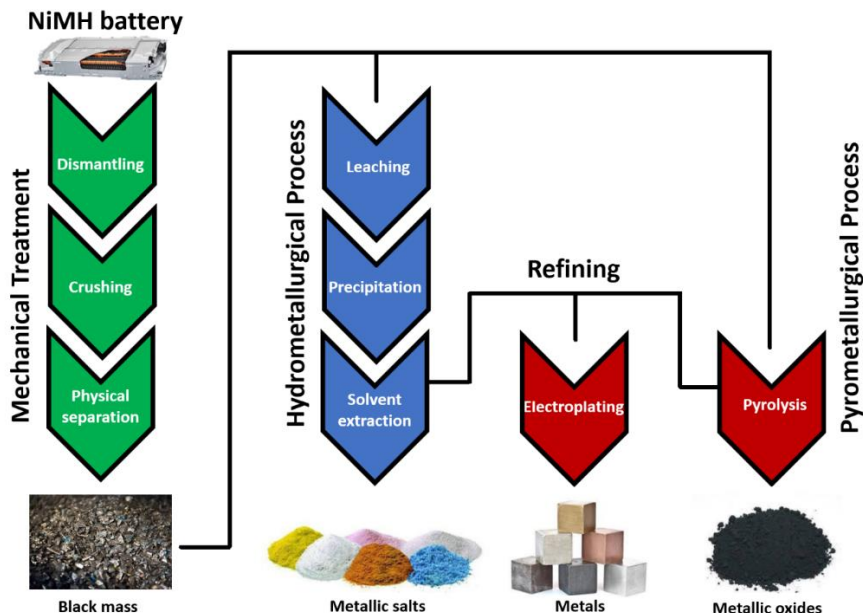


**Figure I.20.** General flowsheet for the recycling of metals from NiMH batteries.

Metal recycling from NiMH batteries is carried out in four main stages.<sup>148</sup> (i) Mechanical separation is used to dismantle the battery and removal of its outer shell. In a second step, the electrochemical storage device is crushed. Physical separation is then applied to the grinded battery. Flotations techniques are usually used to isolate plastics from metallic parts based on their density differences. Using the same principle, cyclonic separation, a vortex separation induced by a stream of gas, can also be used. At the end of the mechanical treatment, a thin powder composed solely of metals and carbon is obtained. Because of its dark color, this material is commonly named as the black mass (BM). (ii) The role of the recycler is then to separate metals from this intermetallic compound. Hydrometallurgy techniques are firstly used to dissolve the metals in an aqueous phase. This step is known as the leaching step and allows the recycler to obtain a concentrated solution of metallic elements. By changing the pH of the solution, selective precipitation of some metals can induce a preliminary separation. The remaining metallic species are then separated by solvent extraction. Similarly to the process of extraction of REE detailed in **part I.2.3**, a complexing agent has to be dissolved in an organic solvent to selectively extract metals. This process uses significant amounts of Volatile Organic Compounds (VOCs) known for their high toxicity and flammability. (iii) Pyrometallurgical process can be used to form oxides or metals by calcining the black mass. Even if this step does not use large amounts of chemicals, calcination is consuming high amounts of energy and allows poor separation of metallic species. In a last step, a (iv) refining process can be performed. After using pyro and/or hydro-metallurgical techniques, all elements are reduced to metallic species using a reducing agent or on a more frequent basis electroplating. It is important to note that this last step is rarely carried out by recycling companies as those processes are mastered by refining industries.<sup>21,145,148,149</sup>

## I.4.2 Leaching and precipitation

### a. Definition

#### *Leaching*

The term “leaching step” used in this work will stand for the dissolution of any metallic species in an ionic form. In other words, leaching allows the oxidation of a metal. This is a key step in hydrometallurgy, a technique working by definition with aqueous solutions. The nature, concentration and temperature of the leaching solution can change with the type of ores or wastes that need to be treated. In a hydrometallurgical process, a strong acid is often used as a leaching agent for two main reasons: (i) Most metallic species are susceptible to undergo hydrolysis at neutral pH and need an acidic media to exist as a free cation. (ii) Strong acids are able to fully dissociate, even at high concentrations, allowing the proton to be reduced to hydrogen while the metal is oxidized. This can be expressed by the following equations according to the Brønsted-Lowry theory.



Where HA, H<sup>+</sup> and A<sup>-</sup> represent the associated acid, the proton and the conjugated base respectively. *Ka* is the acidity constant and describes the strength of an acid as well as its ability to dissociate. When a metal reacts with a proton from the acid, provided the metal redox potential is below that of H<sup>+</sup>, the following equation occurs.



Where *M* represents the metal that needs to be oxidized. *n* is the oxidation state of the metal after leaching. Subscripts (sol), (s) and (g) stand for solution, solid and gas phases.

#### *Precipitation*

Precipitation corresponds to the formation of heterogeneous solid particles in a saturated solution of metal ion. In hydrometallurgy, precipitation stands for the association of a metal *M* by a ligand *L* leading to an insoluble salt *ML* in an

aqueous or an organic solution and is described by the following equations. In aqueous solutions,  $L$  is often the hydroxide anion  $\text{OH}^-$  but may also be another anion such as  $\text{SO}_4^{2-}$ ,  $\text{NO}_3^-$ ,  $\text{Cl}^-$ , ...).



Where  $K_s$  represents the solubility product of the metal. This constant is function of the nature of the solution, the temperature and the concentrations. The stepwise complexation constant can be written as:

$$K_s = \frac{a_{ML}}{a_{M(sol)} \times a_{L(sol)}} \approx \frac{1}{[M]_{(sol)} \times [L]_{(sol)}} \quad (10)$$

Where  $a$  stands for the activity of species.

Selective precipitation in metal separation processes will thus take into account the difference of solubility of one metal species with another species in solution to perform a full precipitation of valuable elements or of impurities.

#### b. Application to NiMH batteries

Selective precipitation of REE has been reported during the last decades for the mining technology.<sup>150,151</sup> This step relies on the difference of solubility of REE and transition metal (TM) in a sulphate media. Briefly, ores can be leached in sulphuric acid.  $\text{H}_2\text{SO}_4$  present two acidities,  $\text{pK}_{a1}$  (-3.0) and  $\text{pK}_{a2}$  (1.9) leading to the formation of  $\text{HSO}_4^-$  and  $\text{SO}_4^{2-}$  respectively. The pH of the solution is then adjusted with a base such as sodium hydroxide (NaOH) or potassium hydroxide (KOH) until a complete precipitation of REE while TM remain in solution as charged ions. The solubility of such rare earth sodium sulphate salts in water has been reported to be below  $7.10^{-4} \text{ mol.L}^{-1}$  in water at  $20^\circ\text{C}$ .<sup>152</sup> This is thus a simple and efficient method to obtain pure rare earth elements.

According to this mining technology, some research groups tried to apply the same principle for the recovery of REE from NiMH batteries. Pietrelli et al. was the first to report the possibility of leaching and precipitating lanthanides from a real NiMH battery in 2002.<sup>153</sup> However only 70 mol % of REE were recovered because of an



inefficient leaching step. This process was optimized and adapted to NiCd batteries in 2005.<sup>154</sup> From then, this work was undertaken by numerous researchers.<sup>155–158</sup>

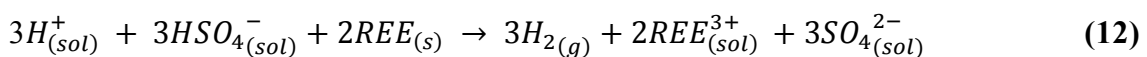
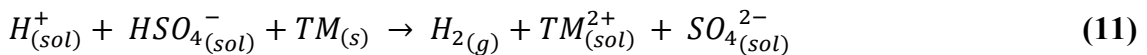
Publications	[H <sub>2</sub> SO <sub>4</sub> ] (mol.L <sup>-1</sup> )	Temperature (°C)	pH precipitation	Yield REE (mol %)
<i>Pietrelli et al. 2002</i> <sup>153</sup>	1.5	20	1.5	70
<i>Rodrigues et al. 2009</i> <sup>157</sup>	2.5	30	2.5	50
<i>Bertuol et al. 2009</i> <sup>155</sup>	6	20	1	98
<i>Innocenzi and Veglio 2011</i> <sup>159</sup>	2	80	1.7	99
<i>Porvali et al. 2017</i> <sup>156</sup>	2	30	2	99

**Table I.6.** Experimental conditions for leaching and precipitation REE from NiMH batteries.

The previous table highlights the heterogeneity of the experimental setup used to achieve a full precipitation of lanthanides. No consensus on the sulphuric acid concentration (1.5 to 6 mol.L<sup>-1</sup>), the temperature (80 °C) and the optimal pH for precipitation was found after 15 years of research. This is most probably linked to the nature, size, model and dismantling process of the NiMH batteries used in these studies that provided such different results.

Unlike what Pietrelli et al.<sup>154</sup> claimed, the precipitate is not a REE sulphate salt but an alkali REE sulphate salt where potassium or sodium, depending on the nature of the base used (NaOH or KOH), is included in the lattice of the salt. This phenomenon has been characterized, reported and reviewed recently by Porvali et al.<sup>156</sup> The mechanism of leaching and precipitation of metals from NiMH batteries is thus depicted in the following equations:

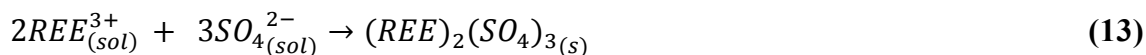
*Leaching:*



During the leaching, the metals are oxidized at the oxidation number (II) and (III) for transition metals and rare earth elements present in NiMH batteries. The proton of the acid is reduced, leading to the formation of hydrogen gas.

*Precipitation:*

Precipitation then occurs when sulphate and REE ions are present in the aqueous solution. Because sulfuric acid is a diacid,  $SO_4^{2-}$  is predominant when the pH is higher than 2. Due to the low solubility of lanthanide sulphate salts, the following reactions occur.



The sulphate rare earth complex  $(REE)_2(SO_4)_3$  formed has been described as highly soluble in water.<sup>152,160</sup> The addition of an alkali metal as well as the increase of the pH allow the formation of a  $Na(REE)(SO_4)_2$  salt.

Relying on previous studies, the optimization of the leaching and precipitation of REE from a real NiMH battery will thus be performed in this PhD and will be described in Chapter II.

c. Leaching in ionic liquids

Leaching using ionic liquids was recently reported and reviewed<sup>148</sup> in the literature to avoid or limit the use of corrosive acids, but also to demonstrate the ability of ILs to oxidize and solubilize a large range of metals. Even if, up to our knowledge, no leaching of NiMH batteries was performed in ionic liquids, those unconventional solvents were used for the dissolution of metallic and oxide ores of gold and silver in the work of Whitehead and co-workers in 2004.<sup>161</sup> Those two metals are commercially extracted by cyanide salts in alkaline solution which present a high toxicity and significant environmental hazard. In this paper, for the first time, an IL, namely 1-butyl-3-methylimidazolium hydrogenosulphate ( $[C_1C_4IM][HSO_4]$ ) presented an enhanced leaching of Au and Ag compared to an aqueous solution containing sulfuric acid. Furthermore, the ability of the ionic liquid to be recycled was highlighted. To prevent the IL from being degraded and to favor the oxidation of metals, iron(III) sulphate was used as an oxidant. This success has been attributed to the high solubility of oxygen in this solvent, even higher than in water. This is due to large ion pairing and dipolar interactions between the oxygen and the anion, influenced by its charge density.<sup>148,161</sup>

Following this breakthrough, some works reported the use of the hydrogensulphate anion for the leaching of many other matrices such as brass ash (*Kilicarslan et al. 2014*),<sup>162</sup> Cu and Fe ores (*Dang et al. 2009*),<sup>163</sup> metals in printed board circuit (*Huang et al. 2014*),<sup>164</sup> (*Zhang et al. 2018*),<sup>165</sup> and REEs in phosphor wastes (*Schaeffer et al. 2017*).<sup>166</sup>

Some cation also showed promising results for leaching applications. A betainium cation  $[\text{Hbet}]^+$  composed of a carboxyl group (**Figure I.21**) was first synthesized by *Nockemann et al.* and used for the complexation of uranyl after being associated to a  $\text{NTf}_2^-$  anion.<sup>167</sup>  $[\text{Hbet}][\text{NTf}_2^-]$  was later used for the leaching of REE in (i) permanent magnets NdFeB (*Dupont, Binnemans et al. 2015*),<sup>168</sup> (ii) phosphor wastes (*Dupont, Binnemans et al. 2015*)<sup>169</sup> and (iii) bauxite ores (*Davris et al. 2016*).<sup>170</sup> Finally, in a recent communication,<sup>171</sup> a super-acidic cation (**Figure I.21**) based on sulfamic acid ( $\text{NH}_3\text{-SO}_3$ ) was associated with a  $[\text{NTf}_2^-]$  anion in order to form an IL with a  $\text{pK}_a$  lower than  $-7$ , again showing the potential of ILs to leach metals.

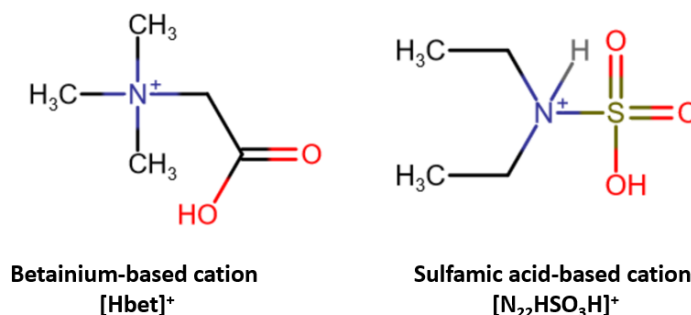


**Figure I.21.** Efficient cations for the leaching of metals  $[\text{Hbet}]^+$  and  $[\text{N}_{22}\text{HSO}_3\text{H}]^+$ .

### I.4.3 IL-based Liquid-liquid extraction

#### a. Definition

Liquid-liquid extraction (LLE) also called solvent extraction can be defined as the difference of distribution of two components, in this work metallic ions between two immiscible liquid phases.<sup>172</sup> The two solvents are in equilibrium each other and allow the separation of elements based on the difference of their chemical potential ( $\mu$ ). Starting from a species A in a solvent 1 (sol1) partitioning in two solutions after LLE using a solvent 2 (sol2), the following equation can be written:

$$\mu_A^{sol1} = \mu_A^{sol2} \quad (15)$$

$$\mu_A^{sol} = \mu_A^0 + RT \ln aA \quad (16)$$

Where  $\mu_A^0$  and  $a$  stand for the standard chemical potential and the activity of species respectively.  $R$  and  $T$  represent the gas constant ( $8.314 \text{ J}\cdot\text{mol}^{-1}\cdot\text{K}^{-1}$ ) and the temperature (K). Combining the two previous equations leads to:

$$\mu_A^{0,sol1} + RT \ln aA^{sol1} = \mu_A^{0,sol2} + RT \ln aA^{sol2} \quad (17)$$

$$\exp\left(\frac{\mu_A^{0,sol1} - \mu_A^{0,sol2}}{RT}\right) = \frac{aA^{sol2}}{aA^{sol1}} = D \quad (18)$$

Where  $D$  is known as the distribution ratio. It is expressed as the ratio of the activities of a species partitioning in two solvents. The higher will be the distribution coefficient, the better is the ability of A to be extracted from sol1 to sol2. However, in the case of liquid-liquid extractions from an aqueous phase to an organic solvent, the concentration of species is often only measured in the aqueous media. The distribution ratio can thus be written as a difference of concentration as follows:

$$D = \frac{aA^{sol2}}{aA^{sol1}} \approx \frac{[sol2]}{[sol1]} = \frac{n_{sol2}}{n_{sol1}} \times \frac{V_{sol1}}{V_{sol2}} = \frac{([sol1]_i - [sol1]_f) \times V_{sol1}}{[sol1]_f \times V_{sol1}} \times \frac{V_{sol1}}{V_{sol2}} \quad (19)$$

$$D = \frac{[sol1]_i - [sol1]_f}{[sol1]_f} \times \frac{V_{sol1}}{V_{sol2}} \quad (20)$$

Where  $V_{sol1}$ ,  $V_{sol2}$  and  $n_{sol1}$ ,  $n_{sol2}$  stand for the volumes (L) and the quantity of matter (mol) of the aqueous and the organic phase respectively.  $[sol1]_i$  and  $[sol1]_f$  represent the initial and final concentrations of the species in solvent 1 (here the aqueous phase) respectively.

To follow the yield of the reaction, extraction efficiency ( $\%E$ ) can also be calculated and is expressed in the following equation:

$$\%E = \left(1 - \frac{[sol1]_f}{[sol1]_i}\right) \times 100 \quad (21)$$

$D$  equals to 1 is similar to a  $\%E$  of 50 % if the volumes of both phases are equal.

Finally, to describe the separation of two metals, a separation factor  $\beta$ :

$$\beta_{A_2}^{A_1} = \frac{D_1}{D_2} \quad (22)$$

With two species  $A_1$  and  $A_2$  in a solvent 1 extracted in a solvent 2 ranging in two distribution coefficients  $D_1$  and  $D_2$  respectively. A high separation factor will stand for an important difference in distribution ratios.

A macroscopic view of a Liquid-Liquid extraction of a yellow metal  $M_1$  from an aqueous phase to a hydrophobic ionic liquid is presented in **Figure I.22**.

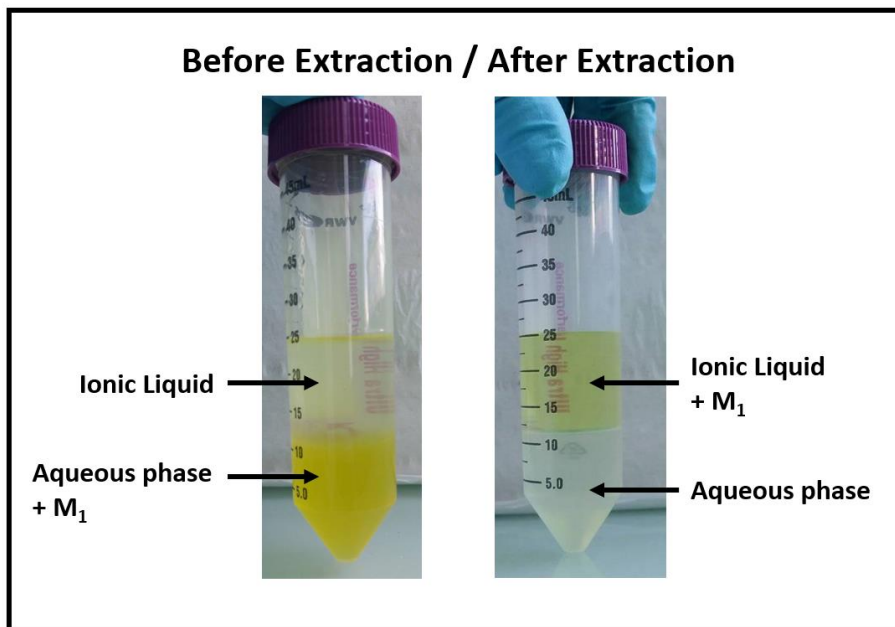


**Figure I.22.** Macroscopic view of an IL-based liquid-liquid extraction of metal. Ce(IV) in nitric acid and  $[C_1C_4Pyrr][NTf_2]$  are used for the aqueous and ionic liquid phases respectively.

b. Extraction of metals with hydrophobic ionic liquids

We have highlighted in **part I.2** of the manuscript that the extraction process of metals is industrially undertaken starting from an aqueous solution where metals are concentrated with the help of a strong acid. Then an organic solvent (kerosene, toluene, heptane etc...) is used for its low polarity and low solubility towards water. An inorganic ligand (Cyanex or [HDEHP]) is diluted in the solvent to form a complex with a metal and thus extract it from an aqueous phase towards the organic solvent.<sup>70–74</sup>

Those processes have major drawbacks towards their safety and their environmental impact. Firstly, most nonpolar organic solvents such as kerosene are known for their high volatility and flammability<sup>173</sup>. Furthermore those VOCs were designated as toxic compounds in numerous publications.<sup>174,175</sup> In this work, we

have chosen to work with safer and less toxic compounds, namely ionic liquids. Please refer to **part I.3** for more information.

Even if the complexation of metals in ionic liquids started around 1985 with the work of *Lipsztajn et al.*,<sup>176</sup> dealing with Fe, Nd and Li in an aluminum chloride IL, *Sheng Dai et al.*<sup>177</sup> were one of the first to report, in 1999, an IL-based LLE by demonstrating the ability of strontium to be extracted as a nitrate complex in [C<sub>1</sub>C<sub>4</sub>IM][NTf<sub>2</sub>]. In the early years of liquid-liquid extraction using ILs, scientists were strictly replacing VOCs with an IL in an extracting process. Therefore, researchers were diluting extractants in the solvent in order to induce metal extraction.<sup>178,179</sup> This was even performed with Cyanex, a famous selective extractant of REE and TM, which was diluted in ILs to achieve the separation of lanthanides<sup>180</sup> and actinides.<sup>181</sup> But, because ILs are charged species and because this induces unique interactions with metal ions, it was quickly reported that these molten salts could replace not only VOCs but also the extractant. In other words, ILs are able to extract metals as pure liquid phase. Extraction of metals from an aqueous solution to a pure ionic liquid phase thus started to be shown in numerous papers and was reviewed by (*Dietz et al. 2011*),<sup>133</sup> (*Abbott et al. 2011*),<sup>134</sup> (*Janssen et al 2015*),<sup>182</sup> (*Billard. 2013*)<sup>136</sup> and very recently by *Schaeffer* and co-workers in 2018.<sup>148</sup> Because a huge amount of combination of ILs and metals can be created, the number of papers dealing with metal extractions in pure ionic liquid is large. As far as we are concerned by the recycling of metals from NiMH batteries, **Table I.7** will review the most striking articles dealing with the extraction of metal ions (Ni, Co, Mn, Fe, La, Ce, Nd, Pr) that can be found in these electrochemical devices using pure ionic liquids.

<b>Metal</b>	<b>Matrix</b>	<b>Ionic Liquid</b>	<b>Optimum <i>D</i></b>	<b>Authors</b>
<b>Ni</b>	NiMH	[P <sub>66614</sub> ][Cl]	0.06	<i>Larsson and Binnemans 2014</i> <sup>183</sup>
	Salt	[P <sub>66614</sub> ][Cl]	0.01	<i>Wellens et al. 2012</i> <sup>184</sup>
	Salt	[THN][NTf <sub>2</sub> ]	0.1	<i>Boudesocque et al. 2016</i> <sup>185</sup>
	Salt	[BuGBOEt][NTf <sub>2</sub> ]	0.5	<i>Zhou et al. 2014</i> <sup>186</sup>
	Salt	[C <sub>4</sub> C <sub>1</sub> IM][PF <sub>6</sub> ]	0.01	<i>Visser et al. 2001</i> <sup>178</sup>
	Salt	[C <sub>6</sub> C <sub>1</sub> IM][PF <sub>6</sub> ]	0.02	<i>Visser et al. 2001</i> <sup>178</sup>
	Salt	[BuGBOEt][DCA]	80	<i>Zhou et al. 2014</i> <sup>186</sup>
	Salt	[THN][DCA]	50	<i>Boudesocque et al. 2016</i> <sup>185</sup>
<b>Co</b>	NiMH	[P <sub>66614</sub> ][Cl]	> 100	<i>Larsson and Binnemans 2014</i> <sup>183</sup>
	Salt	[P <sub>66614</sub> ][Cl]	120	<i>Hoogerstraete et al. 2013</i> <sup>187</sup>
	Salt	[P <sub>66614</sub> ][Cl]	450	<i>Wellens et al. 2012</i> <sup>184</sup>
	Perm. Magnet	[P <sub>66614</sub> ][NO <sub>3</sub> ]	0.01	<i>Hoogerstraete et al. 2014</i> <sup>188</sup>
	Salt	[BuGBOEt][NTf <sub>2</sub> ]	0.1	<i>Zhou et al. 2014</i> <sup>186</sup>
	Salt	[C <sub>4</sub> C <sub>1</sub> IM][PF <sub>6</sub> ]	0.01	<i>Visser et al. 2001</i> <sup>178</sup>
	Salt	[C <sub>6</sub> C <sub>1</sub> IM][PF <sub>6</sub> ]	0.02	<i>Visser et al. 2001</i> <sup>178</sup>
	Salt	[BuGBOEt][DCA]	70	<i>Zhou et al. 2014</i> <sup>186</sup>
<b>Fe</b>	NiMH	[P <sub>66614</sub> ][Cl]	> 100	<i>Larsson and Binnemans 2014</i> <sup>183</sup>
	Salt	[N <sub>1888</sub> ][Cl]	70	<i>Rios et al. 2010</i> <sup>189</sup>
	Salt	[P <sub>66614</sub> ][Cl]	1000	<i>Hoogerstraete et al. 2013</i> <sup>187</sup>
	Salt	[C <sub>8</sub> C <sub>1</sub> IM][NTf <sub>2</sub> ]	0.1	<i>Rios et al. 2010</i> <sup>189</sup>
	Salt	[C <sub>4</sub> C <sub>1</sub> IM][PF <sub>6</sub> ]	0.06	<i>Visser et al. 2001</i> <sup>178</sup>
	Salt	[C <sub>6</sub> C <sub>1</sub> IM][PF <sub>6</sub> ]	0.08	<i>Visser et al. 2001</i> <sup>178</sup>
<b>Mn</b>	NiMH	[P <sub>66614</sub> ][Cl]	> 100	<i>Larsson and Binnemans 2014</i> <sup>183</sup>
	Salt	[P <sub>66614</sub> ][Cl]	10	<i>Hoogerstraete et al. 2013</i> <sup>187</sup>
<b>La</b>	NiMH	[P <sub>66614</sub> ][Cl]	0.05	<i>Larsson and Binnemans 2014</i> <sup>183</sup>
	Salt	[P <sub>66614</sub> ][R <sub>2</sub> POO]	120	<i>Rout and Binnemans 2013</i> <sup>190</sup>
	Salt	[P <sub>66614</sub> ][SCN]	0.02	<i>Larsson and Binnemans 2015</i> <sup>191</sup>
	Salt	[N <sub>1888</sub> ][SCN]	0.5	<i>Larsson and Binnemans 2015</i> <sup>191</sup>
	Salt	[C <sub>4</sub> C <sub>1</sub> IM][C <sub>4</sub> SO <sub>3</sub> ]	80	<i>Kozonoi and Ikeda 2007</i> <sup>192</sup>
<b>Ce</b>	NiMH	[P <sub>66614</sub> ][Cl]	0.06	<i>Larsson and Binnemans 2014</i> <sup>183</sup>
	Salt	[C <sub>8</sub> C <sub>1</sub> IM][PF <sub>6</sub> ]	80	<i>Zuo et al. 2008</i> <sup>88</sup>
	Salt	[P <sub>66614</sub> ][SCN]	0.1	<i>Larsson and Binnemans 2015</i> <sup>191</sup>
	Salt	[N <sub>1888</sub> ][SCN]	1	<i>Larsson and Binnemans 2015</i> <sup>191</sup>
<b>Nd</b>	NiMH	[P <sub>66614</sub> ][Cl]	0.09	<i>Larsson and Binnemans 2014</i> <sup>183</sup>
	Salt	[P <sub>66614</sub> ][SCN]	0.5	<i>Larsson and Binnemans 2015</i> <sup>191</sup>
	Salt	[C <sub>1</sub> C <sub>8</sub> Pyr][C <sub>8</sub> PO <sub>3</sub> H]	100	<i>Zarrougui et al. 2016</i> <sup>118</sup>
<b>Pr</b>	NiMH	[P <sub>66614</sub> ][Cl]	0.07	<i>Larsson and Binnemans 2014</i> <sup>183</sup>
	Salt	[P <sub>66614</sub> ][SCN]	0.3	<i>Larsson and Binnemans 2015</i> <sup>191</sup>
	Salt	[N <sub>1888</sub> ][SCN]	4	<i>Larsson and Binnemans 2015</i> <sup>191</sup>

**Table I.7.** Striking examples of pure hydrophobic ILs used in extraction of metals.

It is interesting to notice that all metals found in NiMH batteries have been studied in extraction experiments using pure hydrophobic ionic liquids. However, even if there is a strong selectivity between Rare Earth Elements and Transition Metals,<sup>190</sup> it seems that very few ILs are able to isolate REE one from another. Extraction of those 4f elements with IL leads to poor distribution ratios. However, an innovative work was presented by *Rout et al. 2013*<sup>190</sup> where the classical hydrophobic cation  $[P_{66614}]^+$  provided by Cytec (Solvay) was combined to a bis(2,4,4-trimethylpentyl)phosphinate  $[R_2POO]^-$ . This IL extracted lanthanum with a distribution coefficient close to 120. This was explained by the ability of phosphinate anions to complex lanthanides. They are the main complexing group found in Cyanex for REE extraction. This principle was also successfully exploited by *Zarrougui et al.* for the extraction of neodymium with an octylphosphite anion grafted to a pyrrolidinium cation ( $[C_1C_8Pyr][C_8PO_3H]$ ). Phosphorus based anion thus seems to be promising complexant of REE. One of the highest extraction yield was obtained for cerium with  $[C_8C_1IM][PF_6]$  and 4 mol.L<sup>-1</sup> of nitric acid.<sup>88</sup> However, this result should be taken with care because the hexafluorophosphate anion is able to degrade in presence of acid. As a result, the highly corrosive and toxic hydrogen fluoride (HF) can be formed. It is thus of little interest to replace VOCs by harmful, dangerous chemicals.

Regarding transition metals, the literature is abundant. On the one hand chloride-based ionic liquids seem to extract efficiently iron, manganese and even cobalt resulting in a poor selectivity of those three metals.<sup>183,187</sup> On the other hand, bis(trifluoromethylsulfonyl)imide ILs present distribution coefficient lower than 1 for all TM. Cobalt and nickel present similar chemical properties and are incredibly hard to separate one from another in purification processes.<sup>44</sup> When Co and Ni are extracted towards pure ionic liquids containing the same cation but  $[NTf_2]^-$  or  $[DCA]^-$  anions, they follow the same extraction trend exhibiting  $D$  below 0.5 and close to 40 accordingly. However, Wellens et al. managed in 2012 to obtain a quantitative separation of Ni<sup>2+</sup> and Co<sup>2+</sup> based on the difference of the complexation constant of those two cations towards a chloride ligand. As a result, they had to use around 8 mol.L<sup>-1</sup> of hydrochloric acid to form a  $[CoCl_4]^{2-}$  complex extracted from the aqueous solution to the  $[P_{66614}][Cl]$ . In other words, the concentration of acid has an impact on the speciation of the metal and thus on the extraction yield.

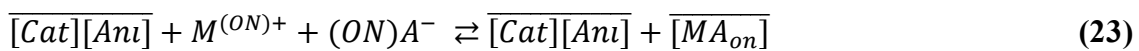


This brings us to the question of the extraction mechanism of metals in pure ionic liquid linked to (i) the interactions between the IL and the metal and (ii) the speciation of the metallic species in solution.

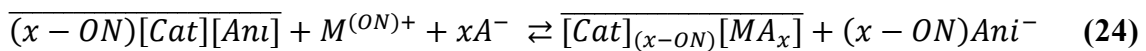
c. Extraction mechanism of metals in pure ILs

The ionic nature of ILs brings new opportunities of speciation, complexation and extraction compared to classical VOCs.<sup>134</sup> Two main extraction mechanisms can occur in those systems and will be depicted in the following equations.

*Ion Pair:*



*Ion Exchange:*



Where species expressed under a bar means they are located in the organic phase. Considering an ionic liquid made of a cation  $Cat^+$  and an anion  $Ani^-$ , a metal  $M$  having an oxidation number  $ON$  can form a neutral complex with an inorganic anion  $A^-$ . This species can be in the aqueous solution by addition of salt or acid. In ion pairing mechanism, the metal form a neutral complex that can be extracted in the organic phase while in ion exchange, a negatively charged complex is formed ( $x > ON$ ). This complex is extracted in the IL phase and binds with the cation of the molten salt. In order to respect the electroneutrality of the solution,  $Ani^-$  is expelled to the aqueous phase. If the anion in water is different from the one in the IL, this can cause a degradation of the solvent.

#### **I.4.4 IL-based Aqueous Biphasic Systems (ABS)**

a. Fundamentals of IL-based ABS

With the aim of developing new extracting techniques of proteins, *Albertsson* reported in *Nature* the first aqueous biphasic system in 1958 using hydrophilic polymers.<sup>193</sup>

A definition of Aqueous Biphasic System was given by *Freire et al.* in a review from 2012.<sup>194</sup> They were briefly defined as two fully water soluble compounds that, in some specific concentration and temperature conditions, can form two immiscible aqueous phases. Soluble compounds can be either a polymer or a salt leading to polymer-polymer, salt-salt or polymer-salt ABS. One of the phase will be defined as an aqueous-rich phase while the other will be a salt or polymer-rich phase.<sup>194</sup> In this work we will be interested in salt-salt ABS and more precisely IL-based ABS. We will define them as:

- An ionic liquid and an inorganic salt that are, for a fixed concentration, pressure and temperature soluble in water when dissolved separately, but forming two immiscible liquid phases when mixed together.

To make a clear distinction between hydrophobic ionic liquids mixed with water forming a unique phase and IL-based ABS, two additional criteria are added:

- The concentration of ionic liquid must be superior to 3 wt. %.
- The concentration of water must be superior to 15 wt. %.

IL-based ABS were firstly proposed by Gutowski, Rogers and.<sup>195</sup> They present the advantage of containing high amounts of water lowering the viscosity of the system. Furthermore, toxic fluorinated anions or long alkyl chain cations used to increase the hydrophobicity of ILs in classical liquid-liquid extractions are removed and replaced by short cation and inorganic hydrophilic anions. As a result, ILs used in ABS are cheaper and safer.

**Figure I.23.A** represents a typical phase diagram of an ABS. The binodal curve in blue represents the limit between a monophasic and a biphasic system at a fixed temperature and can be measured experimentally by titration. The curve is expressed function of the weight percentage or the molar percentage of the salt and the IL. The third component, namely water is not expressed but can be calculated by the following equation.

$$wt. \% water = 100 - wt. \% IL - wt \% salt \quad (25)$$

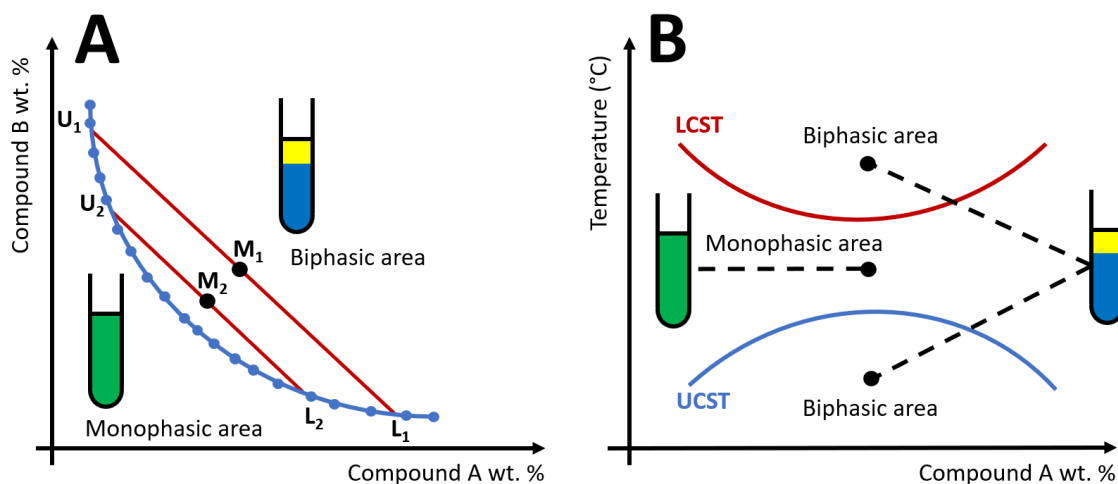


**Figure I.23. A:** Typical phase diagram of an ABS. Binodal curve in blue. Tie lines in red. **B:** Thermomorphic behaviour of an ABS. Red and blue lines, binodal curves for LCST and UCST systems respectively.

Any mixture point  $M_n$  in the biphasic area can be represented by theoretical tie line where  $U_n$  and  $L_n$  represent the composition in ionic liquid, salt and thus in water of the upper phase and the lower phase respectively. Any mixture prepared on the same tie line will lead to similar phase composition and distribution coefficient in the case of extraction. However, they will have different volumes and densities.

ABS are also very sensible to temperature. Two antagonist systems can be found, Lower Critical Solution Temperature (LCST) and Upper Critical Solution Temperature (UCST) tend to form immiscible phases by heating and cooling down the system respectively. Those thermomorphic behaviours are represented in **Figure I.23.B**.

#### b. Mechanism of formation

The mechanisms inducing the formation of a biphasic system starting from two hydrophilic compounds mixed in water are multiple, complex and not always well understood.<sup>85</sup> Among them the salting-out effect plays a major role in the phase demixing. The ionic liquid is partitioned between two phases due to the charge density of the counter anion of a salt. On the one hand, high charge density salts are able to form large hydrated complex.<sup>194</sup> On the other hand due to the delocalized charge on ionic liquid cations, they are weakly solvated by water. As a result, water will preferentially bind with the inorganic salt and will be expelled from the IL-rich phase. Based on this observation, the “salting-out efficiency” of many salts was analysed and compared empirically in the Hofmeister series.

$[\text{PO}_4]^{3-} \leq [\text{SO}_4]^{2-} \leq \text{Cl}^- \leq \text{Br}^- \leq [\text{NO}_3]^- \leq \text{I}^- \leq [\text{ClO}_4]^- \leq [\text{SCN}]^- \leq [\text{NTf}_2]^-$ .<sup>148,196</sup>

The ability to induce a biphasic system can be defined as the minimal necessary amount of a compound A to induce a biphasic solution at a fixed temperature and fixed concentration of a compound B. In this case, using a similar IL, potassium phosphate salt ( $\text{K}_3\text{PO}_4$ ) will be more likely to induce a phase separation than potassium chloride (KCl) or even potassium iodide (KI). This phenomenon has been studied in IL-based ABS by (Shahriari *et al.* 2012).<sup>196</sup>

The choice of the ionic liquid also has a strong impact on the phase separation of an ABS. The impact of the cation in chloride-based ILs on the formation of an ABS induced by a  $\text{K}_3\text{PO}_4$  salt was studied by Neves *et al.* 2009.<sup>197</sup> As a result, the longer the alkyl chain, the more hydrophobic the IL and the stronger was the ability of the system to induce a phase separation. The series  $[\text{C}_6\text{C}_1\text{IM}][\text{Cl}] \geq [\text{C}_7\text{H}_7\text{C}_1\text{IM}][\text{Cl}] \geq [\text{C}_4\text{C}_1\text{IM}][\text{Cl}] \geq [\text{C}_2\text{C}_1\text{IM}][\text{Cl}] \geq [\text{C}_1\text{C}_1\text{IM}][\text{Cl}] \geq [\text{C}_2\text{IM}][\text{Cl}] \geq [\text{C}_1\text{IM}][\text{Cl}] \geq [\text{IM}][\text{Cl}]$  was established based on the ability of long alkyl chain cations to expel water from their chemical environment.<sup>197</sup>

Similarly, the influence of the anion in IL-based ABS was studied by the same group in a different publication with  $[\text{C}_2\text{C}_1\text{IM}]^+$  ionic liquids in ABS induced by a  $\text{K}_3\text{PO}_4$  salt.<sup>198</sup> A strong correlation between the hydrogen bond basicity and the ability to induce a phase separation was highlighted. This relies on previous studies showing that the higher the hydrogen bond acceptance nature of ILs, the lower the ability to form water-based complex and thus the higher the ability to separate the IL from an aqueous phase.<sup>199–201</sup> In line with the previous statement, a series can be established.  $[\text{C}_2\text{C}_1\text{IM}][\text{CF}_3\text{SO}_3] \geq [\text{C}_2\text{C}_1\text{IM}][\text{DCA}] \geq [\text{C}_2\text{C}_1\text{IM}][\text{CH}_3\text{SO}_4] \geq [\text{C}_2\text{C}_1\text{IM}][\text{Br}] \geq [\text{C}_2\text{C}_1\text{IM}][\text{Cl}] \geq [\text{C}_2\text{C}_1\text{IM}][\text{CH}_3\text{CO}_2]$ .<sup>85,198</sup>

### c. IL-based ABS for recycling metals in NiMH batteries?

These emerging systems were widely studied in separation process. However, they were applied for the separation and purification of proteins, DNA, active ingredients and a large range of other (bio)molecular compounds.<sup>129–132,194</sup>

But the neutral and sometimes basic pH of these systems hinders the ability of IL-based ABS to extract and separate metals as they are susceptible to undergo hydrolysis in such conditions. Furthermore, metals are mostly found in acidic media in recycling and extraction processes because of the leaching step. This topic was reviewed by I. Billard in a recent book chapter.<sup>123</sup> Regarding metals

found in NiMH batteries, namely Ni, Co, Mn and Fe for TM and La, Ce, Nd and Pr for REE, only a very few articles were published and are reported in **Table I.8**.

Metal	Matrix	Ionic Liquid	Optimum D	Author
Ni	Salt	[Hbet][NTf <sub>2</sub> ]	0.08	Hoogerstraete et al. 2013 <sup>202</sup>
	Salt	[N <sub>22</sub> hcm][NTf <sub>2</sub> ]	> 1	Blesic et al. 2014 <sup>203</sup>
	Salt	[P <sub>44414</sub> ][Cl]	0.1	Onghena et al. 2016 <sup>204</sup>
Co	Salt	[N <sub>22</sub> hcm][NTf <sub>2</sub> ]	> 1	Blesic et al. 2014 <sup>203</sup>
	Salt	[P <sub>44414</sub> ][Cl]	100	Onghena et al. 2016 <sup>204</sup>
Fe	-	[C <sub>4</sub> C <sub>1</sub> IM][FeCl <sub>4</sub> ]	-	Xie et al. 2011 <sup>205</sup>
	Bauxite Ore	[Hbet][NTf <sub>2</sub> ]	10	Onghena et al. 2015 <sup>206</sup>
Mn	Salt	[Hbet][NTf <sub>2</sub> ]	0.08	Hoogerstraete et al. 2013 <sup>202</sup>
La	Salt	[Hbet][NTf <sub>2</sub> ]	10	Hoogerstraete et al. 2013 <sup>202</sup>
	Bauxite Ore	[Hbet][NTf <sub>2</sub> ]	0.01	Onghena et al. 2015 <sup>206</sup>
Ce	Salt	[Hbet][NTf <sub>2</sub> ]	0.01	Onghena et al. 2015 <sup>206</sup>
Nd	Salt	[Hbet][NTf <sub>2</sub> ]	10	Hoogerstraete et al. 2013 <sup>202</sup>
	Bauxite Ore	[Hbet][NTf <sub>2</sub> ]	0.01	Onghena et al. 2015 <sup>206</sup>
	Salt	[Hbet][NTf <sub>2</sub> ]	10	Hoogerstraete et al. 2013 <sup>207</sup>
Pr	-	-	-	-

**Table I.8.** IL-based ABS used for the extraction of metals found in NiMH batteries.

The betainium functionalized bis(trifluoromethylsulfonyl)imide ionic liquid, namely [Hbet][NTf<sub>2</sub>] was widely studied as an IL-based ABS in several works. Even if this system is not extracting nickel and cobalt, extraction of iron was successfully achieved from a bauxite ore.<sup>206</sup> In this work iron and scandium are thus separated from other REE that present low extraction yield. However, *Vander Hoogerstraete et al. 2013* manage to achieve higher distribution coefficients ( $D = 10$ ) for light REE namely neodymium<sup>207</sup> and lanthanum<sup>202,207</sup> by adding a zwitteronic betaine in the solution. A new (hydrazinocarbonylmethyl)trimethylammonium bis(trifluoromethylsulfonyl)imide ionic liquid, based on the Girard's reagent, named [N<sub>22</sub>hcm][NTf<sub>2</sub>] was synthesized by *Blesic, Seddon and co-workers*.<sup>203</sup> Macroscopic snapshots were reported, a quantitative extraction of both nickel and cobalt was shown, highlighting an interesting new extracting system but no selectivity between these two metals. However this difficult task was carried out by *Onghena et al. 2016*.<sup>204</sup> Relying on the work of *Wellens et al. 2012*<sup>184</sup> the hydrophobic [P<sub>66614</sub>][Cl] IL was replaced by

the fully miscible in water [P<sub>44414</sub>][Cl] IL. Furthermore, the chloride complexation of cobalt, performed with hydrochloric acid in the work of *Wellens and co-workers* was induced by sodium chloride (NaCl). As a result, the separation factor of cobalt from nickel,  $\beta_{Ni}^{Co}$  was reported to be 1000. To conclude, extraction of metals through IL-based ABS is in its early stage. Hydrolysis of the metal, potential addition of the acid, partition of the compounds and selectivity of valuable metals are still pending issues.

## I.4.5 Electrodeposition in ionic liquids

### a. Principle

As described previously a metallic ion can be extracted and loaded in a hydrophobic ionic liquid via liquid-liquid extraction (see **part I.4.3**) and/or via Aqueous Biphasic systems using hydrophilic ILs (see **part I.4.4**). The concentrated metallic ion can then be removed from the IL to an aqueous phase by back extraction and can be eventually precipitated as a salt. However, a different strategy relies on the reduction of the metallic ion in the ionic liquid to a metal in order to recover pure metallic valuable elements. This can be obtained by electrodeposition in IL by inducing a potential difference between two electrodes.<sup>208</sup> Ionic liquids are solely composed of ions which thus make them promising solvents for any charge transportation (see **part I.3.3**).<sup>103</sup> Furthermore, they are also known to have wide electrochemical windows ( $\Delta E_W$ ). An electrochemical window can be defined as the range of potential where no electrochemical reaction takes place with the solvent species. This value can go to 4.5-5 V vs NHE in ILs containing NTf<sub>2</sub> anions and is much higher than what can be undergone in aqueous solutions (1.23 V vs. NHE).<sup>102,209</sup> However no official rule exists to describe the degradation of an IL because oxidation and reduction of species from the solvent are not well established in terms of nature, mechanism and thermodynamic. Furthermore, overpotentials of the reactions are related to the electrode materials and are rarely taken into account. From one paper to another,  $\Delta E_W$  is thus set at different current density values and remains hardly comparable.<sup>210</sup>

In any case, this large electrochemical stability is a strong asset in the reduction of cations. This is the case of REE having low standard reduction potential ( $E^0$ ). This thermodynamic calculated value stands for the potential when a known metallic ion can be reduced in some specific conditions. According to *Bard et al. 1985*,<sup>211</sup> standard reduction potentials are always lower than -2.29 V vs NHE for all light REE studied in this manuscript when reduced from their third oxidation state to a metal ( $\text{Ln(III)} \rightarrow \text{Ln(0)}$ ).

Generated by a potentiostat, electrons ( $e^-$ ) move to an electrode soaked in the solution concentrated in metallic cations ( $M^{NO+}$ ) in order to reduce them to a metal ( $M$ ) according to the following equation.



$ON$  represents the oxidation number of the metallic cation before reduction.

A three-electrode array setup is often used. The potential of the working electrode (WE) is expressed relative to the potential of the reference electrode (RE). No current is going through the latter electrode. While inducing a negative potential, electrons are able, at the interface between the WE and the IL, to reduce metallic cations. At the counter electrode, the reverse process takes place. A schematic view of the use of electrodeposition in ionic liquids in a recycling process is given in **Figure I.24**.

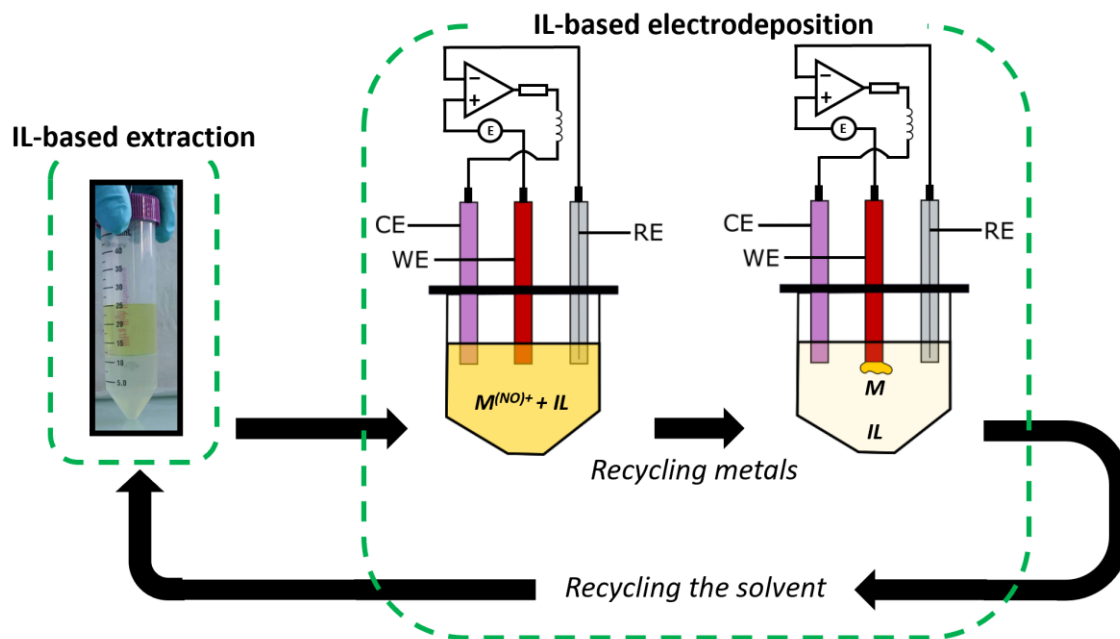


**Figure I.24.** IL-based electrodeposition, as part of a recycling process.

The idea of using a tool such as electrodeposition in ionic liquids relies on the ability to recover pure metals, presenting higher price and interest than precipitated salts. But it is also to perform a regeneration of the solvent. The IL can be cleared from metallic species during the electrodeposition process and can thus be reused again in an extraction step. As mentioned by *Plechkova and Seddon*, being able to reuse the solvent is a highly efficient strategy to decrease the overall price of ionic liquid processes.<sup>83</sup>

#### b. Electrodeposition of REE and TM in ILs

Electrodeposition of metals in ionic liquids was reviewed by *Abbott and co-workers* in 2006<sup>212</sup> and 2013<sup>113</sup> but also by *Liu et al.* in 2016.<sup>213</sup> Similarly to what has been presented for hydrophobic liquid-liquid extraction (**Table I.7**) and for IL-based ABS (**Table I.8**), the most striking reported data on the electrodeposition of REE and TM present in NiMH batteries will be presented in **Table I.9** i.e La, Ce, Nd, Pr, Co, Ni, Mn, Fe. Standard reduction potential for each metal from the third and second oxidation state to the metal for REE and TM respectively will also be reported according to the book from *Bard et al.*<sup>211</sup>



Metal	$E^0$ vs NHE	Ionic Liquid	Applied Potential vs NHE	Authors
Ni	-0.25	[C <sub>4</sub> C <sub>1</sub> IM][Cl]	-0.55	<i>Carlin et al. 1998</i> <sup>214</sup>
		[C <sub>2</sub> C <sub>1</sub> IM][DCA]	-1.1	<i>Deng et al. 2008</i> <sup>215</sup>
Co	-0.28	[C <sub>4</sub> C <sub>1</sub> IM][NTf <sub>2</sub> ]	-1.0	<i>Katayama et al 2005</i> <sup>216</sup>
		[C <sub>4</sub> C <sub>1</sub> IM][Cl]	-0.55	<i>Carlin et al. 1998</i> <sup>214</sup>
		[C <sub>2</sub> C <sub>1</sub> IM][Cl]	-	<i>Yang et al. 2008</i> <sup>217</sup>
Fe	-0.44	[C <sub>4</sub> C <sub>1</sub> IM][Cl]	-0.65	<i>Carlin et al. 1998</i> <sup>214</sup>
		[C <sub>4</sub> C <sub>1</sub> IM][Cl]	-	<i>Endres et al. 2003</i> <sup>218</sup>
Mn	-1.19	[C <sub>4</sub> C <sub>1</sub> Pyr][NTf <sub>2</sub> ]	-1.5	<i>Deng et al. 2007</i> <sup>219</sup>
		[C <sub>4</sub> C <sub>1</sub> Pyr][NTf <sub>2</sub> ]	-1.3	<i>Chang et al. 2008</i> <sup>220</sup>
La	-2.38	[N <sub>1114</sub> ][NTf <sub>2</sub> ]	-2.5	<i>Bhatt et al. 2005</i> <sup>221</sup>
		[C <sub>4</sub> C <sub>1</sub> Pyr][NTf <sub>2</sub> ]	-2.9	<i>Bourbos et al. 2015</i> <sup>222</sup>
		[C <sub>8</sub> C <sub>1</sub> Pyr][NTf <sub>2</sub> ]	-1.3	<i>Legeai et al. 2008</i> <sup>117</sup>
Ce	-2.37	[N <sub>1114</sub> ][NTf <sub>2</sub> ]	-2.3	<i>Hatchett et al. 2013</i> <sup>223</sup>
Nd	-2.32	[P <sub>2225</sub> ][NTf <sub>2</sub> ]	-2.8	<i>Kondo et al. 2012</i> <sup>224</sup>
		[P <sub>2225</sub> ][NTf <sub>2</sub> ]	-2.4	<i>Matsumiya et al. 2014</i> <sup>225</sup>
		[C <sub>8</sub> C <sub>1</sub> Pyr][C <sub>8</sub> PO <sub>3</sub> H]	-2.2	<i>Zarrougui et al. 2016</i> <sup>118</sup>
Pr	-	-	-	-

**Table I.9.** Striking examples of pure ILs used for electrodeposition of metals.

Mostly all light REE found in NiMH batteries were recovered from ionic liquids by electrodeposition. Most of the ILs used are based on the [NTf<sub>2</sub>]<sup>-</sup> anion due to its wide electrochemical window.<sup>221–225</sup> The applied potential to induce the reduction of lanthanides(III) to a metal is in general close from their standard reduction potential. This value is not shifted to lower potential due to the weak interactions between metals and NTf<sub>2</sub><sup>-</sup>. The low affinity of metal cations with bis(trifluoromethylsulfonyl)imide was highlighted by *Bortolini et al. 2015*.<sup>226</sup> However, looking at the characterization of the deposits, the major drawback of most studies is linked to a contamination in fluoride and sulfur. This phenomenon is clearly seen in several studies<sup>117,222,223</sup> via Energy Dispersive Spectroscopy (EDS) from Scanning Electron Microscopy (MEB). As an example, *Hatchett and co-workers*<sup>223</sup> reported that their lanthanum deposit was polluted with 16 wt. % of fluoride and 13 wt. % of sulfur. These two elements were described to be linked to the absorption of the IL on the deposit however they are also highly susceptible to be a result of the degradation of bis(trifluoromethylsulfonyl)imide and thus lead to

the issue of the real electrochemical window of ionic liquids.<sup>210</sup> As a result, these metals can't be recovered in industrial process by electrodeposition.

Manganese(II) was also reduced in [NTf<sub>2</sub>]-based ionic liquids in order to form manganese coatings for supercapacitor electrodes.<sup>219</sup> It has been shown that crystallization and thus the particle size is linked to the overpotential.<sup>220</sup>

Cobalt was successfully deposited in [NTf<sub>2</sub>]<sup>216</sup> and [Cl]<sup>214,227</sup> based ILs while nickel was reduced in [Cl]<sup>214</sup> but also [DCA]<sup>215</sup> based ILs. The latter dicyanamide anion was chosen because of its low viscosity but especially because it is a Lewis base having good ligand properties and thus strong ability to dissolve transition metals.<sup>115</sup> The physicochemical properties of a large range of [DCA]-based IL was highlighted by *MacFarlane et al. 2002*.<sup>228</sup>

The IL-cations are usually made of short alkyl chain (butyl and methyl) imidazolium<sup>214–216,218,227</sup> or pyrrolidinium<sup>117,118,219,220,222</sup> for their relatively low viscosity and good ionic conductivity<sup>208</sup>. However some phosphonium<sup>224,225</sup> and ammonium<sup>221,223</sup> cations were used, for REE electrodeposition for their enhanced electrochemical stability.

Finally, a smart and innovative full process of extraction and electrodeposition of neodymium was performed by *Zarrougui et al. 2016*<sup>118</sup> with an 1-octyl-1-methylpyrrolidinium octylphosphite ionic liquid, namely [C<sub>8</sub>C<sub>1</sub>Pyr][C<sub>8</sub>PO<sub>3</sub>H]. Even if this work does not show the ability of the solvent to isolate one metal from another, it is a great example of the potential of ILs to extract and reduce metals by liquid-liquid extraction and electrodeposition.

## I.5 Specification of the study

---

Nickel metal hydride batteries are currently the dominating technology not only for portable tools but also for Hybrid Electric Vehicles as 70 % of HEVs are powered by NiMH batteries.<sup>18</sup> These electrochemical systems are composed of two electrodes soaked in a potassium hydroxide electrolyte. The positive electrode is composed of nickel hydroxide. The negative electrode can be manufactured using several binary alloys, the so-called AB<sub>5</sub> material being the most popular and efficient one. It will therefore be the material treated in this work. In AB<sub>5</sub>, the letter A stands for Rare Earth Elements. From the most to the least concentrated metals, AB<sub>5</sub> contains lanthanum, cerium, neodymium and praseodymium, the latter being only present as traces. Letter B stands for transition metals, that is, mainly nickel and cobalt with smaller amounts of manganese. The overall negative electrode is often deposited on a nickel-iron alloy.<sup>21,22</sup> As a result, two main categories of metals are present in the active material of a battery, namely Transition Metals (Ni, Co, Mn, Fe) and Rare Earth Elements (La, Ce, Nd, Pr). Since 2010, the European Commission<sup>36</sup> has defined REE as critical raw materials, since more than 97 % of the production is Chinese and only an average of 3 % were recycled in 2017.<sup>38</sup> Furthermore, extracting techniques of REE are extremely polluting using inorganic ligands dissolved in volatile organic compounds (VOCs) such as kerosene, toluene, heptane...etc.<sup>74,75</sup> The production and supply of REE cause violent geopolitical, health, economic and environmental issues.<sup>7</sup> Some transition metals can also have high rate of criticality. This is the case for cobalt, mainly produced with low yields in DR Congo from copper and nickel ores. Because of the increasing need of Co, in NiMH batteries but also and mainly in Li-ion battery, cobalt raises awareness of numerous countries.<sup>42</sup>

One solution to tackle this issue is to develop a recycling process of valuable metals from used NiMH batteries with a low environmental impact. Toxic volatile organic solvents will thus be replaced by safer and greener ionic liquids. The present work will be achieved in compliance with the specifications established between the research laboratory LEPMI and the Recupyl<sup>®</sup> recycling company:

- The main goal of this work is to build a flow sheet for the recycling of metals from NiMH batteries by ionic liquids.
- The work will be carried out with model solutions and with real end-of-life NiMH batteries collected, discharged, shredded and grinded by the industrial partner.
- The first part of the project is to isolate the two main categories of elements found in NiMH batteries, this is to say, Rare Earth Elements and Transition Metals using classical hydrometallurgical process.
- Relying on previous studies regarding Liquid-Liquid Extractions (LLE), Aqueous Biphasic Systems (ABS) and electrodeposition with Ionic Liquids (ILs), effort will be made to develop innovative methods in order to separate TM from REE and each metal from one another.
- Some paths to the evaluation of the overall environmental impact of the process should be given.



---

---

## **CHAPTER II**

# **Separation of Transition Metals from Rare Earth Elements**

## II.1 Introduction

---

**Chapter I** highlighted that NiMH batteries are increasingly used for electrochemical storage as 70 % of hybrid cars are powered by this technology.<sup>18</sup> They contain large amounts of valuable metals, mainly transition metals, Ni, Co and Mn but also rare earth elements, La, Ce, Nd and Pr considered as highly critical materials by the European Commission.<sup>38</sup> To tackle this issue, a recycling process of metals from NiMH batteries will be investigated in this work.

This Chapter will firstly be devoted to the preparation and mechanical treatment of batteries. This will allow to fully identify and characterize the valuable components of real end of life devices. In a second part, the leaching of the battery, this is to say, the dissolution in an aqueous solution containing an acid will be performed. Those investigations will separately be carried out with (i) a spent battery open in a laboratory scale to understand all fundamental mechanisms and (ii) a mixture of several spent batteries to reach a more industrial process. Separation of rare earth elements and transition metals will be undergone in **Chapter 3** and **4** respectively using ionic liquids (ILs). Those unconventional solvents were reported in the literature to be potential efficient extractants of ionic metallic species.<sup>133,134,136</sup> This is why, with the aim of developing a simultaneous oxidation and extraction step, ILs will be investigated as potential leaching phase in a third part. Finally, the last part will be devoted to the separation of the two main families of metals, this is to say transition metals and rare earth elements by selective precipitation.


## II.2 Preparation and mechanical treatment of NiMH batteries

### II.2.1 Laboratory scale black mass production

#### a. The commercial battery

In order to recycle metals from an end-of-life battery, the first step is to be able to open the electrochemical device and to recover the electrodes where the valuable metals can be found. This part of the process was firstly carried out at a laboratory scale with a commercial NiMH battery used in portable tools. Commercial batteries provided by SUPPO<sup>®</sup> were used to optimize our recycling process.

Characteristics	
Battery type	NiMH
Brand	SUPPO
Reference	HPYSC1.5
Geometry	Cylindrical
Height	4.0 cm
Diameter	2.3 cm
Weight	40 g
Voltage	1.2 V
Capacity	3000 mA.h



**Figure II.1.** Characteristics and snapshot of the commercial NiMH batteries from SUPPO<sup>®</sup>

Those batteries referenced as ‘HPY-SC1.5’ by the company SUPPO<sup>®</sup> were commercially used in vacuum cleaners and are considered to be in an end-of-life state. They are organized as cylindrical 4.0x2.3 cm<sup>2</sup> cells (See **part I.1.3**) weighing 40 g each.

For safety reasons, before manipulating the batteries, they were plugged to a resistance during 48 hours to achieve a complete discharge of the system. The



voltage was checked with a multimeter to confirm that the discharge has been successfully carried out.

In a second step, the two sides of the secondary battery, namely the positive and the negative terminals were sawed under a hood. According to what was reported in **CHAPTER I**, regarding cylindrical NiMH batteries, we can observe the layers of electrodes and separator rolled together. No leaks of KOH electrolyte is noted as they are considered as mostly dry systems.<sup>22</sup> Extremities of the sawed battery are represented in **Figure II.2**.

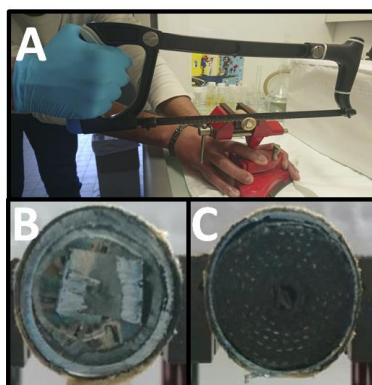


**Figure II.2.** Snapshots of a NiMH commercial battery with sawed extremities. A: The battery is sawed. B: Positive terminal. C: Negative terminal.

From this step, it is possible to push the remaining positive terminal and to extract the rolled electrodes from their outer shell. Layers of negative electrode / Separator / Positive electrode can be found.

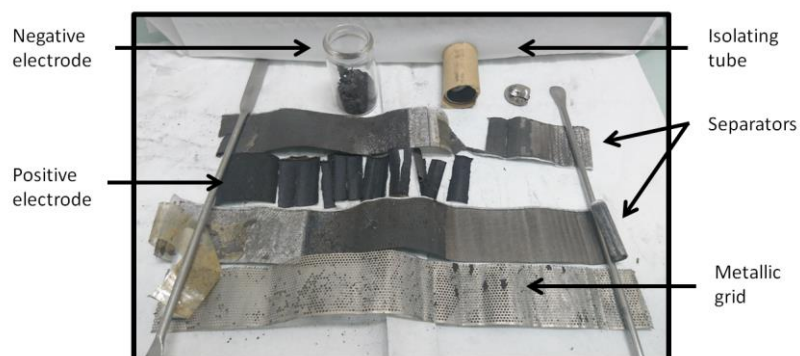


**Figure II.3.** View of a NiMH battery after isolating electrodes and separators.

The negative electrode is deposited on a metallic grid and can easily be scraped in order to recover the active material. The latter is under the form of a thin black metallic powder and is usually named by recycling industries as Black Mass (BM). The negative electrode is the most valuable piece of a NiMH battery as it is, after discharge, an intermetallic compound containing up to 20 and 15 atomic percent of rare earth elements and cobalt respectively for  $AB_5$  binary alloys.<sup>21</sup> REE and Co are now described as highly critical metals (see **part I.2**) and need to be recycled. Therefore, only the intermetallic elements will be treated in this section.

#### b. Purification and characterization

The separator as well as the positive and negative electrodes were qualitatively analysed by Scanning Electron Microscopy using imaging via Backscattered Electron (BSE) and semi-quantitatively evaluated via Energy Dispersive X-Ray Spectroscopy (EDS). **ANNEX 1-A** will be devoted to details on the electronic microscopy experiments.

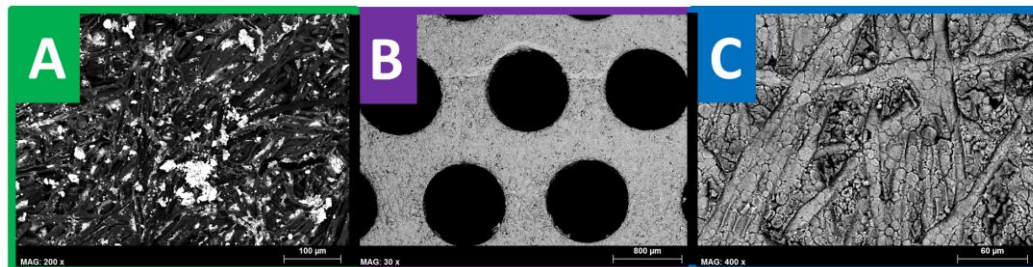


**Figure II.4.** SEM images of different NiMH battery components using BSE. A: Positive electrode (magnification  $\times 200$ ). B: grid (magnification  $\times 30$ ). C: Negative electrode (magnification  $\times 400$ ).

$Ni(OH)_2$  at the positive electrode appears to be under the form of micrometric particles deposited on an organic woven material. Because metals present higher molar masses than organic compounds, the active material is represented by white spots in **Figure II.4-A**. **Figure II.4-B** and **C** represent the metallic grid and the negative electrode active material respectively. The manufacturing technique of the metal hydride found in the negative electrode is in full accordance with the “plasticized technology” described in **part I.1.3**. Spherical particles of 3 to 10  $\mu m$  are homogeneously bound together and deposited on a metallic grid. The

intermetallic compound can be observed in a clear color while the binder is dark/black while analysed by BSE. An elemental analysis of each component was performed via EDS in **Table II.1**.

Elements	Composition (atom. %)		
	A: Positive electrode	B: Grid	C: Negative electrode
<b>Fe</b>	-	27.3 ± 1.1	-
<b>Ni</b>	50.2 ± 2.4	72.7 ± 3.5	30.1 ± 1.5
<b>Co</b>	3.4 ± 0.5	-	7.6 ± 0.8
<b>Mn</b>	1.2 ± 0.2	-	3.7 ± 0.5
<b>REE</b>	-	-	5.2 ± 1.2
<b>K</b>	40.8 ± 4.4	-	53.4 ± 10.1

**Table II.1.** Elemental analysis of different NiMH battery components using EDS.

Similarly to what is reported in the literature regarding negative electrodes manufacture,<sup>21,22</sup> the metallic grid is a nickel iron alloy. Both active materials are contaminated with high amounts of potassium due to the 30 wt. % KOH electrolyte solution used in NiMH batteries. Without surprise, nickel hydroxide, at the positive electrode is doped with approximately 3.4 wt. % Co and minor amounts of manganese as found in the powder. Regarding the negative electrode, it seems that the intermetallic compound is part of the AB<sub>5</sub> alloys that will be treated in this work. This technology is nowadays the most efficient and the most popular on the market.<sup>21</sup> It is mainly composed of nickel, doped with cobalt and manganese. More than 5 wt. % of REEs are found in the powder but it is difficult to differentiate them from one lanthanide to another as (i) the sample is highly contaminated in potassium. (ii) They appear at similar energies on the EDS spectrum.

To remove the electrolyte from the BM, a simple washing step was performed. Because the solubility of KOH is known to increase with temperature unlike most REE salts,<sup>229</sup> the washing solution was composed of MQ-grade pure water (18.2 MΩ.cm at 25 °C) at 40 °C. The mixture of black mass and water was prepared in a ratio 1:10 (mass (g): volume (mL)) and was stirred on a magnetic plate during 30 min without any stirrer because of the high magnetic properties of metals in the electrodes (REE and cobalt are widely used in permanent magnets)<sup>208</sup>. The BM is

filtered on a Büchner setup and the pH of the filtrate was measured with a pH-meter. This process was performed several times until the pH of the filtrate reaches a value below 8. This is an accurate and quick manner to follow the potassium hydroxide dissolution in water as it is known to be a strong basis ( $pK_a = 13.5$ ).<sup>230</sup> The powder was then dried in an oven at 80 °C overnight before being analysed by EDS (**Table II.2**) and X-Ray diffraction (XRD) (**Figure II.5**). XRD analysis will be detailed in **ANNEX 1-B**. The mass of recovered anode was approximately 8 g for each battery.

Elements	Composition (atom. %)
	Washed negative electrode
<b>Fe</b>	-
<b>Ni</b>	$59.2 \pm 3.1$
<b>Co</b>	$12.5 \pm 1.3$
<b>Mn</b>	$6.7 \pm 0.9$
<b>La</b>	$5.7 \pm 1.2$
<b>Ce</b>	$7.8 \pm 1.6$
<b>Nd</b>	$2.3 \pm 0.7$
<b>Pr</b>	$0.8 \pm 0.3$
<b>K</b>	-

**Table II.2.** Elemental analysis of the washed negative electrode using EDS.

No significant energy peak of potassium was detected during the EDS semi-quantitative analysis which confirms that a simple washing step allows to quantitatively remove the electrolyte from the negative electrode. The spectrum confirms that this NiMH battery type is made of an  $AB_5$  negative electrode composed of 59.2 and 12.5 atom. % of nickel and cobalt doped with 6.7 atom. % of manganese. Regarding REEs, the mischmetal is composed of 7.8 and 5.7 atom. % of cerium and lanthanum respectively. Finally, minor rare earth elements can be found such as 2.3 and 0.8 atomic percent of neodymium and praseodymium respectively.

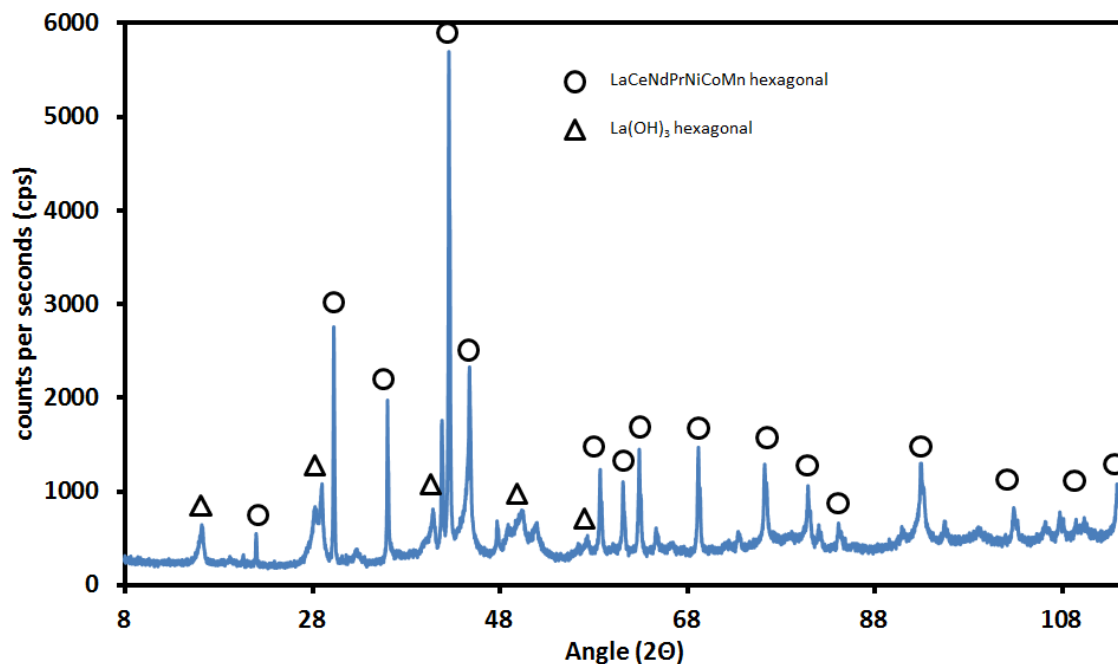


**Figure II.5.** X-ray diffractogram of the washed negative electrode. Circles are used to identify the anode intermetallic material, namely hexagonal LaCeNdPrNiCoMn, while triangles define lanthanum hydroxide hexagonal peaks.

XRD analysis brings information on the structure and composition of the mischmetal. According to the X-ray diffractogram displayed in **Figure II.5**, and in agreement with the literature, the negative electrode is an intermetallic compound made of REE (La, Ce, Nd, Pr) and TM (Ni, Co, Mn). However, the presence of lanthanum hydroxide is also highlighted. One should keep in mind that this battery is in its end of life and has thus undergone some degradation. *Zhou et al. 2013*<sup>231</sup> reported a comprehensive study of the degradation mechanisms of NiMH positive and negative electrodes AB<sub>5</sub> and A<sub>2</sub>B<sub>7</sub>. After cycling AB<sub>5</sub> cells until observing a loss of 80 % of their initial capacity delivery, X-ray diffractograms of the negative electrode were reported. Interestingly, the presence of La(OH)<sub>3</sub> was spotted in the alloys due to the oxidation of the intermetallic compound under the influence of potassium hydroxide electrolyte.<sup>231</sup> This corrosion phenomenon is known to lead to the failure of NiMH secondary batteries and justifies the presence of lanthanum hydroxide in our powder.<sup>21,22,231</sup>

To summarize, the negative electrode has been identified as the most promising part of the NiMH battery because it contains high concentration of valuable metals. We report the possibility of isolating this active material from the positive

electrode, the separator, and the electrolyte by mechanical treatment and a washing step. A full characterization of the powder has been performed and highlights the presence of 59.2 % Ni, 12.5 % Co, 6.7 % Mn, 5.7 % La, 7.8 % Ce, 2.3 % Nd, 0.8 % Pr (data are given in atomic percentages) under the form of an intermetallic compound and lanthanum hydroxide. The latter is a result of the degradation of the electrode at the end-of-life of the device. Interestingly, the overall concentration of REE in the active material is of 16.6 atom. % and is thus twice to ten times superior to what can be found in natural ores such as bastnaesite, loparite and monazite (See part **I.2.3**). This justifies the denomination of “secondary mining” used to describe recycling processes.

This material will be considered as an ideal model raw material, to optimize the recycling process of NiMH batteries.

## **II.2.2 Industrial scale black mass production**

### **a. The Recupyl<sup>®</sup> process**

Opening manually NiMH batteries one by one, and isolating the electrodes is easy to carry out in a laboratory scale process but is not viable in a large scale industrial process. Recupyl<sup>®</sup> is a company recycling in average 720 tons of Li-ion batteries per year. This recycler has thus a strong experience in mechanical treatments of electrochemical devices. In order to build a recycling process for NiMH batteries, black mass was obtained from real end-of-life devices collected, grinded and mechanically treated thanks to the Recupyl<sup>®</sup> facilities according to the following process:

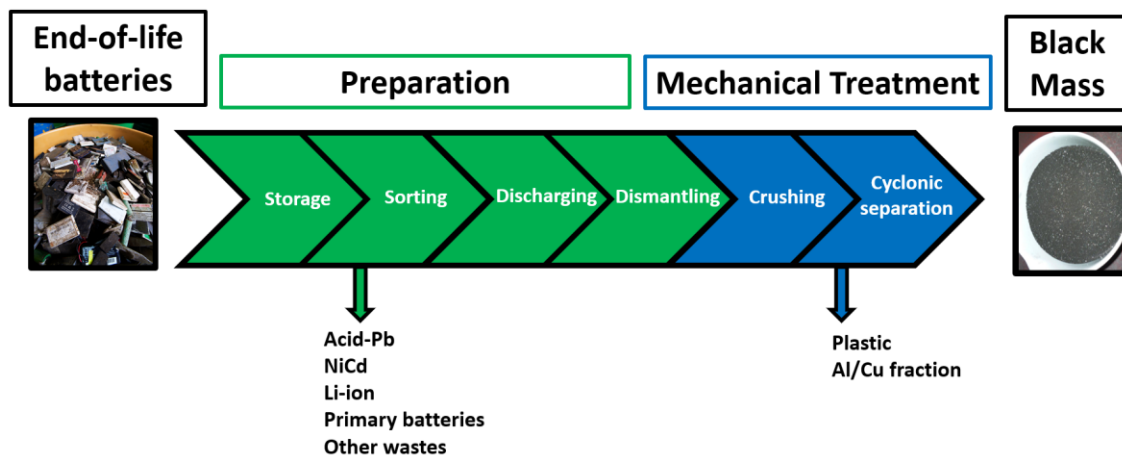


**Figure II.6.** Process for the production of NiMH black mass from the recycler Recupyl<sup>®</sup>.

When end-of-life batteries arrive in the recycling center of Recupyl<sup>®</sup>, they are firstly stored in a vermiculite insulator to prevent the electrochemical systems of creating short circuits. In a second step, they are manually sorted. Li-ion batteries are separated from NiMH systems. Other technologies such as Acid-Pb, primary batteries and NiCd are transferred to appropriate recycling centers. Large automotive modules are discharged for security reasons. They are usually dismantled to remove the plastic outer shell and some strategic components that can return to the automotive constructor. They are subsequently crushed in a hammer mill. This allows the recycler to obtain particles between 1 and 10 mm. A second crusher can even obtain particles below 1 mm. It is important to notice that crushing NiMH batteries can be performed without controlling the atmosphere. This is not the case of Li-ions systems crushed in a carbon dioxide controlled pressure to prevent the organic flammable solvent, and the lithium metallic dendrites from catching fire. In a last step, the metallic powder is separated from plastics and some light metals such as copper and aluminum by a cyclonic separation. The latter separation consists of inducing compressed air in a cone to trigger light particles and isolate them from a heavy metallic fraction. Regarding the Recupyl<sup>®</sup> process using NiMH batteries, this fraction is mainly composed of crushed electrodes and metallic grids and is defined as the black mass (BM). The production rate can reach  $800 \text{ kg}\cdot\text{h}^{-1}$ .

The powder was washed and dried according to the procedure detailed in part II.2.1.

b. Characterization of the black mass

The washed BM was qualitatively analysed by SEM using imaging via BSE and semi-quantitatively evaluated thanks to EDS in **Figure II.7** and **Table II.3** respectively.

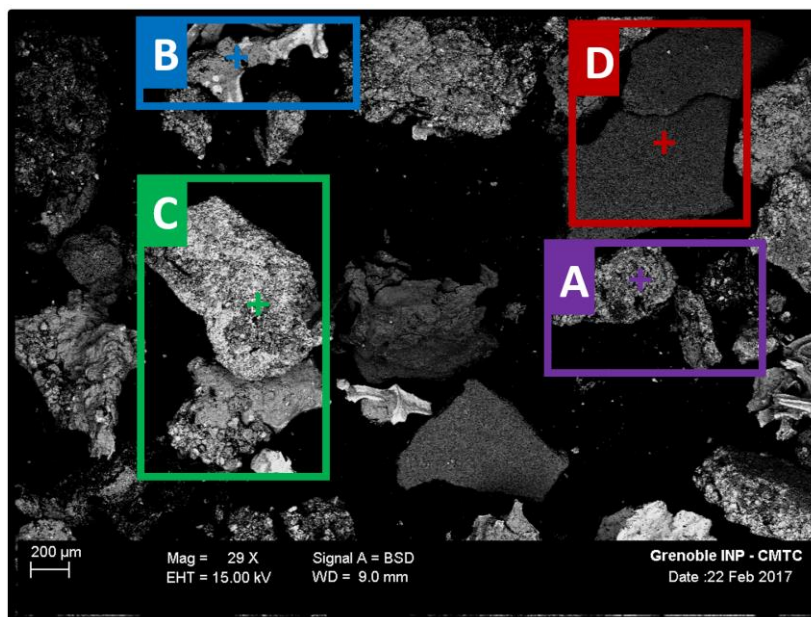


**Figure II.7.** SEM images of washed BM produced at Recupyl<sup>®</sup> (magnification  $\times 29$ ) performed with BSE. Purple A: Positive electrode. Blue B: grid. Green C: Negative electrode. Red D: Other components.

Elements	Composition (atom. %)			
	A: Positive electrode	B: Grid	C: Negative electrode	D: Other component
Fe	$4.9 \pm 0.3$	$9.1 \pm 0.7$	$8.2 \pm 0.6$	$100 \pm 0$
Ni	$88.5 \pm 3.3$	$86.2 \pm 3.5$	$63.4 \pm 3.1$	-
Co	$6.6 \pm 0.2$	$4.7 \pm 0.2$	$10.3 \pm 0.8$	-
Mn	-	$0.2 \pm 0$	$3.7 \pm 0.1$	-
REE	-	$2.1 \pm 0.1$	$14.4 \pm 2.9$	-
K	-	-	-	-

**Table II.3.** Elemental analysis of washed BM produced at Recupyl<sup>®</sup> using EDS.



Unlike what was observed while opening a battery in a laboratory scale process, the powder obtained is much more complex since all the electrodes are mixed together. SEM analysis by BSE displayed in **Figure II.7** presents different grayscales and demonstrates the heterogeneity in the composition of the particles. Four different areas are highlighted in this BM. The metallic grid presenting a characteristic shape framed in blue (area B) is easy to identify. Similarly to what has been shown with the commercial battery from SUPPO<sup>®</sup>, the grid is composed of nickel and iron (see **Table II.1**). However, presence of 4.7 atom. % Co and 2.1 atom. % REE are detected. It is not surprising to find those elements mixed together as the negative electrode containing nickel, cobalt, manganese and REE is deposited on the grid in a NiMH battery. A particle was identified as being part of the negative electrode (area C, framed in green). Even if it is most probably mixed with the metallic grid due to the presence of 8.2 atom. % of iron, the particle confirms the presence of AB<sub>5</sub> negative electrode as 14.4 and 10.3 atom. % REE and Co are present respectively in the intermetallic compound. Darker particles were also spotted in area A (framed in purple) composed of 88.5 atom. % of nickel and small amounts of cobalt. They were identified as the Ni(OH)<sub>2</sub> positive electrode doped with Co (6.6 atom. %). Finally, a fourth and last area, namely D, framed in red was spotted. Those particles are the darkest and seem to be composed of iron oxide. This material does not enter in the composition of the active material of a NiMH battery. However, this can be part of one of the numerous components encapsulating the electrodes. No trace of electrolyte was found in the powder. In a nutshell, the black mass obtained from end-of-life NiMH batteries according to the Recupyl<sup>®</sup> process is a mixture between positive (Ni, Co) and negative electrodes (Ni, Co, Mn, REE), metallic grids (Ni, Fe) and various battery components. Furthermore, because the cyclonic separation does not lead to a full isolation of light particles, some plastic residues can be found in the BM. This black mass will be used in this work as a raw material to build a complete recycling process of NiMH batteries.

## II.3 Leaching

---

### II.3.1 Preliminary tests with an ideal black mass

#### a. Introduction

This part was performed following the supervision of *Malaurie Debon*, during her Master 1 research internship.

The leaching step stands in this work for the dissolution of valuable elements from the BM into an aqueous solution by oxidizing a metal into a cation. For more information on this step, please refer to **part I.4.2**. Before carrying out leaching experiments with the NiMH black mass produced at Recupyl<sup>®</sup>, preliminary experiments were undergone with a model raw material extracted from an end-of-life battery (**part II.2.1**). The literature review from the previous chapter highlighted an important heterogeneity in the conditions needed to obtain a full leaching of NiMH active materials.<sup>154,155,157,159,160</sup> Dissolution of metals was investigated for temperatures ranging from 20 to 80 °C, concentrations ranging from 1 to 6 mol.L<sup>-1</sup> and reaction times ranging from 0.5 to 6 hours. The influence of those three parameters on the leaching of all metals will be now detailed and discussed.

#### b. Experimental

1 g of the recovered negative electrode was mixed with 10 ml of sulfuric acid between 0.5 and 3.0 mol.L<sup>-1</sup> under stirring between 25 and 80 °C. After 10 min to 3 hours of reaction, the leachate was separated from the solid residue by filtration on a Büchner setup. The solid was then washed several times with water. It was then dried on a pre-weighed filter in an oven at 80 °C during 12 hours before being cooled down to room temperature in a desiccator and weighed. In order to follow the efficiency of the reaction, the leaching yield ( $Y_L$ ), expressed in weight percent, was defined according to the following equation.

$$Y_L = \frac{m_f - m_i}{m_{BM}} \times 100 \quad (27)$$

where  $m_{BM}$  stands for the mass of BM initially used in the leaching step, usually, around 1 g.  $m_i$  and  $m_f$  represent the mass of the filter before and after filtration respectively.

The solid residue was scratched and removed from the filter and analysed by SEM. The volume of the leachate was adjusted to 25 ml with H<sub>2</sub>O by transferring the solution in a graduated flask. Controlling the volume of leachate in the latter step is a manner to control the quantity of metal leached and thus the balance of matter for the overall process. Finally, the aqueous solution was analysed using Inductively Coupled Plasma (ICP) in order to measure the concentration of metals in solution. Technical details regarding ICP analysis will be provided in **ANNEX 1-C**.

### c. Results and discussion

#### *Comparison with the literature*

According to the work from *Innocenzi and Vegliò, 2012*,<sup>159</sup> a first leaching experiment, namely *A* was carried out using 2 mol.L<sup>-1</sup> H<sub>2</sub>SO<sub>4</sub> at 80 °C during 3 hours. A second leaching *B* was performed at 20 °C with 1 mol.L<sup>-1</sup> sulfuric acid during 3 hours. The EDS diagram and elemental composition of both solid residues and leachate solutions are displayed in **Figure II.8** and **Table II.4**.

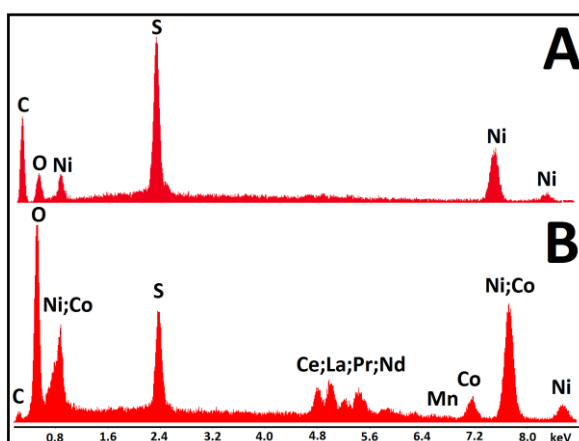


**Figure II.8.** EDS spectra of solid residue after leaching *A*: 2 mol.L<sup>-1</sup> H<sub>2</sub>SO<sub>4</sub> at 80 °C during 3 hours. Leaching *B* 1 mol.L<sup>-1</sup> H<sub>2</sub>SO<sub>4</sub> at 20 °C during 3 hours.

Solid residue composition (atom. %)		Leachate composition (mg.L <sup>-1</sup> )		
Elements	Leaching A	Leaching B	Leaching A	Leaching B
Ni	100 ± 0	65.7 ± 1.1	16690 ± 50	13141 ± 50
Co	-	11.8 ± 0.4	3081 ± 50	2426 ± 50
Mn	-	0.8 ± 0.2	1249 ± 50	659 ± 50
La	-	6.7 ± 0.4	1607 ± 10	1079 ± 10
Ce	-	9.0 ± 0.6	2201 ± 10	1287 ± 10
Nd	-	4.5 ± 1.2	646 ± 10	380 ± 10
Pr	-	1.5 ± 0.8	457 ± 10	285 ± 10

Leaching yield (wt. %)		Leachate composition (mg.g <sup>-1</sup> of BM)		
-	Leaching A	Leaching B	Leaching A	Leaching B
Y <sub>L</sub>	96.37	81.85	-	-

Elements	Ni	Co	Mn	La	Ce	Nd	Pr
	417.3 ± 1.2	77.0 ± 1.2	31.2 ± 1.2	40.2 ± 0.3	55.0 ± 0.3	16.1 ± 0.3	11.4 ± 0.3
		60.7 ± 1.2	16.5 ± 1.2	27.0 ± 0.3	32.2 ± 0.3	9.5 ± 0.3	7.1 ± 0.3

**Table II.4.** Elemental analysis of the solid residue after Leaching A and B by EDS. Only metallic species, namely TM and REE are quantified. Leachate composition analysed by ICP. Leaching yield (Y<sub>L</sub>) calculated by weighing the solid residue.

In full agreement with what was reported in the literature,<sup>159,160</sup> Leaching A leads to the dissolution of more than 96 wt. % of the negative electrode. The remaining residue is mainly composed of nickel and sulfur mixed with carbon particles (**Figure II.8** and **Table II.4**). The presence of sulfur is due to H<sub>2</sub>SO<sub>4</sub>. A thin layer of nickel is still present after leaching and was previously reported to be very difficult to dissolve without the use of oxidant species.<sup>160</sup> As described in **part I.1.3**, the negative electrode is known to be coated with a thin layer of metallic nickel to enhance the conductivity of the active material. However nickel is known to passivate in sulfuric media.<sup>232,233</sup> This phenomenon can hinder the oxidation mechanism of the metal and thus limit its dissolution in the leachate. In our opinion, it is thus of little relevance to use strong oxidant such as oxygen peroxide to recover a negligible amount of passivated nickel. Furthermore, this non-

oxidized metal is already pure and could be separated from the remaining carbon by magnetic-separation. Looking at the leachate, analysed by ICP, all the metal seems to be present in proportion corresponding to the nature of the NiMH negative electrode.

Focusing on experiment *B*, the trend is much different. The leaching yield reaches only 81.8 wt%, which is significantly lower than that obtained in experiment *A*. Regarding the remaining solid residue, it is still composed of TM (Ni 65.7, Co 11.8 and Mn 0.8 wt. %) and REE (La 6.7, Ce 9.0, Nd 4.5 and Pr 1.5 wt. %). Atomic ratios for each element are extremely close to those found in the raw negative electrode before leaching. In other words, no selectivity in the leaching from one metal to another was observed. Transition metals and rare earth elements thus seem to dissolve with the same kinetics. This is confirmed by ICP analysis of the leachate in **Table II.4**. No unexpected ratio of any elements was detected. However, the solution presents for all TM and REE lower concentrations in leachate *B* compared to leachate *A*. For 1 g of negative electrode, leaching *B* is oxidizing and dissolving 88.7 mg of nickel less than in leaching *A*. The values are of 16.4 and 47.0 mg for cobalt and rare earth elements.

### *Results*

According to those 2 preliminary experiments, we will define a leaching as successful if:

- The leaching yield is superior to 90 wt. %
- The remaining solid residue only contains nickel among the valuable elements (Ni, Co, Mn, La, Ce, Nd, Pr).

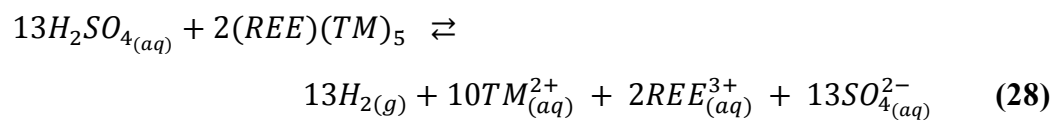
If any of those two conditions is not respected, the leaching will be considered as incomplete. As a result, leaching *A* is considered as successful while *B* is incomplete.

To study the impact of experimental conditions on the leaching efficiency, several tests were carried out using different sulfuric acid concentrations, temperatures and reaction times. Each leaching will be defined to be successful or incomplete according to the two previous conditions. Leaching yields will be reported. Some

experiments will be repeated twice to determine the experimental error. Results are shown in **Figure II.10**.

Visually, all leachates obtained presented light to dark green colors ranging on the amount of nickel in solution. Snapshots are provided in **Figure II.9**.

The previous process leads to an exothermic reaction and produces hydrogen. As a result, heat and bubbles production can be observed in the reactor. The formation of hydrogen and the oxidation of TM and REE by  $H_2SO_4$  for an  $AB_5$  negative electrode is reported in the following equation.



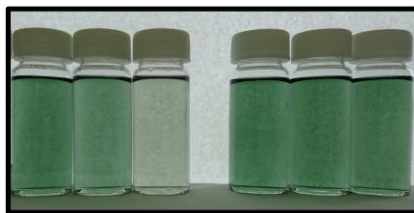


**Figure II.9.** Snapshots of several leachates

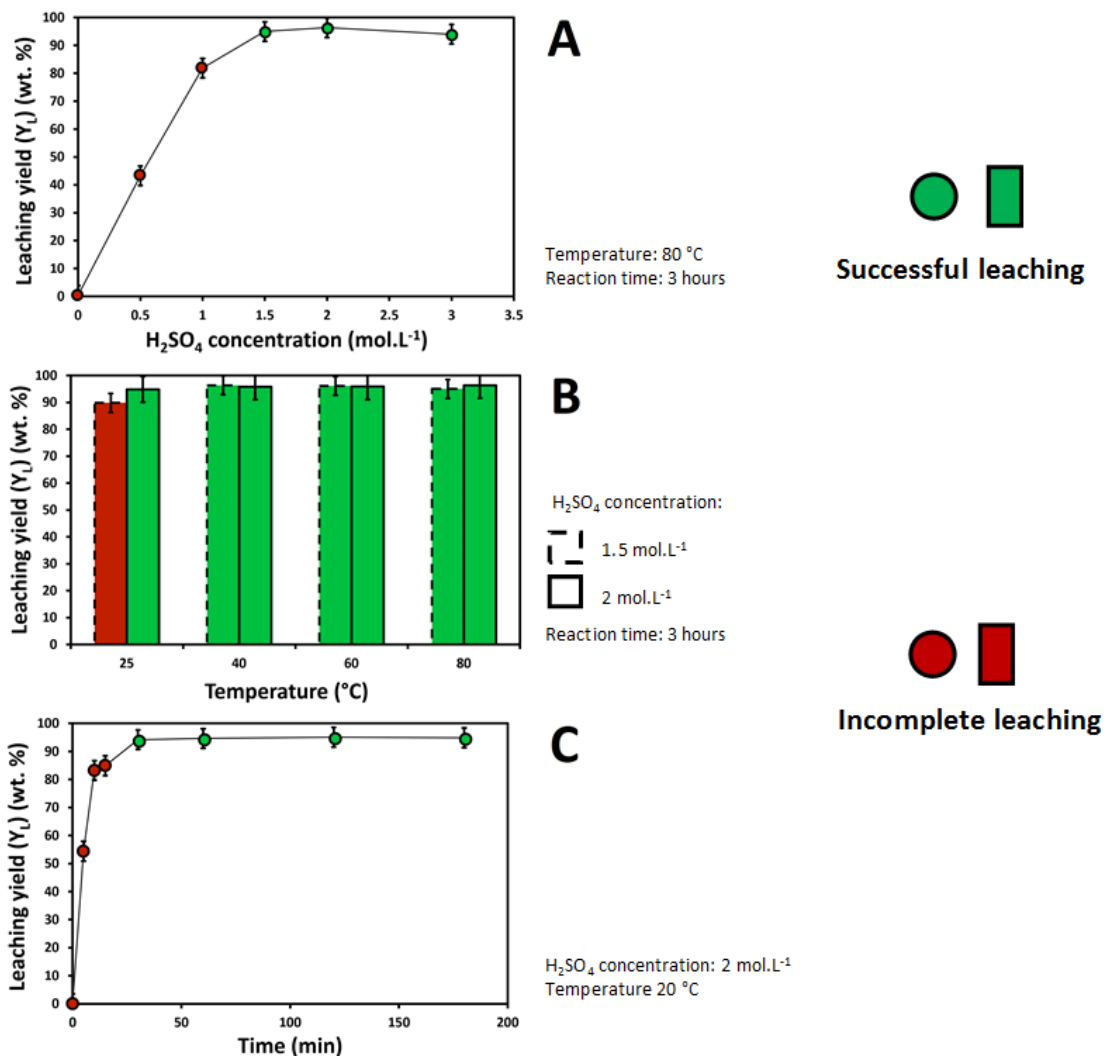


**Figure II.10.** Investigation on the influence of temperature, sulfuric acid concentration and reaction time on the leaching of NiMH negative electrodes.

Green dot or bar refers to a successful leaching while red dot or bar stands for incomplete leaching. A: Influence of the  $H_2SO_4$  concentration from 0 to 3  $mol.L^{-1}$  was investigated at 80 °C for 3 hours reaction time. B: Influence of the temperature from 25 to 80 °C was investigated at 1.5 and 2  $mol.L^{-1}$  in dotted and

full frame line respectively. Reaction time was set to 3 hours. C: Influence of reaction time from 5 to 180 min was investigated at 20 °C using 2 mol.L<sup>-1</sup> H<sub>2</sub>SO<sub>4</sub>.

#### *Optimization of the sulfuric acid concentration*

The first leaching experiments were undertaken at 80 °C with a reaction time of 3 hours. The sulfuric acid concentration was adjusted from 0 to 3 mol.L<sup>-1</sup>. Leaching yield are provided in **Figure II.10-A**. The efficiency of the dissolution of the negative electrode increases with the acidic concentration from 0 to 1.5 mol.L<sup>-1</sup> where  $Y_L$  reaches a value of 95.0 wt. %. Then a plateau is observed from 1.5 to 3 mol.L<sup>-1</sup>, no significant change in the leaching yield is reported in this H<sub>2</sub>SO<sub>4</sub> concentration range. The leaching was considered as incomplete in the range 0 to 1 mol.L<sup>-1</sup> as the solid residue was superior to 10 wt. % of the initial active material mass. Furthermore, Co, Mn and REE were found in the residue, as shown in **Figure II.8-B** and **Table II.4**. However, all leaching experiments carried out at 1.5 mol.L<sup>-1</sup> or at higher concentration led to a solid residue solely composed of passivated nickel.

#### *Characterization of the solid residue*

To confirm the latter statement, XRD analysis of the solid residue after leaching the powder with 2 mol.L<sup>-1</sup> at 25 °C was reported in **Figure II.11**.

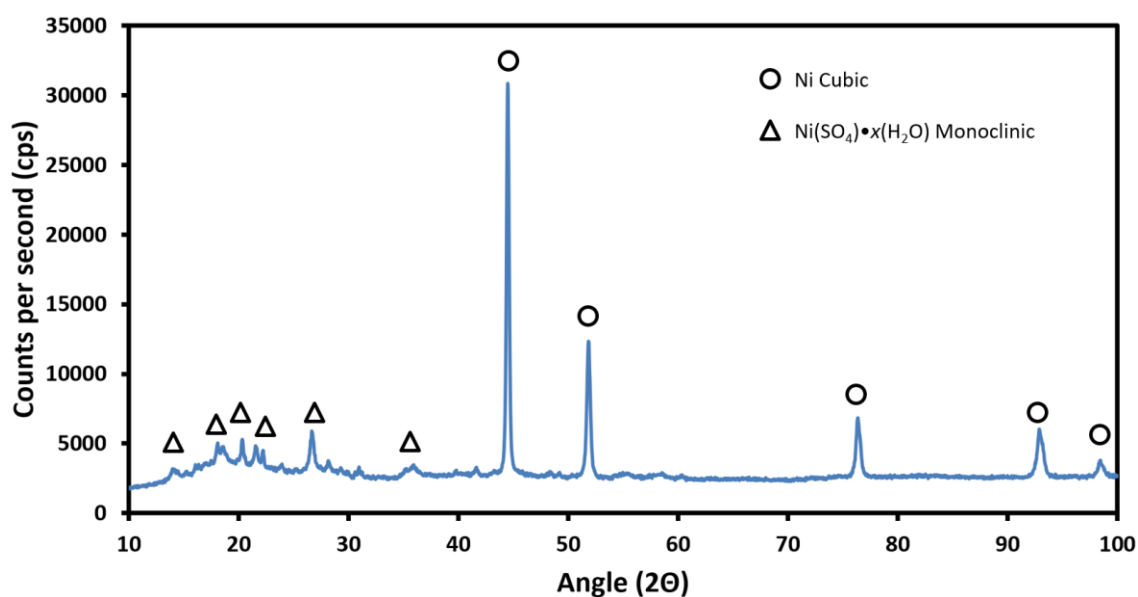


**Figure II.11.** XRD analysis of the solid residue after leaching a NiMH ideal black mass produced at a laboratory scale with H<sub>2</sub>SO<sub>4</sub> 2 mol.L<sup>-1</sup> at 25 °C. Circles and triangles are used to identify nickel cubic and hydrated nickel sulphate monoclinic peaks respectively.



The X-ray diffractogram provided in **Figure II.11** confirms the presence of raw metallic nickel and low amounts of nickel sulphate salts after leaching. It is interesting to compare this result with the X-ray diffractogram of the washed negative electrode provided in **Figure II.5** to appreciate the leaching efficiency of our process as all peaks corresponding to cobalt, manganese and even REE disappeared.

#### *Optimization of temperature*

With the aim of using minimum amounts of acid, leaching at  $1.5 \text{ mol.L}^{-1} \text{ H}_2\text{SO}_4$  was identified as efficient to leach our material at  $80 \text{ }^\circ\text{C}$ . In a further optimization step, the influence of the temperature on the leaching yield was investigated. Results shown in **Figure II.10-B** reveal that the leaching is incomplete at  $80$ ,  $60$  and  $40 \text{ }^\circ\text{C}$ . Experiments carried out at  $25^\circ\text{C}$  led to an incomplete oxidation of metals ( $Y_L = 89.83 \text{ wt. } \%$ ). SEM analysis highlighted the presence of cobalt and REE in the solid residue.

A similar set of experiments was conducted with slightly higher concentrations of acid, namely  $2 \text{ mol.L}^{-1}$ . Results, also presented in **Figure II.10-B** show that leaching was complete, whatever the temperature. At  $25 \text{ }^\circ\text{C}$ ,  $94.86 \text{ wt. } \%$  of the powder is leached. The remaining solid was found to be composed of carbon and nickel only. For an industrial process, a room temperature leaching step is preferred over a process where temperature needs to be monitored. Consequently, leaching using  $2 \text{ mol.L}^{-1} \text{ H}_2\text{SO}_4$  at  $25^\circ\text{C}$  was selected as the best option.

#### *Optimization of reaction time*

Finally, the influence of the reaction time on the leaching of the negative electrode was studied. As shown in **Figure II.10-C**, seven additional leaching experiments were carried out at  $5$ ,  $10$ ,  $15$ ,  $30$ ,  $60$ ,  $120$  and  $180 \text{ min}$ , accordingly. Surprisingly and unlike what is reported in the literature,<sup>154,155,157,160</sup>  $30 \text{ min}$  of reaction time seemed sufficient to achieve a complete leaching of our NiMH negative electrodes. A plateau in the leaching yield is observed between  $30$  and  $180 \text{ min}$  ranging in values of  $94.17$  and  $94.86 \text{ wt. } \%$ .  $3 \text{ h}$  reaction time as used in all previous tests thus appears unnecessary.

During one set of experiments carried out at room temperature (25 °C) and without using a thermostat, the temperature of the solution was found to increase. This is simply due to the oxidation and dissolution of metals that appear to be exothermic reactions. To gain better insight in the leaching step and understand the reasons for an efficient leaching at room temperature, a final leaching experiment was thus undertaken at room temperature with 2 mol.L<sup>-1</sup> H<sub>2</sub>SO<sub>4</sub>. The temperature was monitored with a thermometer in a closed reactor. Evolution of temperature function of reaction time is reported in **Figure II.12**.

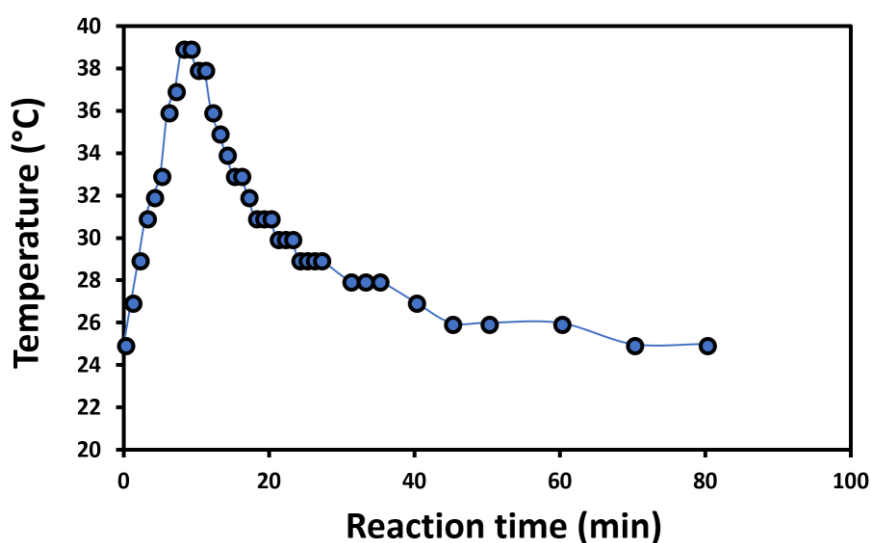


**Figure II.12.** Exothermicity of the leaching reaction

The temperature starting from 25 °C, reached a maximum at 35 °C after 13 min. After that, temperature decreased during 17 min to reach 28 °C. This reveals that increases in temperature can be observed in the reactor, even without heating it up. This phenomenon is favorable to achieve high  $Y_L$  values. It is interesting to notice that after 30 min, the reaction does not produce anymore heat which can be a good indicator to show that the oxidation process has been completed. It is important to point out that those temperature measurements were undergone using 1 g of BM. A scale up of this process using higher amounts of intermetallic powder will most likely lead to higher temperatures during the leaching step.

#### d. Conclusion

Optimization of several parameters, namely, temperature, acidic concentration and reaction time was investigated, with the aim of developing an efficient process for the recycling of metals from NiMH batteries. We showed that the leaching of a model solution can be significantly optimized using  $2 \text{ mol.L}^{-1} \text{ H}_2\text{SO}_4$  at room temperature during a very short amount of time. We report for the first time the ability of reaching a complete dissolution of the negative electrode in only 30 min. However, the difference observed comparing our work to the literature is highly correlated to the mechanical treatment performed to produce the black mass. Because each NiMH brand, will present different manufacture techniques, composition, particle size etc... this work is unlikely to be completely reproducible for all types of NiMH electrochemical systems. To tackle this issue, leaching experiments need to be performed with a large range of different NiMH batteries where the black mass has been produced at an industrial scale.

### II.3.2 Leaching NiMH black mass produced at Recupyl®

#### a. Introduction

This part was performed following the supervision of *Marie Lemire*, during her third-year bachelor internship.

Up to our knowledge, leaching experiments using spent NiMH batteries as Waste Electrical and Electronic Equipment (WEEE) grinded and mechanically treated at an industrial scale were never studied. Most works were performed with new NiMH batteries manually opened in the laboratory.<sup>153,154,234</sup> In the latter works, the leaching process was performed with one type of system, brand and geometry which is interesting for the fundamental understanding of the process but is far from the raw material obtained in a real recycling center. It is worth noticing that *Porvali et al. 2018*<sup>156</sup> used different types of spent NiMH batteries collected in several recycling sites in Sao Paulo, Brazil. However, the mechanical treatment process used is fully manual and can't be directly scaled-up to a real industrial

production. In this part, we will perform leaching experiments with black mass produced at the recycling company Recupyl<sup>®</sup> and thus tackle the issue of the reproducibility of such process at a large scale.

b. Experimental

The black mass production and characterization has been reported in **part II.2.2**. The granulometry of the two BM samples is in line with the mechanical treatment carried out by Recupyl. One powder presents particle size between 1 and 10 mm while the other is composed of particles lower than 1 mm. Snapshots of the BM are given in **Figure II.13**.

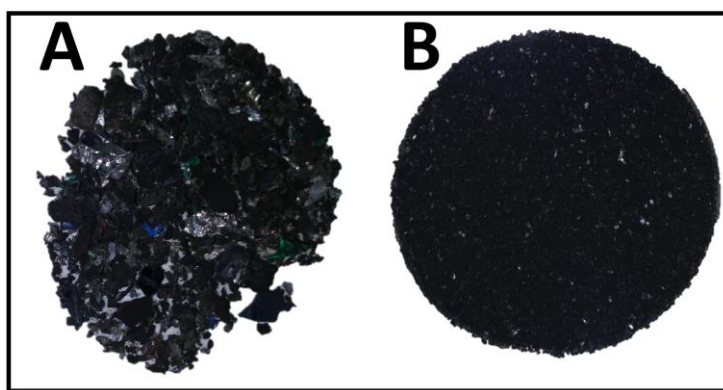


**Figure II.13.** Snapshots of the two different BM granulometries from the Recupyl<sup>®</sup> process. A: particle size between 1 and 10 mm. B: particle size lower than 1 mm.

All leaching experiments were performed during one hour using sulfuric acid ( $\text{H}_2\text{SO}_4$ ), hydrochloric acid ( $\text{HCl}$ ) with concentrations ranging from 0.5 to 10  $\text{mol.L}^{-1}$ . 1 g of BM was used for 10 ml of leaching solution. The mixture was mechanically stirred on a magnetic plate under controlled temperature before being filtrated on a Büchner setup. From then, *the modus operandi* is identical to the one used in **part II.3.1**. The residue was washed several times with water. It was then dried on a pre-weighed filter in an oven at 80 °C during 12 hours before being cooled down to room temperature in a desiccator and weighed. In order to follow the efficiency of the reaction, the leaching yield ( $Y_L$ ), was used. The residue was scratched and removed from the filter. The volume of the leachate was adjusted to 25 ml with  $\text{H}_2\text{O}$  by transferring the solution in a graduated flask. Finally, the aqueous solution was analysed using ICP. The leachate composition is expressed in milligrams of oxidized metal in the aqueous phase per gram of BM. Influence of

the particle size, temperature, nature and concentration of the leaching phase will be studied with the aim of choosing optimum parameters for the leaching of real spent NiMH batteries. Characterization of the solid residue obtained after applying the selected parameters will be undergone by SEM and XRD.

c. Results and discussion

According to the process for the production of black mass at an industrial scale, the separation of light from heavy particle by cyclonic separation is not quantitative. A non-negligible amount of plastic and undesirable components can be present in the BM (see **Figure II.13**). Solid residue and leachate composition will thus be impacted by those new elements. Comparison between experiments will thus be discussed in terms of leaching yield and of amount of oxidized metal per gram of black mass.

*Influence of the size particle.*

Leaching tests were performed with sulfuric and hydrochloric acid between 0.5 and 4 mol.L<sup>-1</sup> at 25, 50 and 75 °C with BM particles above and below 1 mm. Leaching yields are reported in **Figure II.14**.

It appears that whatever the nature of the acid or the temperature,  $Y_L$  is always higher starting from the powder containing particles with a diameter below 1 mm. This is due to the fact these particles exhibit a larger surface area compared to the BM composed with larger particles. Furthermore a reproducibility issue appears when 1 g of BM composed with larger particles is used. For instance, it can contain a large piece of grid or of plastic that will decrease the amount of valuable and oxidable metals. As a result,  $Y_L$  for large particles will vary significantly between two identical experiments and will exhibit an important uncertainty. This issue could be tackled by performing leaching experiments with larger amounts of BM or with a thinner powder. Indeed, the black mass presenting particles below 1 mm is very homogeneous from one test to another while sampling 1 g. Consequently, leaching experiments at 25 °C using 2 mol.L<sup>-1</sup> of sulfuric acid lead to  $Y_L$  of  $45.6 \pm 9.2$  and  $85.1 \pm 2.1$  % respectively for coarse and thin powder. Those values are of  $57.6 \pm 11.5$  and  $74.1 \pm 1.8$  % respectively using hydrochloric acid.

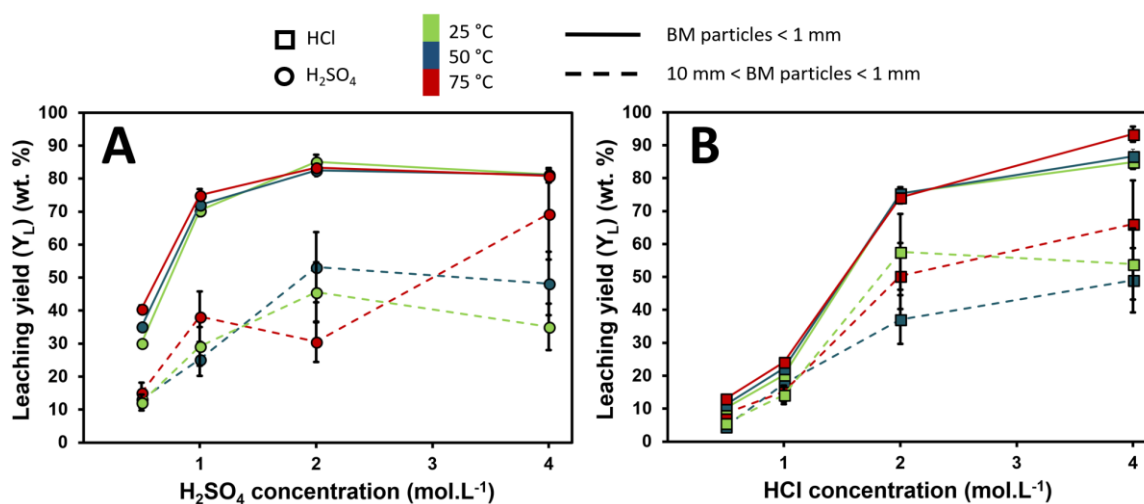


**Figure II.14.** Leaching of NiMH black mass containing particles below 1 mm in full line and with coarse particles between 1 and 10 mm in dotted line. Experiments were undertaken at 25, 50 and 75 °C in green, blue and red respectively. A: The leachate is an aqueous solution containing sulfuric acid. B: The leachate is an aqueous solution containing hydrochloric acid.

#### *Influence of the inorganic acid nature and concentration*

Leaching experiments were performed with hydrochloric and sulfuric acid between 0.5 and 10 mol.L<sup>-1</sup> at 25, 50 and 75 °C with BM particles below 1 mm. Leaching yields but also compositions of some leachates are reported in **Figure II.15**.

Using hydrochloric acid, the leaching yield increases strongly and linearly with the acidic concentration. Y<sub>L</sub> values of 10.2 and 75.4 % are found using 0.5 or 2 mol.L<sup>-1</sup>, accordingly. In this concentration range, the temperature has a little impact on the leaching yield and on the amount of metals oxidized in the leachate. However, regarding REE, it appears that the higher the temperature, the lower the ability to solubilize La, Ce, Nd and Pr. As an example, leaching 1 g of BM with 2 mol.L<sup>-1</sup> HCl led to the presence of 18.2, 11.8 and 1.1 mg of lanthanum at 25, 50 and 75 °C respectively in the leachate. Those values are of 11.9, 5.7 and 2.3 mg for cerium under the same conditions.

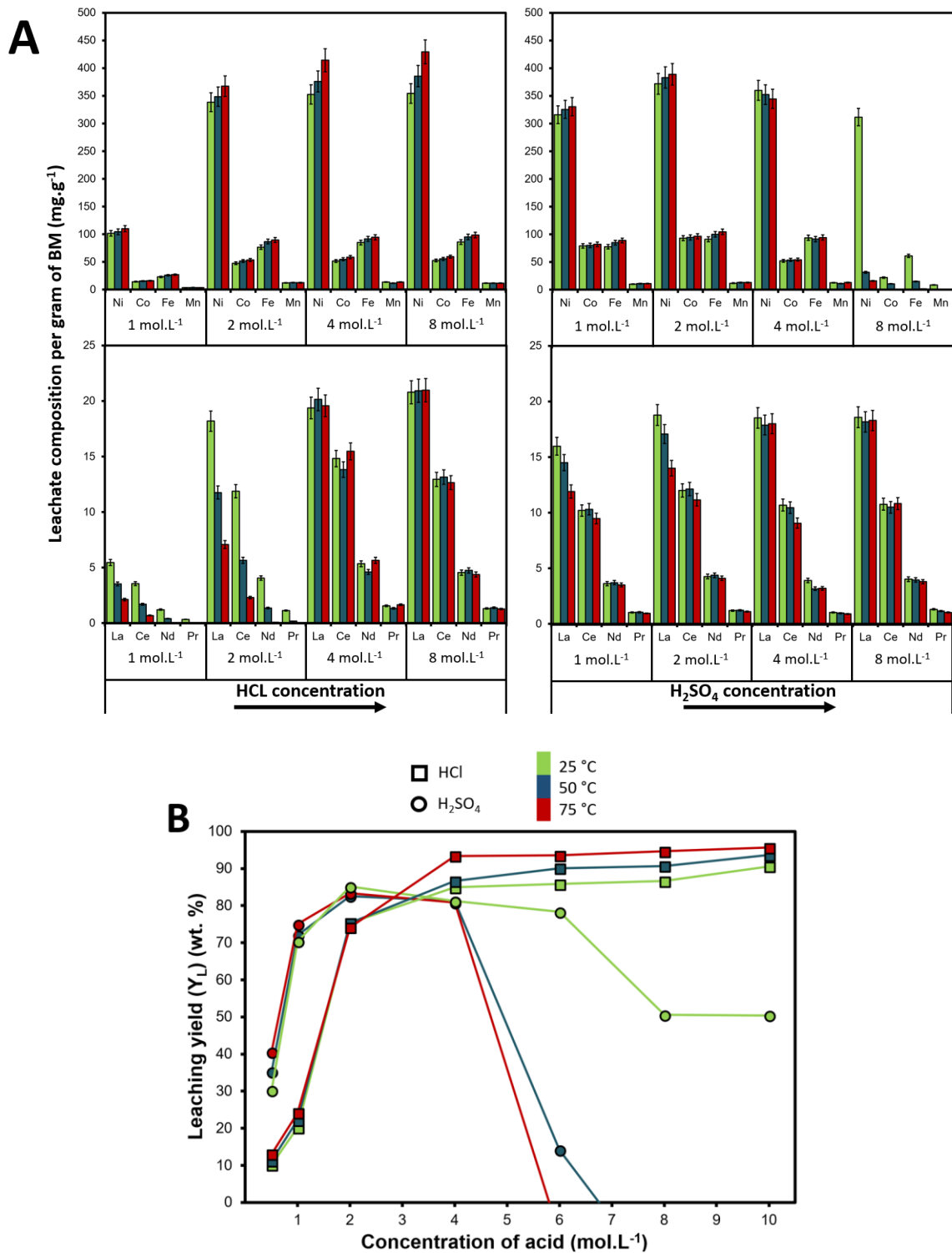


**Figure II.15.** Leaching NiMH black mass produced at Recupyl<sup>®</sup> with particle size below 1 mm. Leachate composed of an aqueous solution containing between 0.5 and 10  $\text{mol}\cdot\text{L}^{-1}$  H<sub>2</sub>SO<sub>4</sub> or HCl. Temperatures were set at 25, 50 and 75 °C in green, blue and red respectively. **A:** composition of metals in the leachate after filtration for experiments at 1, 2, 4 and 8  $\text{mol}\cdot\text{L}^{-1}$  H<sub>2</sub>SO<sub>4</sub> or HCl. **B:** Leaching yield ( $Y_L$ ) for sulfuric and hydrochloric acid in circles and squares respectively.

This phenomenon is closely correlated to the drop in solubility of REE when temperature increases.<sup>230</sup> However, by increasing the concentration of HCl, the solubility of lanthanum, praseodymium and neodymium salts is known to increase.<sup>230</sup> As a result, the influence of temperature on the leaching of REE is compensated by that of the acidity for HCl concentrations between 4 and 8 mol.L<sup>-1</sup>. In this concentration range, the leaching yields reported in **Figure II.15-B** hardly increase. Values of 84.9 and 90.6 % for  $Y_L$  at 2 and 10 mol.L<sup>-1</sup> and 25 °C are obtained. Focusing on the composition of transition metals, **Figure II.15** highlights that one additional metal can be found in the leachate compared to the preliminary leaching with model raw materials performed in **part II.3.1**. Indeed, iron is present in a ratio Ni/Fe close to 4.5 in all cases. The presence of this new metal is not surprising as iron is part of the composition of the metallic grid where the negative electrode is deposited.

Broadly speaking, all TM are increasingly oxidized in the leachate with the temperature. Interestingly, comparing the leaching at 4 mol.L<sup>-1</sup> 25 °C and the one at 8 mol.L<sup>-1</sup> 75 °C which lead to  $Y_L$  of 75.4 and 94.7 % respectively, the amount of recovered nickel, for 1 g of BM increases from 352.4 to 429.6 mg respectively. The amount of cobalt (51.7 and 59.43 mg) and manganese (13.6 and 13.7 mg) does not change significantly when increasing the acidic concentration from 4 to 8 mol.L<sup>-1</sup> and the temperature from 25 to 75 °C. In other words, the little increase of the oxidation yield found between those two experiments is most probably due to the additional leaching of nickel solid residue remaining in the powder as this metal is less likely to passivate in a chloride media compared to a sulphate one.

Results for the leaching experiments carried out with sulfuric acid are presented in **Figure II.15-B**.  $Y_L$  increases from 0.5 to 2 mol.L<sup>-1</sup> reaching a maximum of 85.1 % at 25 °C. H<sub>2</sub>SO<sub>4</sub> thus seem to be more efficient to dissolve the NiMH black than HCl ( $Y_L = 75.4$  %) in this concentration range. Temperature does not seem to have an impact on the global amount of powder leached in this concentration range. Nevertheless, similarly to what was observed with HCl, increasing temperature is slightly favorable to dissolve transition metals but is highly unfavorable in the leaching process of rare earth elements. However, an unexpected trend is reported at high acidic concentrations. In this case, the leaching yield is shown to dramatically drop from 8 mol.L<sup>-1</sup> to 6 mol.L<sup>-1</sup> at 50 and 75 °C. This phenomenon



seems to strengthen with temperature, reaching values of 78.3 and 14.1 % at 25 and 50 °C respectively. At 75 °C, the mass of powder after leaching 1 g of NiMH black mass is close to 1.1 g. Visually, the formation of a precipitate is observed upon leaching the initial BM. This surprising result led us to think that leaching and precipitation reactions occur simultaneously. Increase of the mass of the active material after filtration proves that the metal is oxidized as a free cation before precipitating. A salt or an oxide is formed because of the association with the acid anion or oxygen respectively. Semi-quantitative characterization of the precipitated powder with SEM using EDS was performed in **Figure II.16** and is summarized in **Table II.5**.

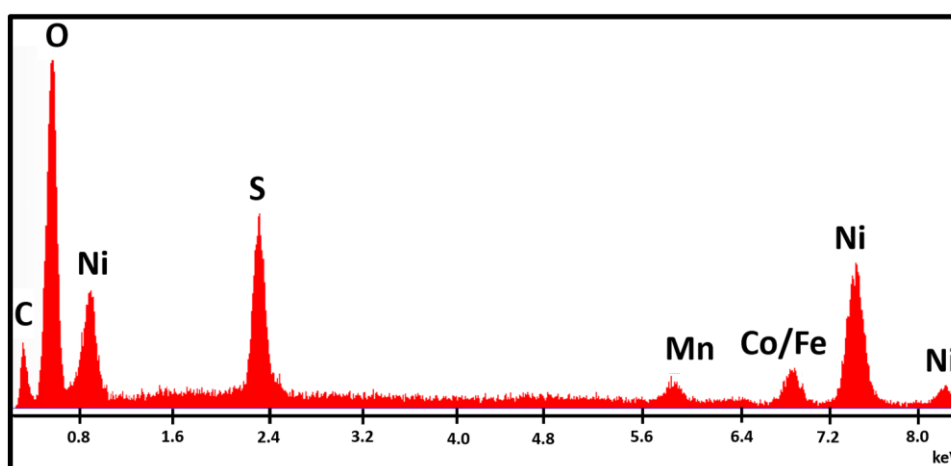
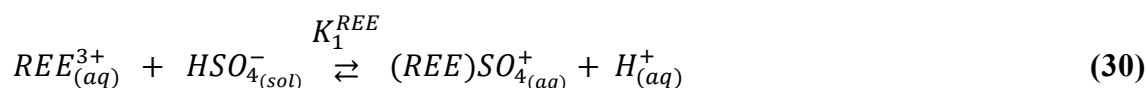
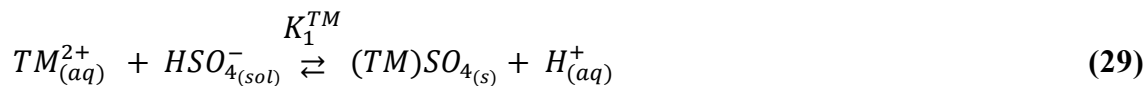


**Figure II.16.** EDS spectra of the precipitate obtained after leaching a NiMH black mass with  $10 \text{ mol.L}^{-1} \text{ H}_2\text{SO}_4$  at 75 °C.

Elements	Composition (atom. %)
Fe	$2.5 \pm 0.1$
Ni	$26.9 \pm 1.3$
Co	$5.6 \pm 0.2$
Mn	$2.3 \pm 0.1$
REE	-
S	$14.5 \pm 5.2$
O	$48.2 \pm 20.2$

**Table II.5.** Elemental analysis of the precipitate obtained after leaching a NiMH black mass with  $10 \text{ mol.L}^{-1} \text{ H}_2\text{SO}_4$  at 75 °C by EDS.

The elemental analysis of the precipitate obtained at 10 mol.L<sup>-1</sup>, 75 °C suggests that the precipitated powder contains more than 14 and 48 atomic percents of sulfur and oxygen respectively. Quantification of the two latter elements should be taken with great care because they are considered as light elements. Therefore, errors given are relatively high. However, we can state that a large amount of sulphate salts was precipitated after leaching. Because H<sub>2</sub>SO<sub>4</sub> has two pKa at -3.0 and 1.9, sulfuric acid will be under the form of a HSO<sub>4</sub><sup>-</sup> cation in our conditions. On the one hand, TM and are able to associate with the hydrogenosulfate ions according to equation (29) leading to the precipitation of a salt. On the other hand, the association between REE and HSO<sub>4</sub><sup>-</sup> leads to the formation of a positively charged complex (equation (30)). By definition the latter specie is fully soluble in water.



Where  $K_1^{TM}$  and  $K_1^{REE}$  represent the first complexation constants of transition metals and rare earth elements respectively.

While adding a large excess of sulphate anions to the solution, basically close to 10 mol.L<sup>-1</sup>, transition metals are able to associate with sulphate ions leading to the formation of (TM)SO<sub>4</sub>. Solubility of NiSO<sub>4</sub> and CoSO<sub>4</sub> are close to 0.26 and 0.19 mol.L<sup>-1</sup> in water at 20 °C<sup>235</sup> and can explain the formation of a precipitate during the leaching.<sup>230</sup> Data for complexation constants of TM and REE in sulphate media are reported from the literature<sup>236</sup> in **Table II.6**.

TM(II)	Complexation ( $K_1^{TM}$ )	Solubility (g / 100 g H <sub>2</sub> O)	REE(III)	Complexation ( $K_1^{REE}$ )
Fe	2.20	38.3	La	1.67
Ni	2.81	40.4	Ce	1.76
Co	2.69	29.5	Nd	1.50
Mn	2.19	63.7	Pr	1.30

**Table II.6.** Data collected in the literature for complexation constants<sup>236</sup> of TM and REE and solubility<sup>235</sup> of Ni, Co, Mn and Fe sulphate salts. All solubility data are given at 20 °C in pure water for (TM)SO<sub>4</sub> salts.

Interestingly, the precipitate obtained does not contain any of the rare earth elements present in AB<sub>5</sub> NiMH negative electrodes as suggested by the EDS analysis in **Figure II.16** and **Table II.5**. This result is confirmed by the ICP analysis performed on the leachate. On the one hand, comparing experiments at 75 °C at 2 and 8 mol.L<sup>-1</sup> the amount of leached nickel and cobalt in the aqueous solution drops from 388.8 to 16.0 and 96.4 to 0.1 mg.g<sup>-1</sup> of BM respectively. On the other hand, the amounts of lanthanum, cerium, praseodymium and neodymium remain constant. Values of 14.0 and 18.3 mg.g<sup>-1</sup> of BM for lanthanum and, 11.2 and 10.8 mg.g<sup>-1</sup> of BM for cerium are obtained at 2 and 8 mol.L<sup>-1</sup> H<sub>2</sub>SO<sub>4</sub> respectively. In other words, this allows us to perform a quasi-quantitative separation of rare earth elements from transition metals by using high concentration of sulfuric acid at 75 °C. In this case, all metals will be oxidized, however, while TM precipitate under sulphate salts, REE are able to stay in solution.

However, the viability of such separation process at an industrial scale suffers from some severe drawbacks. Firstly, the concentration of acid (10 mol.L<sup>-1</sup>) and temperature (75 °C) are rather aggressive conditions. Furthermore, the precipitated transition metals are mixed in the solid residue with plastics and passivated nickel, as a result a supplementary separation process should be undergone.

During the development of a leaching step, we will focus on the dissolution of all metals (TM and REE) using the less harmful conditions. Sulfuric acid is thus a better candidate than hydrochloric acid presenting important issues of corrosion and emission of toxic Cl<sub>2</sub> gas. Nitric acid wasn't even studied because of the risk

of explosion of nitrate derivatives.  $\text{H}_2\text{SO}_4$  thus seems to be the most secured acid to use for Recupyl<sup>®</sup>. Leaching at  $2 \text{ mol.L}^{-1}$  at  $25 \text{ }^\circ\text{C}$  was thus chosen as the optimum conditions to leach a real NiMH black mass powder with particle size lower than 1 mm. At this specific concentration,  $Y_L$  reaches a maximum of 85.1 %, a value higher than the one observed in the same conditions with HCl ( $Y_L = 75.4 \%$ ). Higher concentrations are not recommended as TM are susceptible to undergo precipitation. Higher temperature would significantly decrease the amount of REE in the leachate.

*Comparison between laboratory and industrial scale BM production*

It is also worth noticing that the leaching yield obtained with the selected parameters using an ideal raw material, this is to say,  $2 \text{ mol.L}^{-1} \text{ H}_2\text{SO}_4$ ,  $25 \text{ }^\circ\text{C}$  is of 94.2 % (see **part II.3.1**) and is thus much higher than the one obtained under the same conditions with the black mass produced at Recupyl<sup>®</sup> (85.1 %). Again, performing the grinding step and the mechanical treatment at an industrial scale brings undesirable materials in the BM. Furthermore, one shouldn't forget that the ideal raw material was only composed of the valuable negative electrode, while BM produced at Recupyl<sup>®</sup> is composed of both electrodes which can induce an important modification of the composition of the initial powder and of the leaching mechanisms thereof. As a result, the mass ratio Ni/REE in the leachate were calculated for the ideal BM and the BM produced at Recupyl<sup>®</sup> and are reported in **Table II.7**.

$2 \text{ mol.L}^{-1}$ $\text{H}_2\text{SO}_4$ , $25 \text{ }^\circ\text{C}$	Ideal BM produced at a laboratory scale	BM produced at Recupyl <sup>®</sup>
$Y_L$ (%)	94.2	85.1
Ni/REE	3.4	10.2

**Table II.7.** Comparison of the Ni/REE ratio between an ideal BM and BM produced at an industrial scale.

As expected, because the BM produced at Recupyl<sup>®</sup> is composed of the  $\text{LaNi}_5$  negative electrode but also of the  $\text{Ni}(\text{OH})_2$  positive electrode and the Ni/Fe metallic grid, the concentration of REE decreases in the leachate compared to the treatment of solely negative electrodes performed with the ideal BM produced in a laboratory scale.

*Full characterization after leaching with  $H_2SO_4$  2 mol.L<sup>-1</sup>, 25 °C*

The leachate obtained using 2 mol.L<sup>-1</sup>  $H_2SO_4$  at 25°C during 1 h was fully analysed after filtration, composition of the aqueous phase analysed by ICP and in agreement with **Figure II.15-A** is reported in **Table II.8**.

Element	Leachate composition (mg.g <sup>-1</sup> of BM)
Fe	91.3 ± 1.2
Ni	371.8 ± 1.2
Co	93.2 ± 1.2
Mn	11.9 ± 1.2
La	18.8 ± 0.3
Ce	12.0 ± 0.3
Nd	4.3 ± 0.3
Pr	1.2 ± 0.3

**Table II.8.** Leachate composition after leaching 1 g of BM produced at Recupyl<sup>®</sup> with  $H_2SO_4$  2 mol.L<sup>-1</sup> at 25 °C during 1 hour.

The leachate obtained is a mixture of transition metals (Fe, Ni, Co, Mn) and rare earth elements (La, Ce, Nd, Pr). After leaching 1 g of BM produced at Recupyl<sup>®</sup>, those metals are dissolved in 25 ml of an aqueous solution under the form of ionic species.

Characterization of the remaining solid residue was then performed by scanning electron microscopy in **Figure II.17**.

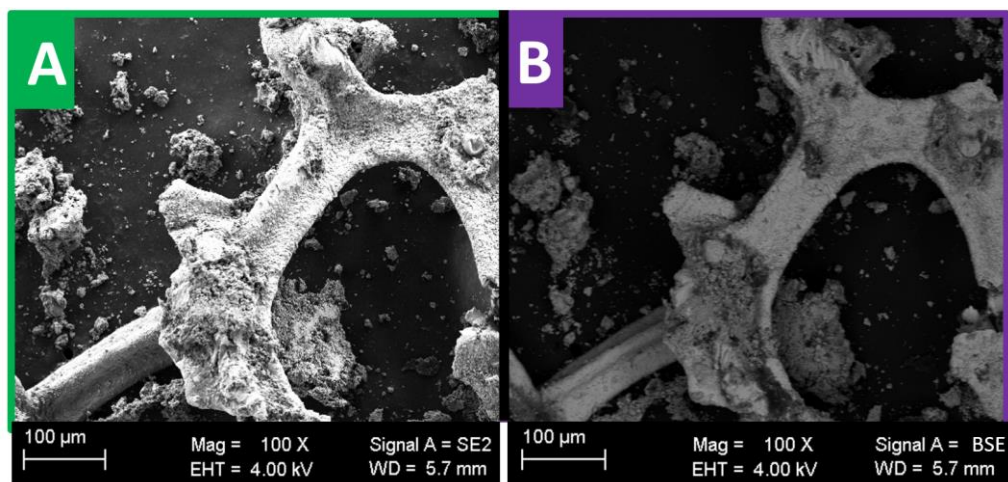


**Figure II.17.** Solid residue analysed by SEM (magnification × 100) after leaching 1 g of BM produced at Recupyl<sup>®</sup> with  $H_2SO_4$  2 mol.L<sup>-1</sup> at 25 °C during 1 hour. A:

Imaging using secondary electrons (SE). B Imaging using Back Scattered Electrons (BSE).

Secondary electron imaging provided in **Figure II.17-A** gives us information on the macroscopic aspect of the residue. Obviously, a large piece of metallic grid withstood oxidation. This is most probably due to the ability of nickel to passivate. Presence of small amounts of powder can be spotted. A SEM snapshot using BSE is shown in **Figure II.17-B**, information on the nature of the residue can be taken from the different grayscales. The light area corresponding to the grid confirms the metallic nature of the particle while the darker areas indicate the presence of “lighter” compounds, most probably salts. In order to confirm the latter statement, elemental analysis was performed by EDS and is reported in **Table II.9**.

<b>Elements</b>	<b>Composition (atom. %)</b>
<b>Fe</b>	$2.7 \pm 0.2$
<b>Ni</b>	$75.4 \pm 1.3$
<b>Co</b>	$0.8 \pm 0.1$
<b>Mn</b>	-
<b>REE</b>	-
<b>S</b>	$5.9 \pm 2.2$
<b>O</b>	$15.2 \pm 10.8$

**Table II.9.** Elemental analysis of the solid residue obtained after leaching a NiMH black mass produced at Recupyl<sup>®</sup> with  $2 \text{ mol.L}^{-1} \text{ H}_2\text{SO}_4$  at  $25 \text{ }^\circ\text{C}$  by EDS.

According to EDS analysis, the solid residue is composed with 75.4, 2.7 and 0.8 atomic percent of nickel, iron and cobalt respectively, most probably corresponding to the metallic grid observed in **Figure II.17**. However, non-negligible amounts of sulfur and oxygen, namely 5.9 and 5.2 atom. % respectively confirm the presence of  $\text{TM}(\text{SO}_4)_{2(s)}$ . This result is in line with the XRD analysis displayed in **Figure II.11** corresponding to the precipitate obtained with the ideal BM. Interestingly, all REE were leached in this step of the process, as no peaks corresponding to La, Ce, Nd or Pr were detected in the EDS spectra.

#### d. Conclusion

Thanks to the facilities from the battery recycler Recupyl<sup>®</sup>, two black mass samples from end-of-life NiMH batteries were produced. Samples were obtained using different mechanical treatments and led to one sample containing particles with diameters below 1mm, and a second sample containing large particles, with diameters typically ranging from 1 to 10 mm. These powder samples containing large amounts of valuable metal such as nickel, cobalt, lanthanum, cerium and neodymium were leached using different acids namely sulfuric and hydrochloric at various concentrations and temperatures. The influence of particles grain size on the leaching yield ( $Y_L$ ) revealed that large coarse powder induces a high uncertainty on  $Y_L$  values. Furthermore, thinner particles always led to higher  $Y_L$  values, due to their larger surface area. Increase in temperature has a positive impact on the leaching of transition metal but decreases the solubility of REE in solution. Using high concentration of sulfuric acid (close to  $10 \text{ mol.L}^{-1}$ ) yielded the precipitation of transition metals. Under such conditions, a  $\text{TM}(\text{SO}_4)_2$  salt was observed. Despite a negligible passivation of Ni using aqueous HCl solutions,  $\text{H}_2\text{SO}_4$  was selected because (i) it presents enhanced leaching yield for concentration of acid lower than  $2 \text{ mol.L}^{-1}$  and (ii)  $\text{H}_2\text{SO}_4$  is less corrosive and harmful than HCl. The latter produces toxic gas such as  $\text{Cl}_2$  and is thus much more problematic from an industrial point of view. As a result,  $2 \text{ mol.L}^{-1} \text{H}_2\text{SO}_4$  during 1 hour at  $25 \text{ }^\circ\text{C}$  was selected as optimum parameters to leach 1 mm particle size NiMH BM. Under these conditions, the leaching yield reaches a maximum of 85.1 wt. %. The remaining 15 wt. % of solid residue are mostly composed of plastics, metallic grids and low amounts of sulphate TM salts (close to 6 atom. %). The leachate is an aqueous solution of 25 ml containing very large amounts of valuable metals, namely 372, 91, 93, 12 mg of nickel, iron, cobalt and manganese respectively and 19, 12, 4, 1 mg of lanthanum, cerium, neodymium and praseodymium respectively after leaching 1 g of BM.

### II.3.3 Possibilities and limitations of using hydrophilic ILs in leaching process

With the aim of performing extraction experiments using ILs, and in order to investigate on the possibility of carrying out leaching and separation of metals in one single IL-based medium, the present section will be dedicated to the leaching of NiMH battery using mixture of acid and ionic liquid in an aqueous phase.

Tributyltetradecylphosphonium chloride, namely  $[P_{44414}][Cl]$  composed of a chloride anion and a quaternary phosphonium cation is fully miscible in pure water but forms 2 phases when contacted with a concentrated HCl solution. The potential of  $[P_{44414}][Cl]$  in leaching metals from a NiMH battery will be studied here. Because the latter IL presents hydrophilic characteristics, mixtures of  $[P_{44414}][Cl]$  and acid will be carried out in an aqueous phase. HCl will be used to reduce the number of ions present in the leaching solutions ( $H^+$ ,  $[P_{44414}]^+$  and  $Cl^-$ ). The potential of  $[P_{44414}][Cl]$  as a novel extraction system will be fully detailed in **Chapter 4**.

#### a. Experimental

1 g of NiMH black mass produced at Recupyl<sup>®</sup> according to **part II.2.2** was leached with 10 ml of aqueous solution at 25, 50 and 75 °C. The leachate was composed of 0, 2 and 4 mol.L<sup>-1</sup> of HCl and 0, 30 and 60 vol. % of  $[P_{44414}][Cl]$ . The nine aqueous solutions were prepared in calibrated flask. Results, acid and ionic liquid concentrations will thus be expressed in volumetric units. Reaction time was set to 1 hour. Similarly to previous leaching experiments, after reaction the mixture was filtered on a Büchner setup. The solid residue was washed several times with water. It was then dried on a pre-weighed filter in an oven at 80 °C during 12 hours before being cooled down to room temperature in a desiccator and weighed. In order to follow the efficiency of the reaction, the leaching yield ( $Y_L$ ), was used.

#### b. Results and Discussion

Leaching yields obtained for the 9 different leaching solutions at 3 different temperatures are provided in **Figure II.18**.



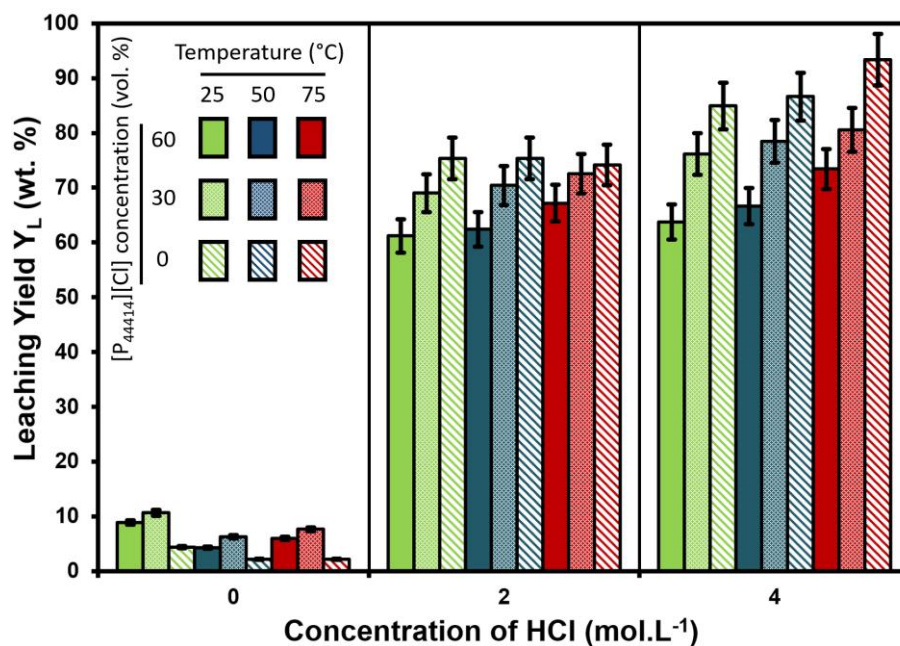


**Figure II.18.** Leaching of NiMH black mass containing particles below 1 mm with sulfuric acid and/or  $[P_{44414}][Cl]$  IL in an aqueous phase. Experiments were undertaken at 25, 50 and 75 °C in green, blue and red respectively. Leachates were composed of 60, 30 and 0 vol. % of  $H_2SO_4$  in full color, light color and striped line respectively. All experiments were carried out at 0, 2 and 4 mol.L<sup>-1</sup> of acid.

As expected, using pure water as leachate solution (0 ; 0) (IL (vol. %) ; HCl (mol.L<sup>-1</sup>)) leads to a poor leaching yield of 7.4 % at 25 °C. At this stage, only a small amount of REE is leached into the solution. REE are known to oxidize in aqueous solutions at 25 °C.<sup>237</sup> Not surprisingly, the leaching yield decreases down to values lower than 2 % at 50 °C because the solubility of lanthanide decreases with temperature.<sup>230</sup> This point was already discussed in **part II.2.1** and justify the use of warm water to wash the NiMH black mass after mechanical treatment. We report that, using pure  $[P_{44414}][Cl]$  in water, the leaching yield will be of 8.9 and 10.7 % for 30 and 60 vol. % IL respectively. Similarly to what has previously been observed, this yield slightly decreases at 50 and 75 °C. In other words, the leaching efficiency of the pure ionic liquid is minor. This leachate thus can't be used to oxidize and dissolve NiMH BM. However, addition of proton via hydrochloric acid can enhance the leaching ability of the aqueous solution leading to  $Y_L$  of 61.2 and 63.7 % for (60 ; 2) and (60 ; 4) respectively. Under those conditions, the solution exhibits a high viscosity due to the presence of the IL. This viscosity can hinder the leaching mechanism of metals because of slow kinetics and agitation. This parameter can be modified by using lower amounts of IL,

which provide a more fluid solution. Use of 30 vol. % of IL thus leaches 69.0 and 76.2 wt. % of the battery using 2 and 4 mol.L<sup>-1</sup> HCl respectively.

c. Conclusion

Using a hydrophilic ionic liquid, namely [P<sub>44414</sub>][Cl] in a leachate solution was reported not to be efficient to oxidize NiMH BM ( $Y_L < 10\%$ ). However, adding acid such as HCl can enhance the leaching yield of the process. Comparing pure acid solutions and mixtures of acid and ionic liquid, the latter leachate solution seems to present lower leaching yields due to its higher viscosity and thus lower kinetics. Nevertheless, viscosity of the solution can be managed by adjusting the concentration of IL. As a result, an aqueous solution containing metallic cations in an ionic liquid could be an interesting media to develop metal extraction processes. The latter step will be fully developed in **Chapter 4**.

## II.4 Selective precipitation

---

### a. Introduction

After performing a leaching step, as detailed previously, Fe, Ni, Co, Mn and La, Ce, Nd, Pr contained in NiMH batteries were leached into an aqueous phase. Using a 2 mol.L<sup>-1</sup> H<sub>2</sub>SO<sub>4</sub> aqueous solution at 25 °C during 1 hour appeared to be the best compromise between efficiency and industrial requirements.

The next step in our under-construction recycling process is to isolate the two main families of metals loaded in the leachate, namely REE and TM. Further theoretical details and review on this step was given in **part I.4.2**. According to the literature, precipitation of rare earth elements can occur in sulphate media by (i) increasing the pH and (ii) adding an alkaline metal.<sup>160</sup> Both steps can occur simultaneously by adding a base such as sodium carbonate Na<sub>2</sub>CO<sub>3</sub>, sodium hydroxide NaOH or potassium hydroxide KOH. Quantitative precipitation of alkaline lanthanide sulphate salts was reported after increasing the pH to values ranging from 1<sup>155</sup> to 2.5<sup>157</sup>.

Starting from our leachate loaded in metals from real grinded NiMH batteries, our goal is thus to perform a quantitative separation of Ni, Co, Mn, Fe from La, Ce, Nd, Pr by performing a selective precipitation of REE. The optimal pH to induce a full precipitation of lanthanides by avoiding any presence of TM will be investigated. Following the recommendation from the recycler Recupyl<sup>®</sup>, sodium carbonate was chosen for this step. This compound is under the form of a thin white powder, is cheaper and easier to handle for an industrial point of view compared to corrosive and hygroscopic NaOH pellets.

### b. Experimental

20 ml of leachate and a magnetic stirrer were transferred in a 50 ml beaker. A calibrated pH electrode was soaked in the latter mixture to follow the pH evolution. In the same time, an aqueous solution of sodium carbonate 1.5 mol.L<sup>-1</sup> was prepared and transferred to a graduated burette. According to preliminary

experiments (not shown), we chose to set the concentration of the  $\text{Na}_2\text{CO}_3$  to  $1.5 \text{ mol.L}^{-1}$  mainly for two reasons. (i) A higher concentration of  $\text{Na}_2\text{CO}_3$  can locally create in the leachate, small areas where the pH becomes basic. This phenomenon can enhance the co-precipitation of transition metals with rare earth elements. (ii) A lower concentration of  $\text{Na}_2\text{CO}_3$  requires by definition a higher volume of aqueous basic solution to increase the pH to a define value. Consequently, the final aqueous solution appears more diluted in metals which can be an issue for hydrometallurgical processes. Very slow addition of the basic solution from the burette to the beaker containing the metallic cations in solution was performed at room temperature (close to  $25 \text{ }^\circ\text{C}$ ) under strong magnetic stirring. Upon addition of the  $\text{Na}_2\text{CO}_3$  solution, a significant bubbling was observed, due to the formation of large amounts of  $\text{CO}_{2(\text{g})}$ . After setting the pH to the selected values, namely pH = 0, 1, 1.5, 1.7, 2, 3, 3.5, 4, 5 and 8, the aqueous solution was filtered in a Büchner setup. When a precipitate was obtained, the latter was then washed with alkaline water and dried on a pre-weighed filter in an oven at  $80 \text{ }^\circ\text{C}$  during 12 hours. Finally, the remaining powder was analysed via Scanning Electron Microscopy (SEM) using Secondary Electrons (SE), Back Scattered Electrons (BSE) and Energy Dispersive X-ray Spectroscopy (EDS). Regarding the leachate, the volume was adjusted to 100 ml and the solution was analysed by Inductively Coupled Plasma (ICP).

### c. Results and Discussion

After drying, the precipitate obtained when pH was set between 1 and 2 has the aspect of a white immaculate powder. Snapshot of the powder is given in **Figure II.19**.

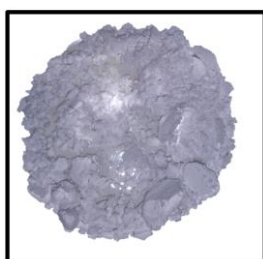


**Figure II.19.** Snapshot of the precipitate obtained while the pH is comprised between 1 and 2 by addition of  $\text{Na}_2\text{CO}_3$   $1.5 \text{ mol.L}^{-1}$  to the leachate.

*Characterization of the leachate*

pH of the leachate in the previously defined conditions does not correspond to the pH of 2 mol.L<sup>-1</sup> H<sub>2</sub>SO<sub>4</sub> because the proton is reduced to hydrogen during the oxidation of metals. The measured pH is thus of -0.25 after leaching. However, we should keep in mind that the latter value suffers from some uncertainty as pH-meters are not calibrated to measure pH lower than 1. The relative amounts of metals present in the leachate, the weight percent of metallic cations still present in the aqueous solution after increasing the pH to values of 0 to 8 will be first detailed. Results are shown in **Figure II.20** and **Table II.10**.

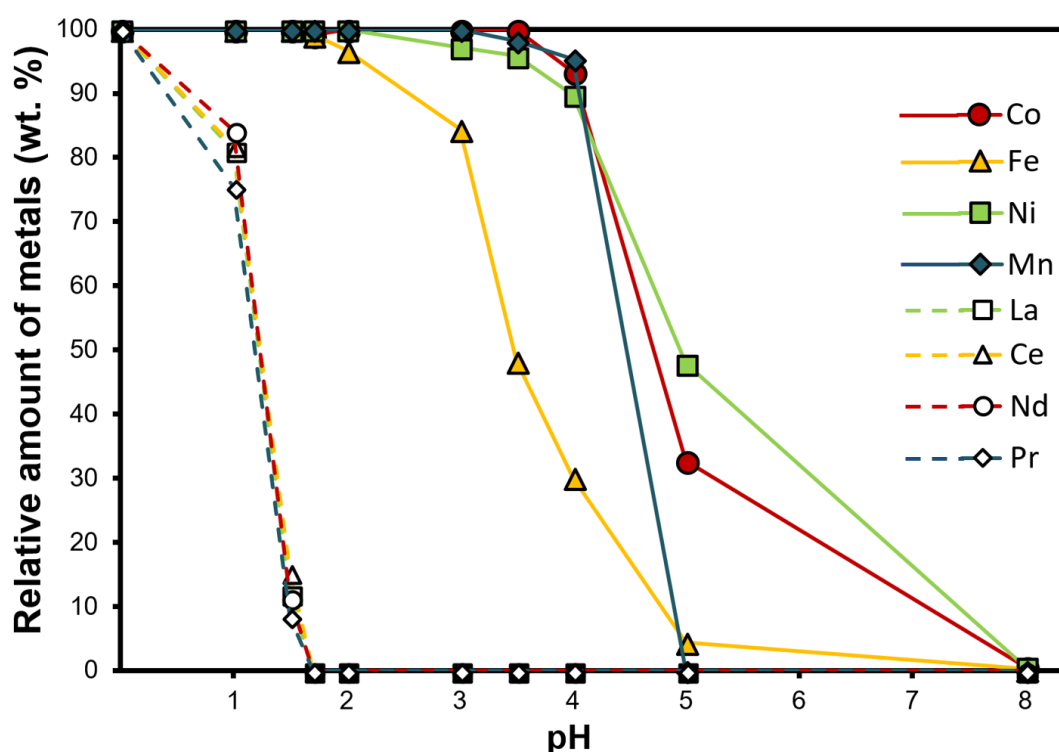


**Figure II.20.** Evolution of the concentration of metals in the leachate while increasing the pH from -0.25 to 8.

When the pH is under 1 no precipitate can be observed in the leachate as suggested by the amount of metals found in the aqueous solution at pH = 0 that are not significantly different from those observed in the initial leachate at pH = - 0.25. By adding more sodium carbonate to the leachate, the pH reaches a value of 1. At this stage, even if all transition metals stay in solution, 15 to 25 wt. % rare earth elements are able to precipitate. This value increases to 85 to 92 wt. % at a pH of 1.5. A quantitative precipitation of REE is finally observed at pH = 1.7 where no

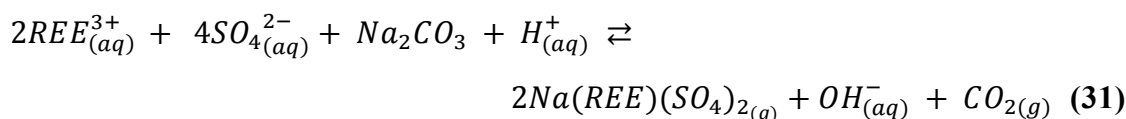
trace of nickel, cobalt, manganese or iron can be detected in the precipitate. It is worth to notice that no selective precipitation between all REE is observed. Lanthanum, cerium, neodymium and praseodymium follow the same precipitation trend in sulphate media.

Precipitation of iron can be observed starting from pH 2 to 5. A co-precipitation of all transition metals, namely nickel, cobalt, manganese and iron is observed from pH 3 to 8.

Composition of the leachate (mg.g <sup>-1</sup> of BM in 100 mL)					
Elements	pH = -0.25	pH = 1.0	pH = 1.5	pH = 1.7	pH = 2
Fe	91.3 ± 1.2	89.9 ± 1.2	91.0 ± 1.2	90.9 ± 1.2	88.2 ± 1.2
Ni	371.8 ± 1.2	369.2 ± 1.2	371.8 ± 1.2	378.3 ± 1.2	371.8 ± 1.2
Co	93.2 ± 1.2	93.4 ± 1.2	92.1 ± 1.2	94.2 ± 1.2	93.4 ± 1.2
Mn	11.9 ± 1.2	11.0 ± 1.2	12.5 ± 1.2	12.4 ± 1.2	11.2 ± 1.2
La	18.8 ± 0.3	15.2 ± 0.3	2.2 ± 0.3	< 0.3	< 0.3
Ce	12.0 ± 0.3	1.6 ± 0.3	0.3 ± 0.3	< 0.3	< 0.3
Nd	4.3 ± 0.3	3.6 ± 0.3	0.5 ± 0.3	< 0.3	< 0.3
Pr	1.2 ± 0.3	0.9 ± 0.3	< 0.3	< 0.3	< 0.3

**Table II.10.** Evolution of the concentration of metals in the leachate while increasing the pH from -0.25 to 1, 1.5, 1.7 and 2.

The increase of pH by addition of sodium carbonate and the following precipitation mechanism of REE can be depicted in the following equation.



The formation of Na(REE)(SO<sub>4</sub>)<sub>2(s)</sub>, OH<sub>(aq)</sub><sup>-</sup> and CO<sub>2(g)</sub> in the previous chemical equation can explain the white precipitate, the pH increase and the formation of bubbles respectively. While some papers depicted the precipitation of lanthanide sulphate salts (REE)<sub>3</sub>(SO<sub>4</sub>)<sub>3(s)</sub> from NiMH batteries,<sup>155,159</sup> Porvali *et al.*<sup>156</sup> brought evidence on the real nature of the precipitate by showing the precipitation of a sodium lanthanide sulphate Na(REE)(SO<sub>4</sub>)<sub>2(s)</sub> from NiMH batteries. Indeed,

according to a previous study,<sup>152</sup> the solubility of  $\text{Na(REE)(SO}_4)_2$  is always lower than  $8.10^{-3} \text{ mol.L}^{-1}$  and is thus much lower than that of  $(\text{REE})_3(\text{SO}_4)_3$ .

Because in those precise conditions, REE are able to quantitatively precipitate while all transition metals stay in the aqueous solution, we defined that increasing the pH at a value of 1.7 using sodium carbonate at  $1.5 \text{ mol.L}^{-1}$  is ideal to perform a separation of La, Ce, Nd and Pr from Ni, Co, Fe and Mn. According to the previous results, evolution of the amount of all metals in those precise conditions is depicted in **Figure II.21**.

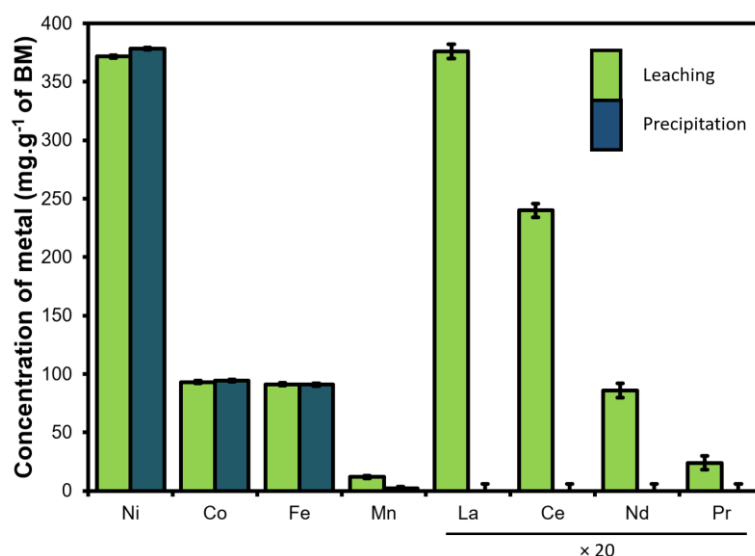


**Figure II.21.** Concentration of metals in the aqueous solution. In green, after leaching at pH -0.25 and in blue after precipitation at pH 1.7. Concentration of La, Ce, Nd and Pr was multiplied by 20 for graphical reason.

#### *Characterization of the precipitate.*

According to the previously defined parameters to induce a quantitative precipitation of REE, the obtained powder was analysed by SEM using SE and BSE for imaging and EDS for elemental analysis. Results are shown in **Table II.1** and **Figure II.22**.

Elements	Composition (atom. %)
La	$5.1 \pm 0.2$
Ce	$3.6 \pm 1.3$
Nd	$2.0 \pm 0.1$
Pr	$0.6 \pm 0.1$
TM	-
Na	$14.2 \pm 2.2$
S	$16.3 \pm 10.9$
O	$58.2 \pm 40.0$

**Table II.11.** Elemental analysis of the precipitate obtained at pH 1.7 by SEM-EDS.

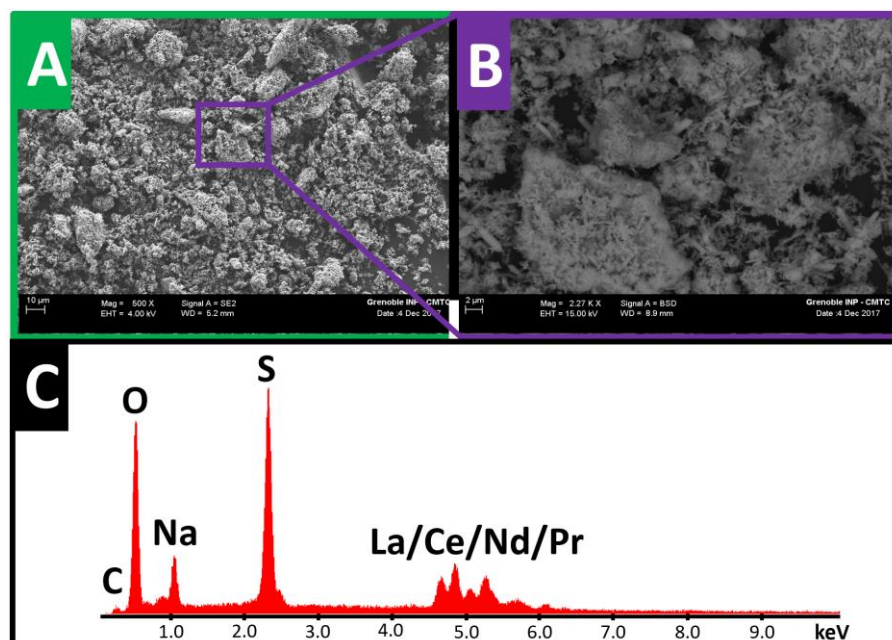


**Figure II.22.** SEM analysis of the precipitate obtained at pH 1.7. A: SE image (magnification  $\times 100$ ). B: BSE image (magnification  $\times 2270$ ). C: Elemental analysis by EDS.

SEM-SE image provided in **Figure II.22-A** gives topological information on the general aspect of the powder. SEM-BSE image shown in **Figure II.22-B** highlights that the powder is chemically homogeneous as only one grayscale can be observed. Finally, elemental analysis of the precipitate given in **Figure II.22-C** and **Table II.11** highlights the presence of 11.3 atomic percents of REE while no trace of TM can be found. This confirms our assumption of a fully quantitative separation of



La, Ce, Nd and Pr from Ni, Co, Fe and Mn. According to the literature and to presence of sulfur (16.3 %) and oxygen (58.2 %) the presence of sulphate ligand is expected. Moreover, 14.2 atom. % of sodium is spotted in the powder. This latter information confirms that the white precipitate is a  $\text{Na}(\text{REE})(\text{SO}_4)_{2(s)}$  salt. The structure of the precipitated powder was thus investigated by XRD in **Figure II.23**.

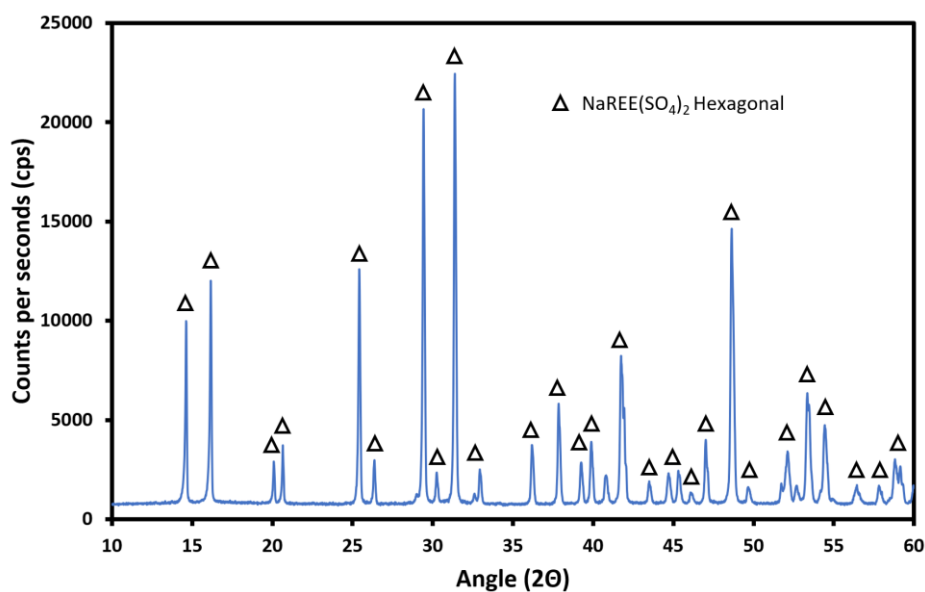


**Figure II.23.** XRD analysis of the precipitate obtained at pH 1.7.

The diffractogram obtained confirms the homogeneity of the compound as only one diffraction pattern was observed. The latter compound is in accordance with our previous results as well as with observations reported by *Provazi et al. 2011*,<sup>160</sup> composed of a sodium lanthanide rare earth sulphate salt, namely  $\text{Na}(\text{REE})(\text{SO}_4)_{2(s)}$ . The latter diffractogram is however unable to make the difference between La, Ce, Nd and Pr salts, however quantification of all REE was already obtained in **Table II.11**.

#### d. Conclusion

In this chapter, we reported a selectively REE precipitation step, thus isolating rare earth elements from transition metals starting from a sulfuric acid leachate loaded with metals from real spent NiMH batteries. To that end, the pH of the leaching solution, initially containing  $2 \text{ mol.L}^{-1} \text{ H}_2\text{SO}_4$  was increased until a pH of 1.7 was

obtained by adding an aqueous solution of  $1.5 \text{ mol.L}^{-1}$  sodium carbonate. Under these conditions, a white precipitate was obtained. On the one hand, characterization of the leachate shows that all REE have been precipitated, as concentrations of La, Ce, Nd and Pr are under the detection limit of the apparatus. On the other hand, characterization of the precipitate highlights no contamination of Ni, Co, Fe and Mn. An homogeneous powder of sodium rare earth sulphate, namely  $\text{Na(REE)(SO}_4)_2(\text{s})$  was identified.

## II.5 Conclusion

---

According to the specifications of the project depicted in **Chapter I**, the first goal was to isolate the two main categories of elements found in NiMH batteries. This is to say, Rare Earth Elements and Transition Metals. To this end, mechanical treatments and classical hydrometallurgical processes were used. They may be summarized as follows:

### *Mechanical Treatment*

- (i) A real spent NiMH battery was opened in a laboratory scale. The negative electrode was fully characterized as it contains large amounts of valuable metals in an intermetallic compound  $\text{La}_{5.7}\text{Ce}_{7.8}\text{Nd}_{2.3}\text{Pr}_{0.8}\text{Ni}_{59.2}\text{Co}_{12.5}\text{Mn}_{6.7}$ . This powder will be used as an “ideal” material in the present work.
- (ii) To scale up this process, a mixture of real spent NiMH batteries was mechanically treated at the recycling company Recupyl<sup>®</sup>. The Black Mass (BM) obtained is composed of the intermetallic negative electrode but also of the positive Ni(OH) electrode, Ni/Fe metallic grids and various plastics. This will be our raw material in the construction of a recycling process.

### *Leaching*

- (i) Optimization of the leaching of 1 g of ideal material was performed and lead to the utilization of 10 ml of  $\text{H}_2\text{SO}_4$  2 mol.L<sup>-1</sup> at 25 °C during 30 min. We claim that 94.2 % of the negative electrode is leached in those conditions. The remaining solid residue is composed of carbon and passivated nickel.
- (ii) A similar trend was observed with the BM produced at Recupyl<sup>®</sup> however the leaching yield is lower because of the presence of plastics and metallic grids.

- (iii) Lower particles offer more efficient and reproducible leaching experiments because of their higher surface area and homogeneity respectively.
- (iv)  $\text{H}_2\text{SO}_4$  is preferred to HCl because this acid presents higher leaching yields for concentrations below  $4 \text{ mol.L}^{-1}$ . Furthermore, sulfuric acid is known to be less corrosive and does not release toxic gases compared to hydrochloric acid.
- (v) According to our optimization studies, 10 ml of  $\text{H}_2\text{SO}_4$   $2 \text{ mol.L}^{-1}$  at  $25^\circ\text{C}$  during 60 min was chosen to leach 1 g of BM produced at Recupyl<sup>®</sup>. In those conditions, the leachate is composed of 91.3, 371.8, 93.2 and 11.9 mg of Fe, Ni, Co and Mn respectively and 18.8, 12.0, 4.3 and 1.2 mg of La, Ce, Nd, Pr respectively in an aqueous solution of 25 mL.

#### *Selective precipitation*

- (i) The pH of the previously described leachate loaded with valuable metals was increased from -0.25 to 1.7 using  $1.5 \text{ mol.L}^{-1}$   $\text{Na}_2\text{CO}_3$  in water. A white precipitate was obtained and separated from the aqueous solution. Analysis of the leachate by ICP lead to no trace of REE. Analysis of the precipitate by SEM and XRD leads to the observation of a  $\text{Na(REE)(SO}_4)_2(\text{s})$  salt. No transition metals contamination was spotted in the powder.

As a result, a quantitative separation of Ni, Co, Mn and Fe from La, Ce, Nd and Pr was obtained from spent NiMH batteries and can be summarized in **Figure II.24**.

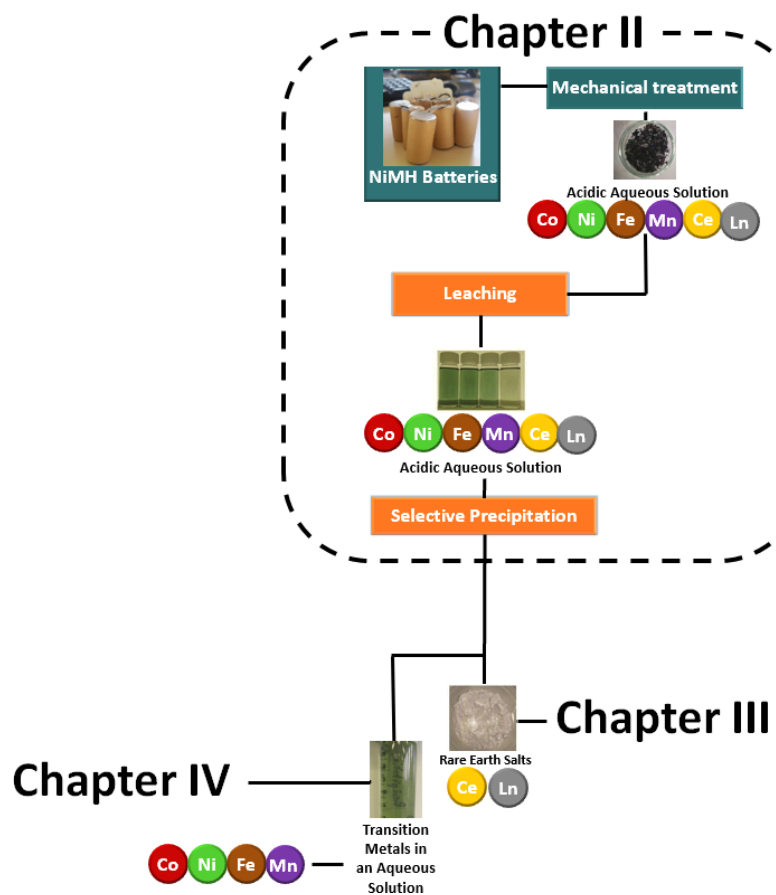


**Figure II.24.** Flowsheet corresponding to the separation of transition metals from rare earth elements.

## **CHAPTER III**

# **Separation of Cerium, Lanthanum, Neodymium and Praseodymium**

## III.1 Introduction

---

According to **Chapter II**, a mixture of rare earth elements was obtained under the form of a  $\text{NaREE}(\text{SO}_4)_2$  salt starting from real spent NiMH batteries. No evidence of nickel, cobalt, manganese or iron was found in the powder highlighting a quantitative separation of REE from TM. Because of the similar properties of lanthanides and thus because of the difficulty of isolating them from one another, 75 to 80 wt. % of those elements are used without performing any separation experiments.<sup>238</sup> As a result, the powder obtained after this precipitation step can already be considered as a valuable product. However, because some applications require the utilization of purified metals in their process, innovative separation technologies for rare earth elements are required.  $\text{NaREE}(\text{SO}_4)_2$  contains La (52 at. %), Ce (33 at. %), Nd (12 at. %) and Pr (3 at. %). This Chapter will thus be devoted to the separation of the two major elements, lanthanum and cerium. On the one hand, separation and recovery of Ce from La, Nd and Pr will be investigated in **part III.2** using oxidation and extraction techniques starting from a model mixture of sulphate salts. On the other hand, based on the results obtained in section **III.2**, a process for the recovery of pure cerium starting from spent NiMH batteries will be studied in **part III.3**. Precipitation and electrodeposition strategies will both be studied in order to recover pure and valuable cerium. Finally, paths to reach the separation of lanthanum from neodymium using pure ionic liquids will be proposed in a last **part (III.4)**.

## III.2 Separation of cerium from lanthanum, neodymium and praseodymium sulphate salts

---

This part is based on the following peer reviewed article:<sup>100</sup>

- Gras.M, Papaiconomou.N, Chainet.E, Tedjar.F, Billard.I, Separation of cerium(III) from lanthanum(III), neodymium(III) and praseodymium(III) by oxidation and liquid-liquid extraction using ionic liquids, *Separation and Purification Technologies* **178** (2017) 169-177.

### III.2.1 Introduction

Cerium is largely used in various applications such as phosphor lamps, polishing media, automotive three way emission catalyst, nickel metal hydride batteries and ceramics.<sup>21,52,239</sup>

Successful separation of cerium(IV) in a mixture of two lanthanides (Gd and Yb) and Th(IV) by liquid-liquid extraction techniques using ionic liquids was reported previously by Zuo et al.<sup>88</sup> The ionic liquid phase used by these authors was 1-octyl-3-methylimidazolium hexafluorophosphate ( $[C_1C_8IM][PF_6]$ ). Nevertheless, the hexafluorophosphate anion is highly susceptible to undergo hydrolysis leading to the formation of hydrofluoric acid.<sup>240</sup> Therefore, another anion, so called bis(trifluoromethanesulfonyl)imide  $[NTf_2]^-$  was considered in our work, since it is chemically stable, does not produce any fluoride anion and exhibits an increased hydrophobicity compared to  $PF_6^-$  anion.<sup>241,242</sup> Two ionic liquids based on the  $[NTf_2]^-$  anion, namely 1-methyl-1-butyl-pyrrolidinium bis(trifluoromethylsulfonyl)imide,  $[C_1C_4Pyr][NTf_2]$  and trihexyl(tetradecyl)phosphonium bis(trifluoromethylsulfonyl)imide,  $[P_{66614}][NTf_2]$ , were used. The former exhibits a low viscosity, which is advantageous for efficient



and rapid liquid-liquid extraction steps, while the latter exhibits an increased hydrophobicity compared to  $[C_1C_4Pyrr][NTf_2]$  because of the long alkyl chains appended onto the cation.<sup>190</sup>

First, cerium(III) will be oxidised in cerium(IV) by dissolved oxygen in a sodium hydroxide solution. Then, after dissolving all metal ions in nitric acid, cerium(IV) will be separated from La(III), Nd(III) and Pr(III) by liquid-liquid extraction using two different ionic liquids, namely  $[C_1C_4Pyrr][NTf_2]$  or  $[P_{66614}][NTf_2]$ , accordingly. Finally, cerium will be recovered by performing a stripping step. Reuse of  $[C_1C_4Pyrr][NTf_2]$  in an extraction process will also be presented by carrying out ten cycles of alternating extraction and stripping steps using the same ionic liquid.

In this chapter after the experimental section, results dealing with the spectrophotometric properties of lanthanides, oxidation of Ce(III) to Ce(IV) and single cerium extraction from nitric acid solutions towards an ionic liquid will be given. Cycling of the ionic liquid in ten consecutive extraction and stripping steps and investigation on a full process for separating cerium from other lanthanides starting from a mixture of lanthanide sulphates will also be presented.

### III.2.2 Oxidation of Ce(III) in alkaline conditions

#### a. Experimental section

In a reactor placed in a temperature-controlled water bath, typically 1 g of cerium(III) sulphate was mixed with 20 mL of sodium hydroxide in water. The concentration of NaOH ranged between 0.2 and 2.0 mol.L<sup>-1</sup>. The mixture was vigorously stirred at 30°C or 50°C. After 3 hours of reaction, the solution was cooled down at room temperature and was filtered under vacuum (Büchner filtration assembly). The precipitate was rinsed with a minimum of water and dried during 12 hours at 50°C. 50 mg of the resulting powder was weighed and dissolved in 15 mL of a solution of 8.0 mol.L<sup>-1</sup> H<sub>2</sub>SO<sub>4</sub>. The aqueous solution obtained was then diluted 250 times with the same stock solution of sulfuric acid and was analysed by UV-visible spectrophotometry.

Additionally, approximately 1 g of cerium(III) sulphate was mixed with various masses of praseodymium(III), lanthanum(III) and neodymium(III) sulphate in

order to have equimolar amounts of each rare earth metal. The mixture was then put in contact with a solution containing  $2.0 \text{ mol.L}^{-1}$  NaOH at  $30^\circ\text{C}$  following the same procedure as that detailed above. Then approximately 12 mg of the resulting sample was dissolved in 10 mL of sulfuric acid  $8.0 \text{ mol.L}^{-1}$ . After diluting the latter solution 30 times using  $8.0 \text{ mol.L}^{-1}$   $\text{H}_2\text{SO}_4$ , the analysis of the solution was carried out by UV-visible spectrophotometry. **ANNEX 1-D** will be devoted to UV-vis analysis.

### b. Measurements

Measurements of the concentrations of Ce(III) and Ce(IV) for the oxidation experiments were obtained using UV-Vis absorption spectroscopy. Calibration solutions containing  $4.0 \times 10^{-4}$  to  $2.0 \times 10^{-3} \text{ mol.L}^{-1}$  Ce(III) or between  $2.0 \times 10^{-5}$  and  $2.0 \times 10^{-4} \text{ mol.L}^{-1}$  Ce(IV) were prepared in  $8.0 \text{ mol.L}^{-1}$   $\text{H}_2\text{SO}_4$ . The Beer-Lambert's law was applied at each maximum absorption wavelengths ( $\lambda_{\text{Ce(III)}} = 242 \text{ nm}$ ,  $\lambda_{\text{Ce(IV)}} = 315 \text{ nm}$ ) obtained from spectra recorded from 200 to 600 nm.<sup>243</sup> In all cases, calibration curves are straight lines and correlation factors above 0.99 were obtained.

Oxidation yield for the precipitated Ce(IV), so called  $Y_{\text{ox}}$  was defined as follows:

$$Y_{\text{ox}} = \frac{n_{\text{Ce(IV)}}}{n_{\text{Ce(III)}}^{\text{Init}}} \times 100 \quad (32)$$

$n_{\text{Ce(IV)}}$  is the number of moles of cerium(IV) that is precipitated after oxidation. It is calculated from the mass of precipitate and the concentration of cerium(IV) measured by the UV-visible spectrophotometer as detailed in the experimental part.  $n_{\text{Ce(III)}}^{\text{Init}}$  corresponds to the number of moles contained in the mass of  $\text{Ce}_2(\text{SO}_4)_3$  (namely 1 g) initially used for these experiments.

### c. Results

#### *Spectroscopic properties of lanthanides*

The spectra of two solutions containing  $4.0 \times 10^{-5}$  Ce(IV) or  $2.0 \times 10^{-3} \text{ mol.L}^{-1}$  Ce(III), in  $8.0 \text{ mol.L}^{-1}$   $\text{H}_2\text{SO}_4$  were recorded. Similarly, the UV-vis spectra of three solutions containing  $1.0 \times 10^{-2} \text{ mol.L}^{-1}$  of either lanthanum, praseodymium or neodymium salts were recorded.  $\epsilon$  values of all REEs were obtained according to the Beer-Lambert law. The molar extinction coefficients of all lanthanides studied

here were plotted against the wavelength and are shown in **Figure III.1**. The maximum absorption wavelengths and the corresponding molecular extinction coefficients for Ce(III) and Ce(IV) are also collected in **Table III.1**.

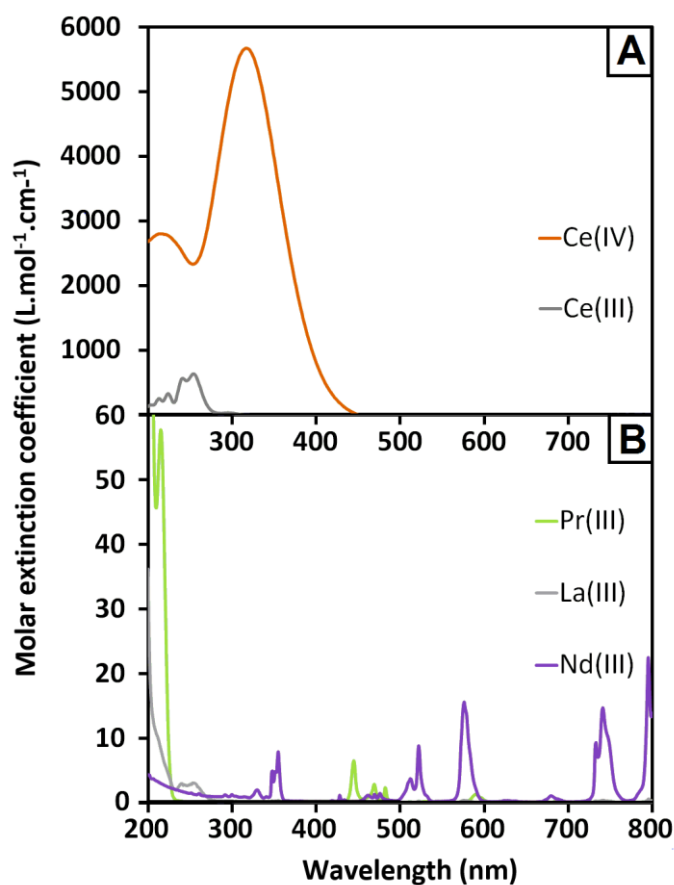


**Figure III.1.** Molar extinction coefficients for **A:** Ce(IV) in orange and Ce(III) in grey lines in 8.0 mol.L<sup>-1</sup> H<sub>2</sub>SO<sub>4</sub> and **B:** Nd(III) in purple, La(III) in grey and Pr(III) in green lines in 8.0 mol.L<sup>-1</sup> H<sub>2</sub>SO<sub>4</sub>

Rare Earth Elements	Molar extinction coefficient ( $\epsilon$ ) (L.mol <sup>-1</sup> .cm <sup>-1</sup> )		
	$\lambda = 212$ nm	$\lambda = 242$ nm	$\lambda = 315$ nm
Ce(IV)	2974.3	2718.4	7865.1
Ce(III)	245.21	590.53	0.70
La(III)	3.23	2.67	0.13
Nd(III)	9.93	1.67	0.90
Pr(III)	50.35	0.2	0.11

**Table III.1.** Molar extinction coefficient for Ce(IV), Ce(III), La(III), Nd(III) and Pr(III) at 212, 242 and 315 nm.

Comparison of the spectra of all lanthanides reveals that Ce(III) and Ce(IV) exhibit strong absorption bands compared to La(III), Pr(III) and Nd(III). These results are in agreement with the literature.<sup>244–246</sup> Besides, the absorption band centred around 315 nm observed on the spectrum of Ce(IV) exhibits a very high  $\epsilon$  value, and does not overlap with the absorption spectra of Ce(III).

At 315 nm, the molecular extinction coefficients of Ce(III), La(III), Nd(III) and Pr(III) never exceed  $1 \text{ L}\cdot\text{mol}^{-1}\cdot\text{cm}^{-1}$ . It can therefore be stated that the influence of Ce(III), La(III), Pr(III) and Nd(III) on the intensity of absorption at 315 nm recorded for a mixture of these lanthanide ions is negligible. Therefore, concentration for Ce(IV) will be measured throughout this part by using the intensity of absorption recorded at 315 nm.

#### *Oxidation of Ce(III)*

The simple oxidation of cerium(III) in cerium(IV) without the other Ln(III) was studied under alkaline conditions. Under such conditions, the insoluble solid of  $\text{Ce}_2(\text{SO}_4)_3$  is known to react and form an insoluble cerium(IV) hydroxide salt,  $\text{Ce}(\text{OH})_4$ .<sup>247</sup> Visually, a change in colour, starting from white for  $\text{Ce}_2(\text{SO}_4)_3$  to yellow is observed. This is a clear indication of the presence of  $\text{Ce}(\text{OH})_4$  in the precipitate. Note that neither  $\text{Ce}_2(\text{SO}_4)_3$ , nor  $\text{Ce}(\text{OH})_3$  or any other lanthanide hydroxide salts are soluble in water. The oxidation yield of Ce(III) was studied at two temperatures, namely 30 and 50 °C respectively. Results are shown in **Figure III.2**.

At 30 °C, a monotonous increase in the oxidation yield ( $Y_{\text{ox}}$ ) with NaOH is observed. Values of 4.2 % and 83.3 % are obtained at 0.2 and 1.0 mol.L<sup>-1</sup> NaOH respectively. At 50°C and from 0.2 to 1.0 mol.L<sup>-1</sup> NaOH,  $Y_{\text{ox}}$  is always higher than the oxidation yield observed at 30°C reaching values of 35.0 and 85.0 % respectively. However, the oxidation yields obtained at 30 and 50 °C appear to converge towards a mostly identical value, namely 87.7 % at 2.0 mol.L<sup>-1</sup> NaOH.

Overall, more than 87 % of  $\text{Ce}_2(\text{SO}_4)_3$  is found to be oxidised in Ce(IV) using a large excess of caustic soda at 30 and 50 °C.

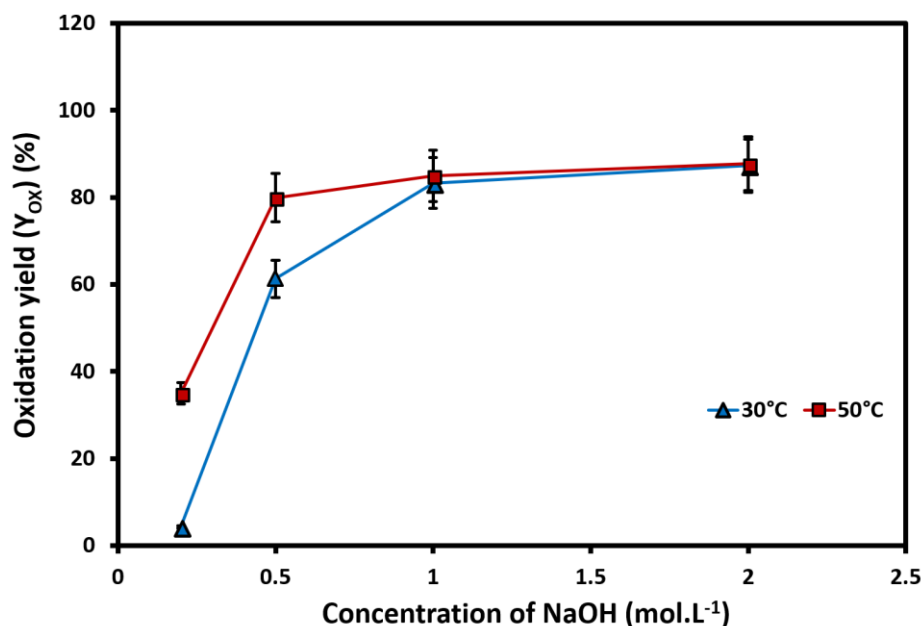
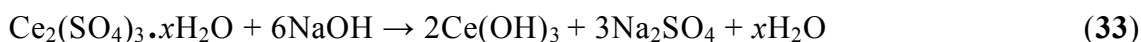


**Figure III.2.** Oxidation yield of cerium for several concentrations of sodium hydroxide. At 30°C: blue triangle, at 50°C: red square.

#### d. Discussion

$\text{Ce}_2(\text{SO}_4)_3$  is a salt exhibiting a low solubility in an alkaline aqueous solution. According to several reports,<sup>151,248,249</sup>  $\text{Ce}_2(\text{SO}_4)_3$ , which exhibits a white colour, reacts with  $\text{OH}^-$  under slightly basic conditions yielding the formation of a  $\text{Ce}(\text{OH})_3$  precipitate, which is also white.<sup>248</sup> The reaction is described in the following equation:



The amount of NaOH required for the previous equation to occur needs to be in slight excess, namely up to 1.25 times its stoichiometric ratio when the reaction occurs at 70°C.<sup>248</sup>

By contrast to this chemical scheme, mixing  $\text{Ce}_2(\text{SO}_4)_3$  in an aqueous solution containing a high concentration of NaOH was reported to yield oxidation of Ce(III) in Ce(IV), and subsequently to the formation of a yellow precipitate of  $\text{Ce}(\text{OH})_4$ .<sup>250,251</sup> According to a revised potential-pH diagram of Ce-H<sub>2</sub>O (reedited in **Figure III.3**), Hayes *et al.*<sup>250,251</sup> demonstrated that even though cerium(III) can form  $\text{Ce}(\text{OH})_3$  under alkaline conditions, oxidation of Ce(III) and subsequent formation of  $\text{Ce}(\text{OH})_4$  is thermodynamically possible when the pH exceeds 10.

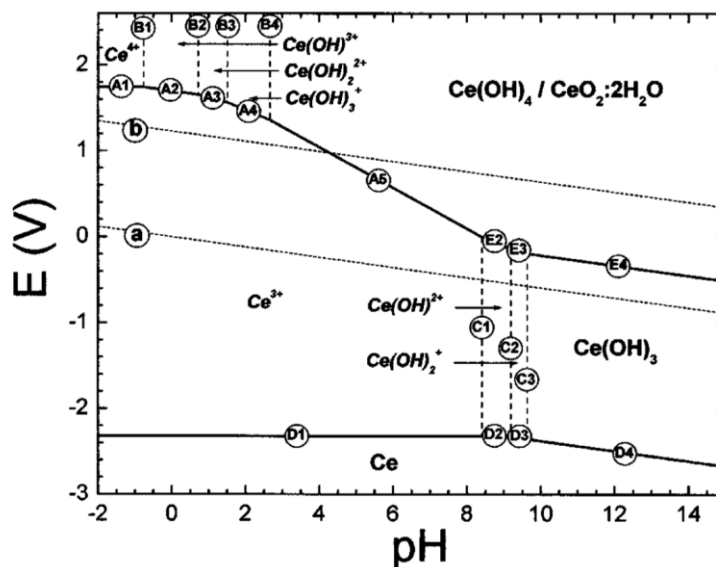


**Figure III.3.** Updated E-pH diagram of Ce-H<sub>2</sub>O system. Reedited from: Hayes et al. The phase stability of cerium species in aqueous systems, *J. Electrochem. Soc.*, **149** (12) C623-C630 (2002).<sup>250</sup>

Indeed, the redox potential for Ce(OH)<sub>3</sub>/Ce(OH)<sub>4</sub> is -0.45 V vs. NHE at pH 14.<sup>250,251</sup> This experimental value is based on the K<sub>s</sub> of Ce(OH)<sub>3</sub> and Ce(OH)<sub>4</sub> found in the literature, respectively  $2.2 \times 10^{-20}$  and  $1.0 \times 10^{-56}$  at 25°C<sup>236,252</sup> and on the redox potential of cerium at pH = 0 which is 1.44 vs. SHE. Since the redox potential of O<sub>2</sub>/OH<sup>-</sup> is typically 0.4 V vs. NHE at pH 14<sup>250,251</sup> one can obtain formation of Ce(OH)<sub>4</sub> through the following equations :



This reaction being the combination of two half reactions, namely the oxidation of Ce(III) and the reduction of O<sub>2</sub>. At this point, it is worthwhile noticing that the low solubility in water of cerium hydroxides reported at 25 °C implies that the amount of cerium remaining in water upon oxidation of Ce(III) is negligible. This implies that all Ce(IV) ions formed precipitate as Ce(OH)<sub>4</sub> and are therefore recovered by filtrating the solution.

In our experiments at 2.0 mol.L<sup>-1</sup> of caustic soda, the amount of NaOH is over 40 times the amount of Ce(III) and the pH is slightly higher than 14. The experimental conditions are thus favourable to the formation of Ce(OH)<sub>4</sub>, as proven by our experimental results gathered in **Figure III.2**. As seen on **Figure III.2**, increasing

the temperature appears to have a positive impact on the oxidation of cerium(III). Only  $0.5 \text{ mol.L}^{-1}$  sodium hydroxide is required at  $50^\circ\text{C}$  compared to  $1.0 \text{ mol.L}^{-1}$  at  $30^\circ\text{C}$  in order to reach a molar fraction of cerium(IV) close to 80 %. This result can be due to an enhancement of the diffusion of oxygen in the reactor which directly impacts the oxidation yield of cerium.<sup>247</sup> Moreover, the higher the pH, the higher the oxidation yield of Ce(III). This result is in accordance with *Hayes et al.* results<sup>250,251</sup> and can be explained considering that the higher the pH, the more thermodynamically favourable is the oxidation of  $\text{Ce(OH)}_3$  in  $\text{Ce(OH)}_4$ .

Please note that the oxidation of cerium(III) sulphate in cerium(IV) hydroxide in caustic soda is an heterogeneous reaction involving a liquid and a solid phase. The kinetics of oxidation is therefore expected to be rather low. Further optimisation of this process could also be envisaged using an ultrasonic setup and/or ozone as an oxidant species.

According to our results, acceptable conditions for oxidizing 1 g  $\text{Ce}_2(\text{SO}_4)_3$  to  $\text{Ce(OH)}_4$  is to use  $2 \text{ mol.L}^{-1}$  of NaOH in water (20 mL) at  $30^\circ\text{C}$  during 3 hours.

### III.2.3 Liquid-Liquid extraction of Ce(IV) by ILs

#### a. Experimental section

##### *Single extraction of lanthanides*

Extraction experiments were carried out in a centrifuging tube, mixing equal volumes of an ionic liquid with a solution containing  $2.0 \times 10^{-2} \text{ mol.L}^{-1}$  of cerium(III), lanthanum(III), neodymium(III), praseodymium (III) and cerium(IV) in aqueous solutions of nitric acid between 1.00 and  $4.00 \text{ mol.L}^{-1}$ .  $[\text{P}_{66614}][\text{NTf}_2]$  or  $[\text{C}_1\text{C}_4\text{Pyrr}][\text{NTf}_2]$  were used accordingly as extracting phase. Additionally, extraction of Ce(IV) from solutions containing 1.00 and  $3.45 \text{ mol.L}^{-1}$  of nitric acid and between  $1.0 \times 10^{-3}$  and  $2.0 \times 10^{-2} \text{ mol.L}^{-1}$  Ce(IV) was carried out using  $[\text{C}_1\text{C}_4\text{Pyrr}][\text{NTf}_2]$ . After stirring the tubes for 20 min on a shaker, centrifugation was carried out for 10 min at 6000 rpm.

All aqueous phases were analysed by ICP-OES before and after extraction experiments.

*Full extraction process of Ce(III) from a mixture of REE sulphate salts*

A mixture of cerium, praseodymium, lanthanum and neodymium sulphate salts was prepared. Oxidation experiment of the latter was carried out in  $2.0 \text{ mol.L}^{-1}$  NaOH at  $30^\circ\text{C}$ . The resulting precipitate was then dissolved in  $3.45 \text{ mol.L}^{-1}$  nitric acid. The amounts of each lanthanide salts and the volume of nitric acid solution were chosen in order to reach a final solution containing  $1.0 \times 10^{-2} \text{ mol.L}^{-1}$  of lanthanide ions. 1 mL of this aqueous phase was then mixed with 1 mL of  $[\text{C}_1\text{C}_4\text{Pyrr}][\text{NTf}_2]$  in a centrifuging tube. The two phases were stirred for 20 min and centrifuged for 10 min at 6000 rpm. Once separated from the ionic liquid, the aqueous phase was analysed by ICP-OES.

*Stripping of Ce(IV) and consecutive extraction cycles*

After extraction of an aqueous solution containing  $1.0 \times 10^{-2} \text{ mol.L}^{-1}$  Ce(IV) and  $3.45 \text{ mol.L}^{-1}$   $\text{HNO}_3$  by  $[\text{C}_1\text{C}_4\text{Pyrr}][\text{NTf}_2]$  in the same conditions as detailed above, the two phases were separated. 1 mL of the organic phase was stripped using 2 mL of  $\text{HNO}_3 = 1.00 \text{ mol.L}^{-1}$ . Within this work, an extraction step followed by a stripping step will be defined as an extraction cycle.

The resulting ionic liquid phase was separated from the aqueous phase and reused in another extraction cycle. Ten consecutive cycles of extraction were carried out. Aqueous phases before extraction and after stripping were analysed by ICP-OES.

b. Measurements

Measurements of the concentrations of lanthanides in their third oxidation state, denoted as Ln, were also carried out using Inductively Coupled Plasma (ICP) analysis. To that end, calibration solutions ranging from  $7 \times 10^{-6}$  to  $7 \times 10^{-4} \text{ mol.L}^{-1}$  Ln ( $\lambda^e \text{ Ce} = 418 \text{ nm}$ ,  $\lambda^e \text{ La} = 379 \text{ nm}$ ,  $\lambda^e \text{ Nd} = 406 \text{ nm}$  and  $\lambda^e \text{ Pr} = 391 \text{ nm}$ ) in 1.00 and  $4.00 \text{ mol.L}^{-1}$   $\text{HNO}_3$  were used. The influence of concentration of nitric acid on the measurement was found to be small, typically within the experimental error. A particular attention was also devoted to interferences that can exist between rare earth emission lines.<sup>253</sup>

According to our experimental protocol, we assume that the minimum and maximum calculable values for  $D$  are  $1 \times 10^{-3}$  and 1400, respectively.

The separation factor of cerium(IV) from lanthanides(III) is a good indicator of the efficiency of the separation and can be described by the following equation:



$$\beta_{Ln(III)}^{Ce(IV)} = \frac{D_{Ce(IV)}}{D_{Ln(III)}} \quad (37)$$

The efficiency of the consecutive extraction cycles, expressed in percentage can be defined by the following equation:

$$E_c = \frac{[Ce(IV)]_s \times V_s}{[Ce(IV)]_0 \times V_{aq}} \times 100 \quad (38)$$

where  $[Ce(IV)]_s$  represents the concentration of cerium(IV) in the stripped phase in  $\text{mol.L}^{-1}$  and  $V_s$  is the volume of the stripped phase in millilitres.

### c. Results

#### *Single extraction of lanthanides*

Extraction of Ce(IV) towards  $[C_1C_4\text{Pyrr}][\text{NTf}_2]$  and  $[P_{66614}][\text{NTf}_2]$  was studied using aqueous solutions containing between 1.00 and 4.00  $\text{mol.L}^{-1}$   $\text{HNO}_3$ . Visually, the influence of the acidity of  $\text{HNO}_3$  is clear. The higher the concentration of the acid, the more intense the yellow colour of the ionic liquid and the less intense that of the aqueous phase after extraction. Snapshots of extraction experiments are collected in **Figure III.4**.

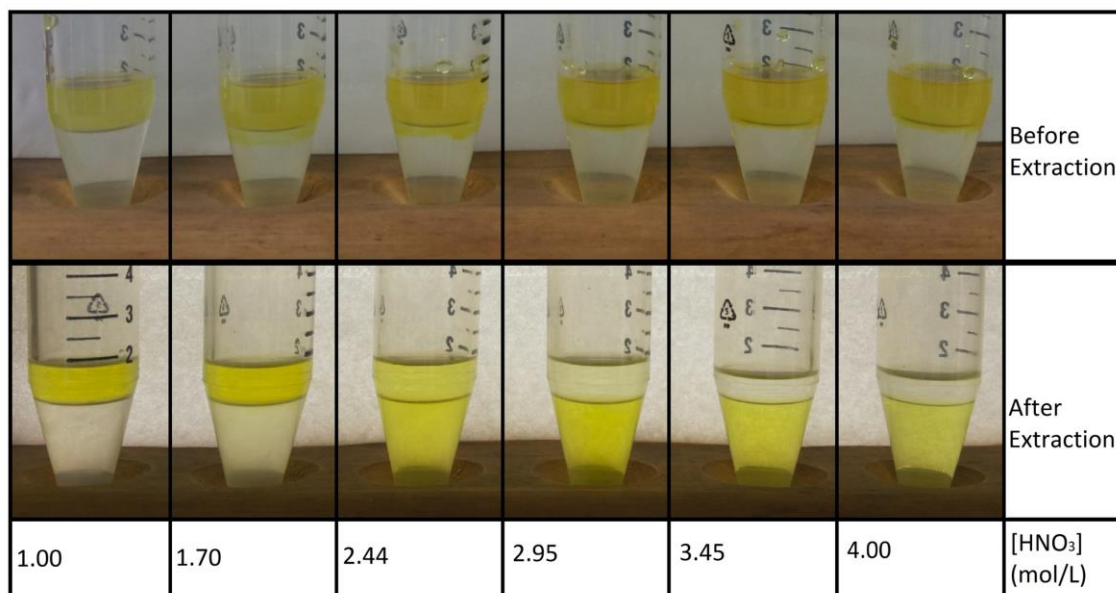


**Figure III.4.** Snapshots of cerium(IV) extractions by  $[P_{66614}][\text{NTf}_2]$  at various concentrations of  $\text{HNO}_3$

Distribution coefficients for Ce(IV) extracted towards  $[C_1C_4Pyrr][NTf_2]$  or  $[P_{66614}][NTf_2]$  are shown in **Figure III.5** and **Figure III.6** respectively. Values for distribution coefficients and separation factors are collected in **Table III.2**.

Experiments carried out using  $[C_1C_4Pyrr][NTf_2]$  (see **Figure III.5**) reveal on the one hand that the distribution coefficients for all Ce(III), La(III), Nd(III) and Pr(III) are negligible at any concentration of nitric acid. On the other hand, extraction of Ce(IV) from the aqueous phase is strongly influenced by the concentration of  $HNO_3$ . Extraction remains low below  $2.44 \text{ mol.L}^{-1} HNO_3$ . Values of 0.01 and 1.03 for  $D$  are obtained at  $1.00$  and  $2.44 \text{ mol.L}^{-1} HNO_3$ , respectively. A strong increase in  $D$  is then observed above  $2.44 \text{ mol.L}^{-1}$  of nitric acid, reaching a value of 109 at  $4.00 \text{ mol.L}^{-1} HNO_3$ . In such a case, extraction of cerium(IV) is considered quantitative. Separation factors of cerium(IV) from lanthanides(III) ( $\beta_{Ln(III)}^{Ce(IV)}$ ) are always above  $6 \times 10^3$  for La(III), Nd(III) and Pr(III) and equal to  $1.71 \times 10^3$  for Ce(III).

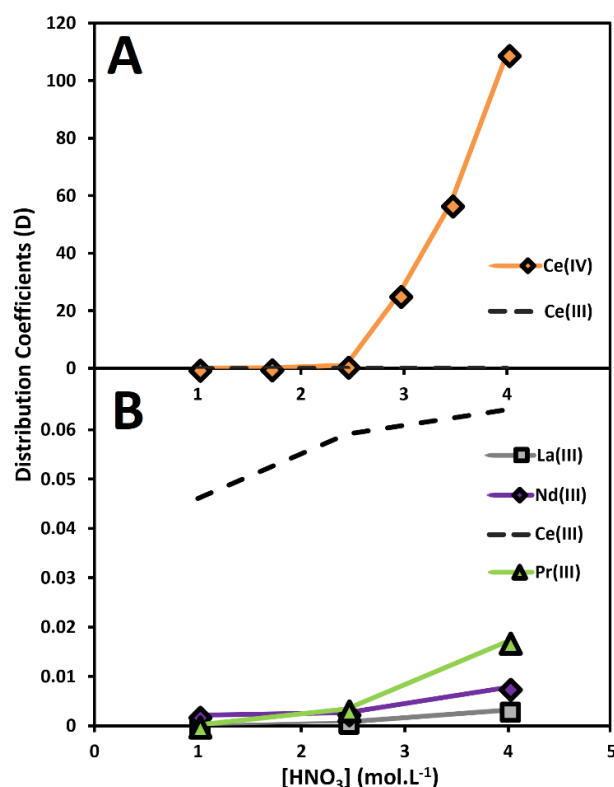


**Figure III.5.** Distribution coefficients for lanthanides ( $[Ln] = 2.0 \times 10^{-2} \text{ mol.L}^{-1}$ ) extracted separately towards  $[C_1C_4Pyrr][NTf_2]$  at various concentrations of  $HNO_3$ . **A:** Cerium(IV) in orange diamond and cerium(III) in black dotted line. **B:** lanthanum(III) in grey square, neodymium(III) in purple diamond, cerium(III) in black dotted line and praseodymium(III) in green triangle.

The situation is quite similar in  $[P_{66614}][NTf_2]$ . Extraction of Ln(III) towards  $[P_{66614}][NTf_2]$  is negligible, as shown in **Figure III.6**, while extraction of cerium(IV) increases markedly over the whole concentration range of  $HNO_3$ .  $D$  starts from 0.62 at  $1.00 \text{ mol.L}^{-1} HNO_3$  and reaches values of 29.0 and 52.3 at  $3.45$  and  $4.00 \text{ mol.L}^{-1} HNO_3$  respectively.

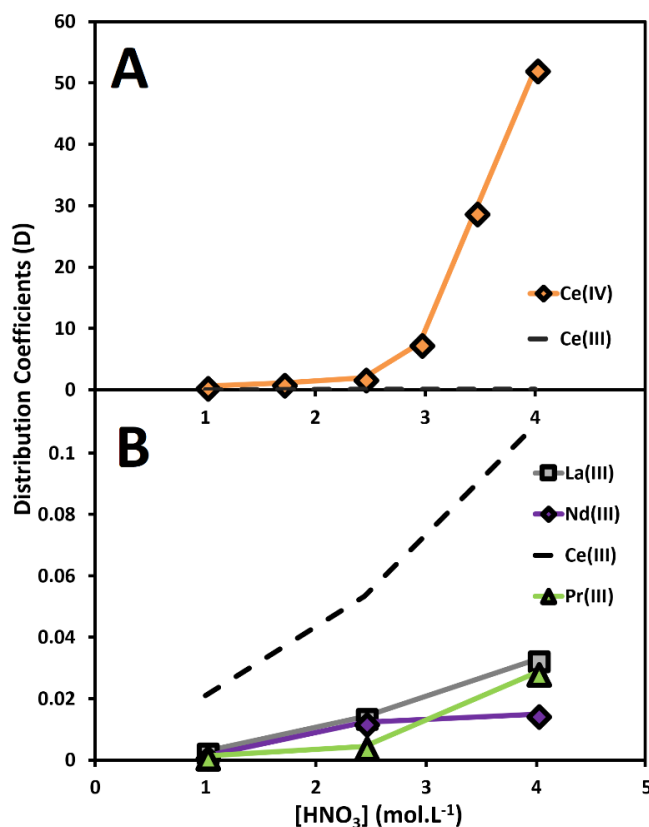


**Figure III.6.** Distribution coefficients of lanthanides ( $[Ln] = 2.0 \times 10^{-2} \text{ mol.L}^{-1}$ ) after single liquid-liquid extractions by  $[P_{66614}][NTf_2]$  at various concentrations of  $HNO_3$ . **A:** Cerium(IV) in orange diamond and cerium(III) in black dotted line. **B:** lanthanum(III) in grey square, neodymium(III) in purple diamond, cerium(III) in black dotted line and praseodymium(III) in green triangle.

Ionic Liquid	D							$\beta_{Ln(III)}^{Ce(IV)}$
	[HNO <sub>3</sub> ] (mol.L <sup>-1</sup> )	1.00	1.70	2.44	2.95	3.45	4.00	
[C <sub>1</sub> C <sub>4</sub> Pyrr][NTf <sub>2</sub> ]	La(III)	$1.41 \times 10^{-4}$	-	$7.70 \times 10^{-4}$	-	-	$3.14 \times 10^{-4}$	$3.48 \times 10^5$
	Nd(III)	$2.10 \times 10^{-3}$	-	$2.65 \times 10^{-3}$	-	-	$7.79 \times 10^{-3}$	$1.40 \times 10^4$
	Pr(III)	$1.66 \times 10^{-4}$	-	$3.42 \times 10^{-3}$	-	-	$1.72 \times 10^{-2}$	$6.36 \times 10^3$
	Ce(III)	$4.61 \times 10^{-2}$	-	$5.92 \times 10^{-2}$	-	-	$6.41 \times 10^{-2}$	$1.71 \times 10^3$
	Ce(IV)	$9.80 \times 10^{-3}$	$2.04 \times 10^{-1}$	1.03	25.6	57.1	109.4	-
[P <sub>66614</sub> ][NTf <sub>2</sub> ]	La(III)	$2.91 \times 10^{-3}$	-	$1.41 \times 10^{-2}$	-	-	$3.28 \times 10^{-2}$	$1.59 \times 10^3$
	Nd(III)	$1.28 \times 10^{-3}$	-	$1.22 \times 10^{-2}$	-	-	$1.49 \times 10^{-2}$	$3.51 \times 10^3$
	Pr(III)	$2.10 \times 10^{-3}$	-	$2.10 \times 10^{-3}$	-	-	$2.58 \times 10^{-2}$	$2.03 \times 10^3$
	Ce(III)	$2.10 \times 10^{-2}$	-	$5.34 \times 10^{-2}$	-	-	$1.09 \times 10^{-1}$	$4.80 \times 10^3$
	Ce(IV)	$6.23 \times 10^{-1}$	1.14	1.94	7.6	29.0	52.3	-

**Table III.2.** Distribution coefficients for lanthanides ([Ln] = 0.02 mol.L<sup>-1</sup>) extracted separately towards [C<sub>1</sub>C<sub>4</sub>Pyrr][NTf<sub>2</sub>] and [P<sub>66614</sub>][NTf<sub>2</sub>] at various concentrations of HNO<sub>3</sub> and their related separation factors of cerium(IV) from lanthanides(III) at 4.00 mol.L<sup>-1</sup> HNO<sub>3</sub>.

Overall, the main difference between the two ionic liquids used here lies in the maximum  $D$  value reached for Ce(IV). At 4.00 mol.L<sup>-1</sup> HNO<sub>3</sub>,  $D$  obtained using [C<sub>1</sub>C<sub>4</sub>Pyrr][NTf<sub>2</sub>] is twice as high as that obtained using [P<sub>66614</sub>][NTf<sub>2</sub>]. This is confirmed by the separation factors of cerium(IV) from lanthanides(III) which are lower for [P<sub>66614</sub>][NTf<sub>2</sub>] ( $1 \times 10^3 < \beta_{Ln(III)}^{Ce(IV)} < 5 \times 10^3$ ) than for [C<sub>1</sub>C<sub>4</sub>Pyrr][NTf<sub>2</sub>].

Extraction of Ce(IV) starting from  $2.0 \times 10^{-2}$  mol.L<sup>-1</sup> Ce(IV) in 3.45 mol.L<sup>-1</sup> HNO<sub>3</sub> using [C<sub>1</sub>C<sub>4</sub>Pyrr][NTf<sub>2</sub>] was also carried out. After centrifugation, the two phases were left in contact during 24 hours before analysis. Visually, the strong yellow colour exhibited by the ionic liquid due to the efficient extraction of Ce(IV), such as the tube on the far right of **Figure III.4**, faded away after 24 hours. Because the aqueous phase did not gain any yellow colour, this could be an indication of a reduction of Ce(IV) back to Ce(III), the latter not exhibiting any colour. This also underlines the necessity of carrying out short stirring and centrifuging steps in the overall recovery process for cerium. When phases are separated, Ce(IV) was found to be stable within the ionic liquid over a period of a few days.

*Impact of cerium(IV) concentrations*

Extraction of Ce(IV) towards  $[C_1C_4Pyrr][NTf_2]$  starting from various initial concentrations of cerium ions was studied using two different  $HNO_3$  concentrations. The distribution coefficients have been plotted against the concentration of Ce(IV) in **Figure III.7**.  $D$  values are also collected in **Table III.3**. At  $2.44 \text{ mol.L}^{-1} HNO_3$ , one can observe a low extraction of cerium(IV) ( $D = 1.03$ ) when starting with  $1.0 \times 10^{-2} \text{ mol.L}^{-1}$  of cerium(IV). Decreasing the metal concentration leads to an increase in the distribution ratio, the latter reaching values of 3.15 and 16.9 using  $5.0 \times 10^{-3}$  or  $1.0 \times 10^{-3} \text{ mol.L}^{-1}$  of cerium(IV) in the aqueous phase accordingly. This phenomenon is even more marked at  $3.45 \text{ mol.L}^{-1} HNO_3$ . In this case,  $D$  values were found to be 57.1 and 246.2 using  $2.0 \times 10^{-2}$  and  $1.0 \times 10^{-3} \text{ mol.L}^{-1}$  cerium(IV) respectively.

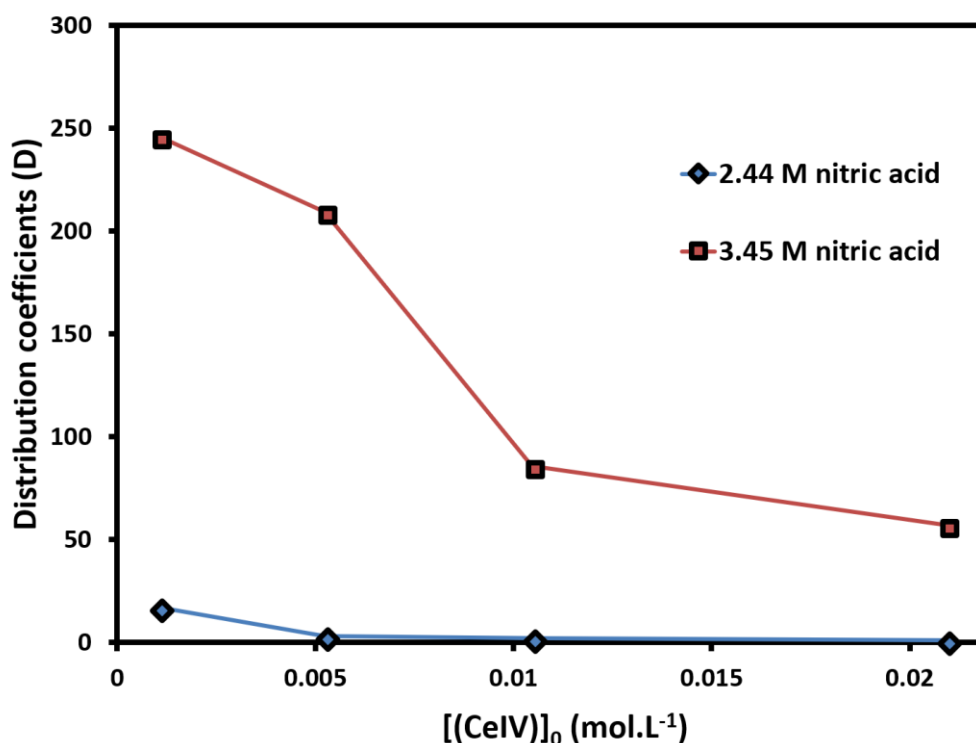


**Figure III.7.** Distribution coefficients for cerium(IV) extracted towards  $[C_1C_4Pyrr][NTf_2]$  at various concentrations of  $[Ce(IV)]_0$  for two different nitric acid concentrations.  $2.44 \text{ mol.L}^{-1} HNO_3$ : blue diamond,  $3.45 \text{ mol.L}^{-1} HNO_3$ : red square.

[Ce(IV)] (mol.L <sup>-1</sup> )	D Ce(IV)	
	2.44 mol.L <sup>-1</sup> HNO <sub>3</sub>	3.45 mol.L <sup>-1</sup> HNO <sub>3</sub>
2.00 × 10 <sup>-2</sup>	1.03	57.11
1.00 × 10 <sup>-2</sup>	2.19	85.68
5.00 × 10 <sup>-3</sup>	3.15	209.41
1.00 × 10 <sup>-3</sup>	16.95	246.20

**Table III.3.** Distribution coefficient for cerium(IV) using [C<sub>1</sub>C<sub>4</sub>Pyrr][NTf<sub>2</sub>] at various concentrations of [Ce(IV)]<sub>0</sub> for two different nitric acid concentrations.

*Full process for the separation of Ce(III) sulphate from other lanthanides*

A two-step process for recovering cerium as Ce(IV) from a mixture of lanthanide salts Ce<sub>2</sub>(SO<sub>4</sub>)<sub>3</sub>, Nd<sub>2</sub>(SO<sub>4</sub>)<sub>3</sub>, LaCl<sub>3</sub>, and PrCl<sub>3</sub> was carried out. According to the results reported above, the experiments were performed solely with [C<sub>1</sub>C<sub>4</sub>Pyrr][NTf<sub>2</sub>]. Oxidation of Ce(III) to Ce(IV) under alkaline pH and in presence of other lanthanides was first carried out. At the end of this step, lanthanides are obtained as insoluble hydroxide salts. In a second step, these hydroxide salts filtered from the solution and washed with water, were dissolved in 3.45 mol.L<sup>-1</sup> HNO<sub>3</sub>. Ce(IV) was then selectively extracted towards [C<sub>1</sub>C<sub>4</sub>Pyrr][NTf<sub>2</sub>]. Results for the extraction of all lanthanides are presented in

**Table III.4.**

Mixture of lanthanides	D	$\beta_{Ln(III)}^{Ce(IV)}$
Ce(IV)	74.9	-
La(III)	2.80 × 10 <sup>-3</sup>	2.68 × 10 <sup>4</sup>
Nd(III)	< 1.00 × 10 <sup>-3</sup>	7.49 × 10 <sup>4</sup>
Pr(III)	2.50 × 10 <sup>-3</sup>	2.97 × 10 <sup>4</sup>

**Table III.4.** Distribution coefficients for lanthanides and separation factors of cerium(IV) from lanthanides(III) extracted towards [C<sub>1</sub>C<sub>4</sub>Pyrr][NTf<sub>2</sub>], subsequently to an oxidation step using NaOH. Extraction carried out using 3.45 mol.L<sup>-1</sup> HNO<sub>3</sub> and 1 × 10<sup>-2</sup> mol.L<sup>-1</sup> lanthanide ions.

In agreement with the results obtained for the oxidation of Ce(III) to Ce(IV) detailed previously, the oxidation yield is 87.1 % in presence of other lanthanides. Under these conditions, it appears that the presence of other lanthanides has no significant influence on the oxidation of Ce(III).

Furthermore and as expected in the extraction step of the process, a clear change in the colour of the aqueous phase was observed within minutes, while the ionic liquid changed from colourless to a strong yellow colour. The distribution coefficient of cerium(IV) was calculated taking into consideration that the initial cerium(IV) concentration in the aqueous phase, namely  $[\text{Ce(IV)}]_0$ , represents 87.1 % of the total cerium concentration in the hydroxide precipitate. Because cerium(III) is very poorly extracted in those conditions, the extraction of the remaining 12.9 % of Ce(III) has been neglected. The distribution coefficient value for Ce(IV) is 74.9 which is in agreement with the value obtained for the single extraction of Ce(IV) ( $D = 85.7$ ). La(III), Nd(III) and Pr(III) are very poorly extracted ( $D < 3.0 \times 10^{-3}$ ). Resulting separation factors of cerium(IV) from La(III), Nd(III) and Pr(III) are high, reaching values of  $2.68 \times 10^4$ ,  $7.49 \times 10^4$ , and  $2.97 \times 10^4$  respectively.

Overall, the process for separating Ce(IV) from Ln(III) appears feasible starting from sulphate lanthanide salts using simple steps.

#### *Stripping of Ce(IV) and consecutive extraction cycles*

Based on the results displayed in **Figure III.5**, stripping was investigated using an aqueous phase containing  $1.00 \text{ mol.L}^{-1} \text{ HNO}_3$ . Over 99.5 % of cerium(IV) was recovered which demonstrates that the back extraction can be carried out efficiently.

According to these results, the recycling of the ionic liquid and its further reuse as an extraction phase were investigated carrying out ten consecutive extraction cycles. According to our previous results detailed above, extraction was carried out starting from  $3.45 \text{ mol.L}^{-1} \text{ HNO}_3$ . The stripping of Ce(IV) from the ionic liquid phase was then carried out using  $1.00 \text{ mol.L}^{-1} \text{ HNO}_3$ . These two steps were then performed ten consecutive times using the same sample of  $[\text{C}_1\text{C}_4\text{Pyrr}][\text{NTf}_2]$ . The efficiency of the consecutive extraction cycles ( $E_c$ ), corresponding to the amount of Ce(IV) recovered from the ionic liquid after each cycle (see eq. 4), was plotted against the number of cycles in **Figure III.8**.

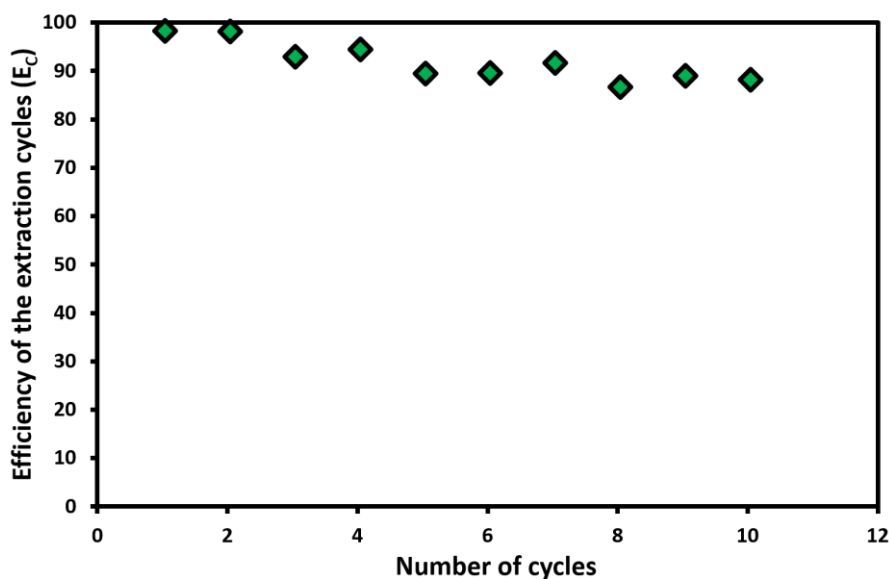


**Figure III.8.** Consecutive extraction steps of cerium(IV) obtained by ten extractions-stripping cycles of  $[\text{Ce(IV)}]_0 = 1.0 \times 10^{-2} \text{ mol.L}^{-1}$  in  $[\text{HNO}_3] = 3.45 \text{ mol.L}^{-1}$  by  $[\text{C}_1\text{C}_4\text{Pyrr}][\text{NTf}_2]$ .

One can observe that 98.8 % of cerium(IV) initially dissolved in  $3.45 \text{ mol.L}^{-1}$   $\text{HNO}_3$  was recovered from the ionic liquid after one extraction cycle. This value slowly decreases as the ionic liquid is reused. After five cycles,  $E_c$  exhibits a value of 90.1 %. After ten cycles, the value for  $E_c$  is 88.7 %. Despite this slight decrease,  $[\text{C}_1\text{C}_4\text{Pyrr}][\text{NTf}_2]$  appears to be promising extracting phase in a consecutive extraction process for cerium. This is a key factor in the development of a whole process for the recovery of cerium from lanthanide powders fitting the principles of green chemistry.<sup>82</sup>

#### d. Discussion

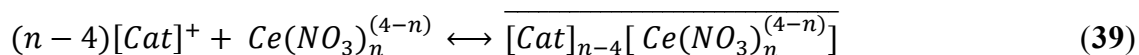
Extraction of Ce(IV) was previously reported using bifunctional ionic liquids derived from phosphine oxide, such as Cyanex<sup>®</sup> 923.<sup>254,255</sup> To the best of our knowledge, only one team worked on extraction of Ce(IV) in nitric acid using a hydrophobic ionic liquid based on an imidazolium cation, namely 1-octyl-3-methylimidazolium hexafluorophosphate ( $[\text{C}_8\text{MIM}][\text{PF}_6]$ ).<sup>88</sup> Competitive extraction of Ce(IV) from nitric acid solutions was carried out in presence of Th(IV), Gd(III) and Yb(III). However because of the decomposition of the  $[\text{PF}_6]^-$  anion and the risk of formation of hydrofluoric acid,<sup>240</sup> the concentration of nitric acid was kept below  $4.00 \text{ mol.L}^{-1}$ .  $D$  for Ce(IV) was reported to increase linearly



from 2 to 62 with  $[\text{HNO}_3]$  ranging from 0.91 to 3.06 mol.L<sup>-1</sup>. In their article, Zuo et al.<sup>88</sup> explained the extraction of Ce(IV) in terms of formation of a negatively charged hexanitratocerate(IV) complex and ion exchange with  $[\text{PF}_6^-]$  anions.

Our results are in general agreement with those presented by Zuo et al. When the concentration of nitric acid is low, typically below 2.44 mol.L<sup>-1</sup>, Ce(IV) is mostly not extracted. As seen in **Figure III.5** and **Figure III.6**, the distribution coefficient for Ce(IV) exceeds 1 when  $[\text{HNO}_3]$  is above 2 or 2.44 mol.L<sup>-1</sup> using  $[\text{P}_{66614}][\text{NTf}_2]$  or  $[\text{C}_1\text{C}_4\text{Pyrr}][\text{NTf}_2]$  accordingly. Between 2.44 and 4.00 mol.L<sup>-1</sup>  $\text{HNO}_3$ ,  $D$  for Ce(IV) obtained using  $[\text{C}_1\text{C}_4\text{Pyrr}][\text{NTf}_2]$  is always higher than that obtained with  $[\text{P}_{66614}][\text{NTf}_2]$  resulting in stronger separation factors of cerium(IV) from lanthanides(III).

These results can be explained by the fact that phosphonium ionic liquids<sup>188</sup> exhibit higher viscosities than other ionic liquids such as  $[\text{C}_1\text{C}_4\text{Pyrr}][\text{NTf}_2]$ , which hinders mixing the two phases and thus the extraction of the metal. However, this may not be the only factor influencing the extraction efficiency. Even though some papers have highlighted the presence of a negatively charged complex of cerium nitrate, namely  $\text{Ce}(\text{NO}_3)_6^{2-}$ ,<sup>256,257</sup> to the best of our knowledge, the speciation of cerium(IV) nitrate complexes as a function of the nitric acid concentration has not been extensively studied yet. It is thus difficult to discuss further which complex is extracted towards the ionic liquid. According to our results, and in agreement with some previous works obtained by our group dealing with the extraction of platinum group metal ions<sup>258,259</sup> showing that such metallic ions are efficiently extracted when they form single or double negatively charged complexes, above 2.44 mol.L<sup>-1</sup>  $\text{HNO}_3$ , such a negatively charged polynitratocerate(IV) complex is most probably formed in the aqueous phase and extracted towards the ionic liquid. Actually, assuming the presence of a negatively charged cerium(IV) complex and assuming that extraction occurs with the help of an ion pair formation, as detailed in a recent article,<sup>259</sup> the lower the concentration of cation, the lower the ion pair formation with a cerium(IV)-nitrate complex. Please note that considering an ion exchange mechanism yields the same result, since it was recently proven that in an ionic liquid, these two mechanisms are actually identical.<sup>259,260</sup> Briefly and following previous results obtained for the extraction of  $\text{PtCl}_6^{2-}$  towards an ionic liquid, the ion pair formation can be described in our case as follows:



$[Cat]^+$  is the ionic liquid cation in the aqueous phase, and the bar refers to the species in the organic phase.  $n$  is superior to 4 in order to obtain a negatively charged complex of cerium. In addition, the solubility in water of the ionic liquid can be written as:



One can deduce that the lower the solubility in water of the ionic liquid, the lower the amount of ionic liquid available in the aqueous phase and the lower the extraction of the metal ion. This is observed experimentally. Moreover, for a given solubility in water of the ionic liquid, hence a given concentration of ionic liquid cation in water, the higher the excess of Ce(IV) compared to  $[Cat]^+$ , the lower the possibility to form hydrophobic ion pairs, and the lower the extraction of Ce(IV). The latter statement is in line with data displayed in **Figure III.7**: for the same ionic liquid and at a given nitric acid concentration, the distribution coefficient for Ce(IV) decreases with the metal concentration. At a concentration of  $HNO_3$  of  $3.45 \text{ mol.L}^{-1}$ ,  $D$  decreases from 86.7 down to 57.1 when the concentration of Ce(IV) increases from  $1.0 \times 10^{-2}$  to  $2.0 \times 10^{-2} \text{ mol.L}^{-1}$ . Using ionic liquids, such a decrease in the distribution coefficient with the initial concentration of metal ions has been observed in many experiments.<sup>183,184,191</sup> This is now known to be in contradiction with the results obtained when classical organic solvents are used as an extracting phase. In the latter case,  $D$  is generally constant as the metal concentration increases, until the saturation of the organic phase, sometimes leading to the formation of a third phase.<sup>261,262</sup> Furthermore, the extraction mechanism of Ce(IV) in NTf2-based IL will release in the aqueous phase some NTf2- anions therefore, the solubility of bis(trifluoromethanesulfonyl)imide anions in water can limit the extraction.

Competitive extraction of Ce(IV) in presence of other lanthanides such as La(III), Ce(III), Ce(IV), Nd(III) and Pr(III) was successfully carried out. Because all lanthanide ions in their third oxidation state do not form any negatively charged complexes in presence of nitrate ions, they remain in the aqueous solution, which

is in agreement with previous results.<sup>88</sup> This explains why Ce(IV) is preferentially extracted compared to other lanthanide(III) ions.

### III.2.4 Conclusion

In this part, a process for recovering cerium from a mixture of lanthanide salts namely cerium, lanthanum, praseodymium and neodymium was investigated. Cerium(III) sulphate was firstly oxidized by oxygen in a reactor containing 2.0 mol.L<sup>-1</sup> NaOH at a temperature of 30°C and after 3 hours of stirring. At that stage, more than 87 % of cerium was oxidized and precipitated out as Ce(OH)<sub>4</sub> while lanthanum, neodymium and praseodymium precipitated as Ln(OH)<sub>3</sub>. Lanthanide hydroxides were then dissolved in 3.45 mol.L<sup>-1</sup> nitric acid before being extracted towards [C<sub>1</sub>C<sub>4</sub>Pyrr][NTf<sub>2</sub>]. The latter gave better results than [P<sub>66614</sub>][NTf<sub>2</sub>]. Only cerium(IV) is loaded in the organic phase. Indeed, the distribution coefficient of cerium(IV) reaches 85.7 when the metal concentration is of 1.0×10<sup>-2</sup> mol.L<sup>-1</sup> while lanthanum, neodymium and praseodymium are very poorly extracted in the ionic liquid ( $D < 3.0 \times 10^{-3}$ ). Our results indicate that liquid-liquid extraction of Ce(IV) can be enhanced by decreasing the metal concentration and increasing the nitric acid molarity. Finally, cerium can easily be recovered in an aqueous phase by performing a simple stripping step using a solution of 1.00 mol.L<sup>-1</sup> HNO<sub>3</sub>. Consecutive extraction and stripping steps were carried out showing that the ionic liquid can be regenerated at least ten times.

To conclude, liquid-liquid extraction of cerium(IV) in a nitric acid solution from heavier lanthanides, such as Gd(III) and Yb(III) respectively was performed by Zuo et al.<sup>88</sup> with [C<sub>8</sub>MIM][PF<sub>6</sub>]. In our work, separation of cerium(IV) from light lanthanides starting from nitric acid solutions towards two ionic liquids, namely, [P<sub>66614</sub>][NTf<sub>2</sub>] and [C<sub>1</sub>C<sub>4</sub>Pyrr][NTf<sub>2</sub>] was carried out. Results imply that cerium(IV) in nitric acid will always be separated after extraction towards a NTf<sub>2</sub><sup>-</sup> based ionic liquid from lanthanides if the competitive metals do not form negatively charged complexes with nitrates.

Based on those results, the previous process will be applied to isolate cerium from a sulphate lanthanide powder obtained from spent NiMH batteries in **Chapter II**.

## III.3 Recovery of cerium from spent

### NiMH batteries

---

#### III.3.1 Extraction of cerium in spent NiMH batteries

##### a. Introduction

According to the results obtained in **Chapter II** and **III** the recovery of pure cerium starting from end-of-life NiMH batteries will be presented here following the *modus operandi* detailed below.

##### b. Experimental section

Starting from 1 g of  $\text{NaREE}(\text{SO}_4)_2$  obtained in **Chapter II**, the powder was mixed with sodium hydroxide  $2 \text{ mol.L}^{-1}$  during 3 hours. After filtration, the solid phase was dried ( $50 \text{ }^\circ\text{C}$  during 12 h) and a small proportion of the obtained powder was dissolved in sulfuric acid for UV-vis analysis following the experimental method developed in **part III.2**.

The yellow powder obtained was dissolved in nitric acid  $4 \text{ mol.L}^{-1}$  in order to obtain a concentration of cerium close to  $1.5 \cdot 10^{-2} \text{ mol.L}^{-1}$ . 20 mL of the following solution was put in contact with 20 mL of  $[\text{C}_1\text{C}_4\text{Pyrr}][\text{NTf}_2]$ . After stirring the tube for 20 min on a shaker, centrifugation was carried out for 10 min at 6000 rpm. The ionic liquid phase was isolated from the bottom aqueous one. Cerium was stripped from the IL using 40 mL of  $\text{HNO}_3$   $1 \text{ mol.L}^{-1}$  in water and shaking for 20 min. Finally, the stripping phase was separated from the organic phase and the pH of the solution was set to 10 adding  $\text{NaOH}$   $2 \text{ mol.L}^{-1}$  under agitation. The remaining precipitate was recovered by filtration and dried during 3 hours in an oven at  $80 \text{ }^\circ\text{C}$  before being analysed by XRD and SEM.

All aqueous phases were analysed by ICP-OES before and after extraction, stripping and precipitation experiments.

c. Results and discussion

The complete flow sheet for cerium recovery starting from  $\text{NaREE}(\text{SO}_4)_2$  is depicted in **Figure III.9**.

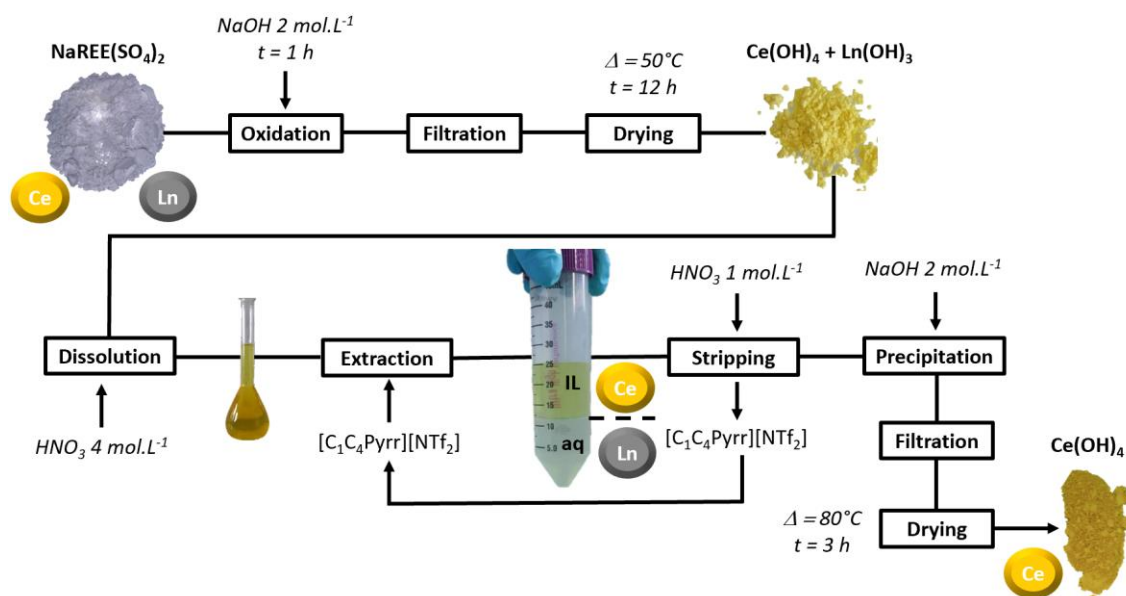


**Figure III.9.** Flow sheet for the recovery of pure cerium hydroxide starting from  $\text{NaREE}(\text{SO}_4)_2$  produced from spent NiMH batteries.

The total concentrations of all lanthanides in aqueous solutions i.e before and after extraction, after stripping and after precipitation are analysed by ICP as well as the concentration of Ce(IV) in the oxidized hydroxide powder is analysed by UV-vis spectrometry and are depicted in **Table III.5**.

Concentration (mg.g <sup>-1</sup> of BM)	Ln(OH) <sub>n</sub>	Aqueous solutions			
	Oxidation	Before extraction	After extraction	Stripping	Precipitation
La	19.40 ± 0.3	19.40 ± 0.3	19.44 ± 0.3	< 0.3	< 0.3
Ce	14.05 ± 0.3	14.05 ± 0.3	1.76 ± 0.3	12.24 ± 0.3	< 0.3
Nd	6.03 ± 0.3	6.03 ± 0.3	6.09 ± 0.3	< 0.3	< 0.3
Pr	2.12 ± 0.3	2.12 ± 0.3	2.11 ± 0.3	< 0.3	< 0.3
Ce(IV)	12.46 ± 0.5	-	-	-	-
Y <sub>OX</sub> (mol. %)	88.7	-	-	-	-
Concentration (g.L <sup>-1</sup> )	-	Before extraction	After extraction	Stripping	Precipitation
La	-	2.90 ± 0.04	2.92 ± 0.04	< 0.04	< 0.04
Ce	-	2.11 ± 0.04	0.24 ± 0.04	0.93	< 0.04
Nd	-	0.90 ± 0.04	0.91 ± 0.04	< 0.04	< 0.04
Pr	-	0.32 ± 0.04	0.32 ± 0.04	< 0.04	< 0.04

**Table III.5.** Mass balance for oxidation, extraction, stripping and precipitation steps in the overall process of cerium separation from lanthanum, neodymium and praseodymium.

Focusing on the oxidation step, more than 88 mol. % of cerium(III) has been oxidized to Ce(IV) as hydroxide salts. The three other REE, namely, lanthanum, neodymium and praseodymium remained in their third oxidation state. This result is in full agreement with our work developed in **part III.2**. Liquid-Liquid extraction performed in nitric acid using [C<sub>1</sub>C<sub>4</sub>Pyrr][NTf<sub>2</sub>] allowed us to extract more than 87 % of the total cerium which represents 97.8 % of Ce(IV). After stripping, the quantity of mater of cerium in the aqueous phase is equal to the difference between the quantity of mater of cerium before and after extraction. In other words, cerium was quantitatively loaded in an aqueous phase by regenerating the ionic liquid during the stripping step.

Finally, no trace of cerium can be found in the aqueous solution after precipitating it under hydroxide by increasing the pH of the solution.

The shape and semi-quantification of the precipitate is shown in **Figure III.10**.

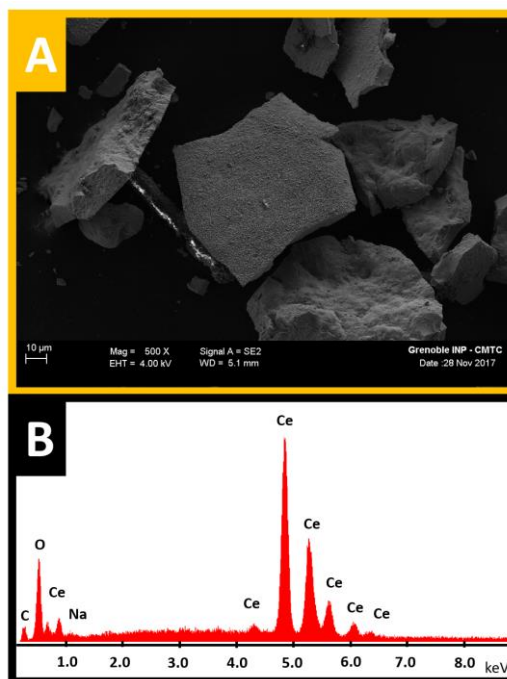


**Figure III.10.** SEM analysis of the recycled cerium obtained from spent NiMH batteries. A: SE image (magnification  $\times 500$ ). B: Elemental analysis by EDS.

Hydroxide particles present a high purity as no other rare earth elements can be spotted. This is strengthened by the absence of lanthanum, neodymium and praseodymium in the aqueous phase before the precipitation step. We thus bring the proof, that cerium contained in spent NiMH batteries can be recycled and recovered after being isolated from all transition and rare earth metals. Efficiency of the overall process is shown in **Figure III.11**.

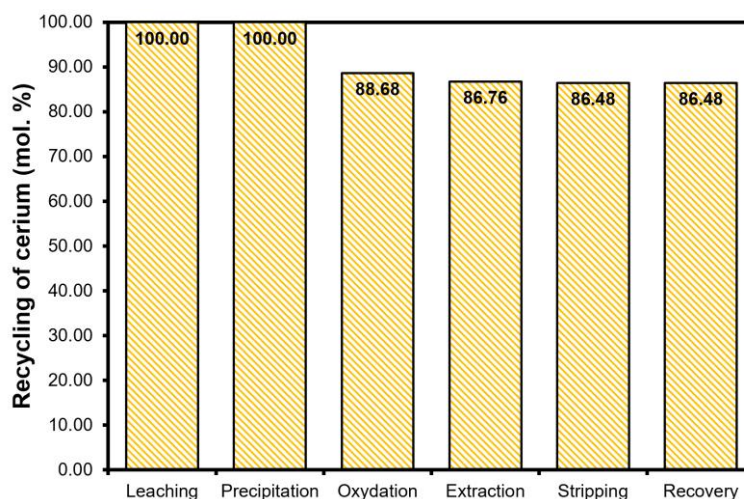


**Figure III.11.** Recycling yield for cerium after each leaching, precipitation, oxidation, extraction, stripping and precipitation steps on the overall recycling process of spent NiMH batteries.

Our results reveal that over 86 molar percent of pure cerium is recycled starting from NiMH batteries. This represents 12.24 mg of Ce extracted per gram of black mass.

It is worth noticing that the less efficient step is the oxidation of Ce(III) to Ce(IV) (oxidation yield of 88.7 mol. %). The difficulty of increasing this yield is related to (i) the heterogeneity of the solid/liquid mixture that hinders the diffusion of oxygen in the hydroxide particle (ii) a passivation mechanism of Ce(OH)<sub>4</sub> to CeO<sub>2</sub>. Several solutions could be investigated:

-An ultrasonic probe could be used to (i) enhance the mixing between the solid and the liquid phase (ii) oxidize cerium to its fourth oxidation state by the production of radicals, ranging on the frequency of the probe.<sup>263</sup>

-According to the potential-pH diagram of Ce-H<sub>2</sub>O system,<sup>250</sup> Ce(III) cations could be oxidized to Ce(IV) in a fully homogeneous acidic aqueous phase by ozone bubbling.

### III.3.2 Electrodeposition of cerium in an ionic liquid: an alternative recovery strategy

This part was carried out in collaboration with Céline Bonnaud during her PhD thesis untitled: “*Towards a recycling process of permanent magnets based on rare earth elements by electrochemistry in an ionic liquid media*”.

#### a. Introduction

In order to study an alternative way to recover pure cerium after it is loaded in an ionic liquid without using a stripping method, electrochemical deposition of cerium(IV) in the IL was investigated.

Starting from Ce(III) carbonate salts, *Hatchett et al. 2012*<sup>223</sup> showed that cerium is able to be reduced to metallic particles after dissolution in [N<sub>4111</sub>][NTf<sub>2</sub>] by using the conjugated acid, HNTf<sub>2</sub>. However, up to our knowledge, consecutive extraction and electrodeposition steps were never reported in the literature for the recovery of cerium. It is worth noticing that neodymium was successfully loaded from an aqueous phase to an ionic liquid based on an octylphosphite anion in the work of *Zarrougui et al. 2017*<sup>118</sup> before being deposited in the ionic liquid. However, this



IL is unable to isolate one rare earth element from another after one extraction step.

In this work, we present the consecutive separation of Ce(IV) from La(III), Nd(III) and Pr(III) by liquid-liquid extraction in  $[\text{C}_1\text{C}_4\text{Pyrr}][\text{NTf}_2]$ , and electrodeposition of cerium in the same media.

b. Experimental section

After performing a liquid-liquid extraction of Ce(IV) in a  $4 \text{ mol.L}^{-1} \text{ HNO}_3$  aqueous solution by  $[\text{C}_1\text{C}_4\text{Pyrr}][\text{NTf}_2]$  depicted in **part III.3.1**, the ionic liquid phase containing approximately  $1.5 \text{ mol.L}^{-1}$  of cerium was sampled and separated from the aqueous phase. A small aliquot of  $[\text{C}_1\text{C}_4\text{Pyrr}][\text{NTf}_2]$  was taken to measure the water content before and after extraction by Karl Fischer titration (**ANNEX 1-E**). 5 mL of the ionic liquid is sampled and poured in a temperature-controlled reactor. A three-electrode array setup is soaked in  $[\text{C}_1\text{C}_4\text{Pyrr}][\text{NTf}_2]$  loaded with Ce(IV). The setup is composed of a gold rotating working electrode (WE) of 0.196 cm diameter, a platinum wire immersed in ferrocene/ferrocenium ( $\text{Fc}/\text{Fc}^+$ ) in equimolar conditions used as a reference electrode (RE). The redox couple was separated from the bulk by a glass frit. A platinum grid was used as a counter electrode (CE). The working electrode is polished with a diamond paste and rinsed before all experiments. All experiments were carried out under hydrodynamic control, the rotating speed of the working electrode being set to 500 rpm. The temperature of the bath was set to  $25 \text{ }^\circ\text{C}$ . Cyclic voltammetry was obtained between -3 and 2 V vs.  $\text{Fc}/\text{Fc}^+$  for neat  $[\text{C}_1\text{C}_4\text{Pyrr}][\text{NTf}_2]$  and between -3 and 0 V vs.  $\text{Fc}/\text{Fc}^+$  for  $[\text{C}_1\text{C}_4\text{Pyrr}][\text{NTf}_2]$  loaded in Ce(IV) after extraction. The scan rate was set to  $0.05 \text{ V.s}^{-1}$ . Electrodeposition of cerium was carried out by chronoamperometry techniques at -2 V vs.  $\text{Fc}/\text{Fc}^+$  during 2 hours. The working electrode is then removed from the ionic liquid phase and washed with water and ethanol. The gold WE was then dried overnight at room temperature before being analysed by SEM.

c. Results and Discussion

Cyclic voltammetry (CV) measurements are shown in **Figure III.12**.

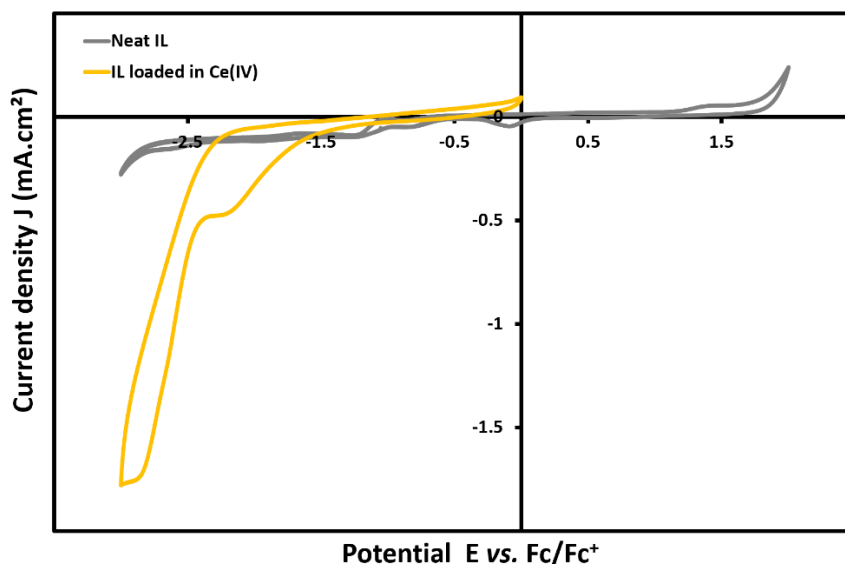
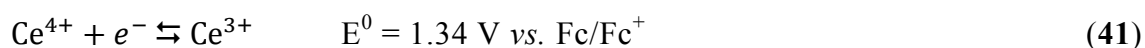


**Figure III.12.** Cyclic voltammetry experiments recorded at a scan rate of  $0.05 \text{ V.s}^{-1}$ . The temperature is set to  $25^\circ\text{C}$  and the rotating speed is 500 rpm. Grey curve: neat  $[\text{C}_1\text{C}_4\text{Pyrr}][\text{NTf}_2]$ . Yellow curve:  $[\text{C}_1\text{C}_4\text{Pyrr}][\text{NTf}_2]$  loaded with Ce(IV) after extraction in a nitric acid media.

CV of the neat IL shows a relatively flat signal between  $-2.5$  and  $1.5 \text{ V vs. Fc/Fc}^+$ . Beyond the latter values, degradation of the solvent takes place and defines the limit of the electrochemical window of  $[\text{C}_1\text{C}_4\text{Pyrr}][\text{NTf}_2]$ . At  $-3.0 \text{ V vs. Fc/Fc}^+$ , the reduction of  $\text{NTf}_2^-$  anion can occur, leading to the formation of  $\text{SO}_2\text{CF}_3^-$  and  $\text{CF}_3^-$ , according to previously reported FTIR measurements.<sup>264</sup> Regarding the IL loaded with cerium after extraction, the trend is much different. Even if the signal is flat in the range  $0$  to  $-1.0 \text{ V vs. Fc/Fc}^+$ , a reduction peak having an onset at  $-1.5 \text{ V vs. Fc/Fc}^+$  can be spotted. A shoulder can be observed at  $-2.2 \text{ V vs. Fc/Fc}^+$  exhibiting a current density ( $j$ ) of  $-0.5 \text{ mA.cm}^2$ . Below that potential,  $j$  drops down to a value close to  $-2.0 \text{ mA.cm}^2$  at  $-3.0 \text{ V vs. Fc/Fc}^+$ . As a result, the electrochemical window of the IL after extraction seems much smaller as the reduction of the solvent is stronger at  $-3.0 \text{ V vs. Fc/Fc}^+$  than what is observed with the neat ionic liquid. Furthermore, unveiled increase in the solubility of water in non-polar ionic liquids were reported when the aqueous phase with which they were in contact had high acidic concentrations (*Ternova et al.* 2004).<sup>265</sup> As a result, the water content, measured by Karl Fischer titration highlighted a concentration of 55.3 and 11234.4 ppm of water in  $[\text{C}_1\text{C}_4\text{Pyrr}][\text{NTf}_2]$  before and after extraction respectively. *Howlett* and co-workers<sup>266</sup> demonstrated the catalytic properties of the  $\text{OH}^-/\text{H}_2\text{O}$  couple on the reduction of the  $\text{NTf}_2^-$  anion thus reducing the electrochemical window of the

IL. Our results highlighting the lower anodic stability of [C<sub>1</sub>C<sub>4</sub>Pyrr][NTf<sub>2</sub>] are thus in agreement with the literature.

However, as mentioned previously, a reduction peak, most probably due to the deposition of cerium on the working electrode is reported between -1.5 and -2.2 V vs. Fc/Fc<sup>+</sup>. The reduction potentials of Ce(IV) and Ce(III) in aqueous solutions are depicted in the following equations. Standard potentials were measured with a NHE reference electrode and are here converted with respect to the Fc/Fc<sup>+</sup> redox couple.<sup>211</sup>



As reported in **part III.2.3**, the yellow colour of cerium in the IL fade away after a few hours which indicates that Ce(IV) is not stable in [C<sub>1</sub>C<sub>4</sub>Pyrr][NTf<sub>2</sub>] and is likely to reduce to Ce(III). Then, the reduction of Ce(III) to metallic cerium seems to occur at higher potential than what is expected in the literature regarding aqueous solutions. This result is in line with the work from *Hatchet et al. 2013*<sup>223</sup> reporting a reduction peak of Ce(III) to Ce<sup>0</sup> at -1.7 V vs. Ag/AgCl using [N<sub>4111</sub>][NTf<sub>2</sub>]. The latter paper highlighted that the ionic liquid media contributed to a favorable electrowinning of cerium.

To bring the proof that cerium can be reduced in an IL and to close the process of Ce recycling from NiMH spent batteries, chronoamperometric experiments were carried out at -2.00 V vs. Fc/Fc<sup>+</sup> during 2 hours on the gold rotating electrode. Current density is plotted as a function of time in **Figure III.13**.

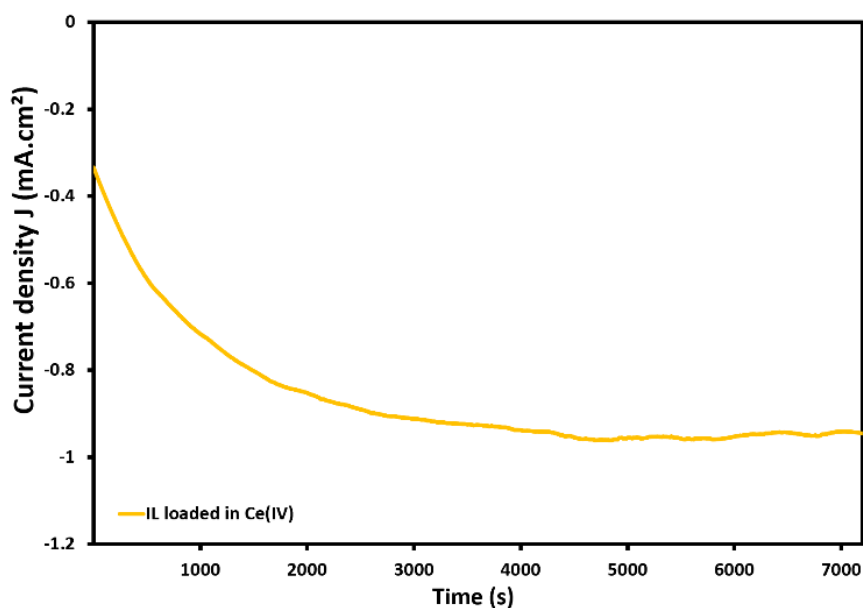


**Figure III.13.** Chronoamperometry experiments for  $[C_1C_4Pyrr][NTf_2]$  loaded in Ce(IV) after extraction in a nitric acid media. A gold rotating electrode and a potential of  $-2.00$  V vs.  $Fc/Fc^+$  during 2 hours is used.

When a potential of  $-2.00$  V vs.  $Fc/Fc^+$  is applied between the WE and the RE, the current density reaches instantly a value of  $-0.33$  mA.cm<sup>2</sup> similar to that observed during cyclic voltammetry at the same potential. A smooth decrease of  $j$  is observed during one hour before reaching a plateau at  $-0.94$  mA.cm<sup>2</sup>. This trend is expected to correspond to the growth of metallic particles on the electrode increasing the conductive surface area and thus the current density measured.<sup>115,215</sup> This assumption was checked thanks to SEM analysis performed on the gold working electrode. Images are provided in **Figure III.14** and EDS semi-quantitative analysis is reported in **Table III.6**.

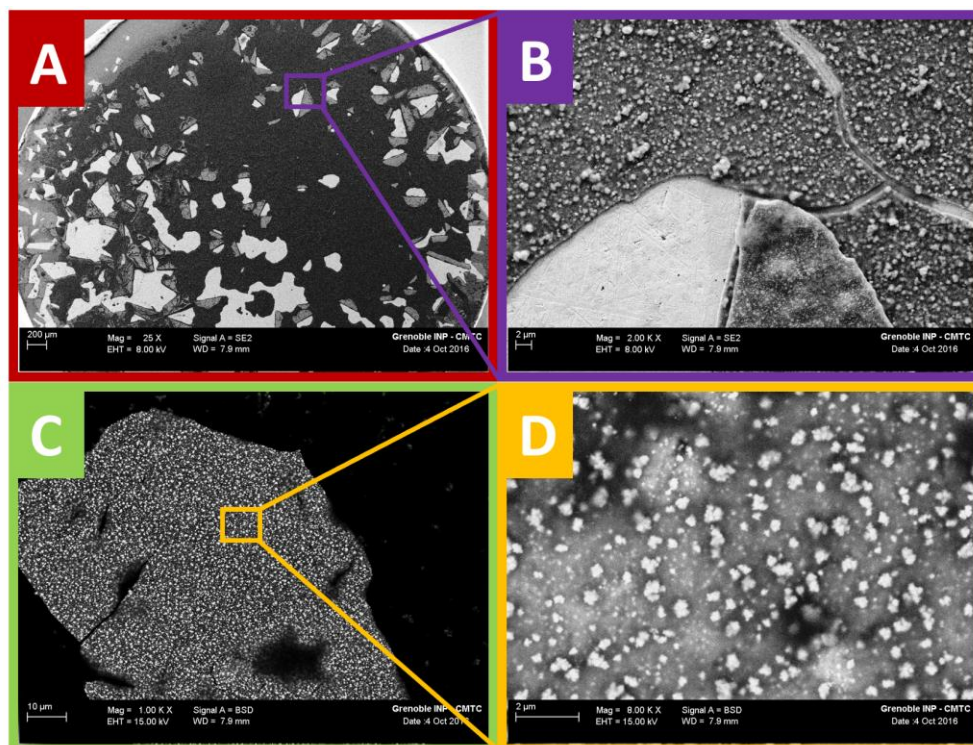


**Figure III.14.** SEM images of the gold electrode after chronoamperometric experiment at  $-2.00\text{ V vs. Fc/Fc}^+$  during 2 hours in  $[\text{C}_1\text{C}_4\text{Pyrr}][\text{NTf}_2]$  loaded in  $\text{Ce(IV)}$  after extraction in a nitric acid media. A and B: Secondary electron (SE) images at a magnification of 25 and 2000 respectively. C and D: Back scattered electron (BSE) images at a magnification of 1000 and 8000 respectively.

Composition (atom. %)	
Elements	Cerium deposit
Ce	$56.25 \pm 2.3$
S	$12.50 \pm$
F	$31.25 \pm$

**Table III.6.** Elemental analysis of the cerium deposit by SEM-EDS

Focusing on image SEM-SE A, taken at a low magnification ( $\times 25$ ), the topography of the whole electrode can be observed. It is mostly covered with a thin black layer. In a few spots, the deposit does not totally adhere to the gold surface (white spots in the image). As a result, some parts of the deposit seem to be turned over (in grey). This is most likely due to the rotation of the electrode and/or the washing process. SEM-SE B image, at a magnification of 1000, provides supplementary information. The deposit is not totally flat as some small aggregates

are spread all over the layer. SEM-BSE images (C and D) provide information on the nature and the homogeneity of the deposit. The two latter images highlight that the aggregates are composed of metallic particles in white. The different greyscale shows that different compounds are present in the deposit. SEM-EDS semi-quantitative analysis cannot differentiate the particles from the deposit which is why a global analysis of the electrode was performed and is reported in **Table III.6**. It reveals that the layer deposited on the gold electrode is composed of 56 atom. % of cerium. No trace of La, Nd and Pr can be spotted. Pure cerium is most probably present in the clear particles observed in images C and D because of the high molar mass of this REE. However, the deposit is also composed of fluorine and sulfur. The presence of the two latter elements is due to (i) an incomplete washing of the ionic liquid trapped in the deposit<sup>117</sup> and (ii) the reduction and degradation of the bis(trifluoromethanesulfonyl)imide anion catalysed by the OH<sup>-</sup>/H<sub>2</sub>O system.<sup>208,264,266</sup> The formation of CF<sub>3</sub><sup>-</sup>, SO<sub>2</sub>CF<sub>3</sub><sup>-</sup> species are susceptible to form insoluble salts by complexing with cerium and could explain the presence of sulphur and fluorine.

Up to our knowledge, deposits of REE in ionic liquids showing no evidence of the degradation of the anion have never been reported. Despite the fundamental interest of performing reduction of lanthanides by electrodeposition in ionic liquids, the interest of such technique in a real industrial recycling process suffers from some strong issues related to the purity of the metal and to the loss of ionic liquid due to the destruction of the anion.

#### d. Conclusion

An alternative technique for the recovery of cerium after separation of Ce(IV) from La(III), Nd(III) and Pr(III) is proposed. We report the ability of cerium to be reduced in [C<sub>1</sub>C<sub>4</sub>Pyrr][NTf<sub>2</sub>] after being extracted in the same ionic liquid from an acidic solution containing nitric acid. This allows us to obtain a complete layer of cerium in our electrode. The IL could thus be regenerated and reused for further extraction cycles. This process can be summed up in **Figure III.15**.

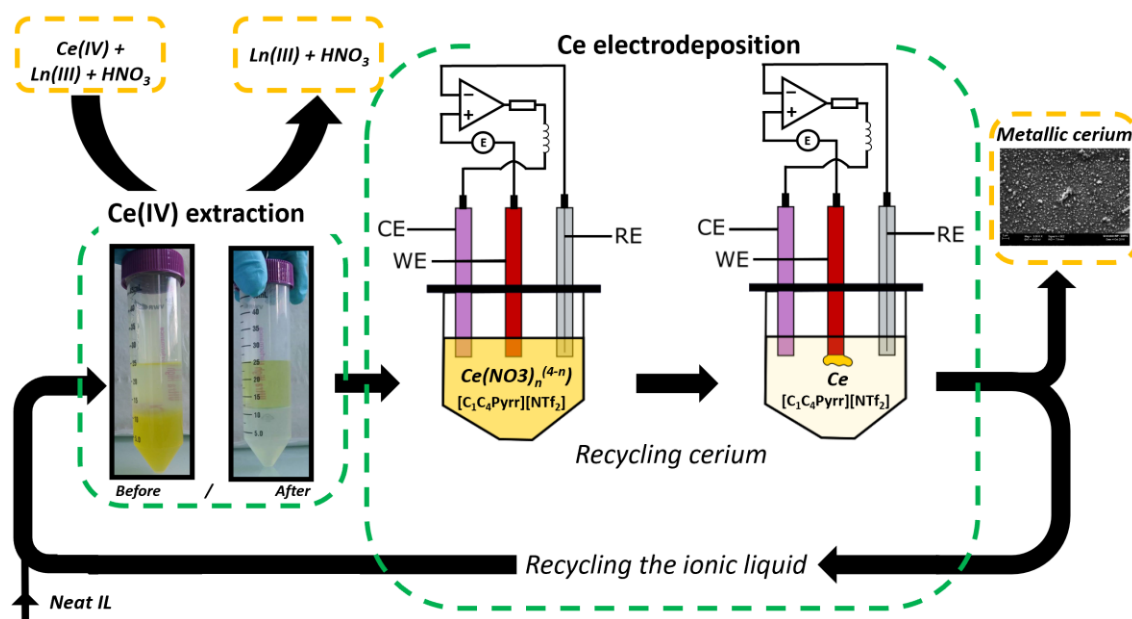


**Figure III.15.** Process for the consecutive extraction and electrodeposition of cerium in  $[C_1C_4Pyrr][NTf_2]$ .

However, the metal is accompanied by large amounts of impurities such as sulfur, fluoride, carbon and oxygen coming from the IL. Because the IL is partly destroyed during the electrowinning process, some fresh  $[C_1C_4Pyrr][NTf_2]$  will need to be added to perform supplementary extraction steps. Furthermore, organic impurities in the metal dramatically impact the value of the recovered rare earth element and hinders any industrial application of this recovery process.

## III.4 Towards the separation of neodymium from lanthanum

### a. Introduction

Lanthanum and praseodymium are always found together in ores such as bastnaesite, loparite and monazite.<sup>53,56</sup> However they can be used for drastically different applications. While 44 and 26 wt. % of extracted lanthanum are used for catalytic conversion and NiMH negative electrodes respectively, neodymium is mainly used (89 wt. %) for permanent magnets. In the latter NdFB alloy, the purity of Nd is crucial to reach high magnetic performance.<sup>267</sup> Separation of lanthanum from neodymium was studied for decades in the literature. Most successful processes are based on the dissolution of an extractant such as di-(2-ethylhexyl) phosphoric acid (DEHPA),<sup>68</sup> **Figure III.16-A**, tributyl phosphate (TBP),<sup>268</sup> **Figure III.16-B**, or a commercial mixture of phosphinic and phosphonic acids named Cyanex 572<sup>®269</sup> and produced by Cytec-Solvay, **Figure III.16-C**.

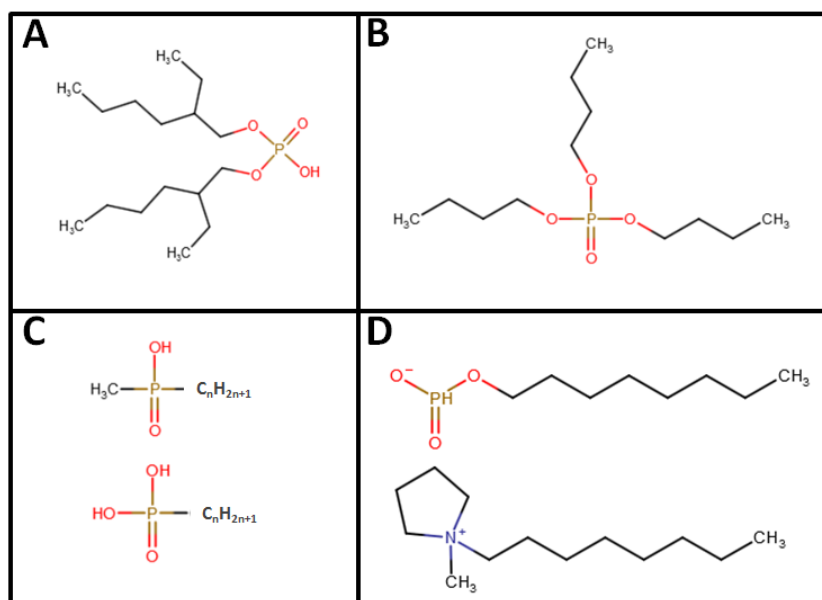


**Figure III.16.** Chemical structures of efficient REE extractants: **A:** di-(2-ethylhexyl) phosphoric acid (DEHPA). **B:** tributyl phosphate (TBP). **C:** Cyanex 572<sup>®</sup> **D:** 1-octyl-1-methylpyrrolidinium octylphosphate ( $[C_1C_8PYR][C_8PO_3H]$ ).



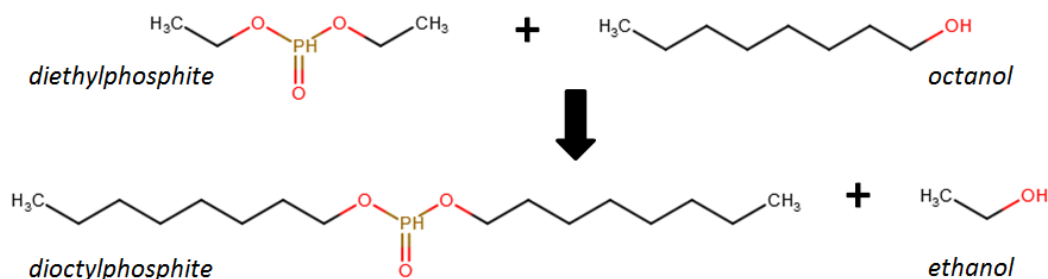
These compounds need to be dissolved in a solvent, typically, aliphatic solvents such as kerosene<sup>75</sup> and heptane.<sup>50,72,74,75</sup> are used. At the end of the extraction step, the solvent as well as the extractant are removed towards a retention pond. Because of poor waste management policies, this toxic, volatile and flammable mixture can be discharged in the environment as it is the case with Chinese groundwaters.<sup>7</sup> A paradox arises where clean technologies such as wind turbines are responsible of dramatic environmental impacts. To tackle this issue, researchers replaced aliphatic solvents by more sustainable media such as ionic liquids. While the neat ILs were unable to extract REE, they showed efficient extraction of REE after dissolving of Cyanex, TBP or DEHPA in an IL.<sup>270,271</sup> To reach higher grade sustainable processes, designing pure ionic liquids as solvent and extractant for the separation of rare earth elements without the use of any solute appears to be challenging. Observing the structure of phosphate-based molecular extractant, *Zarrougui et al.*<sup>118</sup> designed a new family of ILs with an octylphosphite-based anion such as 1-octyl-1-methylpyrrolidinium octylphosphite ( $[C_1C_8PYR][C_8PO_3H]$ ) **Figure III.16-D**. Working solely with neodymium(III), the rare earth metal was extracted from an aqueous phase containing nitric acid. Then, two strategies were successfully carried out for the recovery of both Nd and the IL, (i) precipitation using oxalate and (ii) direct electrodeposition in the IL. The cyclability of the IL was investigated bringing a further gain in the development of greener processes. However, the selectivity of such ionic liquid towards the separation of REE was not investigated. This part will thus be devoted to the investigation of the potential of this new family of IL towards the separation of the two new major lanthanides in solution at the end of the process developed in this chapter, namely, lanthanum and neodymium.

b. Synthesis of  $[C_1C_8PYR][C_8PO_3H]$

Starting from 0.2 mol diethylphosphite, dioctylphosphite was obtained by transesterification using 0.4 mol octanol. The reagents were placed in a round bottom flask heated at 140 °C under reduced pressure and connected to a distillation setup. The mixture was stirred during 6 hours. Ethanol was fully evaporated in the distillate. [1:1] molar ratio of 1-methyl pyridine was added to the round bottom flask after connecting it to a reflux setup. The temperature was set to

160 °C under nitrogen flow and magnetic stirring during 12 hours. The overall reaction can be summarized according to **Figure III.17**.

### Synthesis of dioctylphosphite



### Synthesis of an ionic liquid with an octylphosphite-based anion

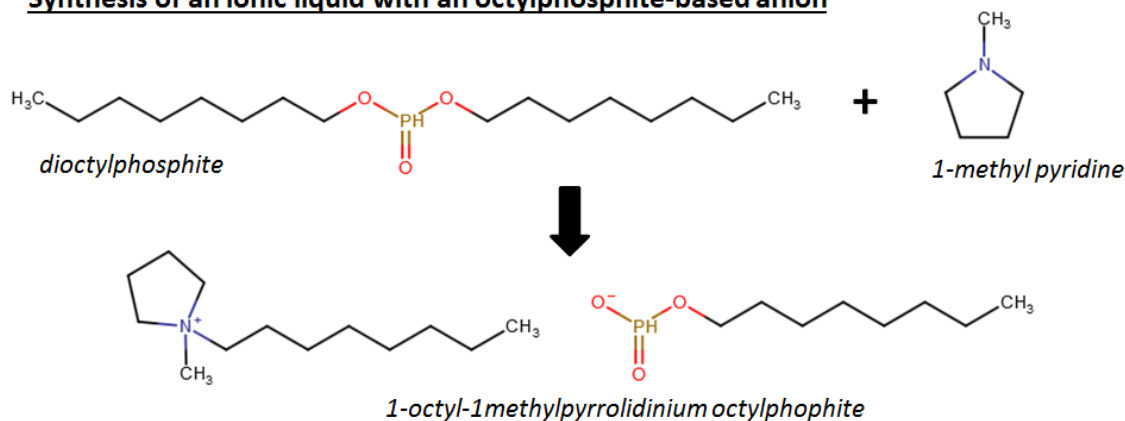


**Figure III.17.** Synthesis flow sheet of [C<sub>1</sub>C<sub>8</sub>PYR][C<sub>8</sub>PO<sub>3</sub>H]

The ionic liquid was then washed three times with water and dried at 80 °C under reduced pressure. Purity and water content in the IL was checked by <sup>1</sup>H NMR (ANNEX 2-A) and Karl Fischer analysis respectively. A small peak (4.1 ppm) attributed to dioctylphosphite was seen in the NMR spectra after 12 hours reaction indicating that the second step is not complete and needs further optimization. Less than 150 ppm H<sub>2</sub>O was found after all drying steps in [C<sub>1</sub>C<sub>8</sub>PYR][C<sub>8</sub>PO<sub>3</sub>H].

#### c. Extraction procedure

Aqueous solutions containing 0.02 mol.L<sup>-1</sup> La(III), Ce(III), Nd(III) and Pr(III) were separately prepared with REE<sub>2</sub>(SO<sub>4</sub>)<sub>3</sub> salts. Using 0.1 mol.L<sup>-1</sup> sulfuric acid, the pH of each solutions was adjusted to 1 and 2. 1 mL of aqueous phase containing a rare earth element was mixed with 1 mL of ionic liquid. After stirring

the tubes for 20 min on a shaker, centrifugation was carried out for 10 min at 6000 rpm.

All aqueous phases were analysed by ICP-OES before and after extraction experiments.

#### d. Results and discussion

Experiments carried out at pH 1 led to a little extraction of lanthanides(III) as the distribution coefficient as found to be lower than 1.2 for all REE.  $D$  seems to decrease with the atomic radius for lanthanum(III), cerium(III) and praseodymium(III). The similar size of praseodymium and neodymium atomic radius, 99.0 and 98.3 pm respectively (see Chapter 1.2.3 Rare earth elements as highly critical raw materials) induces similar distribution coefficients. A comparable trend is observed at pH 1 where  $D_{La} < D_{Ce} < D_{Pr} \approx D_{Nd}$ . This phenomenon has also been reported with organic extractants dissolved in VOCs<sup>269,272,273</sup> and in ILs<sup>271</sup> and is in accordance with our results. Nevertheless, a quantitative extraction of all REE(III) is reported when the pH is increased to a value of 2. Distribution coefficients range between 291 for La to 692 for Pr. Extraction and separation data for  $[C_1C_8PYR][C_8PO_3H]$  are collected in **Figure III.18** and **Table III.7**. Comparatively, distribution ratios and separation factors of Ln(III) at pH 1 and 2 using Cyanex 572<sup>®</sup> diluted in an aliphatic organic solvent are reported according from the claims of Cytec-Solvay industries.<sup>69,272</sup>

		D				$\beta$
		La	Ce	Nd	Pr	Nd/La
$[C_1C_8PYR][C_8PO_3H]$	pH 1	0.89 ± 0.1	1.11 ± 0.1	1.16 ± 0.1	1.20 ± 0.1	1.30
	pH 2	291.05 ± 29	582.40 ± 58	640.19 ± 64	629.00 ± 63	2.20
CYANEX 572 <sup>®</sup>	pH 1	0.01	0.05	0.10	0.08	9.79
	pH 2	0.67	3.00	3.17	3.26	4.75

**Table III.7.** Data for distribution coefficients and separation factors of Ln(III) and Nd/La respectively. Concentrations of REE(III) are of 0.02 and 0.13 mol.L<sup>-1</sup> for pure  $[C_1C_8PYR][C_8PO_3H]$  and Cyanex 572<sup>®</sup> 1.0 mol.L<sup>-1</sup> diluted in an aliphatic solvent respectively. data for Cyanex 572<sup>®</sup> were collected from Cytec-Solvay.<sup>69,272</sup>

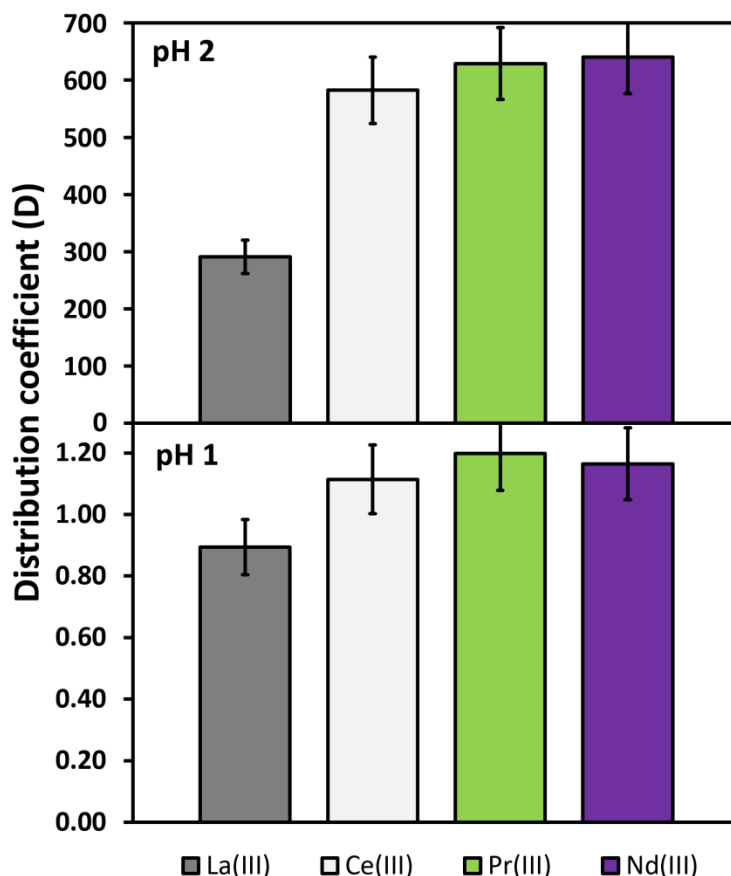
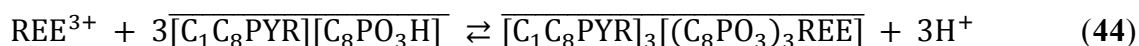


**Figure III.18.** Distribution coefficients of lanthanides ( $[Ln] = 2.0 \times 10^{-2} \text{ mol.L}^{-1}$ ) after single liquid-liquid extractions by  $[C_1C_8PYR][C_8PO_3H]$  in sulfuric acid and water at pH 1 and 2.

The increase of the extraction yield with the pH is linked to the extraction mechanism found in VOCs and in pure IL systems<sup>136</sup> depicted in the following equations:



A lower pH will induce the protonation of the extractant or the ionic liquid which hinders the complexation of the phosphorous compound and the lanthanide.

Interestingly, for the same pH, extraction yields using pure  $[C_1C_8PYR][C_8PO_3H]$  are always higher than for Cyanex 572<sup>®</sup> 1.0 mol.L<sup>-1</sup> diluted in an aliphatic solvent reaching values of 47 and 1 % respectively at pH 1 for lanthanum(III). Both values increase to 99 and 40 % respectively at pH 2. Because leaching steps for metal mining and/or recycling are undergone at low pH, basically under values of 2,

performing quantitative extractions at highly acidic pH is a strong asset in liquid-liquid extraction process. However, looking at the separation factors exhibited in **Table III.7**,  $\beta^{\text{Nd/La}}$  at pH 1 is of 1.3 using  $[\text{C}_1\text{C}_8\text{PYR}][\text{C}_8\text{PO}_3\text{H}]$ . At pH 2 the separation factor is twice as high using commercial Cyanex 572<sup>®</sup> as that obtained using the pure IL. Focusing on greener processes using ionic liquids, the separation of lanthanum from neodymium can't be undergone quantitatively and as efficiently as with commercial organic extractants. A significant difference between the distribution coefficients of neodymium and lanthanum is reported.

e. Conclusion

In this part, a strategy for separating lanthanum from neodymium is investigated. Based on the chemical structure of commercial extractant used to achieve this task, a hydrophobic ionic liquid with a phosphite-based anion, namely 1-octyl-1-methylpyrrolidinium octylphosphite,  $[\text{C}_1\text{C}_8\text{PYR}][\text{C}_8\text{PO}_3\text{H}]$  was synthesized. This IL both acts like an extractant and a solvent which avoids the use of volatile organic compounds.

$[\text{C}_1\text{C}_8\text{PYR}][\text{C}_8\text{PO}_3\text{H}]$  exhibits increasing distribution ratios with the decreasing ionic radius of lanthanides. Separation ratios are of 1.3 and 2.2 at pH 1 and 2 respectively. These results are, in the latter case, twice as low as with Cyanex 572<sup>®</sup>. However, the synthesized  $[\text{C}_1\text{C}_8\text{PYR}][\text{C}_8\text{PO}_3\text{H}]$  appears to be a strong extractant and solvent of lanthanides(III) and presents much higher extraction yields than Cyanex 572<sup>®</sup> at acidic pH. Rare earth elements are quantitatively loaded in the ionic liquid if the pH is of 2 leading to distribution ratios superior to 200 for all lanthanides(III) studied.

Phosphite-based anion ionic liquids thus seem to be a promising new family of ILs for the extraction and/or separation of REE. A large range of optimization could thus be performed to investigate various structures of ILs but also various concentrations, pH, temperatures to reach a more efficient separation of lanthanum from neodymium.

## III.5 Conclusion

---

Starting from the REE powder obtained from the leaching of end-of-life devices as detailed in chapter II, the aim of this chapter was to isolate the two major elements, namely La and Ce. To this end, oxidation of Ce(III), liquid-liquid extraction of Ce(IV), precipitation and electrodeposition of cerium were investigated. They may be summarized as follows:

### *Separation of cerium from lanthanide salts*

- (i) Lanthanide(III) sulphate salts were mixed with 2 mol.L<sup>-1</sup> NaOH in water during 3 hours to oxidize Ce(III) to Ce(IV) hydroxide while lanthanum, neodymium and praseodymium remained in their third oxidation state. We report an oxidation yield of 87 mol. %.
- (ii) Using 4 mol.L<sup>-1</sup> HNO<sub>3</sub> aqueous solutions containing 0.02 mol.L<sup>-1</sup> Ce(IV), La(III), Nd(III), Pr(III) and Ce(IV), liquid-liquid extraction by [C<sub>1</sub>C<sub>4</sub>Pyrr][NTf<sub>2</sub>] was reported and a quantitative separation of Ce(IV) from the other REE was selectively achieved. Distribution ratio (*D*) of 109 for Ce(IV) was obtained. All REE in their third oxidation states presented *D* values below 0.01.
- (iii) The ionic liquid was successfully regenerated by using 1 mol.L<sup>-1</sup> HNO<sub>3</sub> during a stripping step. After 10 consecutive extraction/regeneration steps using the same IL, the overall yield is shown to be of 88.7 %.

### *Recovery of cerium from spent NiMH batteries*

- (i) According to the previous step of the process, over 86 mol. % of cerium was recovered from real spent NiMH batteries.
- (ii) Cerium can be quantitatively precipitated by increasing the pH with NaOH, leading to the formation of pure cerium hydroxide particles.
- (iii) An alternative technique for the recovery of cerium after extraction was investigated. Ce(IV) was directly reduced from the ionic liquid on a gold electrode at a potential of -2 V vs. Fc/Fc<sup>+</sup>. The metallic deposit fully covers the electrode after 2 hours of electrowinning. It suffers,

however, from some organic impurities due to the degradation of the IL on the electrode surface. The precipitation technique will thus be preferred.

In a nutshell, starting from a  $\text{NaREE}(\text{SO}_4)_2$  powder, the process depicted in **Chapter III** allows us to isolate cerium and to recover it as a pure  $\text{Ce}(\text{OH})_3$  salt. The remaining solution is thus mainly composed of lanthanum, 19.44 mg and neodymium, 6.09 mg with small amounts of praseodymium, 2.11 mg as well as the remaining cerium 1.76 mg, per gram of NiMH black mass. This process is summarized in **Figure III.19**.

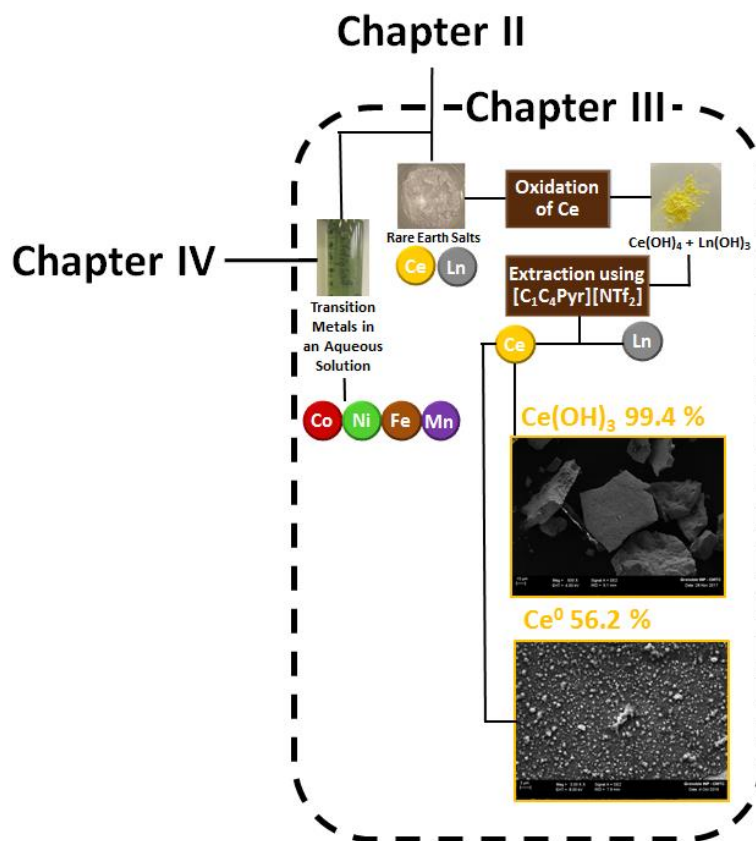


**Figure III.19.** Flowsheet corresponding to the separation of cerium from lanthanum, neodymium and praseodymium

---

---

## **CHAPTER IV**

# **Separation of Cobalt, Nickel, Manganese and Iron**



## IV.1 Introduction

---

The aim of this Chapter is to investigate innovative strategies to isolate and recover all valuable transition metals (TM) from spent NiMH batteries. Among them, cobalt presents the higher criticality level according to a very recent report from the European Commission.<sup>38</sup> In 4 years, its price has more than tripled (85.4 USD.kg<sup>-1</sup> in 2018)<sup>41</sup> due to (i) the hegemony of the production in DR Congo,<sup>51</sup> (ii) its low concentration in ores and (iii) the increasing need in cobalt for electrochemical storage devices. As a result, a particular attention will be devoted to the recovery of pure, valuable cobalt. Nickel production does not suffer from similar tensions on the market, however its price (13.7 USD.kg<sup>-1</sup> in 2018)<sup>41</sup> combined to the important amount of metal found in NiMH batteries, i.e. around 40 wt. % of the black mass strongly increases the interest of recycling Ni. Furthermore, the presence of Ni and Co mixed in ores as well as the similar chemistry of those two elements make their separation difficult and challenging for scientists. This Chapter will firstly give informations on the complexation of cobalt by dicyanamide and highlight the huge gap between the behaviour of a metal and a ligand in water and in an ionic liquid (**part IV.2**). Based on those fundamental results, extraction of cobalt will be undertaken by liquid-liquid extractions. In a second part (**part IV.3**), after highlighting the limitations of classical Aqueous Biphasic Systems (ABS) for metal extractions, the first Acidic Aqueous Biphasic System (AcABS) will be presented from the fundamentals to its ability to extract, isolate and recover a large range of metals. Finally, the last part of this chapter (**part IV.4**) will be devoted to the application of the previous results to the construction of an efficient process to recycle transition metals from NiMH batteries.

## IV.2 Dicyanamide ions as complexing agent of cobalt: from weak ligands in water to strong one in ionic liquids

---

This part is based on the following peer reviewed article:

- [Gras.M](#), [Papaiconomou.N](#), [Chainet.E](#), [Billard.I](#), Dicyanamide ions as complexing agent of cobalt: from weak ligands in water to strong one in ionic liquids, *Solvent extraction and ion exchange* **36** (2018).

### IV.2.1 Introduction

Cobalt is a light metal located on column 9 of the first period of the transition elements in Mendeleïev's table. Because of its magnetic and physical properties, cobalt is used in numerous applications ranging from anti-corrosion alloys<sup>274,275</sup> to catalysis,<sup>276-279</sup> permanent magnets<sup>243,280-282</sup> and electrode materials for rechargeable batteries.<sup>44,217,283,284</sup> Because the production of energy storage devices is strongly increasing with the development of renewable energy sources, portable communication systems and battery-driven electric vehicles, cobalt has become a key metal in nowadays high-end devices.

Ionic liquid-based liquid-liquid extraction is an increasingly popular and efficient process for ion recovery. By definition, liquid-liquid extraction must be performed between two immiscible phases, usually an aqueous one containing the metal ion and an organic phase where the complexation and extraction of the ion occur. Fluorinated ILs based on NTf<sub>2</sub><sup>-</sup> (bis(trifluoromethanesulfonyl)imide) are widely used because they yield extracting phases with an increased hydrophobicity and a

low viscosity.<sup>90,241</sup> Ionic liquids containing a cyclic quaternary ammonium and two alkyl chains, such as 1-butyl-1-methylpyrrolidinium hereafter noted as  $[C_1C_4Pyrr]^+$ , also show a low viscosity which makes them easy to handle.<sup>228</sup> 1-butyl-1-methylpyrrolidinium bis(trifluoromethanesulfonyl)imide ionic liquid is thus a prominent candidate for liquid-liquid extraction because of its low viscosity, hydrophobicity and ability to form ion pairs, yielding an efficient extraction of metals from an aqueous phase. Recent reports have showed that several metals, such as Co, Cu or Pd, could be extracted towards ionic liquids under the form of anionic complexes, namely  $Cl^-$  or  $Br^-$ .<sup>184,188,258</sup> Several studies have reported the speciation of cobalt in aqueous phases containing chloride,<sup>285,286</sup> bromide<sup>286</sup> or dicyanamide<sup>287</sup> anions. With chloride anions for instance, cobalt(II) is able to form a tetrachlorocobaltate(II) complex when the concentration of  $Cl^-$  in the aqueous phase is high, typically above  $8 \text{ mol.L}^{-1}$ . When dicyanamide ions are present in water, V.H. Köhler et al. showed cobalt was only able to coordinate with one such anion.<sup>287</sup>

In ionic liquids, reports dealing with the speciation of such light metals are extremely scarce. Some reports have investigated the speciation of chlorometallates<sup>288,289</sup> or cobalt complexes<sup>290</sup> in ionic liquids and its interest in the extraction of these complexes towards an ionic liquid was discussed. In addition, some evidence for the complexation of Co(II) with three bis(trifluoromethanesulfonyl)imide anions in neat 1-butyl-3-methylimidazolium bis(trifluoromethanesulfonyl)imide was also recently given.<sup>226</sup>

$[DCA]^-$  is an anion exhibiting a significant delocalisation of charge with a light molecular weight. Many ILs based on this anion were found to be liquid at room temperature, to exhibit very low viscosities as well as toxicities significantly lower than those of  $NTf_2$ -based ILs.<sup>115,228</sup> Most DCA-based ILs are however soluble in water and are thus not adapted to the extraction of metal ions from an aqueous phase. One solution would then be to dissolve such an ionic liquid in a hydrophobic one based on  $NTf_2$  anion for instance. Another solution, reported in a few articles, is to combine  $[DCA]^-$  with a large cation, yielding a hydrophobic ionic liquid that was then successfully applied to the liquid-liquid extraction of various metal ions.<sup>186,291</sup> In such studies, the ionic liquid phases were found to exhibit colours not corresponding to the classical chlorometallate or  $NTf_2$ -

metallate complexes. This indicated that  $[\text{DCA}]^-$  was complexing with the metal ions and that it was a good ligand for extracting metals towards an ionic liquid.

So far, however, neither specific details on the speciation of Co(II) in an ionic liquid containing a dicyanamide anion, nor on the competition between two anions, such as  $[\text{NTf}_2]^-$  and  $[\text{DCA}]^-$  from an ionic liquid mixture for the Co(II) coordination sphere were reported. In order to gain insights into the extraction mechanisms of such metal ions extracted towards an ionic liquid phase containing  $[\text{DCA}]^-$  anions, knowledge on the exact speciation of a metal within both the aqueous and ionic liquid phases is crucial.  $[\text{P}_{66614}]^+$  cation was initially chosen because it forms hydrophobic ionic liquids when combined with  $[\text{DCA}]^-$  anions. However, the presence of impurities in phosphonium ILs, hindered using them for spectrometric analysis.  $[\text{C}_1\text{C}_4\text{Pyrr}][\text{NTf}_2]$  was then chosen because it presents a high purity. Furthermore, this cation was used by Bortolini et al. to study the speciation of Co(II) in a  $[\text{NTf}_2]$  ionic liquid. The focus of this work is thus to study the speciation of Co(II) in presence of dicyanamide, in an aqueous phase or in  $[\text{C}_1\text{C}_4\text{Pyrr}][\text{NTf}_2]$ . In order to reduce the number of ions in the IL phase and to ensure a good solubility of the dicyanamide salt in  $[\text{C}_1\text{C}_4\text{Pyrr}][\text{NTf}_2]$ ,  $[\text{C}_1\text{C}_4\text{Pyrr}][\text{DCA}]$  was used as a source of  $\text{DCA}^-$  anion.

In this work, the molar extinction coefficient of Co(II) dissolved in either solvents, as a function of increasing amounts of  $[\text{DCA}^-]$  will be first presented. The concentration ratio  $R = [\text{DCA}^-]/[\text{Co(II)}]$  ranges from respectively 0 to 200 and 0 to 5040 in the aqueous and ionic liquid system. Then, a general model for the Co(II) speciation will be developed in order to describe the experimental spectra recorded. The Co(II) speciation in both phases, as calculated within the model will be detailed and discussed.

Finally, in order to illustrate the interest of our results to the field of liquid-liquid extraction, cobalt(II) will be extracted from an aqueous phase using various  $[\text{DCA}^-]/[\text{Co}]$  ratios towards a mixture of ionic liquids containing various  $[\text{DCA}^-]/[\text{NTf}_2]$  ratios.

## IV.2.2 Construction and fitting of a complexation model

### a. Data Fitting

A complexation chemical model between Co(II) and [DCA]<sup>-</sup> ions was proposed and used to derive a theoretical mathematical expression of the absorbance at a fixed wavelength (see discussion part) as a function of R. This theoretical expression was fitted to the experimental data by use of a home-written Fortran routine, implemented in the MINUIT facilities (CERN Libraries) based on a least square minimization procedure. The  $\chi^2$  convergence criterion was defined as:

$$\chi^2 = \frac{[\sum(A_{cal} - A_{exp})^2]^{\frac{1}{2}}}{(N_{dp} - N_{par})} \quad (45)$$

where  $A_{cal}$  and  $A_{exp}$  are the theoretical and experimental absorbance values, respectively.  $N_{dp}$  and  $N_{par}$  represent the number of data points and of parameters respectively.

### b. Modelling

A general chemical and mathematical model expressing the successive complexations of cobalt by a ligand in a solvent is presented. Because previous papers demonstrated the ability of cobalt to form up to four nitrogen-metal bounds in various complexes,<sup>292,293</sup> this model involves one Co(II) “free” ion, the ligand, denoted  $L$  in the following, and successive  $[\text{Co(II)}L_n]^{(2-n)}$  complexes. In order to get chemical equations and mathematical expressions as general as possible and applicable to both water and ionic liquid systems, complexes  $[\text{Co(II)}L_n]^{(n-2)-}$  were given the same general notation, that is  $X_n$ , with  $n$  indicating the number of [DCA]<sup>-</sup> complexed around the central cation.

Because the presence of water or of  $\text{NTf}_2^-$  anions around Co(II) is not explicitly described using this notation, it clearly does not reflect the exact composition of the first (and second) coordination sphere of Co(II) in water or in IL. It is however correct from a mathematical point of view, since the change of complexation appears to be directly correlated to the increase of [DCA]<sup>-</sup> in a solution of cobalt. In addition, the presence of water or  $\text{NTf}_2^-$  anion initially complexing Co(II) does not change the validity of the treatment presented here. As  $n$  increases in water,

that is, as  $[\text{DCA}]^-$  anions enter the coordination sphere of  $\text{Co(II)}$ , one can reasonably expect some water to be removed from the first coordination sphere. In an ionic liquid, because it is not clear whether  $\text{NTf}_2^-$  will form monodentate or bidentate bonds with  $\text{Co(II)}$ , one can not ascertain how many  $\text{NTf}_2^-$  anions are removed from the coordination sphere of  $\text{Co(II)}$  as one  $[\text{DCA}]^-$  enters it. The notation chosen here is therefore, in our opinion, the one that is the most acceptable considering the lack of specific knowledge on the speciation of  $\text{Co(II)}$  in a neat ionic liquid.

A general chemical equation describing the formation of successive complexes of  $\text{Co(II)}$  with a ligand  $L$  can thus be written as follows:



with  $n = 0$  to 3 in this case. The stepwise complexation constant,  $K_{n+1}$ , can then be written as follows:

$$K_{n+1} = \frac{[X_{n+1}]}{[X_n][L]} \quad (47)$$

where  $[X_n]$  and  $[L]$  denote the concentrations of the metal species and the ligand respectively.

In absence of experimental values for the activity coefficients for the aqueous solutions of  $\text{Co(II)}$  and  $[\text{DCA}]^-$  ion, and because the concentration of ions are relatively low, we considered the solutions to behave ideally, i.e. activity coefficient is equal to 1. Furthermore, because in the ionic liquid phase, our experimental protocol leads to a simple replacement of  $\text{NTf}_2^-$  by  $[\text{DCA}]^-$  ions, both having the same charge, the ionic strength can be considered to remain equal, and the activity coefficients to be constant.  $K_n$  in water and in the ionic liquid are thus ideal and conditional constants, respectively.

At any wavelength, the absorbance  $A$  can be described using the Beer-Lambert's law:

$$A = \sum_n \varepsilon_n [X_n] l + \varepsilon_L [L] l \quad (48)$$

where  $\varepsilon_n$  and  $\varepsilon_L$  stand for the molar extinction coefficients for species  $X_n$  and ligand  $L$ , respectively, and  $[X_n]$  and  $[L]$  correspond to the concentration of these species, respectively.  $l$  is the cell width expressed in cm. As explained above, the

experimental values for the absorbance  $A$  were recorded at 509 or 613 nm in water or IL accordingly.

The set of equations represented by the general equations (47) and (48) are solved as a function of the complexation constant and the molar extinction coefficients using the mass conservation law for Co(II) and the ligand. For clarity reasons, details on the analytical expressions employed for solving this mathematical system are given in ANNEX 2-B supplementary materials file.

In each solvent, the model parameters ( $K_n$ ,  $\varepsilon_{Xn}$  and  $\varepsilon_L$ ) are adjusted in order to describe the experimental absorbance values  $A$  by minimizing the  $\chi^2$  criterion.

### IV.2.3 Co-DCA complexes in water

#### a. Experimental part

In order to study cobalt dicyanamide complexes in water, two stock solutions were used. On the one hand, a solution of cobalt  $5 \times 10^{-3}$  mol.L<sup>-1</sup> in water was prepared. On the other hand, an aqueous solution of cobalt  $5 \times 10^{-3}$  mol.L<sup>-1</sup> and dicyanamide 1 mol.L<sup>-1</sup> was obtained by dissolving cobalt sulphate, sodium dicyanamide and water. By mixing different amounts of the two stock solutions in a quartz cell, solutions containing a constant concentration of  $5 \times 10^{-3}$  mol.L<sup>-1</sup> Co(II) and concentrations of [DCA]<sup>-</sup> varying from 0 to 1 mol.L<sup>-1</sup> can be obtained. In the following, we define  $R$  as the ratio of the initial concentration of [DCA]<sup>-</sup> over the initial cobalt concentration:  $R = [\text{DCA}^-]_{\text{init}}/[\text{Co(II)}]_{\text{init}}$ . For the aqueous samples of this work,  $R$  was thus in the range 0 to 200. UV-vis spectra were recorded using a Cary 50 (Varian) spectrometer with a 1 cm wide quartz cell. Acquisition of all data was performed at 20 °C in the wavelength range of 200 to 800 nm. Pure water was used as a reference sample.

#### b. Results

In aqueous solutions, cobalt sulphate exhibits a light pink colour, due to the formation of a hexaaquacobalt(II) complex. Because of the weak complexation constant of the sulphate and hydrogensulphate anion with cobalt(II),<sup>236</sup> we can infer that the sulphate anion will not disrupt the complexation of cobalt in our conditions. The molar extinction coefficient versus the wavelength of an aqueous

solution of  $5 \times 10^{-3} \text{ mol.L}^{-1}$  Co(II) sulphate is shown in **Figure IV.1** and was obtained by dividing the absorbance of the UV-vis spectrum by the initial concentration of cobalt.

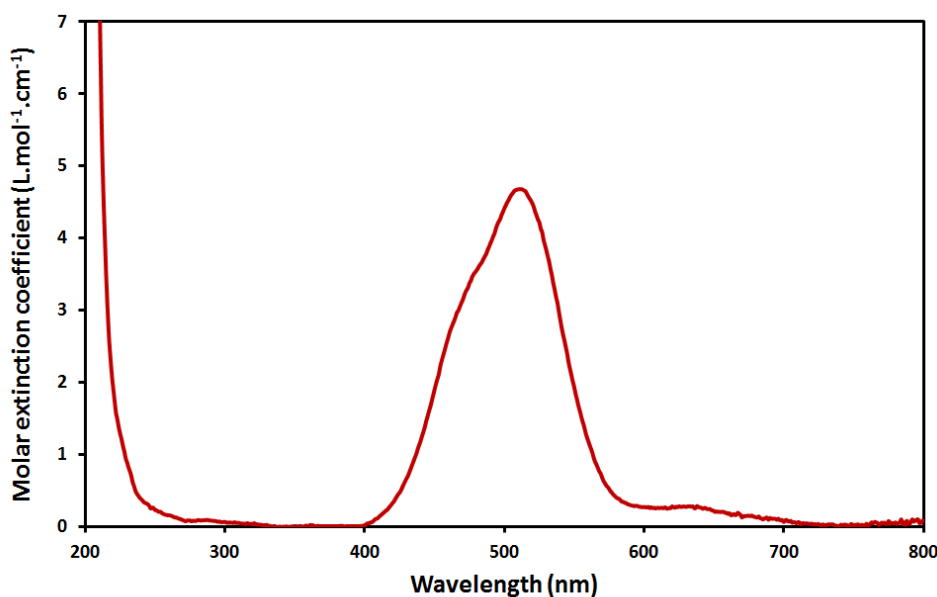
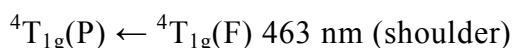
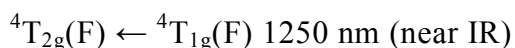


**Figure IV.1.** Molar extinction coefficient of  $\text{CoSO}_4$  in water as function of the wavelength.

A maximum absorption peak centred around 509 nm and exhibiting a molar extinction coefficient of  $4.80 \text{ L.mol}^{-1}.\text{cm}^{-1}$  is observed. A shoulder can be found at 480 nm and no significant absorbance is detected between 600 and 700 nm. This spectrum is in agreement with several previous experimental reports.<sup>286,294</sup> The Tanabe-Sugano diagram of cobalt(II) hexahydrate, which predicts three spin-allowed transitions,<sup>294</sup> is in line with our data for the maximum absorption and the shoulder, while the third predicted peak belongs to the near IR range, as indicated below:



Owing to a very low molar extinction coefficient value in the range 450 – 675 nm (for example,  $\epsilon = 1.4 \times 10^{-3} \text{ L.mol}^{-1}.\text{cm}^{-1}$  at 509 nm) addition of up to  $1 \text{ mol.L}^{-1}$  of  $[\text{DCA}]^-$  has no influence on the baseline in this wavelength range. By contrast, below 450 nm, the  $[\text{DCA}]^-$  spectrum displays a clear increase in absorption.



Absorbance of all UV-vis spectra thus strongly increases because of the impact of the extinction coefficient of the ligand below 450 nm. A UV-vis spectrum of an aqueous solution of  $1 \text{ mol.L}^{-1} [\text{DCA}]^-$  is shown in ANNEX 2-C (supplementary materials) to highlight this phenomenon. However, absorbance of the dicyanamide anion under 450 nm has a low impact on our modelling, because the latter was performed at higher wavelengths.

The molar extinction coefficients versus the wavelength for all 18 aqueous solutions containing varying concentrations of  $[\text{DCA}]^-$  are displayed in **Figure IV.2**. A maximum absorption peak and a shoulder are still observed at 509 and 480 nm respectively whatever the  $R$  value. No major wavelength shift between the different  $[\text{DCA}^-]/[\text{Co(II)}]$  ratios is observed. Nevertheless, absorbance increases with the increasing  $R$  ratio. Furthermore, two shoulders at 595 and 645 nm appear when dicyanamide anion is added to the aqueous solution (see **Figure IV.1** for comparison). These two experimental facts are a clear evidence of a complexation process between  $\text{Co(II)}$  and  $[\text{DCA}]^-$  in water.

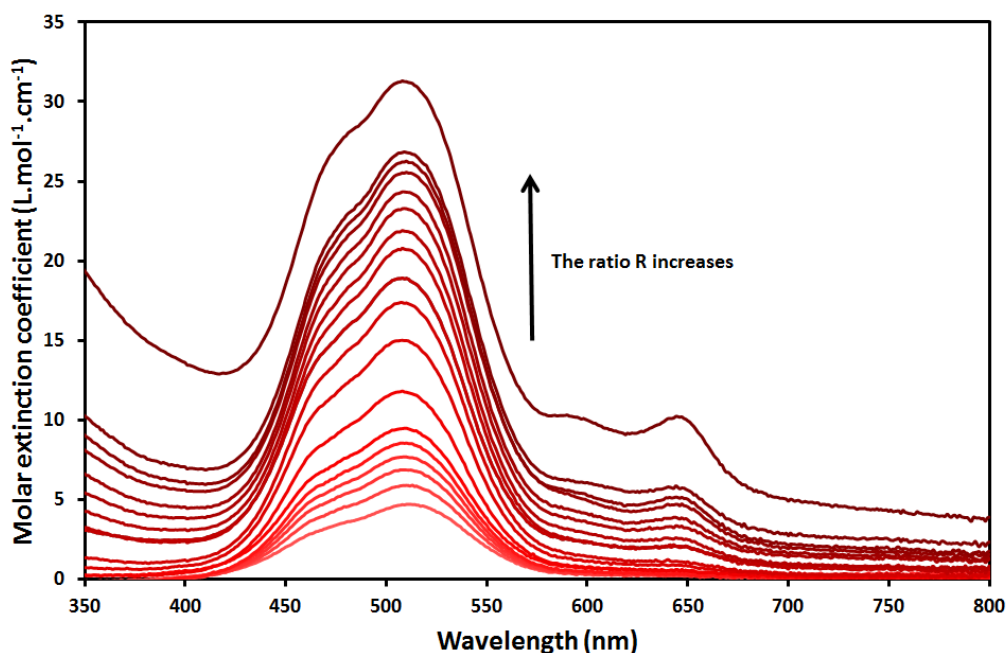


**Figure IV.2.** Molar extinction coefficient for various  $[\text{DCA}^-]/[\text{Co(II)}]$  ratios (0 to 200) in water versus the wavelength.

c. Discussion

Experimental absorbance at 509 nm function of the  $R$  ratio are plotted in **Figure IV.3**. Based on those previous data, we first assumed the simplest complexation scheme, by limiting the chemical model developed in section 4.2.2 to the formation of one complex only named  $X_1$ . Under this hypothesis, the complexation constants  $K_2$ ,  $K_3$  and  $K_4$  and the molar absorption coefficients  $\varepsilon_2$ ,  $\varepsilon_3$  and  $\varepsilon_4$  are all set to 0. The number of parameters is thus reduced to 4,  $\varepsilon_0^w$ ,  $\varepsilon_L^w$ ,  $\varepsilon_1^w$  and  $K_1^w$  with additional superscript  $w$  standing for water.

The adjusted values for the four parameters used within this model are listed in **Table IV.1**. Calculated values for the absorbance at 509 nm are plotted in **Figure IV.3** with respect to the ratio  $R$ . The fitted molar extinction coefficient of the metal  $\varepsilon_0^w = 4.56 \text{ L}\cdot\text{mol}^{-1}\cdot\text{cm}^{-1}$  is close to the experimental value of  $4.80 \text{ L}\cdot\text{mol}^{-1}\cdot\text{cm}^{-1}$  at 510 nm reported in the literature<sup>294</sup> and also very close to our experimental value of  $4.80 \text{ L}\cdot\text{mol}^{-1}\cdot\text{cm}^{-1}$  at 509 nm. The low  $\chi^2$  value ( $7.8 \times 10^{-4}$ ) reflects the good accuracy of the model, as can be seen in **Figure IV.3**. Such a value is much lower than the experimental uncertainty so there is no need to consider additional complexes of higher stoichiometries and this simple model accurately reflects the experimental data. A value of 20.5 is found for the formation constant  $K_1^w$ .

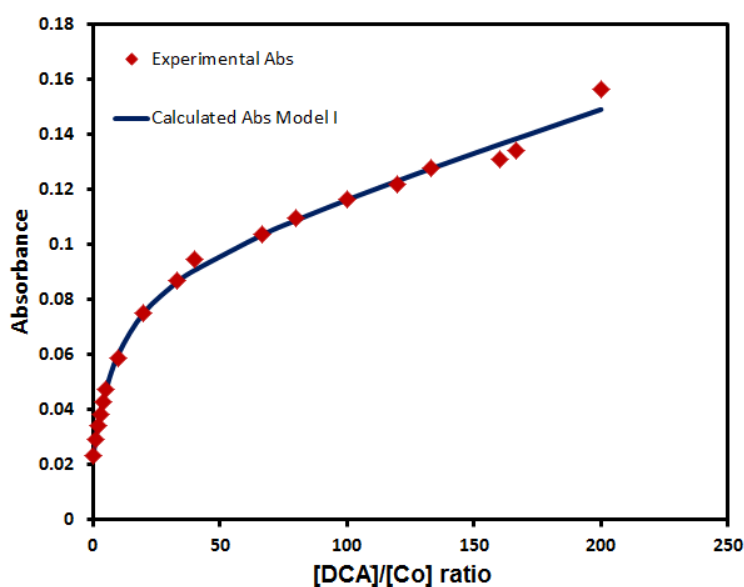


**Figure IV.3.** Experimental and calculated absorbance at 509 nm versus the  $R$  ratio (0 to 200) in water. Diamond: experimental points. Solid line: calculated data according to our model assuming one complex.

This relatively low complex formation value confirms that a significant excess of dicyanamide compared to the concentration of cobalt is needed in order to form  $X_1$ , the single Co-DCA complex in water. The concentrations of the two different cobalt species,  $X_0$  and  $X_1$ , as calculated within the model, are presented in **Figure IV.4** with respect to the ratio  $R$ . The free metallic ion ( $X_0$ ) is gradually consumed to form  $X_1$ . At  $R = 10$ , half of the cobalt reacts with the dicyanamide anion, compared to 96 % of the complex formed when  $[DCA^-]/[Co(II)] = 200$ . The complexation constant is a factor of ca. 15 higher than that obtained for chloride,  $[Co(H_2O)_5Cl]^+$  which exhibits a formation constant of 1.34.<sup>295</sup>

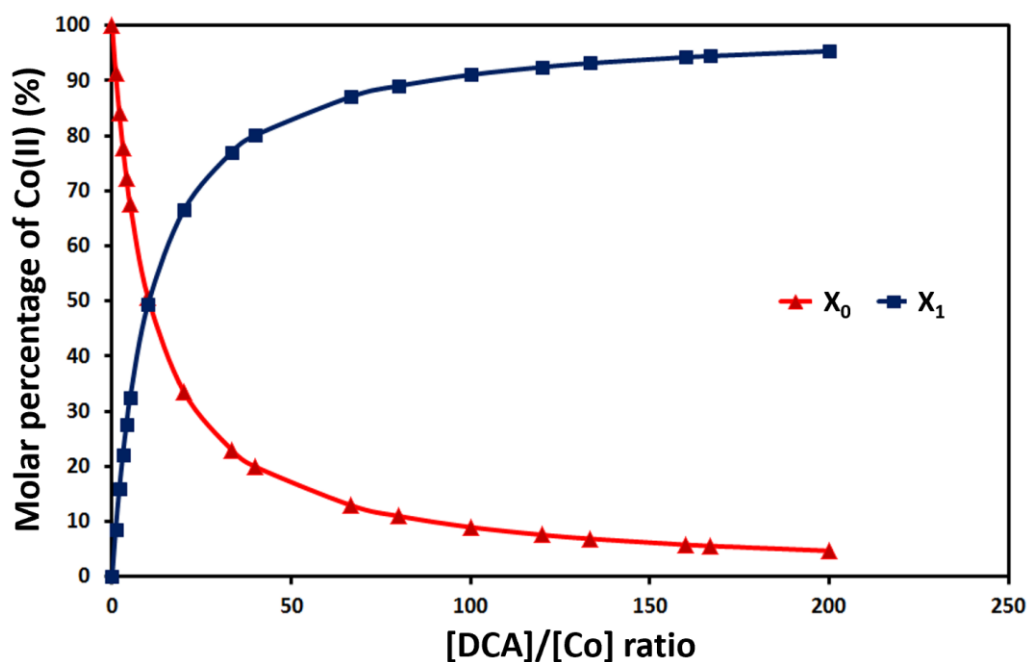


**Figure IV.4.** Chemical speciation for  $[Co(H_2O)_6]^{2+}$  ( $X_0$ ) and  $[Co(H_2O)_5(DCA)]^+$  ( $X_1$ ) for each  $R$  ratio in an aqueous solution. Triangle: ( $X_0$ ) concentration. Square: ( $X_1$ ) concentration.

Co-DCA complexation	
Parameters	Model assuming 1 complex in water
$\epsilon_0$ (L.mol <sup>-1</sup> .cm <sup>-1</sup> )	4.56 ± 1
$\epsilon_1$ (L.mol <sup>-1</sup> .cm <sup>-1</sup> )	1.86×10 <sup>1</sup> ± 1×10 <sup>1</sup>
$\epsilon_2$ (L.mol <sup>-1</sup> .cm <sup>-1</sup> )	0
$\epsilon_3$ (L.mol <sup>-1</sup> .cm <sup>-1</sup> )	0
$\epsilon_4$ (L.mol <sup>-1</sup> .cm <sup>-1</sup> )	0
$\epsilon_l$ (L.mol-1.cm <sup>-1</sup> )	5.9×10 <sup>-2</sup> ± 1×10 <sup>-2</sup>
$K_1$	2.05×10 <sup>1</sup> ± 5
$K_2$	0
$K_3$	0
$K_4$	0
$\chi^2$	7.8×10 <sup>-4</sup>

**Table IV.1.** Calculated parameters for cobalt complexation by dicyanamide in an aqueous solution (Model assuming one complex).

It is important to notice that our chemical model in water describes the complexation of dicyanamidocobalt(II) complexes but is unable to bring any information on the coordination sphere of all complexes. In water the coordination of cobalt is well known, and because H<sub>2</sub>O is a neutral ligand, the charge of the Co-DCA complex will only be influenced by the complexation of [DCA]<sup>-</sup> which is well described by our chemical model.

According to previous literature reports, cobalt(II) hexahydrate is assumed to form a single complex of [Co(H<sub>2</sub>O)<sub>5</sub>(DCA)]<sup>+</sup> in water.<sup>287</sup> V.H. Köhlner,<sup>287</sup> reported a simple chemical model based on the following equation:



The previous equation is in full agreement with our results and confirms the validity of our modelling approach.

#### IV.2.4 Co-DCA complexes in ionic liquids

##### a. Experimental part

Preparation of solutions containing cobalt and dicyanamide ions in ionic liquid [C<sub>1</sub>C<sub>4</sub>Pyrr][NTf<sub>2</sub>] was also conducted starting from two stock solutions.

The first stock solution was prepared by dissolving Co(NTf<sub>2</sub>)<sub>2</sub> and [C<sub>1</sub>C<sub>4</sub>Pyrr][DCA] in [C<sub>1</sub>C<sub>4</sub>Pyrr][NTf<sub>2</sub>] in order to obtain a cobalt concentration of respectively

$8.2 \times 10^{-4}$  mol.L<sup>-1</sup>. The second stock solution results from the dissolution of Co(NTf<sub>2</sub>)<sub>2</sub> ( $8.2 \times 10^{-4}$  mol.L<sup>-1</sup>) in [C<sub>1</sub>C<sub>4</sub>Pyrr][NTf<sub>2</sub>]. A procedure similar to that detailed above in water was used for the sample preparation in the ionic liquid. Various amounts of the two stock solutions were added in a quartz cell. Unlike the metal concentration which remains constant at  $8.2 \times 10^{-4}$  mol.L<sup>-1</sup>, the concentration of [DCA]<sup>-</sup> varied from 0 to 4.13 mol.L<sup>-1</sup> resulting in *R* ranging from 0 to 5040. Note that this protocol was also attempted with a higher concentration of cobalt, namely  $5 \times 10^{-3}$  mol.L<sup>-1</sup> but a blue precipitate appeared when the *R* ratio was superior to 1. The formation of a solid powder has disrupted the UV-vis measurements and forced us to decrease the metal concentration.

All experiments were carried out at 20 °C. A vigorous stirring of all ionic liquid solutions was performed in the quartz cell for a period of 5 to 15 min. Several UV-Vis spectra were recorded until no modification between spectra recorded at successive time intervals was observed. In the following, only the last UV-vis spectrum has been considered. UV-vis spectra were recorded using a Cary 50 (Varian) spectrometer with a 1 cm wide quartz cell. Acquisition of all data was performed in the wavelength range of 200 to 800 nm. Neat [C<sub>1</sub>C<sub>4</sub>Pyrr][NTf<sub>2</sub>] was used as a reference sample.

The water content of the two ionic liquids was determined by using a Titroline® 7500 KF Trace (SI Analytics Karl Fisher). Hydranal® water standard 1.0, containing 1000 ppm of water was used for the device calibration, and results are the average of three measurements. Once dried as described above, [C<sub>1</sub>C<sub>4</sub>Pyrr][NTf<sub>2</sub>] and [C<sub>1</sub>C<sub>4</sub>Pyrr][DCA] were found to contain  $35 \pm 2$  and  $82 \pm 5$  ppm of water, respectively.

## b. Results

### *Co(II) in presence of dicyanamide in [C<sub>1</sub>C<sub>4</sub>Pyrr][NTf<sub>2</sub>]*

Because [C<sub>1</sub>C<sub>4</sub>Pyrr][NTf<sub>2</sub>] and [C<sub>1</sub>C<sub>4</sub>Pyrr][DCA] were of a high purity grade, the latter was used in order to study the speciation of Co(II) in ionic liquid mixtures. Because neat [C<sub>1</sub>C<sub>4</sub>Pyrr][NTf<sub>2</sub>] was found to absorb significantly between 200 and 400 nm, molar extinction coefficients are only shown at wavelengths higher than 400 nm. As observed in an aqueous phase, the solution of [C<sub>1</sub>C<sub>4</sub>Pyrr][NTf<sub>2</sub>] containing only Co(NTf<sub>2</sub>)<sub>2</sub> salt exhibits a light pink colour. The corresponding curve, presented in **Figure IV.5** ( $R = 0$ ), exhibits a maximum absorption wavelength at 506 nm with a molar extinction coefficient of 1.22 L.mol<sup>-1</sup>.cm<sup>-1</sup>. A shoulder can also be spotted at 460 nm. The dissolution of cobalt in another [NTf<sub>2</sub>]<sup>-</sup> based ionic liquid namely 1-butyl-3-methylimidazolium bis(trifluoromethylsulfonyl)imide, [C<sub>1</sub>C<sub>4</sub>Im][NTf<sub>2</sub>] was already investigated and led to a similar spectrum.<sup>226</sup> After drying the IL, the remaining amount of water was found to be three times lower than the amount of cobalt. In this study we thus assume that water does not interfere in the complexation of cobalt by [NTf<sub>2</sub>]<sup>-</sup>. Because whether in an aqueous solution or in a NTf<sub>2</sub>-based ionic liquid, cobalt(II) is solvated by six oxygen atoms leading to an octahedral complex,<sup>226,294</sup> it presents similar molar extinction coefficients in these solvents.

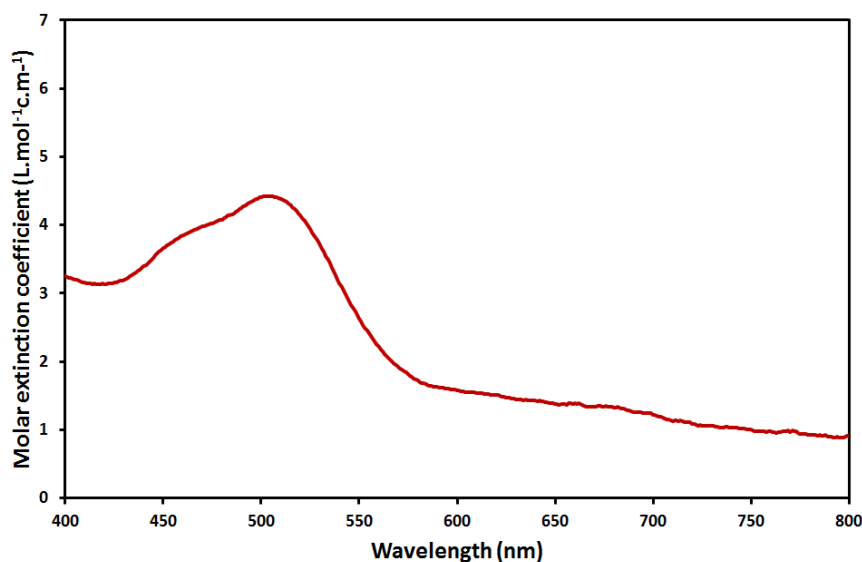


**Figure IV.5.** Molar extinction coefficient of Co(NTf<sub>2</sub>) in [C<sub>1</sub>C<sub>4</sub>Pyrr][NTf<sub>2</sub>] versus the wavelength.

The molar extinction coefficients versus the wavelength obtained for all 27 solutions of [C<sub>1</sub>C<sub>4</sub>Pyrr][NTf<sub>2</sub>] containing Co(II) and various concentrations of

$[\text{DCA}]^-$  are plotted in **Figure IV.6**.

Starting from the solution without  $[\text{DCA}]^-$ , adding a small amount of dicyanamide, for instance  $R = 0.1$ , leads to a drastic change in the absorbance spectrum. The characteristic peaks of cobalt at 506 and 460 nm in  $[\text{C}_1\text{C}_4\text{Pyrr}][\text{NTf}_2]$  are no longer observed. At this ratio, two major peaks can be seen at 589 and 602 nm with molar extinction coefficients of respectively 38.70 and 40.33  $\text{L}\cdot\text{mol}^{-1}\cdot\text{cm}^{-1}$ . Two shoulders can also be observed at 569 and 624 nm. A hypsochromic shift of the two major peaks is highlighted when the ratio  $[\text{DCA}^-]/[\text{Co}(\text{II})]$  is increasing to  $R = 25$ . Indeed, for this ratio, the two previous absorption peaks are shifted towards 594 ( $\epsilon = 521.8 \text{ L}\cdot\text{mol}^{-1}\cdot\text{cm}^{-1}$ ) and 613 nm ( $\epsilon = 527.2 \text{ L}\cdot\text{mol}^{-1}\cdot\text{cm}^{-1}$ ). From  $R = 0$  to  $R = 25$ , the molar extinction coefficient of all spectrum was found to increase and the solution changed from an initial light pink colour to a strong blue colour.

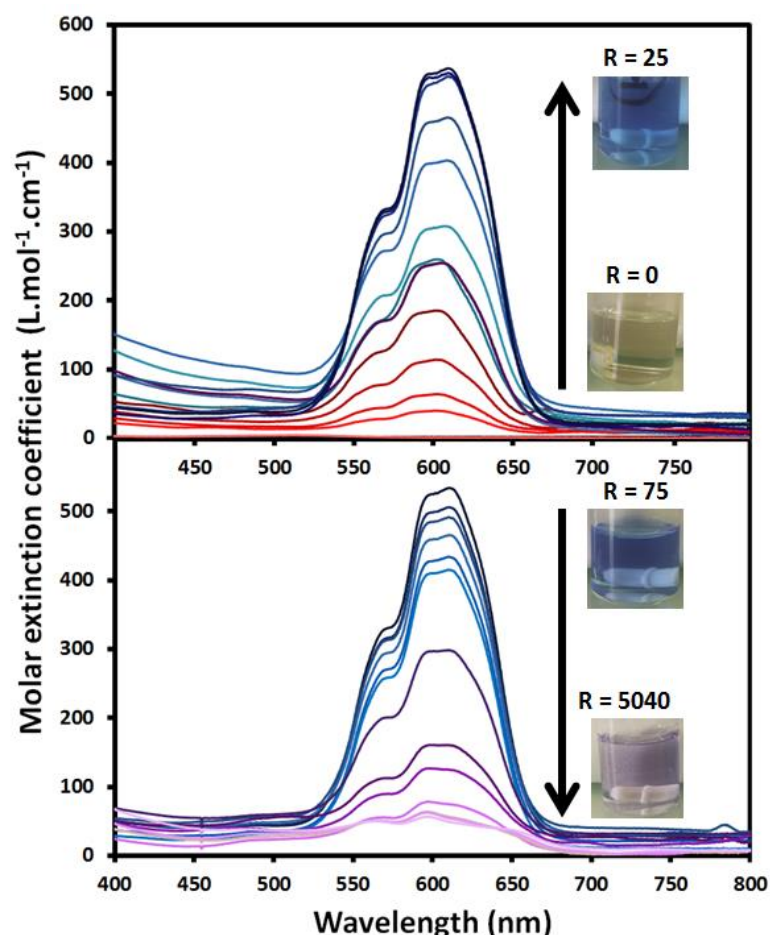


**Figure IV.6.** Molar extinction coefficient of the solution for various  $[\text{DCA}^-]/[\text{Co}(\text{II})]$  ratios ( $R = 0$  to 5040) in  $[\text{C}_1\text{C}_4\text{Pyrr}][\text{NTf}_2]$  versus the wavelength.

When  $R$  increases from 25 to 5040,  $\epsilon$  drops drastically. The strong blue solution

has now a light purple colour as seen in **Figure IV.6**. When the ratio  $[\text{DCA}^-]/[\text{Co(II)}]$  is of 5040, one major peak can be observed at 597 nm with a molar extinction coefficient of  $56.41 \text{ L}\cdot\text{mol}^{-1}\cdot\text{cm}^{-1}$  and two shoulders can be spotted at 569 nm and 655 nm. As observed in an aqueous solution, modifications of the UV-vis spectra with the increasing concentration of  $[\text{DCA}^-]$  are solid evidence of the complexation of Co(II) by dicyanamide anions in an ionic liquid.

#### *Comparison of the two solvents*

In a nutshell, for  $R = 0$ , molar extinction coefficients of cobalt in water and in an  $\text{NTf}_2$ -based IL are rather similar, as seen in **Figure IV.1** and **Figure IV.5**, respectively. As soon as  $R > 0$ , the speciation of cobalt(II) in an aqueous solution differs significantly from that observed in an ionic liquid, as revealed by the UV absorption spectra collected in **Figure IV.2** and **Figure IV.6**.

The analysis of these UV-vis spectra can be refined by examining at a given wavelength, the variation of the experimental absorbance as a function of the  $R$  ratio. To that end, for each solvent, the wavelength exhibiting the highest variation in absorbance was first chosen. This corresponds to 509 and 613 nm for aqueous and ionic liquid phases, respectively. Then, the absorbances at these specific wavelengths were plotted against ratio  $R$ . These curves are presented in **Figure IV.3** and **Figure IV.7** in water and in  $[\text{C}_1\text{C}_4\text{Pyrr}][\text{NTf}_2]$ , respectively.



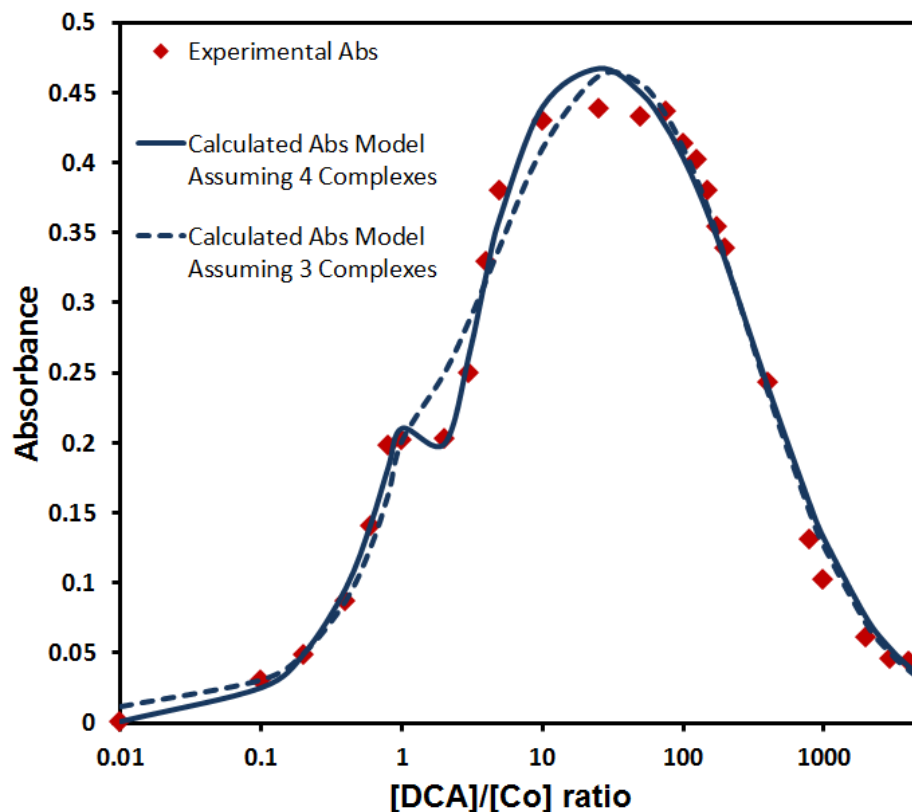


**Figure IV.7.** Experimental and calculated absorbance at 614 nm versus the  $R$  ratio (0 to 5040) in  $[\text{C}_1\text{C}_4\text{Pyrr}][\text{NTf}_2]$ . Diamond: experimental points. Dashed line: calculated value according to our model assuming three complexes. Solid line: Calculated value according to our model assuming four complexes.

In the latter, the x-axis is represented in a logarithmic scale. In water, the increase in absorbance with  $R$  confirms the occurrence of a complexation process. Because no plateau is observed even at  $R = 200$ , we can infer that the complexation of Co(II) is not complete. However, one can assume the presence of at least one complex of Co-DCA exhibiting a molar extinction coefficient significantly larger than that of the “free” cobalt ion in water. Regarding the ionic liquid, the curve’s trend displayed in **Figure IV.7** is more complex and clearly shows features that were previously difficult to highlight when looking at the entire UV-vis spectra. First, absorbance increases from  $R = 0$  to 0.8. Between  $R = 0.8$  and  $R = 2$ , a narrow plateau is observed. Absorbance then increases again until  $R = 25$  before reaching a maximum. Finally, above  $R = 75$ , absorbance decreases. This implies that several complexes of Co-DCA exist in the IL solution depending on the  $R$  value: one dominating the speciation from  $R = 0$  to 0.8, a second one from  $R = 25$  to 75 and a third one above  $R = 75$ . However, the narrow plateau observed in the range  $R =$

0.8-2 is also indicative of (at least) one additional species, displaying a non-negligible contribution to the absorbance in that range.

The existence of several complexes is visually confirmed by the different colours observed in the solution with the increasing  $[\text{DCA}^-]/[\text{Co(II)}]$  ratio. Note that the last complex dominating the speciation of Co(II) in the ionic liquid when  $R$  is superior to 1000 exhibits a very low absorbance.

### c. Discussion

#### *Speciation of Co(II) and dicyanamide in $[\text{C}_1\text{C}_4\text{Pyrr}][\text{NTf}_2]$*

Highlighted in section 4.2.3, the situation in the IL is very different from that in water. In this case and considering the non-monotonous behaviour of the absorbance with respect to the ratio  $R$  (**Figure IV.6**), several dicyanamidocobalt(II) complexes need to be taken into account. In order to describe the absorbance curve reported here, our general model was used in two different ways, assuming the presence of three or four complexes of cobalt(II) with dicyanamide.

In a first approach, the formation of three Co-DCA complexes was assumed. 8 independent parameters, denoted as  $K_m^{IL}$ ,  $\varepsilon_n^{IL}$  and  $\varepsilon_L^{IL}$ , with  $m$  varying from 1 to 3 and  $n$  from 0 to 3 were thus adjusted. The superscript IL stands for the ionic liquid, as these parameters are used to describe the complexation of Co(II) in the ionic liquid. The molar extinction coefficient for the ligand in the ionic liquid,  $\varepsilon_L^{IL}$ , was neglected because  $[\text{C}_1\text{C}_4\text{Pyrr}][\text{DCA}]$  presents an absorbance between 500 and 800 nm, very close to that of  $[\text{C}_1\text{C}_4\text{Pyrr}][\text{NTf}_2]$  (see **ANNEX 2-D** supplementary information file). The increase in absorption observed below 500 nm, as seen in **Figure IV.6** had no influence on our model since the wavelength selected in the ionic liquid was 613 nm. Furthermore, the drastic decrease in absorption observed at high  $[\text{DCA}^-]/[\text{Co(II)}]$  ratio implies that the last complex exhibits very low molar extinction coefficients between 400 and 800 nm. Consequently,  $\varepsilon_3^{IL}$  was approximated to 0, reducing the number of unknown parameters to 6.

In a second approach to describe our experimental results, an additional complex, namely  $X_4$ , corresponding to Co(II) complexed with four dicyanamide anions, was taken into account. In this case, a total of eight parameters were then adjusted.

Fitted values of all parameters for both versions of our model are listed in **Table IV.2**, together with the corresponding  $\chi^2$  values. **Figure IV.7** plots the calculated values for the absorbance at 613 nm against the ratio  $R$  in a logarithmic scale.

Regarding the 3 polydicyanamidocobalt(II) complexes model, that is considering only three cobalt(II) complexes, we observe that, on the one hand, the fit respects the trends of the experimental data from  $R = 75$  to  $R = 5040$ . On the other hand, calculated and measured absorbance values differ from  $R = 0$  to  $R = 50$ . When the  $[\text{DCA}^-]/[\text{Co(II)}]$  ratio is under 10, the calculated data is monotonously increasing and is not recovering the plateau observed experimentally between  $R = 0.8$  and  $R = 2$ . Furthermore, the calculated molar extinction coefficient of cobalt(II) is of  $14.42 \text{ L}\cdot\text{mol}^{-1}\cdot\text{cm}^{-1}$  whereas the experimental  $\epsilon_0^{LL}$  is one order of magnitude lower ( $\epsilon_0^{LL} = 1.22 \text{ L}\cdot\text{mol}^{-1}\cdot\text{cm}^{-1}$ ). Even if the  $\chi^2$  value appears to acceptable compared to the experimental uncertainty, the value for the calculated molar absorption of free Co(II) is too high and the shape of the curve from  $R = 0$  to 10 is not completely satisfying. The assumption considering the presence of only three complexes therefore appears questionable.

Complexation of cobalt by dicyanamide		
Parameters	Model assuming 3 complexes in	Model assuming 4 complexes in
	[C <sub>1</sub> C <sub>4</sub> Pyrr][NTf <sub>2</sub> ]	[C <sub>1</sub> C <sub>4</sub> Pyrr][NTf <sub>2</sub> ]
$\epsilon_0$ (L.mol <sup>-1</sup> .cm <sup>-1</sup> )	$1.44 \times 10^1 \pm 1.4 \times 10^1$	$1.40 \pm 1$
$\epsilon_1$ (L.mol <sup>-1</sup> .cm <sup>-1</sup> )	$2.46 \times 10^2 \pm 1.5 \times 10^1$	$2.97 \times 10^2 \pm 1.5 \times 10^1$
$\epsilon_2$ (L.mol <sup>-1</sup> .cm <sup>-1</sup> )	$6.85 \times 10^2 \pm 1.5 \times 10^1$	$1.95 \times 10^2 \pm 1.5 \times 10^1$
$\epsilon_3$ (L.mol <sup>-1</sup> .cm <sup>-1</sup> )	0	$6.40 \times 10^2 \pm 1.0 \times 10^1$
$\epsilon_4$ (L.mol <sup>-1</sup> .cm <sup>-1</sup> )	0	0 <sup>a</sup>
$\epsilon_l$ (L.mol <sup>-1</sup> .cm <sup>-1</sup> )	0	0
$K_1$	$9.15 \times 10^8 \pm 1.0 \times 10^{16}$	$1.73 \times 10^6 \pm 1.0 \times 10^6$
$K_2$	$2.18 \times 10^2 \pm 5.0 \times 10^1$	$2.71 \times 10^4 \pm 2.0 \times 10^4$
$K_3$	$4.23 \pm 1$	$6.30 \times 10^2 \pm 5$
$K_4$	0	$3.65 \pm 2 \times 10^{-1}$
$\chi^2$	$4.8 \times 10^{-3}$	$3.7 \times 10^{-3}$

**Table IV.2.** Calculated parameters for cobalt complexation by dicyanamide in an aqueous solution (Model assuming one complex) and in [C<sub>1</sub>C<sub>4</sub>Pyrr][NTf<sub>2</sub>] (Model assuming three and four complexes).

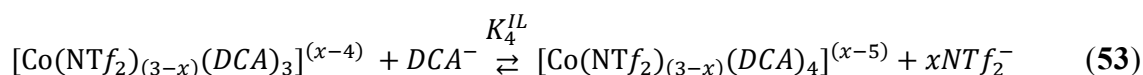
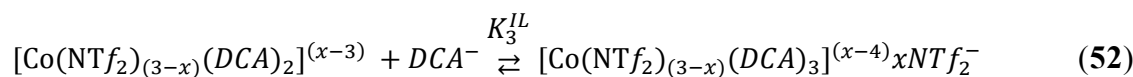
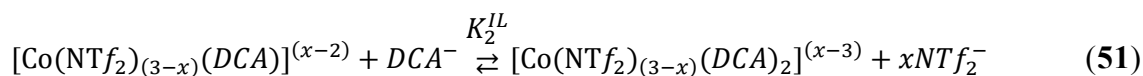
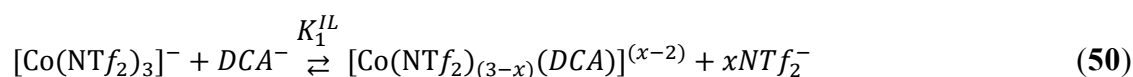
Using the second version of the model based on four dicyanamidocobalt(II) complexes, ( $X_1$  to  $X_4$ ) the  $\chi^2$  now reaches a value of  $3.7 \times 10^{-3}$ , slightly lower than the value obtained when only three complexes are considered. Furthermore, calculated and experimental absorbance values are very close between  $R = 0$  and 10. Strikingly, the local maximum observed between  $R = 0.8$  to 2 is now accurately described. In addition, the calculated molar extinction coefficient of  $X_0$  is now of  $1.40 \text{ L.mol}^{-1}.\text{cm}^{-1}$ , a value very close to the experimental one ( $1.22 \text{ L.mol}^{-1}.\text{cm}^{-1}$ ) measured in this study. Taking into account four complexes thus appears to yield a significantly better description of the absorption data than that obtained when three complexes are considered.

The speciation of cobalt in an ionic liquid based on [NTf<sub>2</sub>]<sup>-</sup> anion was recently studied.<sup>226</sup> Authors revealed that Co(II) is surrounded by three bis(trifluoromethanesulfonyl)imide anions, yielding the formation of a monovalent negative complex [Co(NTf<sub>2</sub>)<sub>3</sub>]<sup>-</sup>. The three NTf<sub>2</sub><sup>-</sup> anions have been found to be bidentate, yielding a hexacoordinated Co(II) ion. In our study, Co(II) is thus

assumed to be under the form of  $[\text{Co}(\text{NTf}_2)_3]^-$  in neat  $[\text{C}_1\text{C}_4\text{Pyrr}][\text{NTf}_2]$ . According to our model, upon addition of dicyanamide anions in  $[\text{C}_1\text{C}_4\text{Pyrr}][\text{NTf}_2]$ , up to four  $[\text{DCA}]^-$  ions are expected to enter the solvation sphere of Co(II). However, because  $\text{NTf}_2^-$  can be either bidentate or monodentate,<sup>226</sup> the exact number of such an anion surrounding Co(II) as  $[\text{DCA}]^-$  increases is not known. Therefore, the only valid general expression for describing the heteroleptic Co(II) complex in  $[\text{C}_1\text{C}_4\text{Pyrr}][\text{NTf}_2]$  is  $[\text{Co}(\text{NTf}_2)_{(3-x)}(\text{DCA})_y]^{(x-y-1)}$  with  $x$  ranging from 0 to 3 and  $y$  from 0 to 4. Note that using this definition, the overall charge of the complex is supposed to be negative.

The spectroscopic data are thus accurately described within a model using five species, namely  $[\text{Co}(\text{NTf}_2)_3]^-$  ( $X_0^{IL}$ ),  $[\text{Co}(\text{NTf}_2)_{(3-x)}(\text{DCA})]^{(x-2)}$  ( $X_1^{IL}$ ),  $[\text{Co}(\text{NTf}_2)_{(3-x)}(\text{DCA})_2]^{(x-3)}$  ( $X_2^{IL}$ ),  $[\text{Co}(\text{NTf}_2)_{(3-x)}(\text{DCA})_3]^{(x-4)}$  ( $X_3^{IL}$ ) and  $[\text{Co}(\text{NTf}_2)_{(3-x)}(\text{DCA})_4]^{(x-5)}$  ( $X_4^{IL}$ ). Each chemical entity has a specific molar extinction coefficient, denoted respectively  $\varepsilon_0^{IL}$ ,  $\varepsilon_1^{IL}$ ,  $\varepsilon_2^{IL}$ ,  $\varepsilon_3^{IL}$  and  $\varepsilon_4^{IL}$ . The formation of these four complexes is governed by four complexation constants ( $K_1^{IL}$ ,  $K_2^{IL}$ ,  $K_3^{IL}$  and  $K_4^{IL}$ ).

The version of our chemical model assuming four Co-DCA complexes can thus be written as follows:



Values of  $1.73 \times 10^6$ ,  $2.71 \times 10^4$ ,  $6.30 \times 10^2$  and 3.65 for the complexation formation constants  $K_1^{IL}$ ,  $K_2^{IL}$ ,  $K_3^{IL}$  and  $K_4^{IL}$  are obtained respectively. Due to a strong complexation constant, the first two complexes are likely to form at  $R < 3$  unlike

the fourth and last Co-DCA complex that will be observed only in the presence of a large excess of dicyanamide anions.

**Figure IV.8** then displays the speciation diagram calculated using the four complexes discussed above. The variation of species concentration in the ionic liquid (in mol. %) is plotted against the R ratio. The concentration of  $[\text{Co}(\text{NTf}_2)_3]^+$  decreases rapidly, reaching 0.1 % at  $R = 2$ . The first complex  $[\text{Co}(\text{NTf}_2)_{(3-x)}(\text{DCA})]^{(x-2)}$  ( $X_1^{IL}$ ) reaches its maximum in the ionic liquid at  $R = 1$  (80.0 %). It then disappears when  $R = 2$  (4.0 %) to the benefit of the second complex  $[\text{Co}(\text{NTf}_2)_{(3-x)}(\text{DCA})_2]^{(x-3)}$  ( $X_2^{IL}$ ) which reaches its maximum (68.7 %) at the same ratio. Regarding the third complex  $[\text{Co}(\text{NTf}_2)_{(3-x)}(\text{DCA})_3]^{(x-4)}$  ( $X_3^{IL}$ ), a continuous growth of the concentration can be observed from  $R = 1$  to  $R = 25$  with a molar percentage of respectively 0.03 and 86.7 %. However  $X_3^{IL}$  fades away from a ratio  $[\text{DCA}^-]/[\text{Co}(\text{II})]$  superior to 25. The last complex, namely  $[\text{Co}(\text{NTf}_2)_{(3-x)}(\text{DCA})_4]^{(x-5)}$  ( $X_4^{IL}$ ) appears at  $R = 3$  and slowly grows until reaching a value of 93.8 % at  $R = 5040$ . When the  $[\text{DCA}^-]/[\text{Co}(\text{II})]$  reaches 5040, there is 6.2 % of  $X_3^{IL}$  remaining in the solution.

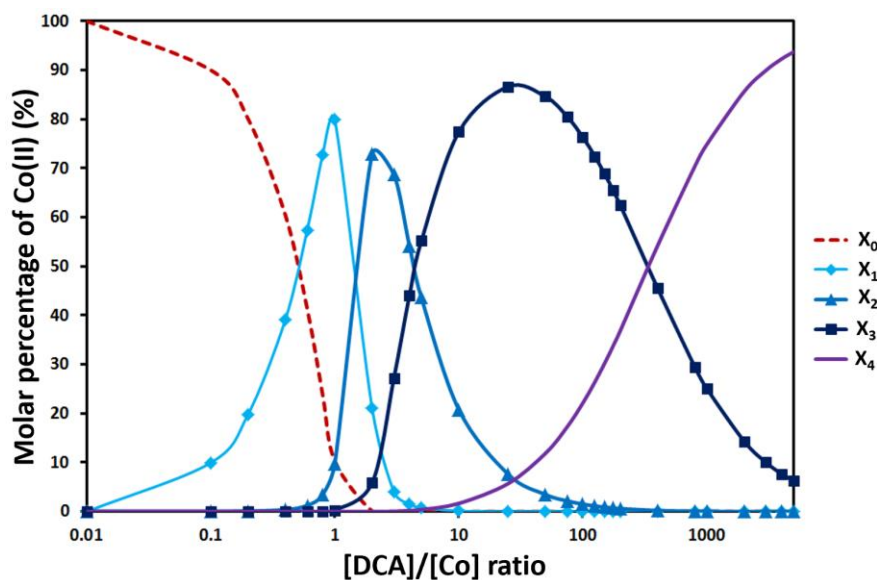


**Figure IV.8.** Chemical speciation for  $[\text{Co}(\text{NTf}_2)_3]^+$  ( $X_0$ ),  $[\text{Co}(\text{NTf}_2)_{(3-x)}(\text{DCA})]^{(x-2)}$  ( $X_1$ ),  $[\text{Co}(\text{NTf}_2)_{(3-x)}(\text{DCA})_2]^{(x-3)}$  ( $X_2$ ),  $[\text{Co}(\text{NTf}_2)_{(3-x)}(\text{DCA})_3]^{(x-4)}$  ( $X_3$ ) and  $[\text{Co}(\text{NTf}_2)_{(3-x)}(\text{DCA})_4]^{(x-5)}$  ( $X_4$ ) for each R ratio in the ionic liquid. Dashed line: ( $X_0$ ) concentration. Diamond: ( $X_1$ ) concentration. Triangle: ( $X_2$ ) concentration. Square: ( $X_3$ ) concentration. Full line: ( $X_4$ ) concentration.

In order to fit with classical representations of speciation diagrams, pDCA (=  $-\log[\text{DCA}]$ ) was calculated and represented in **Figure IV.9**.

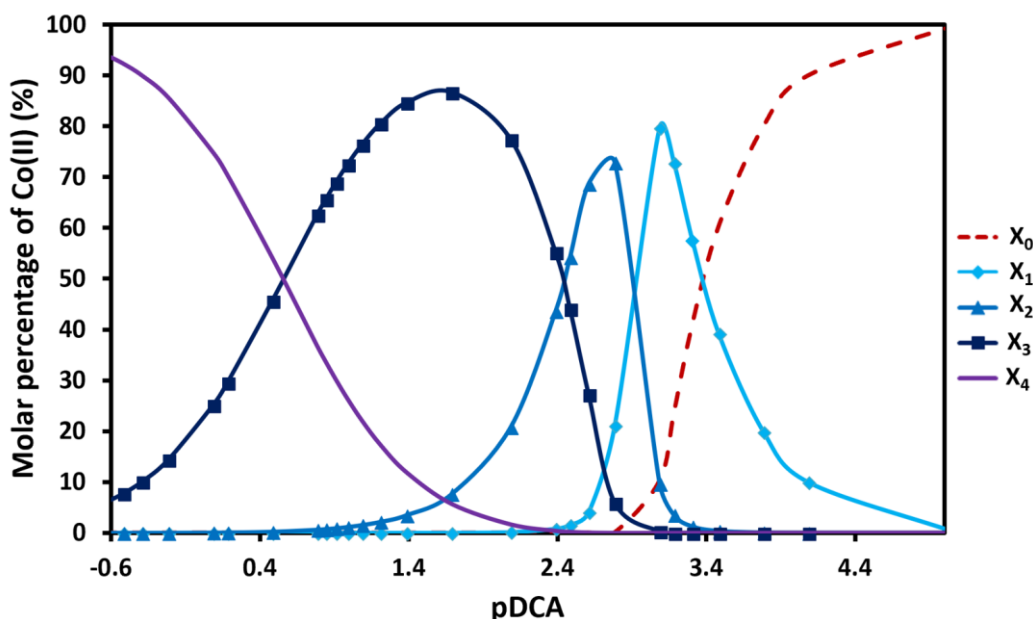


**Figure IV.9.** Chemical speciation for  $[\text{Co}(\text{NTf}_2)_3]^+$  ( $X_0$ ),  $[\text{Co}(\text{NTf}_2)_{(3-x)}(\text{DCA})]^{(x-2)}$  ( $X_1$ ),  $[\text{Co}(\text{NTf}_2)_{(3-x)}(\text{DCA})_2]^{(x-3)}$  ( $X_2$ ),  $[\text{Co}(\text{NTf}_2)_{(3-x)}(\text{DCA})_3]^{(x-4)}$  ( $X_3$ ) and  $[\text{Co}(\text{NTf}_2)_{(3-x)}(\text{DCA})_4]^{(x-5)}$  ( $X_4$ ) function of pDCA in the ionic liquid. Dashed line: ( $X_0$ ) concentration. Diamond: ( $X_1$ ) concentration. Triangle: ( $X_2$ ) concentration. Square: ( $X_3$ ) concentration. Full line: ( $X_4$ ) concentration.

Overall and as expected, dicyanamide anion appears to be a significantly stronger ligand than  $\text{NTf}_2^-$ . The gradual addition of  $[\text{DCA}]^-$  in the coordinating sphere of  $\text{Co}(\text{II})$  rather than an immediate formation of tetracyanamidocobaltate(II) complex is due to the high concentration of  $\text{NTf}_2^-$  in the ionic liquid. Besides,  $K_1^{IL}$  is ca. five orders of magnitude higher than the value for the formation constant of  $[\text{Co}(\text{H}_2\text{O})_5(\text{DCA})]^+$  obtained in water ( $K_1^W = 20.5$ ), while  $K_2^W$ ,  $K_3^W$  and  $K_4^W$  are null in water. We thus can infer that bis(trifluoromethylsulfonyl)imide is a weaker ligand of cobalt than water, a statement that is confirmed by numerous evidences already reported in the literature.<sup>226,242</sup>

#### *Geometry of the complexes*

According to the crystal field theory, molar extinction coefficient of transition metal complexes can drastically change with the geometry of the compound.<sup>294,296,297</sup> In the case of cobalt, low values of  $\epsilon$ , namely under  $100 \text{ L}\cdot\text{mol}^{-1}\cdot\text{cm}^{-1}$  can be linked to an octahedral geometry,<sup>287</sup> as observed for  $[\text{Co}(\text{H}_2\text{O})_6]^{2+}$  ( $\epsilon = 4.5 \text{ L}\cdot\text{mol}^{-1}\cdot\text{cm}^{-1}$ ). A higher extinction coefficient value is most probably due to a

tetrahedral geometry as observed with  $\text{CoCl}_4^{2-}$  that exhibits a molar extinction coefficient of  $615 \text{ L}\cdot\text{mol}^{-1}\cdot\text{cm}^{-1}$  at 690 nm in water.<sup>294</sup> This phenomenon is explained by the inversion centre observed in octahedral complexes that leads to forbidden transitions according to the Laporte law.<sup>296,296,298</sup> Our study indicates that the complex containing three dicyanamide anions in the ionic liquid exhibits a molar extinction coefficient of  $640 \text{ L}\cdot\text{mol}^{-1}\cdot\text{cm}^{-1}$  and a strong blue color, while, adding extra  $\text{DCA}^-$  anions leads to a complex with an inversed centre and thus a negligible absorbance as derived from  $\epsilon_{x4}$  values. We thus suggest that, in accordance with equation (52),  $[\text{Co}(\text{NTf}_2)_{(3-x)}(\text{DCA})_3]^{(x-4)}$  is present in a tetrahedral geometry and becomes octahedral when one dicyanamide anion is added in order to form  $[\text{Co}(\text{NTf}_2)_{(3-x)}(\text{DCA})_4]^{(x-5)}$ . This assumption is strengthened by recent papers dealing with the geometry of cobalt(II) complexes with thiocyanate anions in ionic liquid media.<sup>298,299</sup> In this work tetrahedral complexes exhibit a strong blue colour while a bright red colour is observed for octahedral complexes.

#### IV.2.5 Cobalt extraction by dicyanamide-based ionic liquids

To highlight the importance of studying the speciation of Co-DCA in water, extraction of cobalt from an aqueous phase containing various  $[\text{DCA}]/[\text{Co}]$  ratios with  $[\text{P}_{66614}][\text{DCA}]$  was performed.  $[\text{P}_{66614}]^+$  was used rather than  $[\text{C}_1\text{C}_4\text{Pyrr}]^+$  cation because  $[\text{C}_1\text{C}_4\text{Pyrr}][\text{DCA}]$  is soluble in water. Considering Co(II) interacts mainly with the anions of the ionic liquid, the results obtained in the preceding subsection still hold when  $[\text{P}_{66614}][\text{NTf}_2]$  and  $[\text{P}_{66614}][\text{DCA}]$  are used.

##### a. Experimental part

Firstly, starting from 0.7 mL solutions containing  $5 \times 10^{-3} \text{ mol}\cdot\text{L}^{-1}$  of cobalt and 0 to  $1 \text{ mol}\cdot\text{L}^{-1}$  of sodium dicyanamide in water, 0.7 ml of  $[\text{P}_{66614}][\text{DCA}]$  was added. The  $[\text{DCA}]/[\text{Co}]$  ratio of all solutions before extraction was of 0, 1, 3, 10, 20, 50, 100, 150 and 200 in the aqueous phase. Secondly, 0.7 mL of mixtures containing  $[\text{P}_{66614}][\text{DCA}]$  and  $[\text{P}_{66614}][\text{NTf}_2]$  were prepared to extract  $5 \times 10^{-3} \text{ mol}\cdot\text{L}^{-1}$  of cobalt in an aqueous solution containing  $1 \text{ mol}\cdot\text{L}^{-1}$  of sodium dicyanamide. The weight percentage of  $[\text{P}_{66614}][\text{DCA}]$  in  $[\text{P}_{66614}][\text{NTf}_2]$  was of 0, 25, 50, 75 and 100 wt %.



After stirring and centrifuging the samples during 60 and 15 min respectively, the two phases were separated. The bottom phase, namely the aqueous solution was analysed before and after extraction by Atomic Absorption Spectroscopy (AAS) see ANNEX 1-F. The extraction efficiency was measured thanks to the distribution coefficient ( $D$ ). According to experimental setup, the distribution coefficient of all extraction is given with an error of  $\pm 5\%$ .

### b. Results

Results are expressed in **Figure IV.10**. No extraction of metal was observed when cobalt was in an aqueous solution without dicyanamide ions. However the distribution coefficient ( $D$ ) increases with the  $R$  ratio. Half of the cobalt is extracted at  $R = 3$  ( $D = 1$ ). A quantitative extraction of metal is observed for  $R \geq 100$  leading to a distribution coefficient of 105.

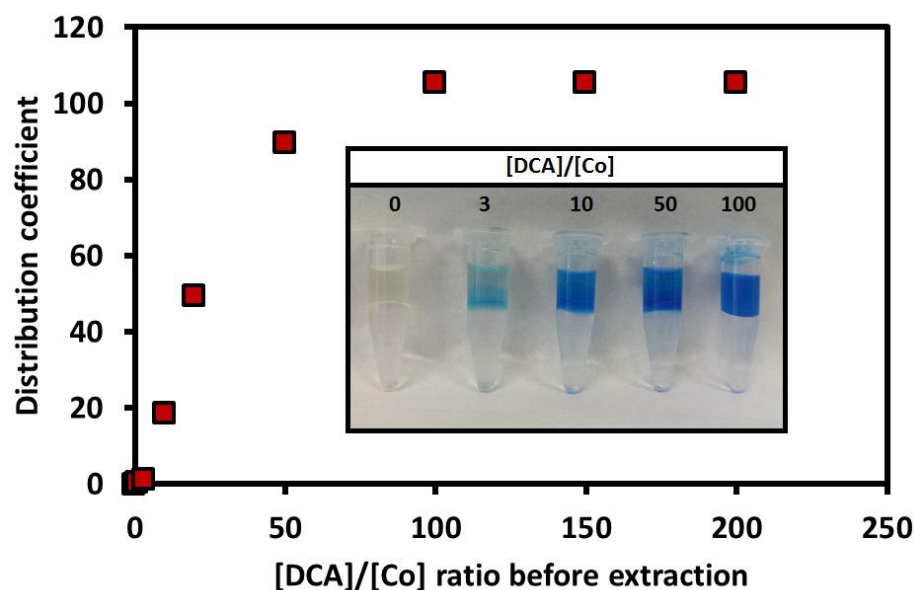


**Figure IV.10.** Extraction of cobalt  $5 \cdot 10^{-3} \text{ mol} \cdot \text{L}^{-1}$  in water with  $[\text{P}_{66614}][\text{DCA}]$  from an aqueous phase containing  $[\text{DCA}]/[\text{Co}]$  ratios of 1, 3, 10, 20, 50, 100, 150 and 200. Snapshots of extraction at ratios of 0, 3, 10, 50, 100 are presented. Ionic liquid phase is on top.

The influence of the DCA-NTf<sub>2</sub> ionic liquid mixtures on the extraction of Co(II) was studied using ionic liquid mixtures containing 0, 25, 50, 75 and 100 wt %  $[\text{P}_{66614}][\text{DCA}]$  in  $[\text{P}_{66614}][\text{NTf}_2]$ . Results are shown in **Figure IV.11**.  $[\text{P}_{66614}][\text{NTf}_2]$  ionic liquid is unable to extract cobalt as the distribution coefficient of such

mixture is close to 0. However the higher is the percentage of dicyanamide, the more efficient is the extraction. The distribution coefficient is thus of 1.4 and 105 for mixtures of 25 and 100 wt % of  $[P_{66614}][DCA]$  in  $[P_{66614}][NTf_2]$  respectively. One should notice that the density of  $[P_{66614}][NTf_2]$  is of 1.11 and is higher than the one of the aqueous phase while the density of  $[P_{66614}][DCA]$  is much lower, namely 0.89. This results in a phase inversion. The organic phase is thus the bottom phase from 0 to 25 wt % and is the top phase from 50 to 100 wt %.

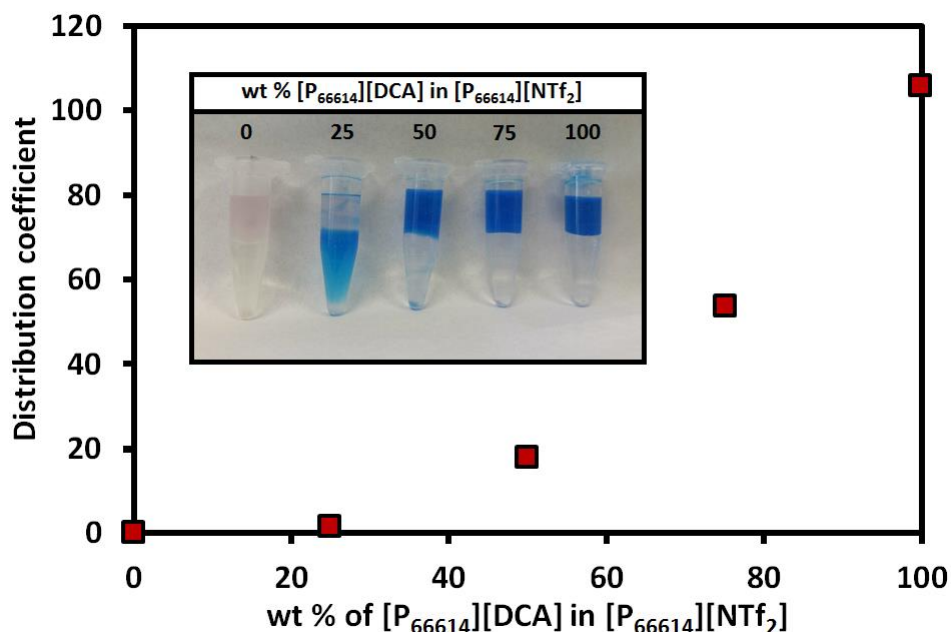


**Figure IV.11.** Extraction of cobalt  $5.10^{-3} \text{ mol.L}^{-1}$  in water and  $1 \text{ mol.L}^{-1}$  of sodium dicyanamide by  $[P_{66614}][DCA]$ - $[P_{66614}][NTf_2]$  mixtures. Weight percentages of  $[P_{66614}][DCA]$  are of 0, 25, 50 and 100 wt %. Snapshots of all extractions are presented. 0 and 25 wt % of  $[P_{66614}][DCA]$ : Aqueous phase is on top. 50, 75 and 100% of  $[P_{66614}][DCA]$ , ionic liquid phase is on top.

c. Discussion: From the speciation to the extraction

The poor extraction observed in the absence of dicyanamide ion in the aqueous phase first reveals that the impurities found in the ionic liquid were not complexing strongly enough with Co(II) to yield an extraction of Co(II) towards the ionic liquid. Besides, because extraction of Co(II) was significantly enhanced in presence of  $[DCA]^-$  and because the colour of Co(II) complexes changed according to the speciation presented in the preceding sections, one can ascertain that the presence of impurities in the phosphonium-based ionic liquids did not play any significant role in the extraction of the metal ion.

A strong correlation can be made between the speciation diagram of Co-DCA in water provided in Figure 5 and the extraction trend of cobalt with various [DCA]/[Co] ratio in water. The  $[\text{Co}(\text{H}_2\text{O})_5(\text{DCA})]^+$  complex predominates in water when the concentration of dicyanamide is 100 times higher than the concentration of cobalt. Similarly, the extraction of cobalt increases with the [DCA]/[Co] ratio until reaching a plateau for  $R \geq 100$ . This result proves that cobalt needs to be under the form of a monodicyanamide complex in order to be extracted towards  $[\text{P}_{66614}][\text{DCA}]$ . In other words, a dicyanamide IL is unable to extract the free metallic cobalt cation solvated in water. Furthermore, the nature of the organic phase also has a significant impact on the cobalt extraction. We reported that DCA ILs present a higher complexation constant of cobalt than what is observed in  $\text{NTf}_2$  ionic liquids or in water. This results in a more efficient extraction of Co(II) as the concentration of dicyanamide increases, as shown in Figure 7. It is important to notice that while cobalt is efficiently extracted from a dicyanamide aqueous medium, the colour of the metal changes from red in the aqueous phase before extraction to a strong blue colour in the ionic liquid. This is characteristic of a difference in complexation of Co(II) in water and in an IL, as demonstrated in this work. Cobalt(II) is thus under the form of a pink octahedral  $[\text{Co}(\text{H}_2\text{O})_5(\text{DCA})]^+$  complex in water. Upon extraction towards the ionic liquid that contains a large amount of dicyanamide ligands, the metal complex changes. According to the UV-Vis spectrum, Co(II) releases its water molecules, three dicyanamide and one or two  $(\text{NTf}_2)^-$  anions complex the metal, leading to a blue  $[\text{Co}(\text{NTf}_2)_{(3-x)}(\text{DCA})_3]^{(x-4)}$  compound. According to the speciation study reported here, it is expected that the apparition of the fourth and last complex, namely  $[\text{Co}(\text{NTf}_2)_{(3-x)}(\text{DCA})_4]^{(x-5)}$  requires a huge excess of ligands compared to the metal and is thus unlikely to be predominant during liquid-liquid extractions. Finally, the exact mechanism, specifically whether the complex change occurs at the interface, or if  $[\text{Co}(\text{H}_2\text{O})_5(\text{DCA})]^+$  passes the interface and changes into  $[\text{Co}(\text{NTf}_2)_{(3-x)}(\text{DCA})_3]^{(x-4)}$  within the ionic liquid is not yet established.

#### IV.2.6 Conclusion

We have investigated and compared the complexation of cobalt by dicyanamide in water and in an ionic liquid,  $[\text{C}_1\text{C}_4\text{Pyrr}][\text{NTf}_2]$ . Strong evidences showed that only

one  $\text{DCA}^-$  is able to complex  $[\text{Co}(\text{H}_2\text{O})_6]^{2+}$  in order to form  $[\text{Co}(\text{H}_2\text{O})_5(\text{DCA})]^+$  in an aqueous solution. Due to a low complexation constant, a large excess of DCA ligand must be added to complex most of the cobalt in water. Regarding the ionic liquid, a model assuming four different complexes  $[\text{Co}(\text{NTf}_2)_{(3-x)}(\text{DCA})]^{(x-2)}$ ,  $[\text{Co}(\text{NTf}_2)_{(3-x)}(\text{DCA})_2]^{(x-3)}$ ,  $[\text{Co}(\text{NTf}_2)_{(3-x)}(\text{DCA})_3]^{(x-4)}$  and  $[\text{Co}(\text{NTf}_2)_{(3-x)}(\text{DCA})_4]^{(x-5)}$  which concentrations are directly related to the  $[\text{DCA}^-]/[\text{Co}(\text{II})]$  ratio is shown to be fully in line with the experimental data. This work underlines the fact that speciation of metal ions in an ionic liquid can be more exotic than that observed in water. In addition, not previously observed complexes, such as the  $[\text{Co}(\text{NTf}_2)_{(3-x)}(\text{DCA})_3]^{(x-4)}$  and  $[\text{Co}(\text{NTf}_2)_{(3-x)}(\text{DCA})_4]^{(x-5)}$ , might show potentially promising physical or chemical properties. As far as liquid-liquid extraction is concerned, extraction mechanisms can thus be significantly influenced by the nature of the metal complex formed within an ionic liquid. For instance, extraction of cobalt(II) using a mixture of hydrophobic ionic liquids based on  $[\text{NTf}_2]^-$  and  $[\text{DCA}]^-$  anion could very well enhance the extraction of this metal within the ionic liquid phase, due to the metal complexes formed with the dicyanamide anion. Optimisation of the metal ion extraction was obtained by carefully choosing the ratio of  $\text{Co}^{2+}$ ,  $[\text{DCA}]^-$  and  $[\text{NTf}_2]^-$  anions in the aqueous and organic phase.

Regarding the recycling of transition metals from NiMH batteries investigated in this chapter, separation of nickel from cobalt is at the center of our attention. However, nickel is known to have similar extraction trends in dicyanamide-based ionic liquids.<sup>185</sup> As a result, a quantitative isolation of those two metals seems difficult in such system. Therefore, the construction of an innovative extraction system must be investigated for the separation of Co from Ni.

## IV.3 Novel ionic liquid-based Acidic Aqueous Biphasic Systems (AcABS): From fundamentals to metal extraction

---

This part is based on the following peer reviewed articles:

- [Gras.M](#), Papaiconomou.N, Schaeffer.N, Chainet.E, Tedjar.F, Coutinho.J.A.P, Billard.I, Ionic-Liquid-Based Acidic Aqueous Biphasic Systems for simultaneous leaching and extraction of metallic ion, *Angewandte Chemie* **58** (2018) 1563-1566.
- Mogilireddy.V, [Gras.M](#), Schaeffer.N, Passos.H, Svecova.L, Papaiconomou.N, Coutinho. J.A.P and Billard.I, Understanding the fundamentals of Acid-Induced Ionic Liquid-based Aqueous Biphasic System, *Physical Chemistry Chemical Physics*, (2018).
- Schaeffer.N, Passos.H, [Gras.M](#), Mogilireddy.V, Leal.J.P, Pérez-Sanchez.G, Gomes.JRB, Billard.I, Papaiconomou.N, Coutinho.J.A.P, Mechanism of ionic liquid-based acidic aqueous biphasic systems formation, *Physical Chemistry Chemical Physics*, **20** (2018) 9839-9846.

And on the following patent:

- (2) Papaiconomou.N, [Gras.M](#), Coutinho.J.A.P, Billard.I, Ionic liquid acid aqueous two phase system, FR3058735A1, 2016

### IV.3.1 Introduction

The major developments in the use of ionic liquids in solvent extraction can be divided into three main categories: ILs are used as the diluting hydrophobic phase

in conjunction with a traditional extracting agent, selective extraction of metals through the IL's anion interaction and task specific ILs.<sup>126,161,300</sup> The ionic nature of ILs results in metal extraction mechanisms from an aqueous phase not possible in conventional organic solvents. The ability of ILs to solvate both charged and neutral metal complexes is the reason behind the various extraction mechanisms in IL mediated solvent extraction processes. More recently, several papers have shown that neat ionic liquids are very successful at extracting several metal ions from aqueous phases.<sup>100,126,191,301</sup> Despite the proven potential of ILs as alternatives to volatile organic compounds in liquid-liquid extraction, some significant drawbacks remain. First, the range of hydrophobic ILs is limited, most being based on fluorinated anions such as bis(trifluoromethanesulfonyl)imide, [Tf<sub>2</sub>N<sup>-</sup>], or on ILs incorporating long alkyl chains.<sup>241,302</sup> Fluorinated ILs are expensive and are not likely to suffer from biodegradation.<sup>303</sup> A collateral problem is that although hydrophobic, these ionic liquids are significantly soluble in the acidic aqueous solutions from which the metal ions are to be extracted, which induces a costly undesirable loss.<sup>12-14</sup> Furthermore, hydrophobic ILs with bulky alkyl chains such as trihexyltetradecyl phosphonium chloride, exhibit high viscosities that hinder their industrial applicability.<sup>15,16</sup>

In order to overcome the difficulties associated with IL-based liquid-liquid extraction systems, such as the limited number of ILs available, their ecotoxicity and their viscosity, we propose an alternative for a 'one-pot' dissolution and separation of metals based on aqueous biphasic system (ABS). During the past decade, so-called aqueous biphasic systems based on ionic liquids have emerged in the literature.<sup>129,195,196,305</sup> ABS are composed of a hydrophilic ionic liquid, water and an (in)organic salt, containing typically a multivalent anion, such as phosphate or sulphate. Depending on the temperature and exact composition, upon mixing of these three compounds two immiscible aqueous phases are eventually formed. One aqueous phase retains most of the IL, while the other is concentrated in the salt. ABS have until now been nearly exclusively applied to the extraction of neutral molecules such as biologically active compounds, dyes, etc.<sup>128,129,194,198</sup> Reported ABS are usually formed with non-fluorinated ILs and as the extraction occurs in an aqueous solution, ABS tackle the issues related to the cost and viscosity of hydrophobic ionic liquids.

However, the acidic media in which metal extraction occurs present new challenges compared to the neutral pH required for the separation of biological compounds.

One of the major limitations of applying such ABS to metallic ion extraction is the difficult handling of metal ions with high sensitivity to hydrolysis and/or precipitation as this requires strong acidic conditions that are apparently incompatible with ABS general composition. Few articles deal with the extraction of metal ions using such hydrophilic ionic liquid-based ABS. The extraction of silver initially dissolved in an aqueous phase containing above  $2 \text{ mol.L}^{-1} \text{ HNO}_3$  using an ABS based on 1-butyl-3-methylimidazolium chloride and potassium phosphate was reported.<sup>306</sup> In this case, however, questions arise concerning the exact speciation of the phosphate anions under such highly acidic conditions. The partition of nitric acid in such a system is also an issue that was not dealt with. With the objective of closing the gap between such ABS and metallic ion extraction from acidic phases, we now report new ABS containing high amounts of acid and only one hydrophilic ionic liquid hereby called acidic ABS (AcABS). This novel AcABS is composed by a hydrophilic ionic liquid, tributyltetradecylphosphonium chloride ( $[\text{P}_{44414}][\text{Cl}]$ ), an acid and water. The acid advantageously plays the role of the inorganic salt, thus tackling the issue of forming ABS in acidic conditions and simplifying the chemical system in terms of number of ions present in solution. It therefore appears to be of crucial importance to overcome the limitations raised by the presence of a large concentration of acid in leaching solutions.

This part dedicated to ABS and to selective liquid-liquid extraction of TM will be divided in two parts. First, fundamentals of acidic aqueous biphasic systems will be presented. Phase diagrams, nature and phase volumes will be analysed to understand the behaviour of these new systems in a large range of temperatures and concentrations. In a second step, the potential of AcABS for metal extraction will be reported. Finally, a strategy for the recovery of metallic cobalt by electrodeposition in an AcABS starting from a solution of mixed Co(II), Ni(II) and Mn(II) will be presented.

### IV.3.2 Fundamentals of Acidic Aqueous Biphasic System

#### a. Experimental part

##### *Phase diagrams*

[P<sub>44414</sub>][Cl] is a hydrophilic ionic liquid, has the appearance of a white waxy material at room temperature. Its melting point is 38.5 °C as determined by the differential scanning calorimetry (DSC) provided in (ANNEX 2-D). This ionic liquid is soluble in any proportion in pure water. However, upon mixing [P<sub>44414</sub>][Cl] with a 37, 96, 6, 85 or 68 wt. % HCl, H<sub>2</sub>SO<sub>4</sub>, H<sub>2</sub>SO<sub>3</sub>, H<sub>3</sub>PO<sub>4</sub> or HNO<sub>3</sub> solution respectively at room temperature, two liquid immiscible phases are sometimes formed. In order to determine at what conditions our system is monophasic or biphasic, the cloud point titration was applied:

Typically, 1 g of an aqueous solution containing 50 to 70 wt. % [P<sub>44414</sub>][Cl] is prepared in a 10 mL vial. The vial is then thermostated at a given temperature using a water bath. Drops of a concentrated acidic solution are then added until the solution becomes cloudy, which is characteristic of the apparition of a biphasic system. Drops of ultrapure water are then added to the vial until the solution becomes clear again. These steps are repeated in order to obtain a series of cloud points, corresponding to the binodal curve that is the border line between the monophasic and biphasic state. In line with previous works, the binodal curve is presented by plotting the amount of ionic liquid as a function of the amount of acid. Experimental errors on the cloud points are in the order of 0.1 wt. %, corresponding to the mass of a drop of about 20 mg. Cloud point titration is schematized in **Figure IV.12**.

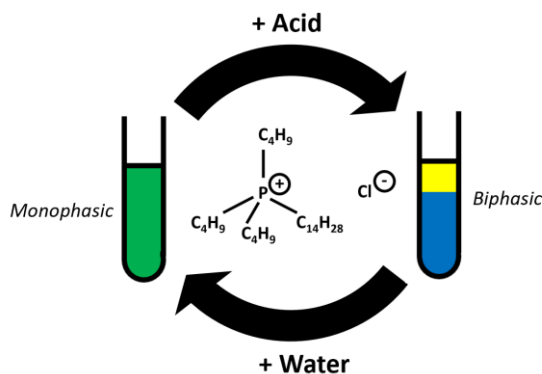


**Figure IV.12.** Scheme for the point titration technique



Finally, phase diagrams of mixed system ABS-AcABS using  $[P_{44414}][Cl]$  / HCl / NaCl / H<sub>2</sub>O were investigated. To that end, the cloud point titration method was used with fixed concentrations of NaCl at 1, 2 and 4 wt. % in order to observe the influence of sodium chloride as an additional salting out agent on the binodal. Those experiments were carried out at 24 °C.

#### *Phase compositions*

Focusing on the  $[P_{44414}][Cl]$  / HCl / H<sub>2</sub>O system, five different mixtures of ionic liquid, acid and water, denoted as A to E, were prepared. Details on their preparation are given in **Table IV.3**.

All mixtures were prepared adding various amounts of ionic liquid to 1 mL of aqueous phase containing concentrations of HCl ranging from 6.0 to 10 mol.L<sup>-1</sup> HCl.

Mixture	Mixture preparation			Amounts of each compound (wt. %)		
	1 mL [HCl] (mol.L <sup>-1</sup> )	[P <sub>44414</sub> ][Cl] (g)	Total mass (g)	[P <sub>44414</sub> ][Cl]	HCl	H <sub>2</sub> O
<b>A</b>	10	0.25	1.40	17.8	25.9	56.3
<b>B</b>	8.0	0.25	1.36	18.1	20.8	61.1
<b>C</b>	6.0	0.25	1.35	18.6	15.7	65.7
<b>D</b>	8.0	0.375	1.48	25.0	19.0	56.0
<b>E</b>	6.6	0.125	1.25	10.2	19.0	70.8

**Table IV.3.** Composition of mixtures A to E of the corresponding  $[P_{44414}][Cl]$  / HCl / H<sub>2</sub>O AcABS formed.

The mixtures were prepared and left over night. If a biphasic system was formed, the two phases were separated and both volumes were measured. The water content of the top phase, known as the IL-rich phase was analysed by Karl Fischer titration while the acidic concentration of the bottom phase known as the acid-rich phase was checked using acid-base titration.

b. Results and discussion*Salting out effect of various inorganic acids*

Phase diagrams for various  $[P_{44414}][Cl]$  / Acid /  $H_2O$  systems at 24 °C using hydrochloric, sulfuric, nitric and sulfurous acid are represented in **Figure IV.13**. For comparison and because the molecular weight of acids are different, the phase diagrams will be expressed in mol per kg of solution ( $mol.kg^{-1}$ ). All binodal curves were obtained by the cloud point titration method. For a fixed temperature, any mixture prepared in the area situated on the left of the binodal will lead to a monophasic mixture. Likewise, any mixture prepared in the area situated on the right of the binodal will lead to a biphasic mixture.

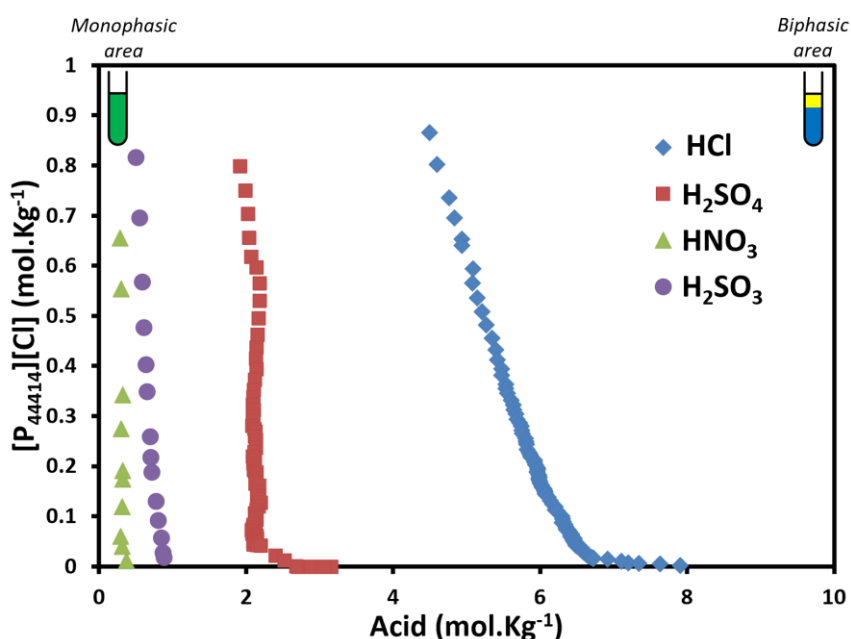


**Figure IV.13.** Binodal curves for various  $[P_{44414}][Cl]$  / Acid /  $H_2O$  AcABS at 24 °C. Blue diamond: HCl, red square:  $H_2SO_4$ , green triangle  $HNO_3$  and purple circle  $H_2SO_3$ .

Results show that the biphasic area can be wider from one acid to another. Using  $0.5 mol.kg^{-1}$  of ionic liquid, more than  $5.5 mol.kg^{-1}$  of hydrochloric acid are required to induce a biphasic solution while this value is  $2 mol.kg^{-1}$  for sulfuric acid. Regarding  $HNO_3$ , a single drop of concentrated acid causes an increase in the turbidity of the solution indicating that two phases are formed. As a result, less than  $0.5 mol.kg^{-1}$  of the latter acid is required to induce the biphasic state. It is worth to notice that experiments using  $H_3PO_4$  were also carried. This inorganic acid was however unable to induce a biphasic solution at 25 °C. Regarding the ability of acids to form solutions with two immiscible phases, from the strongest to

the weakest one, the following series is observed:  $\text{HNO}_3 > \text{H}_2\text{SO}_3 > \text{H}_2\text{SO}_4 > \text{HCl} > \text{H}_3\text{PO}_4$ . These results deviate significantly from the Hofmeister series ( $\text{SO}_4^{2-} > \text{PO}_4^{3-} > \text{Cl}^- > \text{NO}_3^-$ ) an empirical observation describing the ability of ions to induce the salting out of proteins but also, polymers and salts.<sup>196</sup> The deviation between the Hofmeister series and our result can be explained by two main reasons. (i) Concentrated acids are not fully dissociated when the concentration is high. As an example, the binodal of the  $[\text{P}_{44414}][\text{Cl}] / \text{H}_2\text{SO}_4 / \text{H}_2\text{O}$  system is close to  $2 \text{ mol.kg}^{-1}$  for concentrations of IL over  $0.1 \text{ mol.kg}^{-1}$ . In those specific conditions and because the pKa of  $\text{H}_2\text{SO}_4$  are of -3.0 and 1.9,  $\text{HSO}_4^-$  will be the predominant species with small amounts of dissociated  $\text{SO}_4^{2-}$  ions. We can thus infer that the salting out effect of the hydrogenosulphate ion will be different from the sulphate one. (ii) Focusing again on the  $[\text{P}_{44414}][\text{Cl}] / \text{H}_2\text{SO}_4 / \text{H}_2\text{O}$  system, a large range of ions are initially present in the IL, namely,  $[\text{P}_{44414}]^+$  and  $\text{Cl}^-$  and in the aqueous solution, namely,  $\text{HSO}_4^-$ ,  $\text{SO}_4^{2-}$  and  $\text{H}^+$ . After inducing a biphasic solution ( $[\text{P}_{44414}][\text{Cl}] > 0.1 \text{ mol.kg}^{-1}$ ,  $[\text{H}_2\text{SO}_4] > 2 \text{ mol.kg}^{-1}$ ) ions are highly susceptible to exchange from one phase to another. As a result,  $[\text{P}_{44414}][\text{Cl}]$  forms  $[\text{P}_{44414}][\text{HSO}_4]$  in presence of concentrated sulphuric acid. This phenomenon was highlighted by *Mogilireddy et al. 2018*<sup>307</sup> in a recent paper from our group. Using a weight ratio of IL:Acid of 1:2, more than 63 and 14 molar percent of chloride ions from  $[\text{P}_{44414}][\text{Cl}]$  were exchanged with nitric and hydrogenosulphate ions using  $\text{H}_2\text{SO}_4$  and  $\text{HNO}_3$  as salting out agents respectively. This ion exchange is a well-known mechanism in ionic liquid synthesis as nitrate or hydrogenosulphate ILs can be prepared by addition of concentrated  $\text{HNO}_3$ <sup>308</sup> or  $\text{H}_2\text{SO}_4$ <sup>309</sup> respectively in chloride-based ionic liquids. However the newly formed IL,  $[\text{P}_{44414}][\text{NO}_3]$  is not fully soluble in water anymore but can be considered as a hydrophobic IL. As a result, this system can't be defined as an Aqueous Biphasic System according to the definition given in **Chapter I**. This fully justifies the formation of two phases at low concentration of acid for the system  $[\text{P}_{44414}][\text{Cl}] / \text{HNO}_3 / \text{H}_2\text{O}$  and explains the deviation observed between binodal curves in **Figure IV.13** and the Hofmeister series.

*Temperature impact on phase diagrams*

To avoid any ion exchange, the following study will focus on the  $[P_{44414}][Cl] / HCl / H_2O$  AcABS. The binodal curve observed at 24 °C in **Figure IV.13** is compared with similar systems at various temperatures in **Figure IV.14**. The three-dimension diagram of the latter system is given in **Figure IV.15**.

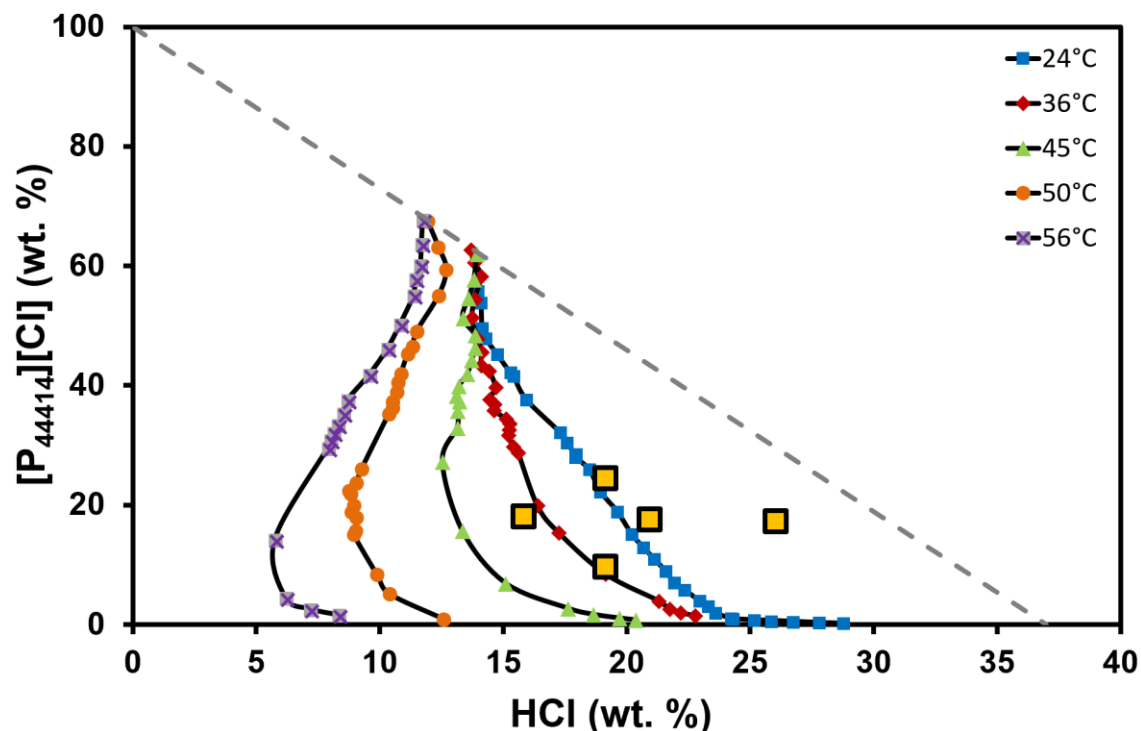


**Figure IV.14.** Binodal curves for  $[P_{44414}][Cl] / HCl / H_2O$  AcABS. Blue square: 25 °C, red diamond: 36 °C, green triangle: 45 °C, orange circle: 50 °C, Purple square: 56 °. Mixture points from A to E are represented in large yellow squares. Points  $[IL] > 30$  wt. % were measured by V.Mogilireddy during her post-doctoral position.

Lowering the temperature of a biphasic system can turn it into monophasic state, which corresponds to the behaviour of a system presenting a lower critical solution temperature (LCST). LCST behaviour has previously been observed for several phosphonium-based IL in classical ABS.<sup>310,311</sup> As shown in **Figure IV.14** and **Figure IV.15**, two domains appear. In the first domain, below 50 wt. % of ionic liquid, the concentration of acid required to induce a biphasic system is strongly dependent on the temperature. While at 24 °C a solution with 15 wt. % of  $[P_{44414}][Cl]$  requires 20 wt. % of HCl to form two phases, at 56 °C, 6 wt. % HCl is enough to obtain a phase separation in the same mixture.

This is not the case of the second domain, for concentration of  $[P_{44414}][Cl]$  higher than 50 wt. % where temperature has a negligible effect on the position of the

binodal centered around  $13 \pm 1$  wt. % HCl. Surprisingly, from 45 to 56 °C, over 20 wt. % IL, the concentration of HCl needed to induce two phases is decreasing with the increasing concentration of IL. Binodals will thus form what was described as an onion shape.<sup>307</sup>

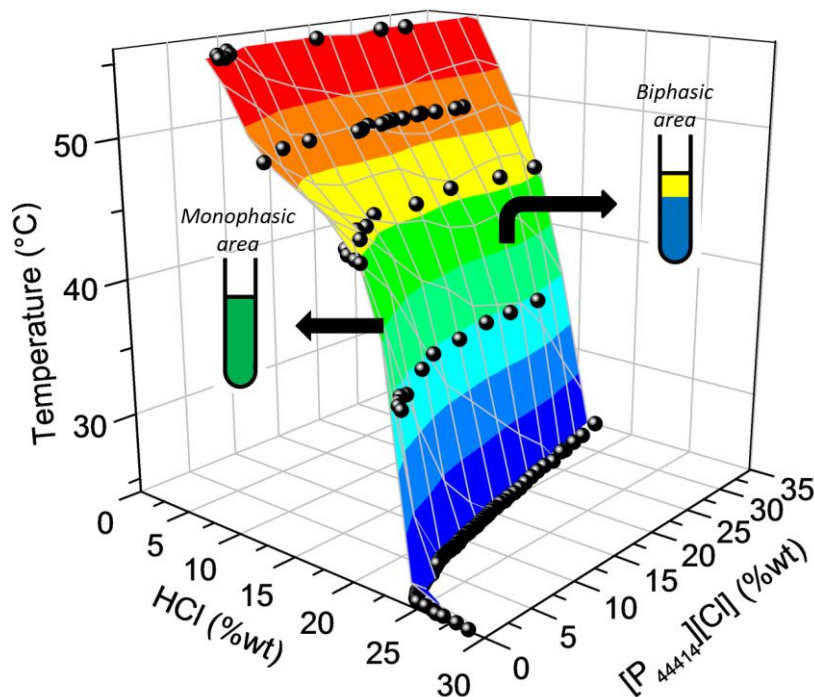


**Figure IV.15.** 3D phase diagram of  $[P_{44414}][Cl]$  / HCl / H<sub>2</sub>O from 25 to 56 °C. *Mixed systems ABS-AcABS*

Onghena et al.<sup>204</sup> recently reported the formation of ABS using  $[P_{44414}][Cl]$  and NaCl and their application to the separation of cobalt from nickel. A comparison of the phase diagrams for these systems shows that they have a similar shape and temperature dependency, albeit weaker for the NaCl system, with this system presenting a much larger biphasic region. The phase separation requires a significantly higher concentration of chloride in the case of  $[P_{44414}][Cl]$  / HCl / H<sub>2</sub>O compared to that required in  $[P_{44414}][Cl]$  / NaCl / H<sub>2</sub>O which is around 17.6 wt.% and 5.7 wt.% respectively at 30 wt.%  $[P_{44414}][Cl]$ . However most metals, e.g. platinum and iron, are not stable in solution at the high pH of this system,<sup>237</sup> while the AcABS allows the extraction of metals directly from the leachate just by adding  $[P_{44414}][Cl]$ . To increase the biphasic region of AcABS system and provide stability of metallic ions in an acidic pH, mixed systems were investigated. Phase diagrams of  $[P_{44414}][Cl]$  / HCl-NaCl / H<sub>2</sub>O with 1, 2 and 4 wt. % NaCl at 24 °C are reported in **Figure IV.16**.

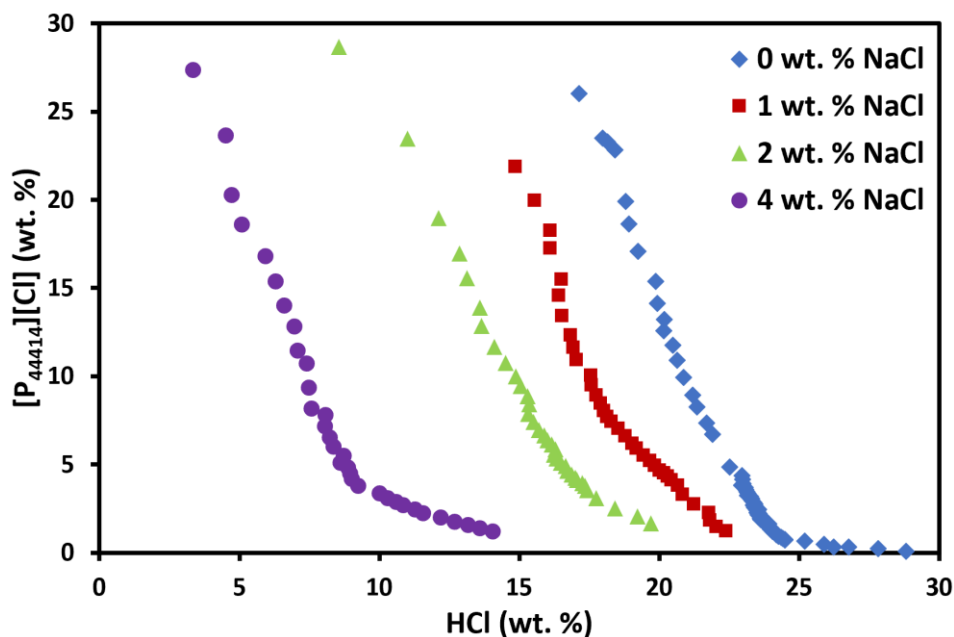


**Figure IV.16.** The effect of NaCl concentration on the binodal curve of  $[P_{44414}]Cl$ -HCl- $H_2O$  system at 24 °C. All binodal points containing NaCl were measured by N.Schaeffer during his post-doctoral position.

Interestingly, while at 15 wt. % IL, 20 wt. % HCl is needed to induce a biphasic solution at 24 °C, this value drops to 16, 13 and 6 wt. % when 1, 2 and 4 wt. % respectively of NaCl are added. This synergetic effect of HCl and NaCl offers to mixed systems ABS-AcABS the ability to set the concentration of acid of a bath to an appropriate value, function of the desired applications.

The overall phase diagrams bring the proof that biphasic solutions can be induced by a salt, an acid or both forming ABS, AcABS or ABS-AcABS respectively. They present an important thermomorphic behaviour in a large range of temperature and concentration which highlights the tuneability of those novel potential extraction systems.

#### *Phase compositions*

Snapshots of a  $[P_{44414}]Cl / HCl / H_2O$  solution heated from 24 to 50 °C during 10 min containing Fe(III) and Co(II) are shown in **Figure IV.17**.

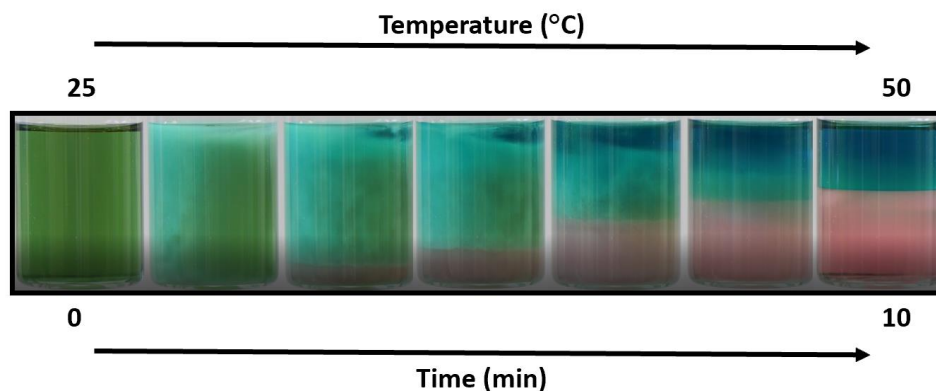


**Figure IV.17.** Snapshots of  $[P_{44414}][Cl]$  / HCl / H<sub>2</sub>O AcABS with Fe(III) and Co(II) from 24 to 50°C. Metals are only present to provide coloring of both phases.

Demixion phenomenon while heating  $[P_{44414}][Cl]$  / HCl / H<sub>2</sub>O AcABS stems from fast exchanges of components from one phase to another through volutes until an equilibrium is reached. After 10 min of heating, the two phases are well separated and stable. If the sample is cooled down to room temperature, only a strong agitation of the AcABS can lead to the re-formation of the monophasic system. Questions remain regarding the composition and volumes of both phases with the evolution of temperature and concentrations.

Five different mixture points A to E were prepared according to their composition depicted in **Table IV.3**. These mixture points have been plotted in **Figure IV.14**. The evolution of the volume of both phases, of the water content of the top phase (the IL-rich phase) and of the acidic concentration of the bottom phase (acid-rich phase) were investigated at 24 and 50 °C for all mixture points. Results are gathered in **Table IV.4**.

Mixture	Phase volumes				Water-content		HCl-content			
	24 °C		50 °C		24 °C	50 °C	24 °C	50 °C		
	Upper (mL)	Lower (mL)	Upper (mL)	Lower (mL)	Upper (wt. %)	Upper (wt. %)	Lower (wt. %)	Lower (mol.L <sup>-1</sup> )	Lower (wt. %)	Lower (mol.L <sup>-1</sup> )
<b>A</b>	0.45	0.85	0.35	0.95	17.5	15.3	29.4	9.2	28.7	9
<b>B</b>	0.40	0.88	0.35	0.93	23.3	13.3	25.3	7.8	25.2	7.8
<b>C</b>	-	-	0.60	0.68	-	43	-	-	17.1	5.1
<b>D</b>	0.70	0.68	0.63	0.75	26.1	20.3	25.1	7.7	24.8	7.6
<b>E</b>	-	-	0.23	0.98	-	31.0	-	-	21.6	6.5

**Table IV.4.** Behaviour of both phases in terms of volumes, water content of the IL-rich phase and HCl content of the acid-rich phase at 24 and 50 °C.

For mixtures exhibiting a phase separation, the compositions of the upper and lower phases are related by tie lines.<sup>312,313</sup> Since the lower part of the binodal curves in **Figure IV.14** are very close to the x-axis, the acid rich phase contains very little ionic liquid while the upper phase contains essentially all the ionic liquid. The latter statement was verified by NMR quantification in a recent paper from our group where less than 1 wt. % of the IL can be found in all acid-rich phases.<sup>307</sup> The water content is the lowest for mixture point A at 24 °C and reaches a maximum for mixture point C at 50 °C with weight percentages of 17.5 and 43.0 respectively. Regarding the HCl concentration in the lower phase, it decreases with increasing temperature due to the transfer of water from the IL-rich phase.

As shown in **Table IV.4**, it appears that for a given mixture, the amount of water in the upper phase decreases with temperature. Similarly, for that same mixture, the volume of the upper phase is found to decrease with temperature. Combining these results with the fact that the ionic liquid is almost only present in the upper phase, the influence of the temperature on the phase separation of an AcABS can be depicted according to **Figure IV.18**.

With the increase in temperature, the formation of a biphasic solution results from water and HCl being expelled from the initially monophasic mixture and forming an essentially ionic liquid-free lower phase. As the temperature increases, more



water and HCl are expelled, yielding an increase in the volume of the lower phase and a decrease in the volume of the upper phase.

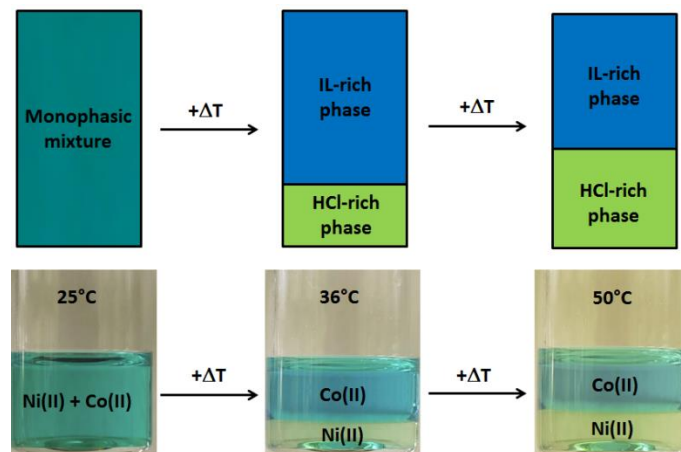


**Figure IV.18.** Influence of the temperature on the phase splitting. The HCl-rich phase is assumed to be completely depleted in ionic liquid. Metals are only present to provide coloring of both phases

The LCST-type behaviour of the AcABS is related to the strong polar/electrostatic interactions between the water and the ions and the unfavorable negative contribution to the entropy of mixing with increasing temperature.<sup>314</sup>

Overall, the ability to separate highly acidic solutions into two phases in presence of an ionic liquid by increasing the temperature allows the development of metal recycling processes combining leaching and extraction of metal ions. AcABS systems offer the ability to leach a metal towards a mixture and then partition the metals ions between two aqueous phases formed upon heating up the initial aqueous leaching liquor.

### IV.3.3 Acidic Aqueous Biphasic systems for metal extraction

#### a. Experimental part

Starting from [P<sub>44414</sub>][Cl] / HCl / H<sub>2</sub>O AcABS, five mixtures containing 30 wt. % IL and increasing concentration of HCl ranging from 10 to 30 wt. % were prepared. These five mixtures were used to study separately the partitioning of Co(II), Ni(II), Fe(III) or Mn(II) metal ions at 0.1 mol.L<sup>-1</sup> at 50 °C, representing all the transition metals found in NiMH batteries.

The separation of Co(II) from Ni(II), two difficult metals to isolate, found together in natural ores was studied in an additional set of experiments. A solution containing both metal ions at a concentration of  $0.1 \text{ mol.L}^{-1}$  was extracted with  $[\text{P}_{44414}][\text{Cl}] / \text{HCl} / \text{H}_2\text{O}$  AcABS mixtures forming an AcABS with a concentration of IL of 30 wt. % at  $24 \text{ }^\circ\text{C}$  (20, 25, 30 wt. % IL) and at  $50 \text{ }^\circ\text{C}$  (10, 15, 20, 25, 30 wt. % IL) according to the phase diagrams reported in **Figure IV.14**.

#### b. Measurements

Tubes were stirred in a rotator during two hours until complete dissolution of the IL and placed in a heating bath for 6 hours. Aliquots of the upper and lower phases were then taken and the concentration of metals determined with the help of an AAS apparatus. Please note that unlike the analysis reported previously in the case of the extraction of metal ions using ionic liquid, the concentrations of metal ions were measured in both phases. The mass conservation law was confirmed ( $\pm 5 \%$ ). All concentrations were determined after cooling down aliquots at  $24 \text{ }^\circ\text{C}$  when necessary.

The distribution coefficient (D) and the extraction yield (%E) were calculated as follows:

$$D = \frac{\frac{[\text{M}]_0 V_{\text{initial}}}{V_{\text{low}}} - [\text{M}]_{\text{low}}}{[\text{M}]_{\text{low}}} \times \frac{V_{\text{low}}}{V_{\text{up}}} \quad (54)$$

$$\%E = \frac{\frac{[\text{M}]_0 V_{\text{initial}}}{V_{\text{low}}} - [\text{M}]_{\text{low}}}{\frac{[\text{M}]_0 V_{\text{initial}}}{V_{\text{low}}}} \times 100 \quad (55)$$

$[\text{M}]_0$  is the concentration in  $\text{mol.L}^{-1}$  ( $25 \text{ }^\circ\text{C}$ ) of metal in mixtures A to E before extraction (i.e before addition of the IL).  $V_{\text{initial}}$  is the volume in ml of the mixture before extraction and addition of IL.  $[\text{M}]_{\text{low}}$  is the concentration in  $\text{mol.L}^{-1}$  of the metal ion in the lower phase after extraction.  $V_{\text{low}}$  and  $V_{\text{up}}$  are respectively the volumes at  $25 \text{ }^\circ\text{C}$ , expressed in mL, of the lower and upper phase after extraction.

The separation factor of cobalt(II) from nickel(II) was calculated as described by the following equation:

$$\beta_{Co}^{Up} = \frac{D_{Co}}{D_{Ni}} \quad (56)$$

In addition, the proportions of each metal ion in the upper ( $x_{Co}^{Up}$ ) and lower ( $x_{Ni}^{Low}$ ) phases were calculated as following:

$$x_{Co}^{Up} = \frac{[Co]^{up}}{[Ni]^{up} + [Co]^{up}} \quad (57)$$

$$x_{Ni}^{Low} = \frac{[Ni]^{low}}{[Ni]^{low} + [Co]^{low}} \quad (58)$$

With superscripts up and low standing for the upper and lower phases, respectively.

### c. Results and discussion

#### *Single extraction of TM found in NiMH batteries by AcABS*

The highly acidic aqueous solutions yielding biphasic systems in this study are representative of the solutions employed as leaching phases in industrial processes for the production/recycling of metals. We therefore present in this section results for the extraction and separation of leached metallic ions using AcABS. This represents a major advantage as no pH adjustment is required, with AcABS formation relying on the acidity of the leaching solution.

Extraction yields of cobalt(II), nickel(II), manganese(II) and iron(III) using [P<sub>44414</sub>][Cl] / HCl / H<sub>2</sub>O AcABS at 50°C are given in **Figure IV.19**.

The four metals studied follow very different trends. Iron(III) is always quantitatively extracted toward the IL-rich phase leading to an extraction yield over 98 % whatever the concentration of acid. This is not the case of nickel(II) that remains in the acid-rich phase after extraction until 25 wt. % of HCl (%E < 5 %). However, a small extraction can be noticed at 30 wt. % hydrochloric acid where approximately 10 molar percents of nickel are loaded to the top phase. Extraction yields of manganese are continuously increasing with the acidic concentration reaching a maximum of 40 % extraction at 30 wt. % of acid. Similarly, %E for Co(II) is increasing with [HCl] however this phenomenon occurs from 10 to 25 wt. % HCl where the extraction yield of cobalt reaches a maximum

of 93 wt. %. Increasing the concentration of acid to 30 wt. % leads to a decrease of the extraction yield of cobalt (%E = 85 %).

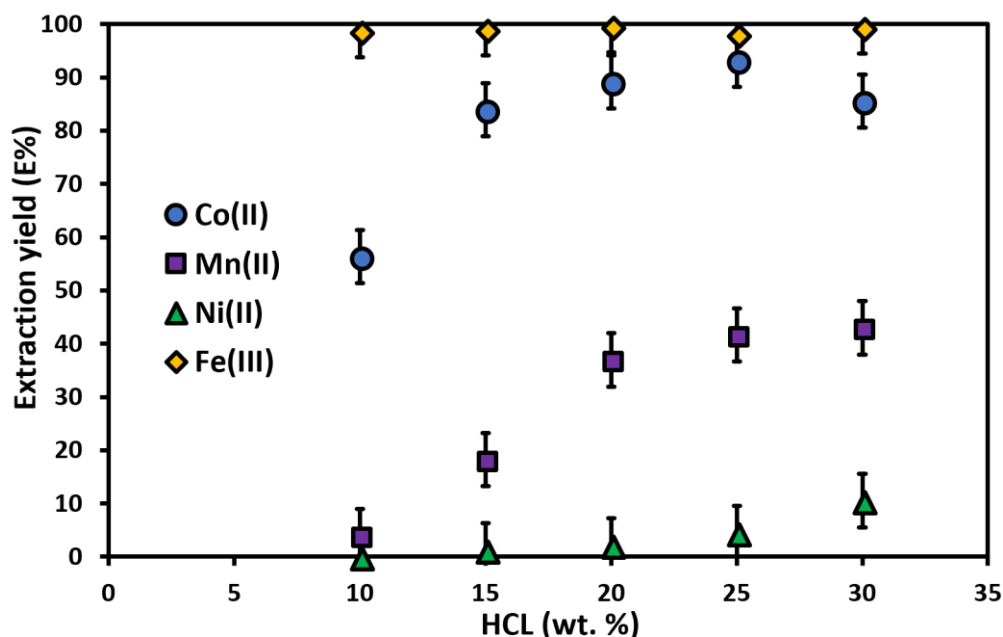
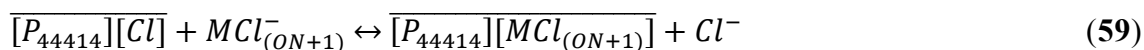


**Figure IV.19.** Extraction efficiency of single ion solution of 0.1 mol.L<sup>-1</sup> Co(II), Ni(II) or Mn(II) chloride in [P<sub>44414</sub>]Cl-HCl-H<sub>2</sub>O AcABS using 30 wt.% [P<sub>44414</sub>]Cl as a function of HCl concentration at 24 °C.

In order to get a better understanding of the mechanisms underlying the extraction of the metal ions studied here, we will briefly recall the insights gained for the extraction of various metals towards hydrophobic ionic liquids-based systems. Previous studies have shown that metal ions forming anionic complexes such as AuCl<sub>4</sub><sup>-</sup>, IrCl<sub>6</sub><sup>2-</sup>, PtCl<sub>6</sub><sup>2-</sup>, PdCl<sub>4</sub><sup>2-</sup>, RhCl<sub>6</sub><sup>3-</sup>, CoCl<sub>4</sub><sup>2-</sup> etc. are extracted efficiently using simple hydrophobic ionic liquids without any extracting agent.<sup>183,301,315</sup> In all these studies, the extraction mechanism is ascribed to the formation of a hydrophobic pair between the anionic metal complex and the cation of the ionic liquid. In addition, recent reports have demonstrated that because of the non-negligible solubility in water of ionic liquids, when the latter are used as the extracting phase, ion pair formation and anion exchange mechanisms actually describe the same mechanism.<sup>316</sup> On this basis, we suggest the following mechanism as described through the following equation.



Where species expressed under a bar means they are located in the organic phase. M stands for the metal and ON refers to its oxidation number.

Ni(II) exhibits a limited coordination with chloride anions, highlighted by the low complexation constant of  $\text{NiCl}^+$  ( $k_1^{\text{NiCl}^+} = 0.07$ ).<sup>24</sup> The inability of Ni(II) to form anionic chloro-complexes in water results in low extraction yields due to its inability to form an ion pair with the IL cation. The intermediate complexation constant of Mn(II) with  $\text{Cl}^-$  ( $k_1^{\text{MnCl}^+} = 0.33$ ) compared to Ni(II) and Co(II) ( $k_1^{\text{CoCl}^+} = 0.40$ )<sup>24</sup> is reflected in its extraction efficiency (**Figure IV.19**). Contrary to nickel, iron has one of the strongest ability to complex with chlorides among the transition metals ( $k_1^{\text{FeCl}^{2+}} = 1.96$ ), in other words, a large excess of chlorides vs Fe(III) is not needed to achieve a complete formation of  $\text{FeCl}_4^-$  and thus a quantitative extraction. In the case of Co(II), its speciation is known to change significantly depending on the ratio concentration of metal on concentration of chloride ions. For instance, at 24 °C, for a fixed amount of cobalt(II),  $\text{Co}(\text{H}_2\text{O})_6^{2+}$  is formed in pure water, while  $\text{CoCl}_3^-$  and  $\text{CoCl}_4^{2-}$  are found at high concentrations of HCl.<sup>236</sup> Indeed, the third and fourth complexation constants at 25°C are of 7.65 and 2.77 respectively.<sup>236</sup>

In all cases, extraction of Co(II) using this AcABS led to ionic liquid-rich phases exhibiting a blue color, as shown in **Figure IV.18**. This color and the corresponding absorption spectra are characteristic of negatively charged complexes such as  $\text{CoCl}_3^-$  or  $\text{CoCl}_4^{2-}$ . Previous reports studying the extraction of Co(II) using  $[\text{P}_{66614}][\text{Cl}]$  pointed out towards a predominant  $\text{CoCl}_4^{2-}$  species within the ionic liquid phase.<sup>184</sup> In our case, the presence of such tetrachlorocobaltate(II) complex is easily explained by the fact that all ionic liquid-rich phases contain a large amount of  $\text{Cl}^-$  originating from the HCl and the ionic liquid itself as confirmed by UV-Vis analysis of the IL phase after extraction (**ANNEX 2-E**).

#### *Separation of nickel from cobalt by AcABS*

As a proof of concept of the application of these new acidic ABS in the separation of metal ions, the competitive extraction of Co(II) and Ni(II), relevant to the recycling of NiMH batteries but also in natural ores, was studied at 24 and 50 °C.

Results for the study of the separation of Ni(II) from cobalt(II) are reported in **Table IV.5**.

	Co(II)			Ni(II)			$\beta_{Co}^{Up}$	$x_{Co}^{Up}$	$x_{Ni}^{Low}$
	HCl (wt.%)	% E	D	% E	D				
24 °C	20	87.7	14	<2.00	<0.05	280	0.98	0.89	
	25	93.7	19	<2.00	<0.05	380	0.98	0.94	
	30	87.1	13	8.4	0.09	144	0.91	0.88	
50 °C	10	56.7	3.2	<2.00	<0.05	64	0.97	0.69	
	15	71.8	9.9	<2.00	<0.05	198	0.97	0.78	
	20	88.5	17	<2.00	<0.05	340	0.98	0.89	
	25	97.7	21	<2.00	<0.05	420	0.98	0.98	
	30	88.8	17	11.3	0.14	121	0.89	0.89	

**Table IV.5.** Extraction yields (%E), distribution coefficients (D), separation factors ( $\beta_{Co}^{Up}$ ) and mole fractions of cobalt in the upper phase ( $x_{Co}^{Low}$ ) and of nickel in the lower phase ( $x_{Ni}^{Low}$ ) using [P<sub>44414</sub>][Cl] / HCl / H<sub>2</sub>O ([IL] = 30 wt. %) at 24 and 50 °C. Initial concentrations for all metals were 0.1 mol L<sup>-1</sup>.

The extraction yields for each metal are very similar to those obtained in the single extraction experiments. Ni(II) partitions preferentially to the lower phase, whereas Co(II) is extracted towards the upper phase. Values for the separation factor appear to differ significantly depending on the initial composition of the mixture and the temperature at which extraction is carried out. At all temperatures, the highest values for  $\beta_{Co}^{Up}$  are obtained with mixtures containing 25 wt. % HCl. This value corresponds to the optimal acidic concentration where cobalt is quantitatively extracted and nickel fully remains in the bottom phase.

At 50 °C, distribution ratios are systematically higher than those obtained at 24 °C. The highest value for cobalt is of 21 for the mixture at 25 wt. % HCl.

Values for  $x_{Co}^{up}$  and  $x_{Ni}^{Low}$  are also given in **Table IV.5**. IL-rich phases from mixture using 25 wt. % HCl at 24 and 50 °C exhibit the highest purity values for  $x_{Co}^{up}$  of 0.98 in both cases. The purity of Ni(II) in the corresponding HCl-rich phases is however higher for the mixture at 50 °C compared to the one at 24 °C.

From an application point of view, values for  $x_{Co}^{up}$  and  $x_{Ni}^{Low}$  reveal that both metal ions are quantitatively separated between the two phases, that is Co(II) in the upper and Ni(II) in the lower phase, using 30 wt. % [P<sub>44414</sub>][Cl], 25 wt. % HCl at 50 °C.

Nevertheless, such process will be considered as successful if the metal can be recovered after performing an extraction step. Relying on those results, electrochemical investigations will be carried out to perform electrowinning of cobalt directly in the IL-rich phase after extraction.

### IV.3.4 Recovery of cobalt by electrodeposition in ABS-AcABS

#### a. Experimental part

Electrochemical investigations including chronoamperometry and cyclic voltammetry (CV) were carried out using a Metrohm Autolab potentiostat controlled with the GPES software. A three-electrode system was used consisting of a glassy carbon (GC) working electrode (3 mm diameter), an iridium counter electrode and a silver chloride (Ag/AgCl) reference electrode. The working electrode was polished with diamond paste, rinsed and dried prior to all measurements.

All voltammograms of single 0.1 mol.L<sup>-1</sup> Co(II) aqueous solutions were obtained at 24 °C and at a scanning rate of 0.01 V.s<sup>-1</sup>, [P<sub>44414</sub>][Cl] concentration (from 0 to 20 wt.%) and HCl concentration (0 to 8 mol.L<sup>-1</sup>).

Chronometric deposition experiments were performed in the following three systems: ABS, AcABS and ABS-AcABS (with and without the addition of water). Compositions of all systems are depicted in **Table IV.6**. After extraction from a single metal solution containing 0.1 mol.L<sup>-1</sup> of CoCl<sub>2</sub>.6H<sub>2</sub>O or a mixed solution of 0.1 mol.L<sup>-1</sup> of CoCl<sub>2</sub>.6H<sub>2</sub>O, NiCl<sub>2</sub>.6H<sub>2</sub>O and MnCl<sub>2</sub>.4H<sub>2</sub>O, the IL-rich phase was isolated from the aqueous one. Extraction yields, in line with the previous part on metal extraction are shown in **Table IV.6**.

<b>Composition (wt. %)</b>	<b>AcABS</b>	<b>ABS</b>	<b>ABS-AcABS</b>
[P <sub>44414</sub> ][Cl]	30	30	30
HCl	25	0.0	3.7
NaCl	0.0	7.6	7.6
<b>Extraction yield (%)</b>	<b>AcABS</b>	<b>ABS</b>	<b>ABS-AcABS</b>
Co(II)	95.8	96.2	99.0
Mn(II)	39.8	40.7	43.2
Ni(II)	<2.00	<2.00	<2.00

**Table IV.6.** Composition of the ABS, AcABS and ABS-AcABS systems studied and their related extraction yields at 50 °C.

CV experiments were carried out under diffusion control in a potential range of -2.50 to 2.00 V *vs.* Ag/AgCl at a scan rate of a 0.01 V.s<sup>-1</sup>. Electrodeposition of metals was undertaken by chronoamperometry under diffusion control at a fixed potential of -2.00 V *vs.* Ag/AgCl during one hour. The three systems namely, AcABS, ABS and ABS-AcABS depicted in **Table IV.6** were studied.

A fourth system was considered to investigate the impact of the water content on the deposition. After isolating the phases from the system ABS-AcABS, the top phase was separated and diluted in a minimum of water (around 0.2 g of water per gram of IL-rich phase) until the solution colour transitioned from a deep blue to light red. This well-known colour change is due to the transition of blue chloride-complexes (CoCl<sub>4</sub><sup>2-</sup> or CoCl<sub>3</sub><sup>2-</sup>) to the formation of a red cobalt hexahydrate complex, Co<sup>2+</sup>(H<sub>2</sub>O)<sub>6</sub>.<sup>24</sup> This system is referred to as “ABS-AcABS-diluted” in this work.

Obtained deposits were analysed by SEM-Energy Dispersive Spectroscopy (SEM-EDS) and SEM-Secondary Electrons (SEM-SE) for single metal extractions. Metallic deposits obtained after selective deposition of cobalt in multielemental solutions were analysed through XRD. In the latter case, the metal was fully leached in 5 mL of 4 mol.L<sup>-1</sup> nitric acid (HNO<sub>3</sub>) in order to investigate (i) the purity of the metal and (ii) the Faradic efficiency of the electrodeposition ( $E_F$ ). The Faradic yield corresponds to the ratio between the experimental and theoretical conversion of Co(II) to Co(0) during electrodeposition.  $E_F$  was calculated according to the following equation:



$$E_F = \frac{C_{Co} \times V_{HNO_3}}{\frac{\int_0^t I(t) dt}{nF}} \times 100 \quad (60)$$

where  $C_{Co}$  represents the concentration of cobalt in  $\text{mol.L}^{-1}$  in the aqueous phase containing nitric acid, used to leach the deposits.  $V_{HNO_3}$  is the volume of the nitric acid solution in L.  $I$  (A) represents the current produced during chronoamperometry measurements for a given time  $t$  in seconds.  $F$  and  $n$  stand for the Faraday constant and the charge of the metal.

#### b. Results and discussion

##### *Electrochemical behaviour of Co(II) in ABS-AcABS systems*

Having demonstrated the separation of Co(II) from Ni(II) and Mn(II) in AcABS and ABS-AcABS (**part IV.3.3**) as well as the partitioning of the system components (**part IV.3.3**) relevant to the subsequent deposition of Co(II), the electrochemical behaviour of studied system is now investigated.

The influence of the hydrophilic IL  $[P_{44414}][Cl]$  in aqueous solutions on the reduction potential of Co(II) was investigated and the results are presented in **Figure IV.20**.

The presence of the IL in aqueous solution reduces the reduction of water to hydrogen kinetics (*cf.* **Figure IV.20-A**), in line with the wide electrochemical window of phosphonium-based ILs.<sup>102,317</sup> Co(II) is known to reduce to metallic cobalt at a potential of -0.28 V *vs.* NHE, this is to say, -0.50 V *vs.* Ag/AgCl.<sup>211</sup> In accordance with the literature, the CV of an aqueous  $0.1 \text{ mol.L}^{-1}$  Co(II) solution (**Figure IV.20-A**, dashed line) presents an inset reducing peak at -0.42 V and a minimum at -1.0 V *vs.* Ag/AgCl. A large oxidation peak is also observed from 0.42 to 0.59 V *vs.* Ag/AgCl, confirming that the process is reversible. The addition of increasing amounts of  $[P_{44414}][Cl]$  from 0 to 10 wt. % IL results in a decrease in the cathodic peak potential for cobalt ( $E_{Co}^{Red}$ ) from -0.42 to -1.06 V *vs.* Ag/AgCl. When the concentration of IL exceeds 10 wt.%, the reduction peak potential remains constant (*cf.* **Figure IV.20-B**).

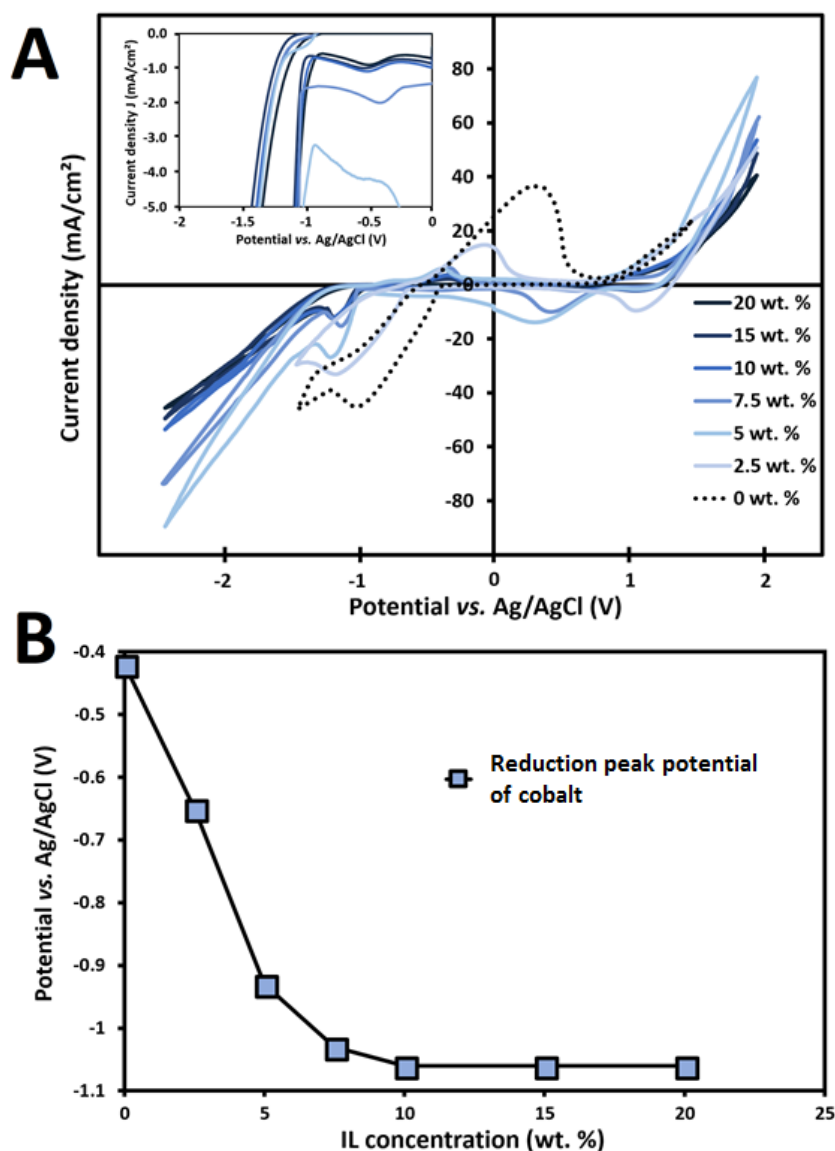


**Figure IV.20.** (A) CV experiments at a  $0.01 \text{ V}\cdot\text{s}^{-1}$  scan rate of various solutions containing  $0.1 \text{ mol}\cdot\text{L}^{-1}$  of Co(II) and concentration of  $[\text{P}_{44414}][\text{Cl}]$  ranging between 0 (black dotted line) and 20 wt. % (light to dark blue colours). (B) Evolution of the inset peak corresponding to the reduction of Co(II) to Co(0) as a function of the concentration of  $[\text{P}_{44414}][\text{Cl}]$ .

This shift in the reduction peak is a strong indication of a change in the complexation of Co(II) in the presence of the chloride anions from the IL. The anionic cobalt complexes  $\text{CoCl}_3^-$  and  $\text{CoCl}_4^{2-}$  are the predominant complexes reported in chloride based ILs.<sup>188,204,295,318</sup> Furthermore, whilst the  $\text{CoCl}_3^-$  was shown to be electrochemically active in ILs, the complex  $\text{CoCl}_4^{2-}$  was not.<sup>319</sup> This suggests that a high chloride concentration is inhibiting to the deposition of Co(0). However, in accordance with the Nernst law, complexation of chlorides is insufficient to explain such a shift in the reduction potential. The electrochemical

kinetic behaviour of nickel electrodeposition was previously studied in acidic aqueous phases and lead to the intermediate formation of Ni(OH) adsorbed species.<sup>320–322</sup> Similarly, cobalt is assumed to present the following reduction mechanism in water:



Elevated concentrations of ILs could inhibit the formation of the intermediate complex cobalt(I) hydroxide adsorbed species and therefore reduce the kinetic of reduction of Co. The intensity of all reduction peaks decreases with the increasing IL concentration. This can be linked to the higher viscosity and therefore lower kinetics of the IL-concentrated systems compared to the pure water system. Finally, an unveiled trend can be observed for mixtures containing 5 wt. % [P<sub>44414</sub>][Cl] or more with the emergence of a small reduction peak close to -0.5 V vs. Ag/AgCl (**Figure IV.20-A**, inset). This can be attributed to the reduction of Co(II) to Co(I). ILs provide a better environment for the stabilization of intermediate metal oxidation states compared to water. For example, the presence of water was shown to significantly affect the voltammetric behaviour of Co(II) in the ethylammonium nitrate IL and the oxidation of Co(II) to Co(III).<sup>323</sup>

CV analysis at a scan rate of 0.01 V.s<sup>-1</sup> and 24 °C on a GC working electrode was carried out in the four systems AcABS, ABS and ABS-AcABS (both undiluted and diluted) after extraction from 0.1 mol.L<sup>-1</sup> Co(II) solutions. The solution compositions of the studied systems are listed in **Table IV.6**. The CV scans are presented in **Figure IV.21**. Electrodeposition of Co(II) was performed during one hour on a GC electrode under agitation. The electrodes were qualitatively and semi-quantitatively analysed via SEM-SE and SEM-ESD respectively. The morphology and composition of the obtained deposits are presented in **Figure IV.22** and **Table IV.7** respectively.

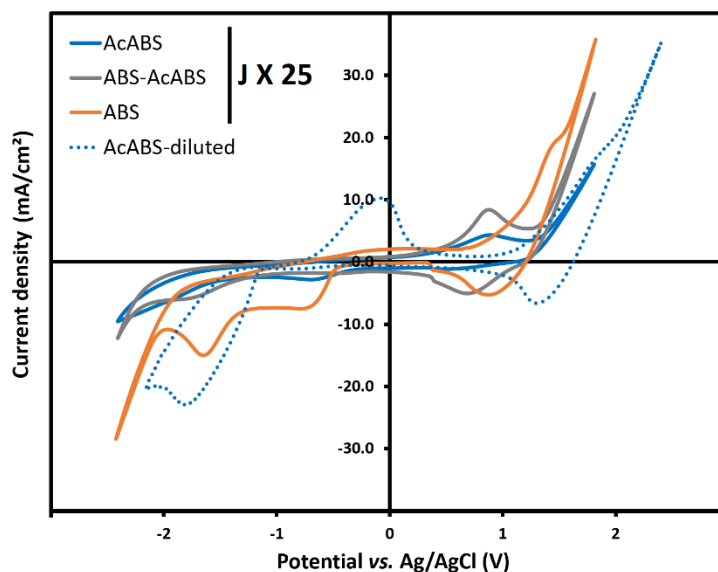


**Figure IV.21.** CV of various systems after extraction of cobalt in an aqueous solution containing  $0.1 \text{ mol.L}^{-1} \text{ Co(II)}$ . Scanning rate:  $0.01 \text{ V.s}^{-1}$ . Current densities (J) are multiplied by 25 for the ABS, AcABS and ABS-AcABS.

Starting with the ABS system, first reported by *Onghena et al.*<sup>204</sup> composed of  $[\text{P}_{44414}][\text{Cl}]-\text{NaCl}-\text{H}_2\text{O}$ , a reduction peak ( $\text{Co(II)}$  to  $\text{Co(0)}$ ) with an onset point at  $-1.07 \text{ V vs. Ag/AgCl}$  can be observed (**Figure IV.21**, orange line). This is in full agreement with our previous result showing that  $E_{\text{Co}}^{\text{Red}} = -1.06 \text{ V vs. Ag/AgCl}$  for systems containing 10 wt. % or more  $[\text{P}_{44414}][\text{Cl}]$ . After inducing a potential of  $-2.00 \text{ V vs. Ag/AgCl}$  to the solution, EDS analysis of the obtained deposit on the GC electrode surface indicates a high purity cobalt deposit of 98.9 at.% (**Table IV.7**).

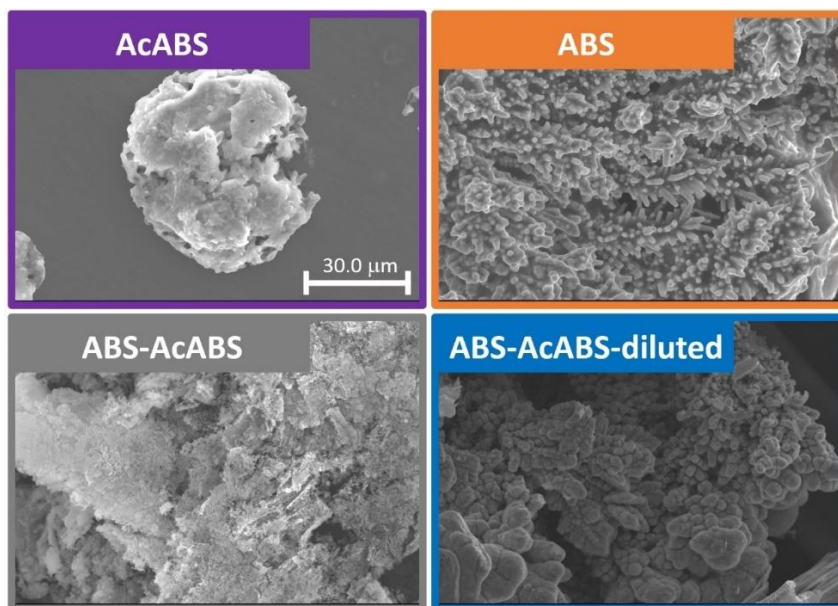


**Figure IV.22.** SEM-SE images (magnification  $\times 1000$ ) of working electrodes after 1 hour of electrodeposition at  $-2.00$  V vs. Ag/AgCl.

Systems	Elemental analysis (at.%)		
	Co	Cl	P
ABS	$98.9 \pm 12.3$	$1.1 \pm 0.5$	-
AcABS	$52.7 \pm 23.3$	$44.7 \pm 18.3$	$2.6 \pm 1.6$
ABS-AcABS	$92.6 \pm 12.5$	$6.9 \pm 6.3$	$0.5 \pm 0.1$
ABS-AcABS-diluted	$95.6 \pm 16.3$	$3.3 \pm 2$	$1.1 \pm 0.6$

**Table IV.7.** Elemental analysis of the electrodeposited deposits obtained in ABS, AcABS and ABS-AcABS (undiluted and diluted) systems after extraction from solution containing  $0.1 \text{ mol.L}^{-1}$  Co(II).

No significant quantities of chloride or phosphonium are recorded. The morphology of the obtained deposit is that of micrometer-scale dendrites, characteristic of metallic cobalt in aqueous solutions.<sup>44</sup>

Despite the lack of visible Co(0) reduction peak in the  $[\text{P}_{44414}]\text{Cl}/\text{HCl}/\text{H}_2\text{O}$  AcABS (**Figure IV.21**, full blue line), small particles were identified on the GC electrode after electrodeposition. This is a direct consequence of the large concentration of acid after extraction in the top phase ( $[\text{H}_3\text{O}]^+ = 3.0 \pm 0.26 \text{ mol.L}^{-1}$ ). In such an acidic environment, cobalt particles can be leached back in the aqueous solution after deposition. Two concomitant but opposing phenomena emerge: (i) the

reduction of Co(II) at the negative overpotential and (ii) the oxidation of Co(0) due to the HCl concentration. As a result, the particle seen in **Figure IV.22** and analysed in **Table IV.7** is composed of only 52.7 mol.% of cobalt and 44.7 mol.% of chloride, characteristic of an ongoing leaching phenomenon.

To avoid leaching during the electrodeposition step, a mixed ABS-AcABS system containing [P<sub>44414</sub>]Cl/NaCl/HCl/H<sub>2</sub>O is evaluated (composition provided in **Table IV.6**). This system was studied both in its undiluted and diluted form to establish the impact of water and therefore Co(II) complexation, on the quality of the Co(0) deposits. In the CV of undiluted ABS-AcABS,  $E^{\text{Red}}_{\text{Co}}$  appears at -1.12 V vs. Ag/AgCl (**Figure IV.21**, grey line), similar to that obtained in the ABS system. The composition of the obtained deposit is 92 at. % of cobalt and only 7 at. % chloride. This represents a significant increase in the deposit purity compared to that obtained in AcABS. The presence of Cl<sup>-</sup> is assigned to (i) the presence of residual [P<sub>44414</sub>]Cl in the final deposit and (ii) to the small leaching effect from the persistent presence of HCl ( $[\text{H}_3\text{O}]^+ = 0.35 \pm 0.04 \text{ mol.L}^{-1}$ ). SEM-SE analysis of the working electrode surface after deposition reveals its complete coverage by a large layer of deposit (*cf.* **Figure IV.22**). The deposit presents a sheet-like structure with no observable dendrites. This is probably due to the etching of the deposit surface by the remaining HCl after oxidation of Co(0) present in the dendritic structures of high surface area.

To gain a better understanding on the role of water in the studied system, the IL-rich phase (top phase) of the mixed system ABS-AcABS was isolated after extraction and diluted. The system was diluted through dropwise addition of water until a shift in the solution colour from blue to light red was observed. The addition of water enables the transition of Co(II) deposition from an IL environment to one where the IL is present as an additive in aqueous media. Performing the deposition of Co(II) in aqueous media compared to IL increases the kinetics of mass transport thereby raising the Faradic efficiency of the process. An additional positive effect of dilution on the Faradic efficiency is the change in Co(II) coordination from chlorocobalt complexes to Co(II) hexahydrate.

Dilution of the system results in an upshift in the onset of the reduction peak to -0.90 V vs. Ag/AgCl. The dilution influences the complexation of cobalt-chloride complexes, thereby increasing in accordance with Nernst's law. A deposit

composed of large dendrites was visually observed, further confirmed by SEM-SE (*cf.* **Figure IV.22**). Elemental analysis of the deposit highlights a quasi-pure material composed of 95.5 mol. % cobalt. In light of these results,  $[P_{44414}]Cl/NaCl/HCl/H_2O$  mixture stands out as promising medium for the recovery of metallic cobalt. The morphology and composition of the obtained deposits can be altered by varying the NaCl to HCl ratio and water content, resulting in highly tailored cobalt deposits. However, extraction results displayed in **Figure IV.19** and **Table IV.6** indicate that around 40 wt. % of Mn(II) can be co-extracted with Co(II). The question of the selectivity of such a process, starting from an aqueous solution containing a mixture of Co(II), Mn(II) and Ni(II) thus arises.

#### *Selective electrodeposition of Co(II) from Ni(II) and Mn(II)*

After extraction of a mixture of  $0.1 \text{ mol.L}^{-1}$  of Co(II), Ni(II), Mn(II) from ABS and ABS-AcABS systems (compositions provided in **Table IV.6**) chronoamperometry experiments at  $-2V$  vs Ag/AgCl were carried out to selectively reduce cobalt to its metallic state. Results are given in **Figure IV.23**.

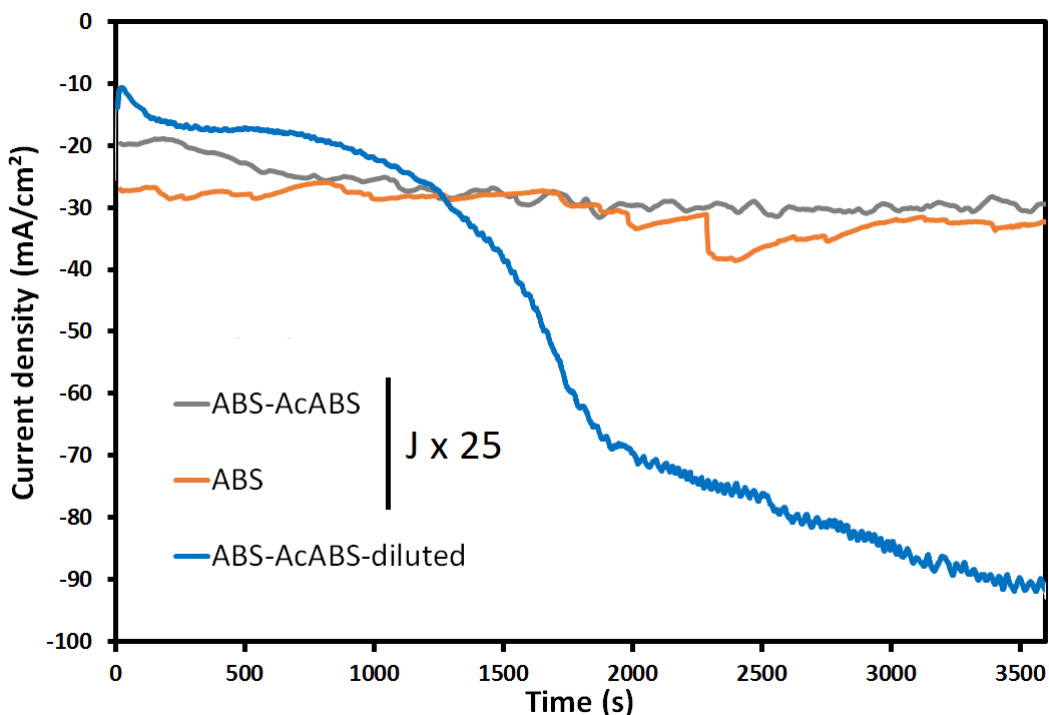


**Figure IV.23.** Chronoamperometry experiments using a potential of  $-2.00 V$  vs. Ag/AgCl for 1 hour. Current densities (J) are multiplied by 25 for ABS and ABS-AcABS systems.

Current densities for all experiments suffer from some oscillations as a result of hydrogen evolution from the reduction of water and/or of  $[H_3O]^+$ . This is visually confirmed during experiments by the formation of hydrogen bubbles at the interface between the solution and the GC working electrode. Hydrogen can partly cover the surface of the electrode, reduce its reactive area and thus the overall current density. The current density slowly decreases with time during deposition in all systems, characteristic of metallic deposition. The reduction of a conductive material such as cobalt can increase the surface area of the electrode and thus the current density in absolute value. This phenomenon is particularly pronounced in the ABS-AcABS-diluted system where the current density is multiplied by a factor of 8 in one hour. The lower viscosity and chloride complexation of this system are beneficial for an efficient deposition of metals. Quantitative compositional analysis of the deposits for the systems presented in **Figure IV.23** and their respective Faradic efficiencies are displayed in **Table IV.8**.

<b>Deposit Composition</b>	<b>Extraction Systems</b>		
	<b>ABS-AcABS</b>	<b>ABS</b>	<b>ABS-AcABS-diluted</b>
<b>Co (mg)</b>	$0.30 \pm 5 \times 10^{-3}$	$0.29 \pm 5 \times 10^{-3}$	$7.2 \pm 0.1$
<b>Mn (mg)</b>	$< 5 \times 10^{-3}$	$< 5 \times 10^{-3}$	$< 5 \times 10^{-3}$
<b>Ni (mg)</b>	$< 5 \times 10^{-3}$	$< 5 \times 10^{-3}$	$< 5 \times 10^{-3}$
<b>E<sub>F</sub> (%)</b>	28.9	31.6	59.7
<b>Co electroplated (mol. %)</b>	0.91	0.82	2.51

**Table IV.8.** ICP analysis performed for ABS, ABS-AcABS and ABS-AcABS diluted systems. The composition of deposits and Faraday efficiencies ( $E_F$ ) are given for all systems.



For all studied systems, no trace of manganese and nickel were recorded, confirming that solely cobalt is reduced as a metallic species. This is to be expected as Ni(II) is not extracted to the IL-rich phase (*cf.* **Table IV.6**), and Mn(II) presents a reduction potential of  $-1.41\text{ V vs. Ag/AgCl}$ , lower than that of Co(II) ( $-0.5\text{ V vs. Ag/AgCl}$ ).<sup>211</sup> In addition, Mn(II) is also likely to form complexes with chloride anions present in the system, thereby further shifting its reduction potential to lower values and avoiding any co-deposition of Mn(II) with Co(II).

The efficiency of Co(II) reduction is low in the undiluted ABS and ABS-AcABS systems with a final deposit mass of 0.30 mg and 0.29 mg respectively. Faradic efficiencies indicate that around 30 % of the electrons generated by the potentiostat are used for the reduction of Co(II) to metallic Co(0) in these systems. Inducing a potential of  $-2.00\text{ V vs. Ag/AgCl}$  results in an important reduction of water and/or proton to hydrogen. The low energetic yields hinder the industrial application for such processes.

Deposition yields are significantly improved after dilution, with close to twenty fourfold increase in the deposit mass to 7.2 mg in the system ABS-AcABS-diluted. This results in a twofold increase in the Faradic efficiency to a value of 59.7 %. The faradic yields reported here are reasonably satisfying and were obtained without any optimization of the electrochemical process. At  $-2\text{ V vs. Ag/AgCl}$ , water or  $[\text{H}_3\text{O}]^+$  present in the medium are expected to be reduced significantly. Carrying out the experiments at a more positive potential would most probably lead to better yields due to a less pronounced reduction of water or  $[\text{H}_3\text{O}]^+$ . Experiments carried out at  $-1.5\text{ V vs. Ag/AgCl}$  revealed that deposition of Co(II) was possible, whereas assigning a potential of  $-1\text{ V vs. Ag/AgCl}$  at the GC electrode did not yield any reduction of Co(II). It is worth highlighting that the electric charge is of 0.3 and 14 A.s for the undiluted and diluted ABS-AcABS systems respectively. As a result, even if the Faradic yield is twice higher with the ABS-AcABS-diluted, more electrons will be devoted to the reduction of water in the latter system. However, the cobalt deposition kinetics is more than 24 times faster in the diluted systems which significantly improves results obtained compared to pure ILs. After 1 hour of chronoamperometric measurements, only 2.5 mol. % of cobalt ions were reduced. This proves that the bath did not suffer from any significant concentration depletion. Larger

surface electrodes are required to recover the metal in an acceptable length of time.

The crystalline structure of the deposits obtained at the end of the chronoamperometry experiments were analysed by XRD analysis with the spectra depicted in **Figure IV.24**.

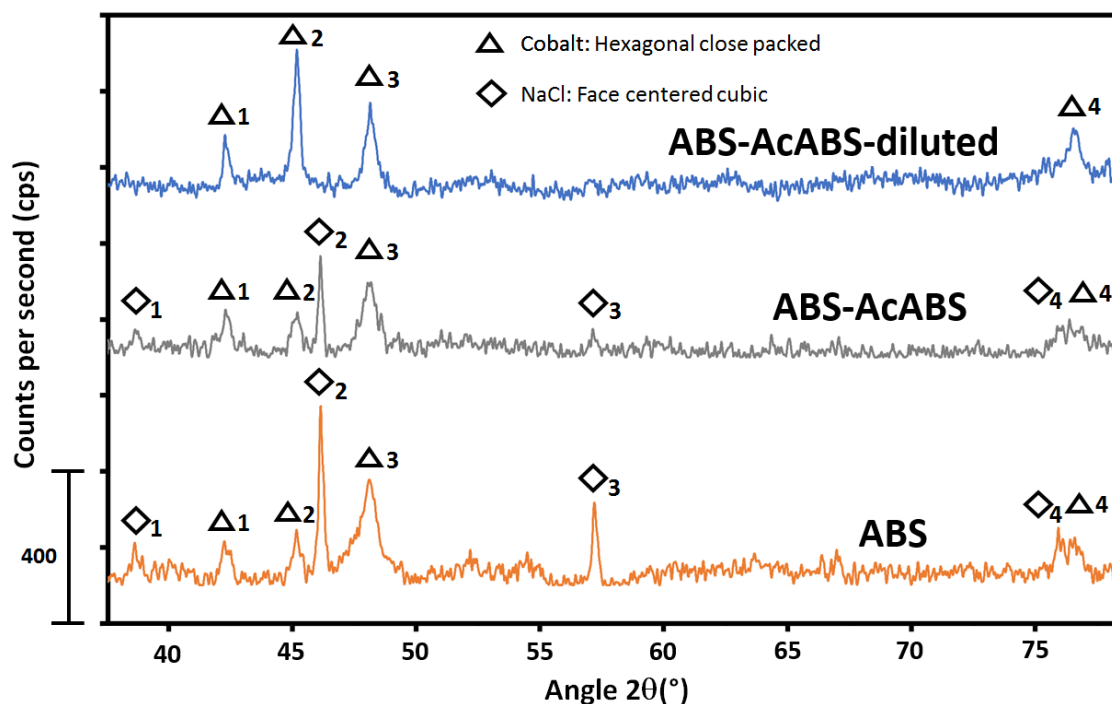


**Figure IV.24.** XRD diffractograms of deposits obtained after extraction of metals from a mixed solution containing  $0.1 \text{ mol.L}^{-1}$  Co(II), Ni(II) and Mn(II) and electrodeposition at a potential of  $-2.00 \text{ V}$  vs. Ag/AgCl during 1 hour.

NaCl crystals are highlighted in the ABS-AcABS and ABS systems. This is not surprising as these two solutions contain an important initial NaCl concentration (7.6 wt.%) to induce the formation of two phases. Near the electrode, the deposition of cobalt in ABS-AcABS and ABS systems will most likely release chloride anions from the metallic complexes and locally saturate the solution in NaCl inducing the crystallisation of the latter salt. All deposits are composed of metallic cobalt crystallized in a hexagonal close packed lattice. However, there are differences in the crystallization of cobalt in the ABS and ABS-AcABS compared to the ABS-AcABS-diluted system. Focusing on the cobalt metallic peaks 2 ( $p_2$ ) and 3 ( $p_3$ ) at  $44.6$  and  $47.5^\circ$

respectively, the ratio  $p_2 / p_3$  differs from one system to another. These two peaks correspond to the crystal orientation (111) and (101) respectively of metallic cobalt.<sup>324</sup> Concerning the ABS-AcABS-diluted system,  $p_2$  presents a higher intensity than  $p_3$  resulting in a ratio of 1.51. The opposite phenomenon is reported for ABS-AcABS and ABS systems leading to a ratio of 0.51 and 0.47 respectively. This phenomenon highlights a preferential (101) crystalline orientation of metals electrodeposited in concentrated IL solutions compared to diluted IL solutions. Such changes in the crystalline nature of deposits due to the presence of IL was previously reported for the deposition of copper in the presence of  $[C_4mim][HSO_4]$  as additive.<sup>325</sup>

The versatility of IL-based ABS and AcABS was recently highlighted for its application in metal extraction<sup>168,203,204</sup> but it is here shown that it can be extended to the electrodeposition of metals. The hydrophilicity of the extracting solution allows to tune and enhance the efficiency of the recovery of pure cobalt and to modify the properties of the resulting deposits.

### IV.3.5 Conclusion

A new family of extracting systems based on a water-soluble ionic liquid and an inorganic acid is presented, namely AcABS. These systems form two immiscible phases in presence of concentrations of acid, salt or both resulting in a AcABS, ABS or mixed ABS-AcABS. Regarding  $[P_{44414}][Cl] / HCl / H_2O$  system, the latter phenomenon occurs above a given threshold that increases with decreasing temperature (5 wt. % HCl at 56 °C and 20 wt. % HCl at 24 °C). The lower phase is largely depleted in ionic liquid, while the upper phase contains most of the ionic liquid, as well as some acid/salt and water. A LCST-type behaviour was observed for these systems with two mutually immiscible phases being formed by heating monophasic aqueous solutions containing  $[P_{44414}][Cl]$  and HCl or NaCl.

The results obtained are a proof of concept of the successful application of these new AcABS to metal ion extraction processes. These systems display several advantages over other extracting solvents. Unlike classical systems based on an organic solvent and an extracting agent,  $[P_{44414}][Cl]/HCl/H_2O$  exhibits a thermotropic behaviour. This allows the mixing of the compounds to be done in a homogeneous phase at a given temperature, while phase separation occurs by

simply heating up the solution, avoiding kinetic limitations related to the mass transport between two-immiscible systems. Moreover, this type of system does not require fluorinated anions as it is the case for most hydrophobic ionic liquids. This represents a significant benefit both from environmental and economic points of view. By varying the HCl concentration and the chloride source (either NaCl or HCl), selective separation of Co(II) from Ni(II) was achieved whilst controlling the partition of the various system constituents. The distribution of HCl was found to have a profound influence on the subsequent electrodeposition of Co(II). To address this, a mixed ABS-AcABS extraction system was proposed which combines the advantages of the AcABS and ABS systems. By varying the water content of the [P<sub>44414</sub>]Cl-rich phase after extraction and separation of Co(II) from Ni(II), high quality dendritic deposits of pure metallic cobalt were obtained in presence of Mn(II) impurities. Furthermore, ABS-AcABS systems can be tailored to obtain metal deposits with varied properties. The results presented in this work demonstrate the applicability of AcABS for a ‘one-pot’ approach for the sequential leaching, solvent extraction and electrodeposition of metals.

## IV.4 Separation of transition metals from spent NiMH batteries

---

### IV.4.1 Introduction

In **Chapter II**, a quantitative separation of rare earth elements from transition metals is reported. A REE sodium sulphate precipitate is obtained while all transition metals remain in an aqueous solution. The latter solution is composed of 91 mg Fe, 378 mg Ni, 94 mg Co and 12 mg Mn in 100 mL of aqueous solution containing sulfuric acid (pH = 1.7) after treatment of 1 g of black mass. Even if the sulphate media was identified as an optimal solution, some leaching experiments using hydrochloric acid and/or [P<sub>44414</sub>][Cl] were also conducted in **Chapter II**, leading to an aqueous solution containing in some specific conditions similar amounts of transition metals. Nevertheless, this leachate is mixed with La, Nd, Ce and Pr as no selective precipitation can be conducted in hydrochloric media.

Starting from both leachates solution using H<sub>2</sub>SO<sub>4</sub> or HCl obtained in **Chapter II** and based on the previous extraction results using AcABS in **Chapter IV**, this part will be devoted to the separation of transition metals from spent NiMH batteries.

### IV.4.2 Inducing an AcABS from leachate solutions: A versatile process

#### a. Experimental part

##### *Biphasic formation from various leachates*

Starting from leachates obtained at 6, 8 and 10 mol.L<sup>-1</sup> HCl (practical details, leaching yields and leachate compositions are detailed in **part II.3.2, Figure II.15**), 5 g of [P<sub>44414</sub>][Cl] were added to 10 mL of aqueous solution. A biphasic system was formed at 50 °C. After 3 hours of demixing, the aqueous phase was analysed by ICP to determine the extraction yield of all metals.

A similar procedure was applied to the leachate at  $2 \text{ mol.L}^{-1} \text{ H}_2\text{SO}_4$  after precipitation of rare earth elements at pH 1.7. Various amounts of NaCl (1, 2 and  $3 \text{ mol.L}^{-1}$ ) were added to the aqueous solution in order to (i) induce a biphasic system and (ii) form cobalt complexes with chlorides to enhance metallic extraction.

More information regarding this solution is provided in **Chapter II**, leaching yields and leachate composition are given in **part II.3.2 / Figure II.15** while precipitation data and metal compositions are shown in **part II.3.3 / Table II.10**.

For clarity reasons, the composition in metals of leachate using  $8 \text{ mol.L}^{-1} \text{ HCl}$  and  $2 \text{ mol.L}^{-1} \text{ H}_2\text{SO}_4$  after precipitation of rare earth elements at pH 1.7 are given in the following table.

<b>Elements</b>	<b>HCl 8 M pH &lt; 1</b> (mg of BM in 25 mL)	<b>H<sub>2</sub>SO<sub>4</sub> 2 M pH 1.7</b> (mg of BM in 100 mL)
<b>Fe</b>	$85.0 \pm 1.2$	$88.2 \pm 1.2$
<b>Ni</b>	$352.4 \pm 1.2$	$371.8 \pm 1.2$
<b>Co</b>	$51.7 \pm 1.2$	$93.4 \pm 1.2$
<b>Mn</b>	$13.7 \pm 1.2$	$11.2 \pm 1.2$
<b>La</b>	$19.4 \pm 0.3$	< 0.3
<b>Ce</b>	$14.8 \pm 0.3$	< 0.3
<b>Nd</b>	$5.3 \pm 0.3$	< 0.3
<b>Pr</b>	$1.6 \pm 0.3$	< 0.3

**Table IV.9.** Reminder of aqueous solutions compositions after leaching using  $8 \text{ mol.L}^{-1} \text{ HCl}$  and leaching using  $\text{H}_2\text{SO}_4$  followed by a precipitation step at a pH of 1.7. Data are given for the treatment of 1 g of black mass.

Extraction systems previously detailed using  $[\text{P}_{44414}][\text{Cl}]$ , acid and sometimes NaCl are depicted in **Table IV.10**.

	[Acid] <sub>i</sub> (mol.L <sup>-1</sup> )	V aq (mL)	m [P <sub>44414</sub> ][Cl] (g)	[P <sub>44414</sub> ][Cl] (wt. %)	[Acid] (wt.%)	
HCl	6	10	5	31.25	7.2	
	8	10	5	30.67	17.1	
	10	10	5	30.12	21.5	
	[NaCl] <sub>i</sub> (mol.L <sup>-1</sup> )	V aq (mL)	m [P <sub>44414</sub> ][Cl] (g)	[P <sub>44414</sub> ][Cl] (wt. %)	[Acid] (wt.%)	[NaCl] (wt. %)
H <sub>2</sub> SO <sub>4</sub> 2 M	1	10	5	29.79	7.3	3.5
	2	10	5	28.79	7.1	6.7
	3	10	5	27.85	6.9	9.8

**Table IV.10.** AcABS and ABS-AcABS systems formed using [P<sub>44414</sub>][Cl] / HCl / H<sub>2</sub>O and [P<sub>44414</sub>][Cl] / H<sub>2</sub>SO<sub>4</sub> / NaCl / H<sub>2</sub>O systems respectively.

*Flow sheet for the separation of Co / Fe / Ni / Mn*

Using the leachate at 2 mol.L<sup>-1</sup> H<sub>2</sub>SO<sub>4</sub> after precipitation of rare earth elements at pH 1.7, an extraction step, (denoted as extraction 1) using 27.8, 6.9 and 9.8 wt. % IL, acid and sodium chloride respectively was performed. After 3 hours of demixion, the top IL-rich phase was isolated from the bottom acid-rich phase. (i) In the IL-rich phase 1 mL H<sub>2</sub>SO<sub>4</sub> 4 mol.L<sup>-1</sup> per 3 mL of IL-rich phase at 25 °C was added. A biphasic system was observed, this step will be denoted as extraction 2. (ii) In the acid-rich 1 phase, electrowinning of nickel was performed using chronoamperometry techniques at – 0.5 V vs. Ag/AgCl during 2 min 30 seconds. A three-electrode system was used consisting of a copper rotating working electrode (3 mm diameter), a platinum counter electrode and a silver chloride (Ag/AgCl) reference electrode. The rotating speed of the WE was set to 2000 rpm.

Both phases before and after extraction 1 and 2 were analysed by AAS. Images and semi quantification of the metallic deposit are provided thanks to SEM and EDS analysis respectively.

The previous *modus operandi* can be summarized by the following flowsheet in **Figure IV.27**.

b. Results and discussion:*Leachate using HCl*

According to results provided in **Chapter II**, NiMH spent batteries can be treated by hydrochloric acid leading to a leaching yield close to 90 wt. % using 8 mol.L<sup>-1</sup> HCl. A hydrophilic ionic liquid, namely [P<sub>44414</sub>][Cl] can straightforwardly be added to the leachate to induce in some particular conditions a biphasic system simultaneously oxidizing and extracting metals. Extraction yields for leachates using 6, 8 and 10 mol.L<sup>-1</sup> are reported in **Figure IV.25** for all transition metals. REE are not represented as the extraction yield of all lanthanides studied was under 0.05 %.

In full accordance with the results obtained previously for the [P<sub>44414</sub>][Cl] / HCl / H<sub>2</sub>O system, iron is quantitatively extracted whatever the concentration of hydrochloric acid due to its high complexation constant.<sup>236</sup> Less than 43 % of cobalt is extracted at 6 mol.L<sup>-1</sup> (7.2 wt. % acid). Similarly to what was observed in **part IV.3.3** of this chapter, Co(II) can be fully extracted (98.6 %) when the HCl concentration is 21 wt. % (10 mol.L<sup>-1</sup>). Not surprisingly nickel is never loaded to the IL-rich phase in those conditions. Manganese is partly extracted in this HCl range with a %E increasing with the acidic concentration reaching a value of 40 % at 10 mol.L<sup>-1</sup>. In the latter conditions, cobalt and iron can thus be isolated from nickel, lanthanum, neodymium and praseodymium. Both phases will be however containing manganese.

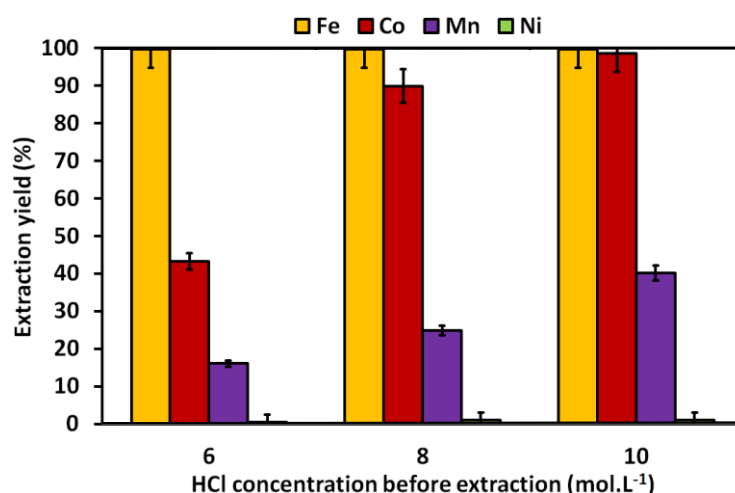


**Figure IV.25.** Extraction yields of iron, cobalt, manganese and nickel for leachates using 6, 8 and 10 mol.L<sup>-1</sup> HCl after addition of approximately 30 wt. % of [P<sub>44414</sub>][Cl] at 50 °C.



*Leachate using H<sub>2</sub>SO<sub>4</sub>*

Sulfuric acid was identified in this work as the most suitable acid to perform a leaching step as (i) it is less corrosive and explosive than hydrochloric and nitric acid respectively (ii) it allows the recycler to perform a precipitation step by increasing the pH which selectively isolates transition metals from REE. In order to separate the four remaining TM, [P<sub>44414</sub>][Cl] and NaCl can be added to the system forming a mixed ABS-AcABS. Extraction yields of iron, nickel, cobalt and manganese are reported in **Figure IV.26** function of the initial concentration of sodium chloride in the aqueous solution.

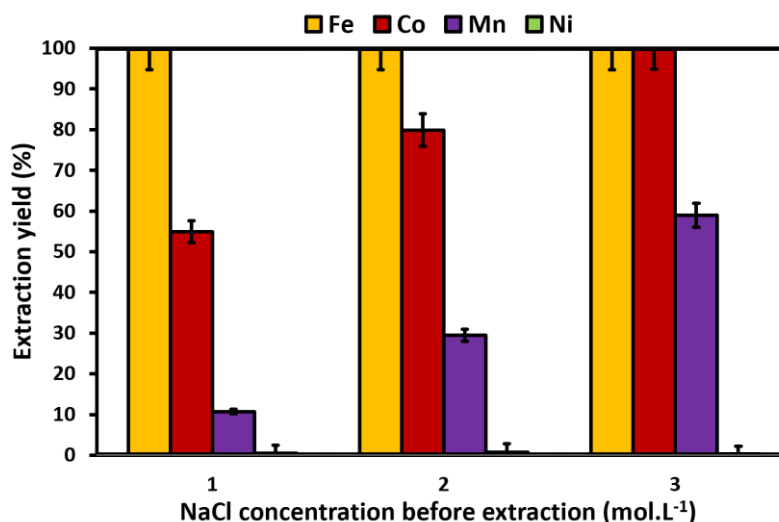


**Figure IV.26.** Extraction yields of iron, cobalt, manganese and nickel for leachates using 2 mol.L<sup>-1</sup> H<sub>2</sub>SO<sub>4</sub> after a precipitation step at pH 1.7. 1, 2 or 3 mol.L<sup>-1</sup> NaCl was added to the solution before extraction with approximately 30 wt. % of [P<sub>44414</sub>][Cl] at 50 °C.

While iron(III) is again fully loaded to the IL-rich phase, and nickel is never extracted, cobalt and nickel show increasing extraction yields with the NaCl concentration. Interestingly, when the ABS-AcABS presents low concentrations of chlorides, namely 3.5, 6.7 and 9.8 wt. % NaCl, extraction yields remain high leading to values of 54.9, 79.9 and 99.8 wt. %. It is worth noticing that cobalt is more diluted in this solution than in the HCl leachate. Co(II) concentration range from 944 to 2068 ppm respectively because of the additional precipitation step. Diluting the metal will thus allow the ratio [Cl<sup>-</sup>]/[Co(II)] to be higher and enhance the formation of CoCl<sub>3</sub><sup>-</sup> complexes. Inducing an ABS-AcABS using 3 mol.L<sup>-1</sup> NaCl in the aqueous phase, leads to a mixture composed of 27.9 wt. % [P<sub>44414</sub>][Cl], 6.9 wt. % H<sub>2</sub>SO<sub>4</sub> and 9.8 wt. % NaCl is an interesting option in the process of

separation of transition metals from spent NiMH batteries as two metals, iron and cobalt are fully separated from nickel even if manganese is distributed in both phases. The latter statement is reinforced by the fact that cobalt and nickel are often mixed together in alloys<sup>43</sup> and ores<sup>44</sup> and are challenging to separate one from another because of similar chemical properties.<sup>42,188,204</sup> Starting from the latter extraction system, a flow sheet is proposed to reach an efficient separation of those four transition metals.

*Flow sheet for the separation of TM from spent NiMH batteries*

The flow sheet for the separation of cobalt, iron, nickel and manganese by ABS-AcABS is proposed in **Figure IV.27**. Composition of each phases after extraction is given in **Table IV.11**.

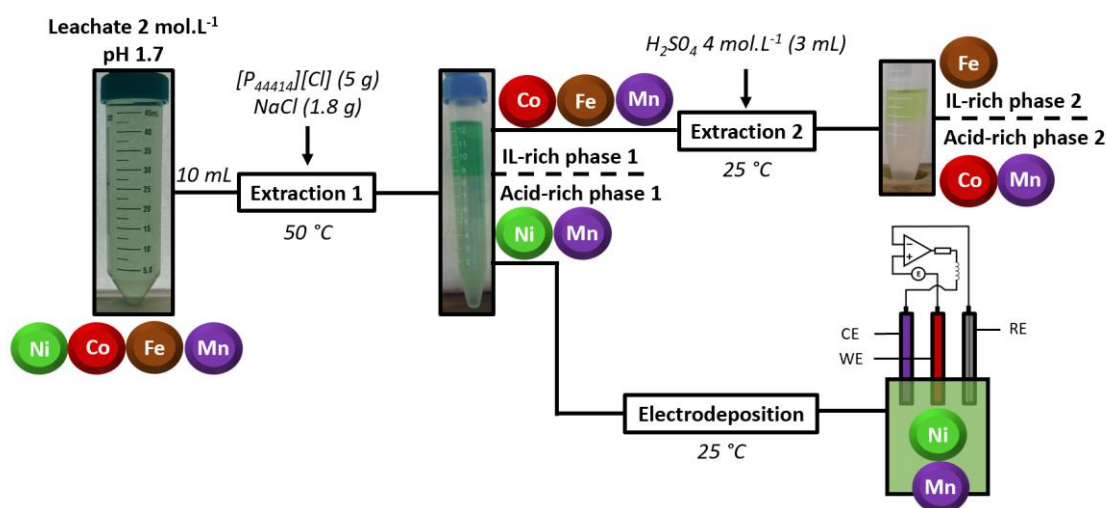


**Figure IV.27.** Flow sheet for the separation of transition metals from spent NiMH batteries by ABS-AcABS.

	Metal concentration (mg.g <sup>-1</sup> ) of BM				
	Initial solution	extraction 1		extraction 2	
		IL-rich phase 1	Acid-rich phase 1	IL-rich phase 2	Acid-rich phase 2
Fe	88.2	88.3 ± 0.5	< 0.5	87.1 ± 0.5	< 0.5
Co	93.4	92.5 ± 0.5	< 0.5	9.2 ± 0.5	83.7 ± 0.5
Mn	11.2	6.5 ± 0.5	4.6 ± 0.5	< 0.5	3.7 ± 0.5
Ni	371.8	< 0.5	370.1 ± 5.0	< 0.5	< 0.5

**Table IV.11.** Concentration of Fe, Co, Mn and Ni in both IL and Acid-rich phases during extraction 1 and 2 by ABS-AcABS.

Extraction 1 is carried out with an AcABS [P<sub>44414</sub>][Cl] / H<sub>2</sub>SO<sub>4</sub> / NaCl / H<sub>2</sub>O system at 50 °C. Such an AcABS is formed due to the salting out effect of sulfuric acid and sodium chloride shown in **part IV.3.2** of this chapter. The bottom phase is green because of the presence of nickel, not extracted at all in the IL-rich phase. The top, ionic liquid-rich phase also exhibits a green color due to the co-extraction of yellow FeCl<sup>4-</sup> and blue CoCl<sup>3-</sup> / CoCl<sup>4-</sup> complexes (*cf.* **Figure IV.27**). This is confirmed by results in **Table IV.11** showing that cobalt and iron are quantitatively separated from nickel and are present in the IL-rich phase. The latter phase can be isolated from the bottom one and after addition of sulfuric acid (4 mol.L<sup>-1</sup>). In that case, another biphasic solution is induced, so-called extraction 2. This is not a surprising result as we previously bring the proof (see **part IV.3.2**) that 2 mol.kg<sup>-1</sup> of H<sub>2</sub>SO<sub>4</sub> is enough to induce an AcABS for low concentrations of [P<sub>44414</sub>][Cl] (under 0.05 mol.kg<sup>-1</sup>). The resulting biphasic solution presented in **Figure IV.27** is composed of a yellow top phase and a red bottom one. Information gathered in **Table IV.11** reports that Fe(III) is fully extracted towards the IL-rich phase compared to only 10 %. The bottom phase is thus composed of 83.7 and 3.7 mg per gram of black mass with concentrations of iron and nickel beyond the detection limits. This separation of iron from cobalt derives from the poor chloride content of the mixture during extraction 2, unable to fully extract cobalt but presenting a sufficient Fe(III)/Cl<sup>-</sup> ratio to quantitatively complex iron in FeCl<sup>4-</sup> and extract it by an ion exchange mechanism towards the IL rich phase. Cobalt can thus be reduced from an aqueous solution containing manganese according to the process developed in **part IV.3.3** in order to recover a pure Co(0).

Similarly, acid rich phase 1 containing solely nickel (98.7 wt. %) and manganese (1.23 wt. %) can be treated in order to recover pure nickel. The deposition of pure nickel or Ni/Mn alloys in an aqueous solution has been widely performed in the literature<sup>275,326–328</sup> and is not a major challenge in this process as their reduction potential are separated by 0.935 V. ( $E^0 \text{Ni}^{2+} = -0.47 \text{ V vs. Ag/AgCl}$  ;  $E^0 \text{Mn}^{2+} = -1.185 \text{ V vs. Ag/AgCl}$ ).<sup>211</sup> Chronoamperometry curve observed after applying -0.5 V vs. Ag/AgCl during 160 seconds is reported in **Figure IV.28**.

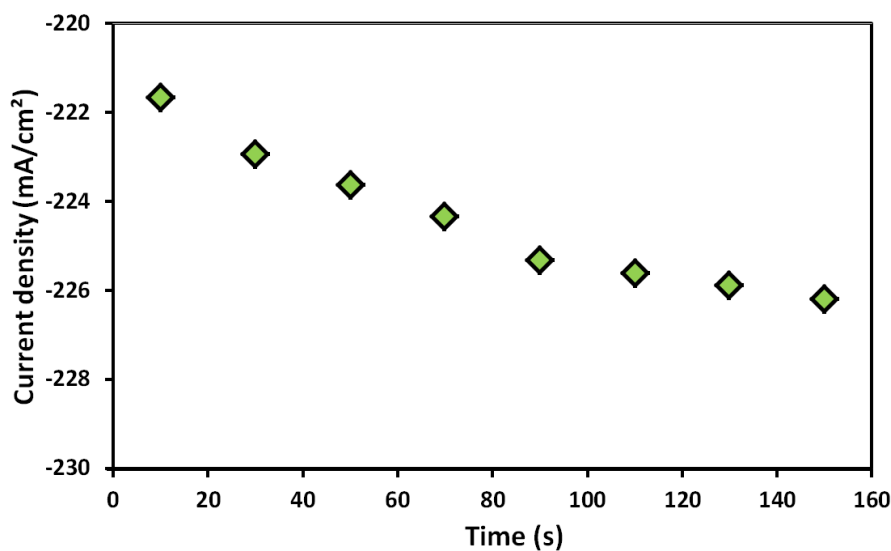


**Figure IV.28.** Chronoamperometry measurements, the potential applied is of -0.5 V vs. Ag/AgCl during 160 seconds in the IL-rich phase.

The low current densities observed during chronoamperometry measurements justify the short times needed to induce the reduction of nickel. It is worth noticing that, thanks to the precipitation step, carried out previously, the pH has been increased to a value of 1.7. This hinders the reduction of proton leading to a more favorable electrodeposition of Ni. Furthermore, sodium chloride, used as a salting out agent brings  $\text{Cl}^-$  ions to the bath, increasing the conductivity of the aqueous media. For this reason,  $10 \text{ g.L}^{-1}$  of NaCl are added to the *WATTS* bath used for industrial nickel electroplating.<sup>329</sup> It is worth noticing that  $\text{H}_3\text{BO}_3$  can be used as a pH buffer in the range 1.5 – 2.5.<sup>329</sup> Because the pH of our solution was of 1.7, boric acid wasn't necessary in this case.

After 160 seconds of chronoamperometric measurements at -0.5 V vs. Ag/AgCl, the copper electrode was analysed by SEM, SE and EDS, results are shown in **Figure IV.29** and **Table IV.12**.

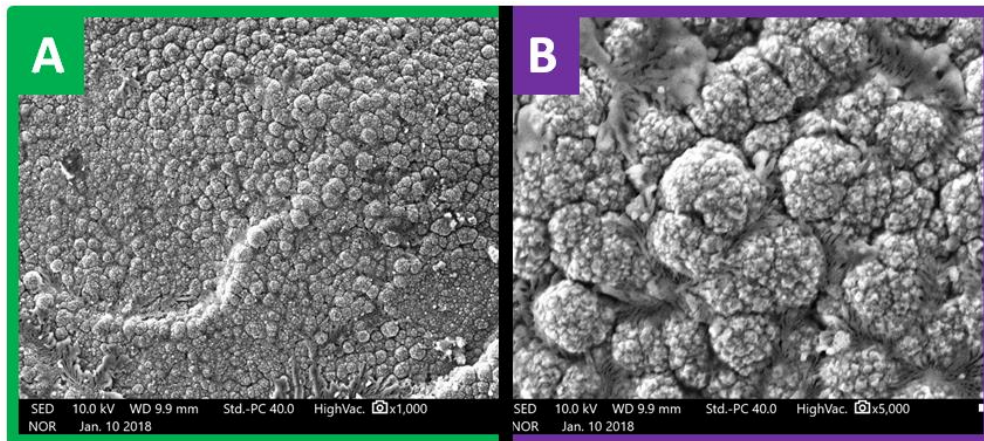


**Figure IV.29.** SEM analysis of the deposit obtained on a copper electrode after electroplating nickel at  $-0.5$  V vs. Ag/AgCl during 160 sec A: SE image (magnification  $\times 1000$ ). B: SE image (magnification  $\times 5000$ ).

Elements	Composition (atom. %)
Ni	$99.2 \pm 0.2$
Mn	$0.2 \pm 0.1$
Co	-
Fe	-
REE	-

**Table IV.12.** Elemental analysis of the deposit obtained on a copper electrode after electroplating nickel at  $-0.5$  V vs. Ag/AgCl during 160 sec. Transition metals, except from copper are considered.

According to SEM analysis, the copper electrode is completely recovered with nickel after 2 min 30 sec electroplating. A fine-grained structure is observed, characteristic of metallic nickel.<sup>326,328</sup> The metal obtained is composed of a ratio Ni:Mn of 99.2:0.2 which can be considered as a satisfying purity for Ni recovered from a recycling process using spent NiMH batteries.

#### IV.4.3 Conclusion

Starting from a solution of transition metals obtained from spent NiMH batteries, and relying on the results obtained on the separation of nickel, cobalt and manganese by AcABS, a flow sheet is proposed to recover pure strategic transition metals.

A biphasic solution can be induced by leaching a spent NiMH battery by hydrochloric or sulfuric acid. [P<sub>44414</sub>][Cl] can straightforwardly be mixed to the leachate using 2 mol.L<sup>-1</sup> H<sub>2</sub>SO<sub>4</sub> at pH 1.7 after addition of 3 mol.L<sup>-1</sup> NaCl. Sodium chloride will both act as a salting out and a complexing agent. In those conditions, a biphasic solution is formed allowing a quantitative separation of iron(III) and cobalt(II) from nickel(II). Manganese is distributed between the both phases. The tuneability of AcABS is reported as sulfuric acid can be used to induce a supplementary biphasic solution isolating Fe(III) from Co(II) and Mn(II). Finally, cobalt and nickel mixtures containing manganese impurities can be purified by electrodeposition as their reduction potential is differentiated by more than 0.9 V.<sup>211</sup> As a proof of concept, nickel from real spent NiMH batteries was electroplated on a copper electrode and exhibited a metallic purity of 99.2 at. %.

Nickel was found to represent more than 65 wt. % of the active material of nickel metal hydride batteries.<sup>21</sup> Scaling up this result to a HEV battery, such as the one found in the Toyota Prius car, up to 5 kg of nickel could be recovered for each battery by the process developed in this work. The price of nickel is currently of (data from July 2018) 14.9 USD.kg<sup>-1</sup>. Furthermore, considering that 700 Million hydride cars are currently produced in the world each year, we can infer that approximately 84000 tons of nickel could be recycled when the batteries will reach their end-of life. This data cannot be neglected as it represents 29 wt. % of the world nickel production.

## IV.5 Conclusion

---

The main objective of this part was to carry fundamental and applied investigations on the development of novel extracting technologies for the separation of transition metals found in NiMH batteries, i.e. nickel, cobalt, iron and manganese. A particular attention was devoted to cobalt, presenting the higher critical level among the transition metals and nickel highly concentrated (over 65 wt. %) in NiMH black mass. Results can be highlighted as follows:

### *Cobalt complexation by dicyanamide in H<sub>2</sub>O and in an IL*

- (i) In water, only one dicyanamide ion (DCA<sup>-</sup>) is able to complex Co<sup>2+</sup>. When the ratio  $R = \text{DCA}/\text{Co}$  is of 100, 90 molar percent of the latter complex is formed leading in a complexation constant of 20.5.
- (ii) In an ionic liquid, the complexation is drastically different as  $R = 1$  leads to the complexation of more than 80 mol. % of Co(II) by dicyanamide. From a ratio DCA/Co in the range 10 to 500, cobalt is mainly complexed by three [DCA]<sup>-</sup>. However, an unveiled compound appears using high excess of ligand as four [DCA]<sup>-</sup> were reported to complex 90 mol. % of cobalt for  $R = 2000$ .
- (iii) Finally, a correlation between the predominance of various complexes and distribution ratios after liquid-liquid extraction of cobalt from an aqueous phase towards an ionic liquid is reported.

### *Fundamentals of the first ionic liquid-based AcABS*

- (i) An aqueous biphasic solution can be induced by a fully miscible ionic liquid in water such as [P<sub>44414</sub>][Cl] mixed with an acid. The inorganic salt, used as a salting out agent in classical ABS is in this work replaced by H<sub>2</sub>SO<sub>4</sub>, HCl or HNO<sub>3</sub>.
- (ii) We report the first deviation of the Hofmeister series. The ability of inorganic acids to induce a biphasic solution follows the series HNO<sub>3</sub> > H<sub>2</sub>SO<sub>3</sub> > H<sub>2</sub>SO<sub>4</sub> > HCl > H<sub>3</sub>PO<sub>4</sub>. This can be explained by the speciation of acids and the ion exchange mechanism.

- (iii) A strong thermomorphic behaviour is observed in the  $[P_{44414}][Cl]$  / HCl /  $H_2O$  system, a mixture using 30 wt. % IL and 15 wt. % acid is shown to be monophasic at 24 °C but forms two phases at 50 °C.
- (iv) Mixed ABS-AcABS systems using  $[P_{44414}][Cl]$  / HCl-NaCl /  $H_2O$  allows to decrease the concentration of acid needed to induce a biphasic solution by adding sodium chloride as a salting out agent.

*Ionic-liquid based AcABS for metal extraction and recovery*

- (i) Focusing on the  $[P_{44414}][Cl]$  / HCl /  $H_2O$  AcABS using 30 wt. % IL and 25 wt. % HCl, Fe(III) and Co(II) can quantitatively be loaded towards the IL-rich phase while nickel remains in the acid-rich phase. Manganese is always distributed between both phases with a distribution ratio increasing with the HCl concentration.
- (ii) As a proof of concept, cobalt and nickel, two metals often mixed together in natural ores and industrial alloys were isolated with a separation factor over 400 by 30 wt. %  $[P_{44414}][Cl]$  and 25 wt. % HCl in an aqueous solution at 50 °C.
- (iii) Starting from a mixture of Ni(II), Mn(II) and Co(II), cobalt was extracted by a mixed ABS-AcABS system and recovered by electroplating from the IL-rich phase. Ranging on the concentration of acid and water, significative differences in the metallic appearance and crystallography is reported. This strengthens the tuneability aspect of AcABS, for metal extraction but also for metal electrodeposition.

*Separation of transition metal from spent NiMH batteries*

- (i) The formation of a biphasic solution can be induced by straightforwardly adding  $[P_{44414}][Cl]$  to leachates using hydrochloric or sulfuric acid providing a simultaneous leaching/extraction of metals from spent NiMH batteries.
- (ii) Starting from the leachate using 2 mol.L<sup>-1</sup>  $H_2SO_4$  after precipitation of REE at pH 1.7, the ionic liquid (30 wt. %) and NaCl (9.8 wt. %) are added to the aqueous solution. As a result, Ni(II) is isolated from Co(II) and Fe(III).
- (iii) Based on previous results, a flow sheet for the separation of all TM and the recovery of nickel (99.2 at. %) by electrodeposition is reported.



This work can be integrated in the recycling process of metals from spent NiMH batteries and is summarized in **Figure IV.30**.

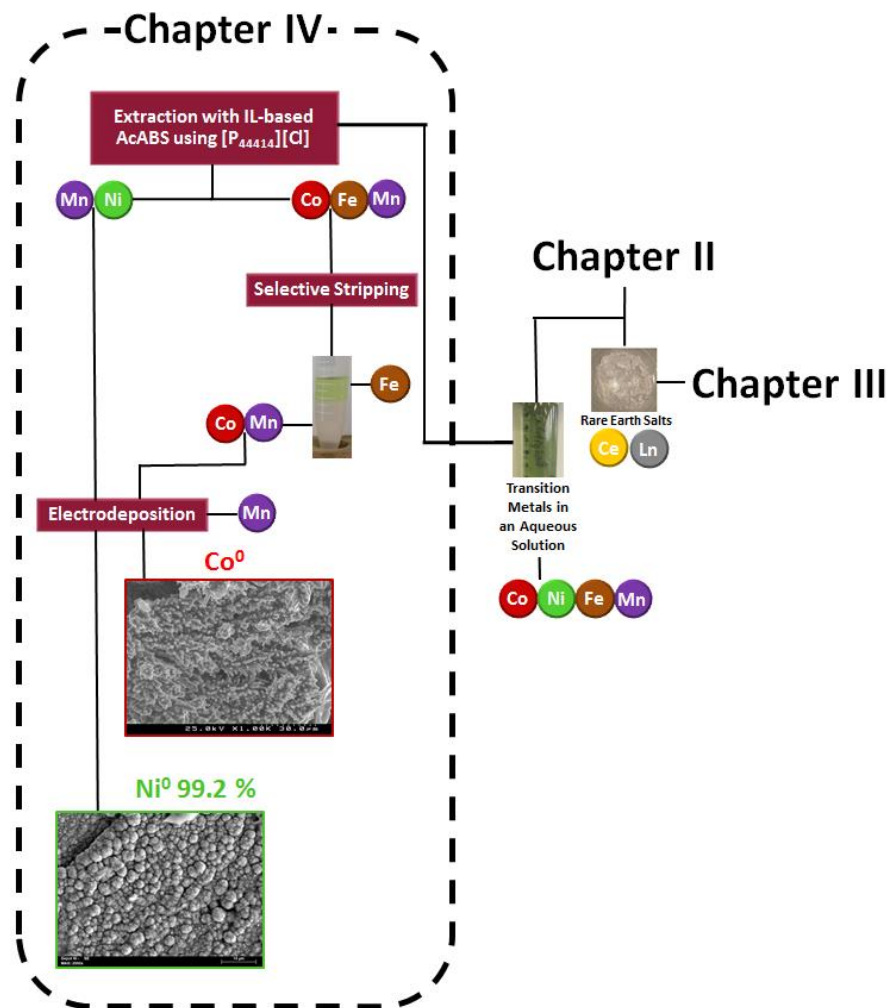


**Figure IV.30.** Flowsheet corresponding to the separation of cobalt, nickel, manganese and iron.

---

---

## Conclusion and Perspectives

*“From the strategies established...”*

To fit economic and environmental requirements linked to the criticality of metals, recycling of devices producing or storing energy has been identified as a driving force. This work is thus focusing on the recovery of transition metals and rare earth elements from NiMH batteries. Based on the expertise of the recycling company Recupyl<sup>®</sup>, spent batteries were mechanically treated in an industrial scale to obtain a concentrated fraction of strategic metals, namely, the black mass (BM). This material was fully characterized by microscopic and spectroscopic techniques to identify the nature and composition of the BM. While toxic and flammable solvents are commercially used to perform efficient extractions of metals, this project aimed the development of greener process through the use of ionic liquids (ILs). A panel of hydrometallurgical and electrochemical strategies were investigated during this work and can be summarized as follows:

(i) Leaching and selective precipitation

Sulfuric acid is an excellent candidate for the leaching of the black mass as more than 85 wt. % of the material can be oxidised and dissolved in the leachate using 2 mol.L<sup>-1</sup> acid at room temperature. The remaining solid phase is composed of plastics, carbon and passivated nickel. Increasing the pH by addition of sodium carbonate until reaching a value of 2 allows the rare earth elements to quantitatively precipitate as sodium sulphate salts (NaLn(SO<sub>4</sub>)<sub>2</sub>). All transition metals remain in the leachate.

(ii) Liquid-liquid extraction

Hydrophobic ionic liquids are known to act both as a solvent and an extractant during liquid-liquid extraction processes. This strategy is proposed for the separation of cerium(IV) from lanthanum(III), neodymium(III) and praseodymium(IV) in an aqueous phase containing 4 mol.L<sup>-1</sup> HNO<sub>3</sub> after oxidation of cerium(III) in a basic heterogeneous media. The IL showing the highest

separation factors ( $\beta$ ) of cerium towards lanthanides is the 1-methyl-1-butyl-pyrrolidinium bis(trifluoromethylsulfonyl)imide,  $[C_1C_4\text{Pyrr}][\text{NTf}_2]$  ( $\beta_{Ln(III)}^{Ce(IV)} > 1000$ ). Based on the extraction of cobalt by  $\text{NTf}_2$ -based ILs in a dicyanamide (DCA) media, fundamentals aspects of liquid-liquid extraction was studied and correlated with the speciation of Co-DCA complexes formed in the aqueous phase, but also in the ionic liquid. Dicyanamide is reported to be a strong complexing agent of cobalt in  $\text{NTf}_2$ -based ILs but a weak one in water leading in calculated complexation constants  $K_1$  of  $1.73 \times 10^6$  and  $2.05 \times 10^1$  respectively. The formation of  $\text{CoDCA}^+$  complex in water is nevertheless mandatory to induce the extraction towards the IL phase and is predominant for DCA/Co ratios higher than 100.

### (iii) Acidic aqueous biphasic systems (AcABS)

For the first time, we report the ability of a fully soluble ionic liquid in water, namely trihexyltetradecyl phosphonium chloride,  $[P_{44414}][\text{Cl}]$  to form a biphasic solution ranging on the concentration of inorganic acid and on the temperature. As an example, using 0.5 moles of IL per kg of solution, 5.1, 2.2, and 0.34 mol.kg<sup>-1</sup> of HCl, H<sub>2</sub>SO<sub>4</sub> and HNO<sub>3</sub> respectively are required to induce a phase separation. Both biphasic and monophasic domain were explored and characterised to apply those systems to metal extraction. Ranging on the complexation of the metal by the inorganic acid, metals are shown to be extracted to the top phase defined as the IL-rich phase. Furthermore, the difficult separation of cobalt(II) from nickel(II) is achieved with a separation factor of 420 at 50 °C using 30 wt. % of IL and 25 wt. % of HCl. A simultaneous leaching/extraction step can thus be considered.

### (iv) Electrodeposition

Starting from a metal loaded in a hydrophobic IL or in a hydrophilic IL-rich phase after extraction, electrodeposition of cerium or cobalt respectively was shown to be an encouraging strategy for metal recovery. Metallic cerium was reduced on a gold electrode after performing chronoamperometry at -2 V vs. Fc/Fc<sup>+</sup>. Nevertheless, evidence of sulfur and fluorine elements coming from the IL anion strongly decreases the purity of the obtained metal. On the contrary, cobalt(II) was reduced in an AcABS with high purity rates. Another proof of the tuneability of AcABS is

reported as different crystallographic and morphologic structures of  $\text{Co}(0)$  are found depending on the concentrations of  $[\text{P}_{44414}][\text{Cl}]$  and water.

According to those results, and in agreements with the specifications from this project, a flowsheet for the recycling of metals from spent NiMH batteries is proposed in **Figure V.1**.

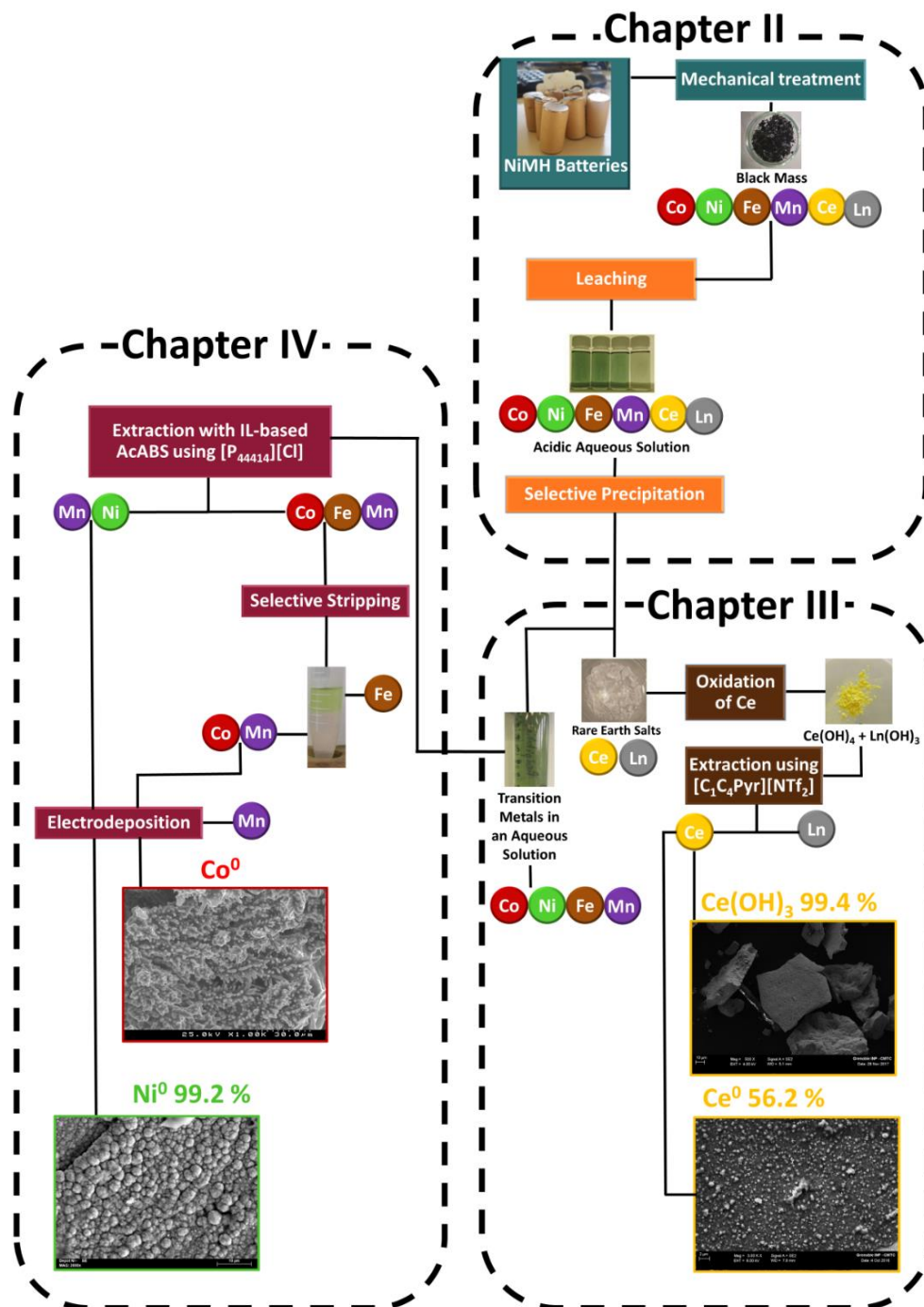


**Figure V.1.** Flowsheet for the recycling of metals from NiMH batteries.

“...to the prospects opened.”

(i) Oxidation of cerium(III)

Oxidation step of Ce(III) sulphate in Ce(IV) hydroxide is the less efficient step among the Ce recovery as approximately 88 mol. % of the latter REE is oxidized. This result can be attributed to the heterogeneous, solid/liquid reaction but also to the passivation of a thin surface layer of cerium hydroxide. Furthermore, a large amount of chemicals are used as oxidation takes place in alkaline media while liquid-liquid extraction using [C<sub>1</sub>C<sub>4</sub>Pyrr][NTf<sub>2</sub>] takes place in a nitric acid aqueous solution. According to the potential-pH diagram of cerium,<sup>237,250</sup> we report the ability of Ce(III) to be oxidised by oxygen at alkaline pH. Such an oxidation is also possible at highly acidic pH(< 0) using ozone.

After dissolution of Ce<sub>2</sub>(SO<sub>4</sub>)<sub>3</sub> 0.02 mol.L<sup>-1</sup> in 4 mol.L<sup>-1</sup> HNO<sub>3</sub>, an ozone generator connected to a pump allowed a 100 mL solution to be in contact with ozone bubbles at a flow rate of 2.6 mol.h<sup>-1</sup>. The flow rate was calculated thanks to the titration of I<sub>2</sub> by Na<sub>2</sub>S<sub>2</sub>O<sub>3</sub> after oxidation of KI. Snapshots of aliquot taken from the solution are given in **Figure 2**.

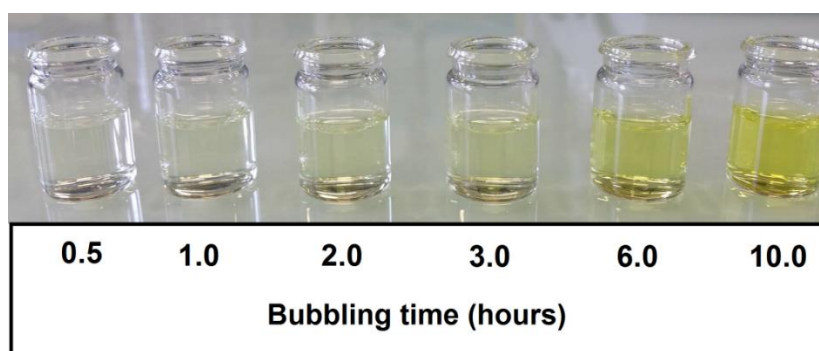


**Figure V.2.** Ce(III) 0.02 mol.L<sup>-1</sup> in 4 mol.L<sup>-1</sup> HNO<sub>3</sub> after 10 hours bubbling of 2.6 mol.h<sup>-1</sup> O<sub>3</sub>.

The increasing yellow colouration with the bubbling time indicates that Ce(III) is able to be oxidized by ozone in Ce(IV) directly in nitric acid. This would allow a direct liquid-liquid extraction starting from the latter solution. However the oxidation yields remains difficult to evaluate by classical analytical techniques such as UV-vis spectrophotometry because of the similar absorption of NO<sub>3</sub><sup>-</sup> and Ce<sub>4</sub><sup>+</sup> ions at wavelength lower than 400 nm.<sup>244</sup> Nevertheless, oxidation in acidic media by O<sub>3</sub> appears to be an encouraging strategy and could be investigated.

## (ii) Life cycle assessment (LCA) for a better understanding of the process

In many parts of the process, different strategies are proposed e.g. oxidizing cerium in alkaline or acidic media and recovering cerium by a precipitation or an electrodeposition step. It is however difficult to define which solution is the most favorable on an economic and environmental point of view. This can be investigated by LCA analysis which is currently undergone by the G-scope laboratory from Grenoble, France. Our collaboration is focusing on the recycling of 1 kg of BM starting from mechanical treatments down to cerium recovery. Preliminary results demonstrate that the recycling of the IL phase has tremendous influence on all environmental impacts. However the difficulty to obtain reliable information on the synthesis of bis(trifluoromethylsulfonyl)imide ILs in an industrial scale provides important uncertainty in our results. Based on the recycling process of metals from spent NiMH batteries, the potential and limitation of ILs will be demonstrated in a forthcoming study. Based on published data, the impact of the anion, the cation and waste is analysed. (Optimisation of the model is currently investigated). **Figure V.3** demonstrates that the anion containing sulphur and fluorine atoms is the most impacting. This strengthens the use of hydrophilic ILs based on chloride anions in AcABS for metal recycling.

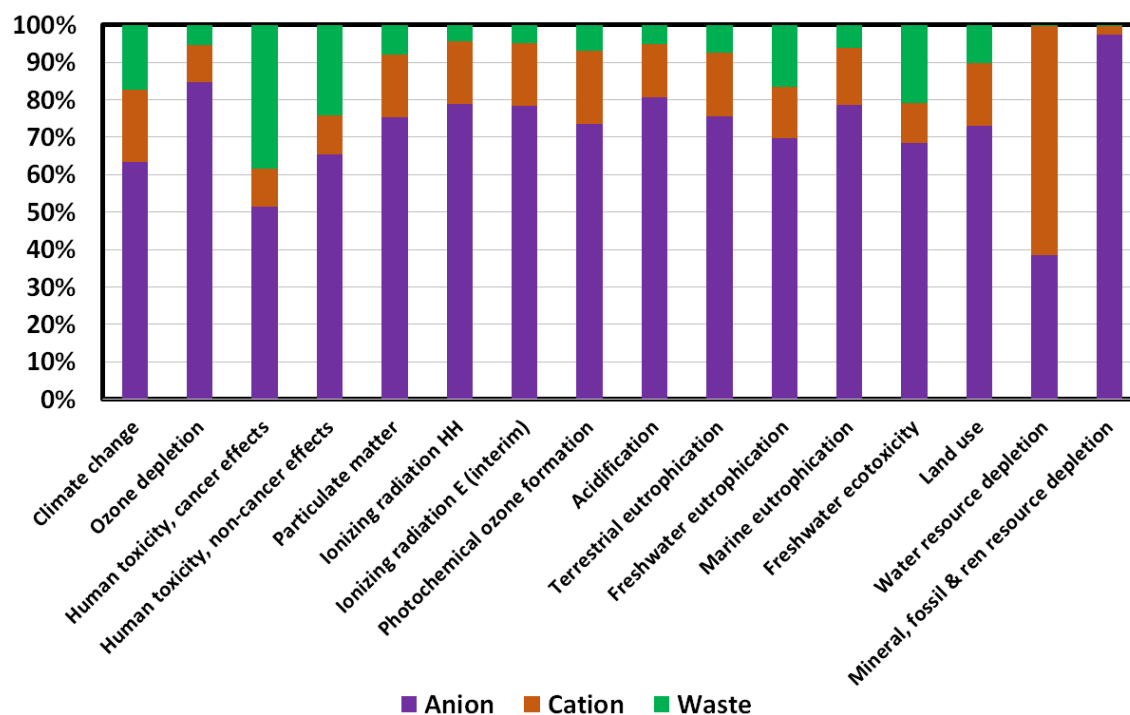


**Figure V.3.** Modelling the impact of the anion, the cation and waste during the synthesis of  $[C_1C_4Pyrr][NTf_2]$ . Method used: ILCD 2011 Midpoint + V1.05. Data are provided by Florence Betmont from G-Scop laboratory.

(iii) Recovery of Pt and Co from proton exchange membrane fuel cells (PEMFC)

Broadly speaking, innovative extraction systems developed in this project such as acidic aqueous biphasic systems could be of particular interest for recycling strategic metals from other spent devices. Furthermore, one of the major advantages of AcABS is to straightforwardly extract metals from highly acidic leachates. In other words, those systems could perfectly fit to the recovery of metal suffering from hydrolysis. This is the case of platinum contained in PEM fuel cells. Within a PEMFC, two crucial parts are relevant to recycle: the proton exchange membrane and the electrode material forming the Membrane Electrode Assembly (MEA).<sup>330</sup> Platinum is a metal exhibiting one of the highest prices on the market, typically above 20 k\$.kg<sup>-1</sup> in march 2016.<sup>331</sup> Because of its price, the limited availability of this metal in earth's crust, the fact that such a metal is currently used in many high end (telecommunications, aerospace) or everyday applications (catalytic converters, jewellery, etc.) and that it can currently hardly be substituted by other metals,<sup>332</sup> finding alternative and sustainable ways of recycling platinum is justified. Briefly, starting from a real spent MEA, the material was treated with 200 mL of aqueous solution containing 3 vol.% H<sub>2</sub>O<sub>2</sub> in HCl 12 mol.L<sup>-1</sup>. The leaching step was carried out at 25 °C during 5 hours. Concentrations of 1.2x10<sup>-2</sup> and 4.8x10<sup>-3</sup> mol.L<sup>-1</sup> for platinum(IV) and cobalt(II) were respectively measured. Addition of 30 wt. % of [P<sub>44414</sub>][Cl] allowed to quantitatively extract 99.8 % of Pt(IV) and 85.2 % of Co(II). Selective precipitation of [P<sub>44414</sub>]<sub>2</sub>[PtCl<sub>6</sub>] occurred by addition of HCl 1 mol.L<sup>-1</sup> to the IL-rich phase. The process in development can be summarized by **Figure V.4**.

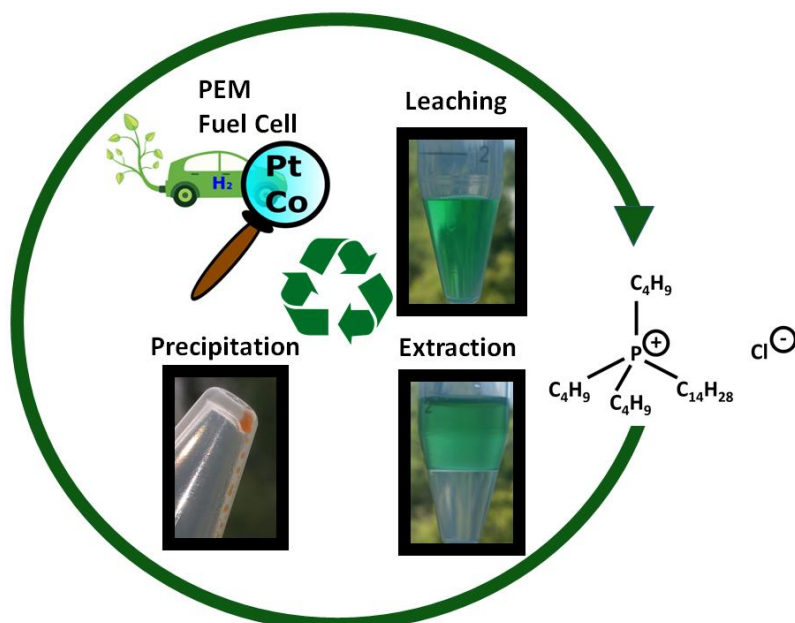


**Figure V.4.** Recycling process of platinum from spent PEMFC currently developed.





---

---

## References

- (1) Hublin, J.-J.; Ben-Ncer, A.; Bailey, S. E.; Freidline, S. E.; Neubauer, S.; Skinner, M. M.; Bergmann, I.; Le Cabec, A.; Benazzi, S.; Harvati, K.; et al. New Fossils from Jebel Irhoud, Morocco and the Pan-African Origin of Homo Sapiens. *Nature* **2017**, *546* (7657), 289–292.
- (2) *The international system of units (SI)*, 8. éd.; Bureau International des Poids et Mesures, Ed.; BIPM: Sèvres, 2006.
- (3) Berna, F.; Goldberg, P.; Horwitz, L. K.; Brink, J.; Holt, S.; Bamford, M.; Chazan, M. Microstratigraphic Evidence of in Situ Fire in the Acheulean Strata of Wonderwerk Cave, Northern Cape Province, South Africa. *Proc. Natl. Acad. Sci.* **2012**, *109* (20), E1215–E1220.
- (4) James Watt's Fire Engines Patent Act, 1775 (15 Geo 3 c. 61).
- (5) International Atomic Energy Agency, <https://www.iaea.org/> (Accessed March 2018).
- (6) Université de Grenoble Encyclopédie de l'énergie, <http://encyclopedie-energie.org> (Accessed March 2018).
- (7) Pitron, G. *La Guerre Des Métaux Rares, La Face Cachée de La Transition Énergétique et Numérique*; Les Liens qui Libèrent, 2018.
- (8) United Nations Environment Programme; REN21 Secretariat; Frankfurt School UNEP Collaborating Centre for Climate & Sustainable Energy Finance. *Renewables 2016 global status report.*; 2016.
- (9) Rifkin, J. *The Third Industrial Revolution: How Lateral Power Is Transforming Energy, the Economy and the World*; Palgrave MacMillan, 2011.
- (10) Solar Impulse Foundation, <http://aroundtheworld.solarimpulse.com/> (Accessed March 2018).
- (11) Gras, M. A Novel Ionic Liquid Electrolyte for Sodium-Ion Batteries, Deakin University, Internship report, 2015.
- (12) Volta, A. On the Electricity Excited by the Mere Contact of Conducting Substances of Different Kinds. *Philos. Trans. R. Soc. Lond.* **1800**, *90*, 403–434.
- (13) Navarathinam, N.; Lee, R.; Chesser, H. Characterization of Lithium-Polymer Batteries for CubeSat Applications. *Acta Astronaut.* **2011**, *68* (11–12), 1752–1760.

- (14) Etiemble, A. Étude de Matériaux Hydrurables Par Émission Acoustique: Application Aux Batteries Ni-MH. PhD Thesis, Lyon, INSA, PhD thesis, 2013.
- (15) Gille, B. *Histoire Des Techniques: Prolégomènes à Une Histoire Des Techniques*; Encyclopédie de la Pléiade; Encyclopédie de la Pléiade, Gallimard, 1978.
- (16) Directive 2006/66/ CE of the European Parlement Relative to Batteries and Accumulators. *Off. J. Eur. Com.* **2006**, 14.
- (17) Beccu, K. Accumulator Electrode with Capacity for Storing Hydrogen and Method of Manufacturing Said Electrode, Patent US3669745A, June 1972.
- (18) Avicenne Consulting Firm, [Http://Www.Avicenne.Com](http://www.avicenne.com) (Accessed March 2018).
- (19) Waluś, S.; Robba, A.; Bouchet, R.; Barchasz, C.; Alloin, F. Influence of the Binder and Preparation Process on the Positive Electrode Electrochemical Response and Li/S System Performances. *Electrochim Acta* **2016**, 210, 492–501.
- (20) Blanchard, R.; Martin, V.; Mantoux, A.; Chatenet, M. Cobalt Porphyrin and Salcomine as Novel Redox Shuttle Species to Enhance the Oxygen Evolution Reaction in LiO<sub>2</sub> Batteries. *Electrochim Acta* **2018**, 261, 384–393.
- (21) Reddy, T. B. *Linden's Handbook of Batteries*, 4th ed.; Mc Graw Hills, 2011.
- (22) Caillon, G. Les Accumulateurs Portables. *Techniques Ing.* **2001**, E2140.
- (23) Gilliam, R.; Graydon, J.; Kirk, D.; Thorpe, S. A Review of Specific Conductivities of Potassium Hydroxide Solutions for Various Concentrations and Temperatures. *Int. J. Hydrog. Energy* **2007**, 32 (3), 359–364.
- (24) Wang, C.; Sun, J.; Liu, H. .; Dou, S. .; MacFarlane, D.; Forsyth, M. Potential Application of Solid Electrolyte P11OH in Ni/MH Batteries. *Synth. Met.* **2005**, 152, 57–60.
- (25) Züttel, A. Hydrogen Storage Methods. *Naturwissenschaften* **2004**, 91 (4), 157–172.
- (26) Pistoia, G.; Wiaux, J.; Wolsky, S. *Used Battery Collection and Recycling*, Elsevier Science Publishers.; 2001.
- (27) Cuevas, F.; Joubert, J.-M.; Latroche, M.; Percheron-Guégan, A. Intermetallic Compounds as Negative Electrodes of Ni/MH Batteries: *Appl. Phys. Mater. Sci. Process.* **2001**, 72 (2), 225–238.

- (28) Van Vutch, J.; Kuijpers, f; Bruning, H. Reversible Room Temperature Absorption of Large Quantities of Hydrogen by Intermetallic Compounds. *Philipps Res. Rep.* **1970**, *25*, 133–140.
- (29) Percheron-Guégan, A.; Lartigue, C.; Achard, J. C.; Germi, P.; Tasset, F. Neutron and X-Ray Diffraction Profile Analyses and Structure of LaNi<sub>5</sub>, LaNi<sub>5</sub>- XAl<sub>x</sub> and LaNi<sub>5</sub>- XMn<sub>x</sub> Intermetallics and Their Hydrides (Deuterides). *J. Common Met.* **1980**, *74* (1), 1–12.
- (30) Petit Férey, M. A. Élaboration et Caractérisation d'alliages Hydrurables de Type AB<sub>x</sub> (A= La, Mg; B= Ni et X= 3 à 4) En Vue de Leur Utilisation Comme Matière Active Pour Électrode Négative d'accumulateur Ni-MH. PhD Thesis, Université Paris-Est, PhD thesis, 2008.
- (31) Johnson, J.; Harper, E. M.; Lifset, R.; Graedel, T. E. Dining at the Periodic Table: Metals Concentrations as They Relate to Recycling. *Environ. Sci. Technol.* **2007**, *41* (5), 1759–1765.
- (32) Serfati, C.; Le Billon, P. Mondialisation et conflits de ressources naturelles. *Ecol. Polit.* **2007**, *34* (1), 9.
- (33) Graedel, T. E.; Barr, R.; Chandler, C.; Chase, T.; Choi, J.; Christoffersen, L.; Friedlander, E.; Henly, C.; Jun, C.; Nassar, N. T.; et al. Methodology of Metal Criticality Determination. *Environ. Sci. Technol.* **2012**, *46* (2), 1063–1070.
- (34) Halada, K.; Shimada, M.; Ijima, K. Forecasting of the Consumption of Metals up to 2050. *Mater. Trans.* **2008**, *49* (3), 402–410.
- (35) Erdmann, L.; Graedel, T. E. Criticality of Non-Fuel Minerals: A Review of Major Approaches and Analyses. *Environ. Sci. Technol.* **2011**, *45* (18), 7620–7630.
- (36) European Commission. Critical Raw Materials for the EU. **2010**, 0–85.
- (37) European Commission. Report on Critical Raw Materials for the EU. **2014**, 0–41.
- (38) European Commission. Report on Critical Raw Materials for the EU. **2017**, 0–519.
- (39) IUPAC. *Nomenclature of Inorganic Chemistry*, 3rd ed.; Blackwell Scientific Publications: Oxford, 1990.
- (40) Foucault, A.; Raoult, J.; Platevoet, B. *Dictionary of Geology*, 8th ed.; Dunod, 2014.
- (41) Info Mine, [Http://Www.infomine.com/chartsanddata](http://www.infomine.com/chartsanddata) (Accessed March 2018).
- (42) King, A. Battery Builders Get the Cobalt Blues, [Http://Www.chemistryworld.com](http://www.chemistryworld.com) (Accessed March 2018). *Chemistry World*.

- (43) Hannis, S.; Bide, T. *Cobalt*; British Geological Survey, 2009.
- (44) Crundwell, F. K.; Moats, M. S.; Ramachandran, V.; Robinson, T. G.; Davenport, W. G. *Extractive Metallurgy of Nickel, Cobalt and Platinum Group Metals*; Elsevier, 2011.
- (45) Tesla, <https://www.tesla.com/models> (Accessed March 2018).
- (46) Musk, E. Millions of Teslas, 500-Miles Range Coming. *CNBC*.
- (47) Hulot, N. « Nous Visons La Fin de La Vente Des Voitures à Essence et Diesel d'ici à 2040 », <http://www.lemonde.fr> (Accessed March 2018). *Le Monde*.
- (48) French Ministry of the Ecological Transition, <http://www.statistiques.developpement-durable.gouv.fr>, (Accessed March 2018).
- (49) Chez Tesla, Elon Musk Rompt Avec La Méthode Toyota, <https://www.usinenouvelle.com> (Accessed in March 2018).
- (50) Hocquard, C. New Energy, New Risks. *Talk ENSTA 08-02-18 InnoEnergy Conf*.
- (51) DR Congo Signs New Mining Law despite Companies' Opposition, <http://www.bbc.com> (Accessed March 2018).
- (52) Binnemans, K.; Jones, P. T.; Blanpain, B.; Van Gerven, T.; Yang, Y.; Walton, A.; Buchert, M. Recycling of Rare Earths: A Critical Review. *J. Clean. Prod.* **2013**, *51*, 1–22.
- (53) Merriman, D. A Review of the Global Supply of Rare Earths. *RSC Environmental Chem. Group* **2013**, *32*.
- (54) Bavard, F. Complexation Des Cations Lanthanides Trivalents Par Des Ligands Azotés et Oxygénés : Études Physico - Chimiques de l'association et de La Sélectivité En Solution. *CEA Grenoble Univ. Grenoble Alpes* **2004**, 233.
- (55) Pyykko, P. Relativistic Effects in Structural Chemistry. *Chem. Rev.* **1988**, *88* (3), 563–594.
- (56) Binnemans, K.; Jones, P. T.; Müller, T.; Yurramendi, L. Rare Earths and the Balance Problem: How to Deal with Changing Markets? *J. Sustain. Metall.* **2018**, *4* (1), 126–146.
- (57) Shelby, J. Rare Earths as Major Components in Oxide Glasses. *Key Eng Mater* **1994**, *94*, 1–42.
- (58) Gutfleisch, O.; Willard, M. A.; Brück, E.; Chen, C. H.; Sankar, S. G.; Liu, J. P. Magnetic Materials and Devices for the 21st Century: Stronger, Lighter, and More Energy Efficient. *Adv. Mater.* **2011**, *23* (7), 821–842.

- (59) Labbé, J. .; Lefebvre, G. Panorama Du Marché Des Terres Rares. *COMES Commity Strateg. Met. Semin.* **2016**.
- (60) Hedrick, J.; Sinha, S. Cerium-Based Polishing Compounds: Discovery to Manufacture. *J Alloys Compd* **1994**, *207*, 377–382.
- (61) Falconnet, P. The Economics of Rare Earths. *J. Common Met.* **1985**, *111*, 9–15.
- (62) USGS Data Sheets, <https://Minerals.USgs.Gov/Minerals> (Accessed March 2018).
- (63) US department of the Interior; US deological survey. Rare Earth Metals. Critical Ressources for High Technology. *USGS Rep.* **2002**.
- (64) Simoni, M.; Kuhn, E. P.; Morf, L. S.; Kuendig, R.; Adam, F. Urban Mining as a Contribution to the Resource Strategy of the Canton of Zurich. *Waste Manag.* **2015**, *45*, 10–21.
- (65) Arshi, P. S.; Vahidi, E.; Zhao, F. Behind the Scenes of Clean Energy: The Environmental Footprint of Rare Earth Products. *ACS Sustain. Chem. Eng.* **2018**, *6* (3), 3311–3320.
- (66) Robinson, B. H. E-Waste: An Assessment of Global Production and Environmental Impacts. *Sci. Total Environ.* **2009**, *408* (2), 183–191.
- (67) Vahidi, E.; Zhao, F. Environmental Life Cycle Assessment on the Separation of Rare Earth Oxides through Solvent Extraction. *J. Environ. Manage.* **2017**, *203*, 255–263.
- (68) Talens Peiró, L.; Villalba Méndez, G. Material and Energy Requirement for Rare Earth Production. *JOM* **2013**, *65* (10), 1327–1340.
- (69) Cytec Solvay Group, [Http://www.Cytec.Com/Products](http://www.Cytec.Com/Products) (Accessed March 2018).
- (70) Saleh, M. I.; Bari, M. F.; Saad, B. Solvent Extraction of Lanthanum(III) from Acidic Nitrate-Acetato Medium by Cyanex 272 in Toluene. *Hydrometallurgy* **2002**, *63* (1), 75–84.
- (71) Reddy, M. L. .; Bosco Bharathi, J. .; Peter, S.; Ramamohan, T. . Synergistic Extraction of Rare Earths with Bis(2,4,4-Trimethyl Pentyl) Dithiophosphinic Acid and Trialkyl Phosphine Oxide. *Talanta* **1999**, *50* (1), 79–85.
- (72) Jia, Q.; Tong, S.; Li, Z.; Zhou, W.; Li, H.; Meng, S. Solvent Extraction of Rare Earth Elements with Mixtures of Sec-Octylphenoxy Acetic Acid and Bis(2,4,4-Trimethylpentyl) Dithiophosphinic Acid. *Sep. Purif. Technol.* **2009**, *64* (3), 345–350.

- (73) Tian, M.; Jia, Q.; Liao, W. Studies on Synergistic Solvent Extraction of Rare Earth Elements from Nitrate Medium by Mixtures of 8-Hydroxyquinoline with Cyanex 301 or Cyanex 302. *J. Rare Earths* **2013**, *31* (6), 604–608.
- (74) Wu, D.; Niu, C.; Li, D.; Bai, Y. Solvent Extraction of Scandium(III), Yttrium(III), Lanthanum(III) and Gadolinium(III) Using Cyanex 302 in Heptane from Hydrochloric Acid Solutions. *J. Alloys Compd.* **2004**, *374* (1–2), 442–446.
- (75) Panda, N.; Devi, N.; Mishra, S. Solvent Extraction of Neodymium(III) from Acidic Nitrate Medium Using Cyanex 921 in Kerosene. *J. Rare Earths* **2012**, *30* (8), 794–797.
- (76) Du, X.; Graedel, T. E. Uncovering the Global Life Cycles of the Rare Earth Elements. *Sci. Rep.* **2011**, *1*:145.
- (77) Duclos, L.; Lupsea, M.; Mandil, G.; Svecova, L.; Thivel, P.-X.; Lafort, V. Environmental Assessment of Proton Exchange Membrane Fuel Cell Platinum Catalyst Recycling. *J. Clean. Prod.* **2017**, *142*, 2618–2628.
- (78) Zaimes, G. G.; Hubler, B. J.; Wang, S.; Khanna, V. Environmental Life Cycle Perspective on Rare Earth Oxide Production. *ACS Sustain. Chem. Eng.* **2015**, *3* (2), 237–244.
- (79) Bontron, C. En Chine Les Terres Rares Tuent Des Villages. *Le Monde*. 2012.
- (80) Adwen, [Http://Www.Adwenoffshore.Com/](http://www.adwenoffshore.com/) (Accessed March 2018).
- (81) Anastas, P. T.; Williamson, T. C. Green Chemistry: An Overview. In *Green Chemistry*; Anastas, P. T., Williamson, T. C., Eds.; American Chemical Society: Washington, DC, 1996; Vol. 626, pp 1–17.
- (82) Anastas, P.; Eghbali, N. Green Chemistry: Principles and Practice. *Chem Soc Rev* **2010**, *39* (1), 301–312.
- (83) Plechkova, N. V.; Seddon, K. R. Applications of Ionic Liquids in the Chemical Industry. *Chem Soc Rev* **2008**, *37* (1), 123–150.
- (84) Walden, P. Molecular Weights and Electrical Conductivity of Several Fused Salts. *Bull Acad Imper* **1914**, 405–422.
- (85) Passos, H. Development and Characterization of New Extraction Platforms Using Ionic-Liquid-Based Aqueous Biphasic Systems, Aveiro University, PhD thesis, 2017.
- (86) Web of Knowledge, [Http://Www.Webofknowledge.Com,](http://www.webofknowledge.com/) (Accessed March 2018).

- (87) MacFarlane, D.; Kar, M.; Pringle, J. *Fundamentals of Ionic Liquids: From Chemistry to Applications*, Wiley.; 2017.
- (88) Zuo, Y.; Liu, Y.; Chen, J.; Li, D. Q. The Separation of Cerium(IV) from Nitric Acid Solutions Containing Thorium(IV) and Lanthanides(III) Using Pure [C<sub>8</sub>Mim]PF<sub>6</sub> as Extracting Phase. *Ind. Eng. Chem. Res.* **2008**, *47* (7), 2349–2355.
- (89) Earle, M. J.; Seddon, K. R. Ionic Liquids: Green Solvents for the Future. In *Clean Solvents*; Abraham, M. A., Moens, L., Eds.; American Chemical Society: Washington, DC, 2002; Vol. 819, pp 10–25.
- (90) Jacquemin, J.; Husson, P.; Padua, A. A. H.; Majer, V. Density and Viscosity of Several Pure and Water-Saturated Ionic Liquids. *Green Chem* **2006**, *8* (2), 172–180.
- (91) Salminen, J.; Papaiconomou, N.; Kumar, R. A.; Lee, J.-M.; Kerr, J.; Newman, J.; Prausnitz, J. M. Physicochemical Properties and Toxicities of Hydrophobic Piperidinium and Pyrrolidinium Ionic Liquids. *Fluid Phase Equilib* **2007**, *261* (1–2), 421–426.
- (92) Thuy Pham, T. P.; Cho, C.-W.; Yun, Y.-S. Environmental Fate and Toxicity of Ionic Liquids: A Review. *Water Res.* **2010**, *44* (2), 352–372.
- (93) Zhao, D.; Liao, Y.; Zhang, D. Toxicity of Ionic Liquids. *Clean Soil Air Water* **2007**, *35* (1), 42–48.
- (94) MacFarlane, D. R.; Forsyth, M.; Howlett, P. C.; Pringle, J. M.; Sun, J.; Annat, G.; Neil, W.; Izgorodina, E. I. Ionic Liquids in Electrochemical Devices and Processes: Managing Interfacial Electrochemistry. *Acc. Chem. Res.* **2007**, *40* (11), 1165–1173.
- (95) Paulechka, Y. U.; Zaitsau, D. H.; Kabo, G. J.; Strechan, A. A. Vapor Pressure and Thermal Stability of Ionic Liquid 1-Butyl-3-Methylimidazolium Bis(Trifluoromethylsulfonyl)Amide. *Thermochim. Acta* **2005**, *439* (1–2), 158–160.
- (96) Rebelo, L. P. N.; Canongia Lopes, J. N.; Esperança, J. M. S. S.; Filipe, E. On the Critical Temperature, Normal Boiling Point, and Vapor Pressure of Ionic Liquids. *J. Phys. Chem. B* **2005**, *109* (13), 6040–6043.
- (97) Smiglak, M.; Reichert, W. M.; Holbrey, J. D.; Wilkes, J. S.; Sun, L.; Thrasher, J. S.; Kirichenko, K.; Singh, S.; Katritzky, A. R.; Rogers, R. D. Combustible Ionic Liquids by Design: Is Laboratory Safety Another Ionic Liquid Myth? *Chem. Commun.* **2006**, No. 24, 2554–2556.



- (98) Zhang, Y.; Gao, H.; Joo, Y.-H.; Shreeve, J. M. Ionic Liquids as Hypergolic Fuels. *Angew. Chem. Int. Ed.* **2011**, *50* (41), 9554–9562.
- (99) Long Chen; Sharifzadeh, M.; Mac Dowell, N.; Welton, T.; Shah, N.; Hallett, J. P. Inexpensive Ionic Liquids: [HSO<sub>4</sub>]-Based Solvent Production at Bulk Scale. *Green Chem.* **2014**, *16* (6), 3098–3106.
- (100) Gras, M.; Papaiconomou, N.; Chainet, E.; Tedjar, F.; Billard, I. Separation of Cerium(III) from Lanthanum(III), Neodymium(III) and Praseodymium(III) by Oxidation and Liquid-Liquid Extraction Using Ionic Liquids. *Sep. Purif. Technol.* **2017**, *178*, 169–177.
- (101) Hilder, M.; Gras, M.; Pope, C.; Kar, M.; MacFarlane, D.; Forsyth, M.; O'Dell, L. A. Effect of Mixed Anions on the Physicochemical Properties of a Sodium Containing Alkoxyammonium Ionic Liquid Electrolyte. *Phys Chem Chem Phys* **2017**, *24*, 17461–17468.
- (102) MacFarlane, D. R.; Tachikawa, N.; Forsyth, M.; Pringle, J. M.; Angell, C. A. Energy Applications of Ionic Liquids. *Energy Env. Sci* **2014**, *7* (1), 232–250.
- (103) Armand, M.; Endres, F.; MacFarlane, D. R.; Ohno, H.; Scrosati, B. Ionic-Liquid Materials for the Electrochemical Challenges of the Future. In *Materials for Sustainable Energy*; Macmillan Publishers Ltd, UK, 2010; pp 129–137.
- (104) Ishikawa, M.; Sugimoto, T.; Kikuta, M.; Ishiko, E.; Kono, M. Pure Ionic Liquid Electrolytes Compatible with a Graphitized Carbon Negative Electrode in Rechargeable Lithium-Ion Batteries. *J. Power Sources* **2006**, *162* (1), 658–662.
- (105) Lewandowski, A.; Świdarska-Mocek, A. Ionic Liquids as Electrolytes for Li-Ion Batteries—An Overview of Electrochemical Studies. *J. Power Sources* **2009**, *194*, 601–609.
- (106) Forsyth, M.; Yoon, H.; Chen, F.; Zhu, H.; MacFarlane, D. R.; Armand, M.; Howlett, P. C. Novel Na<sup>+</sup> Ion Diffusion Mechanism in Mixed Organic–Inorganic Ionic Liquid Electrolyte Leading to High Na<sup>+</sup> Transference Number and Stable, High Rate Electrochemical Cycling of Sodium Cells. *J. Phys. Chem. C* **2016**, *120* (8), 4276–4286.
- (107) De Souza, R. F.; Padilha, J. C.; Gonçalves, R. S.; Dupont, J. Room Temperature Dialkylimidazolium Ionic Liquid-Based Fuel Cells. *Electrochem. Commun.* **2003**, *5* (8), 728–731.

- (108) Armel, V.; Pringle, J. M.; Forsyth, M.; MacFarlane, D. R.; Officer, D. L.; Wagner, P. Ionic Liquid Electrolyte Porphyrin Dye Sensitised Solar Cells. *Chem. Commun.* **2010**, *46* (18), 3146–3148.
- (109) Wang, P.; Zakeeruddin, S. M.; Moser, J.-E.; Humphry-Baker, R.; Grätzel, M. A Solvent-Free,  $\text{SeCN}^- / (\text{SeCN})^{3-}$  Based Ionic Liquid Electrolyte for High-Efficiency Dye-Sensitized Nanocrystalline Solar Cells. *J. Am. Chem. Soc.* **2004**, *126* (23), 7164–7165.
- (110) Abraham, T. J.; MacFarlane, D. R.; Pringle, J. M. Seebeck Coefficients in Ionic Liquids – Prospects for Thermo-Electrochemical Cells. *Chem. Commun.* **2011**, *47* (22), 6260–6262.
- (111) Wilkes, J. S. A Short History of Ionic Liquids—from Molten Salts to Neoteric Solvents. *Green Chem.* **2002**, *4* (2), 73–80.
- (112) Zhao, Y.; VanderNoot, T. J. Electrodeposition of Aluminium from Nonaqueous Organic Electrolytic Systems and Room Temperature Molten Salts. *Electrochimica Acta* **1997**, *42* (1), 3–13.
- (113) Abbott, A. P.; Frisch, G.; Ryder, K. S. Electroplating Using Ionic Liquids. *Annu. Rev. Mater. Res.* **2013**, *43* (1), 335–358.
- (114) Endres, F.; Abbott, A.; MacFarlane, D. R. *Electrodeposition from Ionic Liquids*; Wiley VCH, 2008.
- (115) Deng, M.-J.; Chen, P.-Y.; Leong, T.-I.; Sun, I.-W.; Chang, J.-K.; Tsai, W.-T. Dicyanamide Anion Based Ionic Liquids for Electrodeposition of Metals. *Electrochem. Commun.* **2008**, *10* (2), 213–216.
- (116) Ishii, M.; Matsumiya, M.; Kawakami, S. Development of Recycling Process for Rare Earth Magnets by Electrodeposition Using Ionic Liquids Media. *ECS Trans.* **2013**, *50* (11), 549–560.
- (117) Legeai, S.; Diliberto, S.; Stein, N.; Boulanger, C.; Estager, J.; Papaiconomou, N.; Draye, M. Room-Temperature Ionic Liquid for Lanthanum Electrodeposition. *Electrochem. Commun.* **2008**, *10* (11), 1661–1664.
- (118) Zarrougui, R.; Mdimagh, R.; Raouafi, N. Highly Efficient and Eco-Friendly Extraction of Neodymium Using, Undiluted and Non-Fluorinated Ionic Liquids. Direct Electrochemical Metal Separation. *Sep. Purif. Technol.* **2017**, *175*, 87–98.
- (119) Welton, T. Ionic Liquids in Catalysis. *Coord. Chem. Rev.* **2004**, *248* (21–24), 2459–2477.

- (120) P'Pool, S. J.; Klingshirn, M. A.; Rogers, R. D.; Shaughnessy, K. H. Kinetic Study of the Oxidative Addition of Methyl Iodide to Vaska's Complex in Ionic Liquids. *J. Organomet. Chem.* **2005**, *690* (15), 3522–3528.
- (121) Wheeler, C.; West, K. N.; Eckert, C. A.; Liotta, C. L. Ionic Liquids as Catalytic Green Solvents for Nucleophilic Displacement Reactions. *Chem. Commun.* **2001**, *10*, 887–888.
- (122) Qiao, C.-Z.; Zhang, Y.-F.; Zhang, J.-C.; Li, C.-Y. Activity and Stability Investigation of [BMIM][AlCl<sub>4</sub>] Ionic Liquid as Catalyst for Alkylation of Benzene with 1-Dodecene. *Appl. Catal. Gen.* **2004**, *276* (1–2), 61–66.
- (123) Freire, M. G. *Ionic-Liquid-Based Aqueous Biphasic Systems*; Green Chemistry and Sustainable Technology; Springer Berlin Heidelberg: Berlin, Heidelberg, 2016.
- (124) Bara, J. E.; Gabriel, C. J.; Hatakeyama, E. S.; Carlisle, T. K.; Lessmann, S.; Noble, R. D.; Gin, D. L. Improving CO<sub>2</sub> Selectivity in Polymerized Room-Temperature Ionic Liquid Gas Separation Membranes through Incorporation of Polar Substituents. *J. Membr. Sci.* **2008**, *321* (1), 3–7.
- (125) Bates, E. D.; Mayton, R. D.; Ntai, I.; Davis, J. H. CO<sub>2</sub> Capture by a Task-Specific Ionic Liquid. *J. Am. Chem. Soc.* **2002**, *124* (6), 926–927.
- (126) Huddleston, J. G.; Willauer, H. D.; Swatloski, R. P.; Visser, A. E.; Rogers, R. D. Room Temperature Ionic Liquids as Novel Media for 'Clean' Liquid–Liquid Extraction. *Chem. Commun.* **1998**, No. 16, 1765–1766.
- (127) McFarlane, J.; Ridenour, W. B.; Luo, H.; Hunt, R. D.; DePaoli, D. W.; Ren, R. X. Room Temperature Ionic Liquids for Separating Organics from Produced Water. *Sep. Sci. Technol.* **2005**, *40* (6), 1245–1265.
- (128) Domínguez-Pérez, M.; Tomé, L. I. N.; Freire, M. G.; Marrucho, I. M.; Cabeza, O.; Coutinho, J. A. P. (Extraction of Biomolecules Using) Aqueous Biphasic Systems Formed by Ionic Liquids and Aminoacids. *Sep. Purif. Technol.* **2010**, *72* (1), 85–91.
- (129) Louros, C. L. S.; Cláudio, A. F. M.; Neves, C. M. S. S.; Freire, M. G.; Marrucho, I. M.; Pauly, J.; Coutinho, J. A. P. Extraction of Biomolecules Using Phosphonium-Based Ionic Liquids + K<sub>3</sub>PO<sub>4</sub> Aqueous Biphasic Systems. *Int. J. Mol. Sci.* **2010**, *11* (4), 1777–1791.

- (130) Passos, H.; Trindade, M. P.; Vaz, T. S. M.; da Costa, L. P.; Freire, M. G.; Coutinho, J. A. P. The Impact of Self-Aggregation on the Extraction of Biomolecules in Ionic-Liquid-Based Aqueous Two-Phase Systems. *Sep. Purif. Technol.* **2013**, *108*, 174–180.
- (131) Ventura, S. P. M.; Sousa, S. G.; Freire, M. G.; Serafim, L. S.; Lima, Á. S.; Coutinho, J. A. P. Design of Ionic Liquids for Lipase Purification. *J. Chromatogr. B* **2011**, *879* (26), 2679–2687.
- (132) Ventura, S. P. M.; de Barros, R. L. F.; de Pinho Barbosa, J. M.; Soares, C. M. F.; Lima, Á. S.; Coutinho, J. A. P. Production and Purification of an Extracellular Lipolytic Enzyme Using Ionic Liquid-Based Aqueous Two-Phase Systems. *Green Chem.* **2012**, *14* (3), 734–740.
- (133) Dietz, M. L. Ionic Liquids as Extraction Solvents: Where Do We Stand? *Sep. Sci. Technol.* **2006**, *41* (10), 2047–2063.
- (134) Abbott, A. P.; Frisch, G.; Hartley, J.; Ryder, K. S. Processing of Metals and Metal Oxides Using Ionic Liquids. *Green Chem.* **2011**, *13* (3), 471–481.
- (135) Génand-Pinaz, S.; Papaiconomou, N.; Leveque, J.-M. Removal of Platinum from Water by Precipitation or Liquid–Liquid Extraction and Separation from Gold Using Ionic Liquids. *Green Chem.* **2013**, *15* (9), 2493–2502.
- (136) Billard, I. Ionic Liquids: New Hopes for Efficient Lanthanide/Actinide Extraction and Separation? In *Handbook on the Physics and Chemistry of Rare Earths*; Elsevier, 2013; Vol. 43, pp 213–273.
- (137) ERAMIN Project, <https://www.era-min.eu/> (Accessed March 2018).
- (138) Elkind, E. Reuse and Repower: How to Save Money and Clean the Grid with Second-Life Electric Vehicle Batteries. *Berkley Publ.* 37.
- (139) Schneider, E. L.; Kindlein, W.; Souza, S.; Malfatti, C. F. Assessment and Reuse of Secondary Batteries Cells. *J. Power Sources* **2009**, *189* (2), 1264–1269.
- (140) Schneider, E. L.; Oliveira, C. T.; Brito, R. M.; Malfatti, C. F. Classification of Discarded NiMH and Li-Ion Batteries and Reuse of the Cells Still in Operational Conditions in Prototypes. *J. Power Sources* **2014**, *262*, 1–9.
- (141) Hu, W.-K.; Kim, D.-M.; Jang, K.-J.; Lee, J.-Y. Studies on Co-Free Rare-Earth-Based Hydrogen Storage Alloys. *J. Alloys Compd.* **1998**, *269* (1–2), 254–258.

- (142) Lenain, C.; Aymard, L.; Tarascon, J.-M. Electrochemical Properties of  $Mg_2Ni$  and  $Mg_2Ni_2$  Prepared by Mechanical Alloying. *J. Solid State Electrochem.* **1998**, *2* (5), 285–290.
- (143) Rousselot, S.; Gazeau, A.; Guay, D.; Roué, L. Influence of Pd on the Structure and Electrochemical Hydrogen Storage Properties of  $Mg_{50}Ti_{50}$  Alloy Prepared by Ball Milling. *Electrochim Acta* **2010**, *55* (3), 611–619.
- (144) Cui, N.; Luan, B.; Liu, H. K.; Zhao, H. J.; Dou, S. X. Characteristics of Magnesium-Based Hydrogen-Storage Alloy Electrodes. *J. Power Sources* **1995**, *55* (2), 263–267.
- (145) Worell, E.; Reuter, M. *Handbook of Recycling*, 1st ed.; Elsevier, 2014.
- (146) ADEME. Piles et Accumulateurs. *ADEME Rep.* **2014**, 1–17.
- (147) SNAM, <https://www.snam.com> (Accessed March 2018).
- (148) Schaeffer, N.; Passos, H.; Billard, I.; Papaiconomou, N.; Countinho, J. Recovery of Metals from Waste Electrical and Electronic Equipment (WEEE) Using Unconventional Solvents Based on Ionic Liquids. *Publ. Yet.*
- (149) *Electronic Waste: Recycling Techniques*; Veit, H. M., Moura Bernardes, A., Eds.; Topics in mining, metallurgy and materials engineering; Springer: Cham, 2015.
- (150) Guichard, F.; Church, T. M.; Treuil, M.; Jaffrezic, H. Rare Earths in Barites: Distribution and Effects on Aqueous Partitioning. *Geochim. Cosmochim. Acta* **1979**, *43* (7), 983–997.
- (151) Kul, M.; Topkaya, Y.; Karakaya, I. Rare Earth Double Sulfates from Pre-Concentrated Bastnasite. *Hydrometallurgy* **2008**, *93* (3–4), 129–135.
- (152) Lokshin, E. P.; Tareeva, O. A.; Ivlev, K. G.; Kashulina, T. G. Solubility of Double Alkali Metal (Na, K) Rare-Earth (La, Ce) Sulfates in Sulfuric/Phosphoric Acid Solutions at 20°C. *Russ. J. Appl. Chem.* **2005**, *78* (7), 1058–1063.
- (153) Pietrelli, L.; Bellomo, B.; Fontana, D.; Montereali, M. R. Rare Earths Recovery from NiMH Spent Batteries. *Hydrometallurgy* **2002**, *66* (1), 135–139.
- (154) Pietrelli, L.; Bellomo, B.; Fontana, D.; Montereali, M. Characterization and Leaching of NiCd and NiMH Spent Batteries for the Recovery of Metals. *Waste Manag.* **2005**, *25* (2), 221–226.
- (155) Bertuol, D. A.; Bernardes, A. M.; Tenório, J. A. S. Spent NiMH Batteries—The Role of Selective Precipitation in the Recovery of Valuable Metals. *J. Power Sources* **2009**, *193* (2), 914–923.

- (156) Porvali, A.; Wilson, B. P.; Lundström, M. Lanthanide-Alkali Double Sulfate Precipitation from Strong Sulfuric Acid NiMH Battery Waste Leachate. *Waste Manag.* **2018**, *71*, 381–389.
- (157) Rodrigues, L. E. O. C.; Mansur, M. B. Hydrometallurgical Separation of Rare Earth Elements, Cobalt and Nickel from Spent Nickel–Metal–Hydride Batteries. *J. Power Sources* **2010**, *195* (11), 3735–3741.
- (158) Innocenzi, V.; Ferella, F.; De Michelis, I.; Vegliò, F. Treatment of Fluid Catalytic Cracking Spent Catalysts to Recover Lanthanum and Cerium: Comparison between Selective Precipitation and Solvent Extraction. *J. Ind. Eng. Chem.* **2015**, *24*, 92–97.
- (159) Innocenzi, V.; Vegliò, F. Recovery of Rare Earths and Base Metals from Spent Nickel–Metal Hydride Batteries by Sequential Sulphuric Acid Leaching and Selective Precipitations. *J. Power Sources* **2012**, *211*, 184–191.
- (160) Provazi, K.; Campos, B. A.; Espinosa, D. C. R.; Tenório, J. A. S. Metal Separation from Mixed Types of Batteries Using Selective Precipitation and Liquid–Liquid Extraction Techniques. *Waste Manag.* **2011**, *31* (1), 59–64.
- (161) Whitehead, J. A.; Lawrance, G. A.; McCluskey, A. Green Leaching: Recyclable and Selective Leaching of Gold-Bearing Ore in an Ionic Liquid. *Green Chem.* **2004**, *6* (7), 313.
- (162) Kilicarslan, A.; Saridede, M. N.; Stopic, S.; Friedrich, B. Use of Ionic Liquid in Leaching Process of Brass Wastes for Copper and Zinc Recovery. *Int. J. Miner. Metall. Mater.* **2014**, *21* (2), 138–143.
- (163) Dong, T.; Hua, Y.; Zhang, Q.; Zhou, D. Leaching of Chalcopyrite with Brønsted Acidic Ionic Liquid. *Hydrometallurgy* **2009**, *99* (1–2), 33–38.
- (164) Chen, M.; Huang, J.; Ogunseitan, O. A.; Zhu, N.; Wang, Y. Comparative Study on Copper Leaching from Waste Printed Circuit Boards by Typical Ionic Liquid Acids. *Waste Manag.* **2015**, *41*, 142–147.
- (165) Zhang, Y.; Chen, M.; Tan, Q.; Wang, B.; Chen, S. Recovery of Copper from WPCBs Using Slurry Electrolysis with Ionic Liquid [BSO<sub>3</sub>HPy]·HSO<sub>4</sub>. *Hydrometallurgy* **2018**, *175*, 150–154.
- (166) Schaeffer, N.; Feng, X.; Grimes, S.; Cheeseman, C. Recovery of an Yttrium Europium Oxide Phosphor from Waste Fluorescent Tubes Using a Brønsted Acidic Ionic Liquid, 1-

- Methylimidazolium Hydrogen Sulfate: Recovery of an Yttrium Europium Oxide Phosphor from Waste Fluorescent Tubes. *J. Chem. Technol. Biotechnol.* **2017**, *92* (10), 2731–2738.
- (167) Nockemann, P.; Van Deun, R.; Thijs, B.; Huys, D.; Vanecht, E.; Van Hecke, K.; Van Meervelt, L.; Binnemans, K. Uranyl Complexes of Carboxyl-Functionalized Ionic Liquids. *Inorg. Chem.* **2010**, *49* (7), 3351–3360.
- (168) Dupont, D.; Binnemans, K. Recycling of Rare Earths from NdFeB Magnets Using a Combined Leaching/Extraction System Based on the Acidity and Thermomorphism of the Ionic Liquid [Hbet][Tf<sub>2</sub>N]. *Green Chem.* **2015**, *17* (4), 2150–2163.
- (169) Dupont, D.; Binnemans, K. Rare-Earth Recycling Using a Functionalized Ionic Liquid for the Selective Dissolution and Revalorization of Y<sub>2</sub>O<sub>3</sub>:Eu<sup>3+</sup> from Lamp Phosphor Waste. *Green Chem.* **2015**, *17* (2), 856–868.
- (170) Davris, P.; Balomenos, E.; Pantias, D.; Paspaliaris, I. Selective Leaching of Rare Earth Elements from Bauxite Residue (Red Mud), Using a Functionalized Hydrophobic Ionic Liquid. *Hydrometallurgy* **2016**, *164*, 125–135.
- (171) Dupont, D.; Renders, E.; Raiguel, S.; Binnemans, K. New Metal Extractants and Super-Acidic Ionic Liquids Derived from Sulfamic Acid. *Chem. Commun.* **2016**, *52* (43), 7032–7035.
- (172) Müller, E.; Berger, R.; Blass, E.; Sluyts, D. Liquid-Liquid Extraction. *Ullmanns Encycl. Ind. Chem.* **2008**, 1–54.
- (173) Bane, S. P. M.; Ziegler, J. L.; Boettcher, P. A.; Coronel, S. A.; Shepherd, J. E. Experimental Investigation of Spark Ignition Energy in Kerosene, Hexane, and Hydrogen. *J. Loss Prev. Process Ind.* **2013**, *26* (2), 290–294.
- (174) Carpenter, P.; Geary, D.; Myers, R.; King, J. Petroleum Hydrocarbon Toxicity Studies. *Toxicol. Appl. Pharmacol.* **1975**, *36*, 443–456.
- (175) Heipieper, H. J.; Weber, F. J.; Sikkema, J.; Keweloh, H.; de Bont, J. A. M. Mechanisms of Resistance of Whole Cells to Toxic Organic Solvents. *Trends Biotechnol.* **1994**, *12* (10), 409–415.
- (176) Lipsztajn, M.; Osteryoung, A. Electrochemistry in Neutral Ambient-Temperature Ionic Liquids. 1. Studies of Iron(III), Neodymium(III), and Lithium(I). *Inorg. Chem.* **1985**, *24* (5), 716–719.

- (177) Dai, S.; Ju, Y. H.; Barnes, C. E. Solvent Extraction of Strontium Nitrate by a Crown Ether Using Room-Temperature Ionic Liquids †. *J. Chem. Soc. Dalton Trans.* **1999**, *8*, 1201–1202.
- (178) Visser, A. E.; Swatloski, R. P.; Reichert, W. M.; Davis Jr., J. H.; Rogers, R. D.; Mayton, R.; Sheff, S.; Wierzbicki, A. Task-Specific Ionic Liquids for the Extraction of Metal Ions from Aqueous Solutions. *Chem. Commun.* **2001**, No. 1, 135–136.
- (179) Visser, A. E.; Swatloski, R. P.; Reichert, W. M.; Griffin, S. T.; Rogers, R. D. Traditional Extractants in Nontraditional Solvents: Groups 1 and 2 Extraction by Crown Ethers in Room-Temperature Ionic Liquids. *Ind. Eng. Chem. Res.* **2000**, *39* (10), 3596–3604.
- (180) Rout, A.; Binnemans, K. Influence of the Ionic Liquid Cation on the Solvent Extraction of Trivalent Rare-Earth Ions by Mixtures of Cyanex 923 and Ionic Liquids. *Dalton Trans.* **2015**, *44* (3), 1379–1387.
- (181) Cocalia, V. A.; Jensen, M. P.; Holbrey, J. D.; Spear, S. K.; Stepinski, D. C.; Rogers, R. D. Identical Extraction Behavior and Coordination of Trivalent or Hexavalent F-Element Cations Using Ionic Liquid and Molecular Solvents. *Dalton Trans.* **2005**, *11*, 1966–1971.
- (182) Janssen, C. H. C.; Macías-Ruvalcaba, N. A.; Aguilar-Martínez, M.; Kobrak, M. N. Metal Extraction to Ionic Liquids: The Relationship between Structure, Mechanism and Application. *Int. Rev. Phys. Chem.* **2015**, *34* (4), 591–622.
- (183) Larsson, K.; Binnemans, K. Selective Extraction of Metals Using Ionic Liquids for Nickel Metal Hydride Battery Recycling. *Green Chem* **2014**, *16* (10), 4595–4603.
- (184) Wellens, S.; Thijs, B.; Binnemans, K. An Environmentally Friendlier Approach to Hydrometallurgy: Highly Selective Separation of Cobalt from Nickel by Solvent Extraction with Undiluted Phosphonium Ionic Liquids. *Green Chem.* **2012**, *14* (6), 1657–1665.
- (185) Boudesocque, S.; Mohamadou, A.; Dupont, L.; Martinez, A.; Déchamps, I. Use of Dicyanamide Ionic Liquids for Extraction of Metal Ions. *RSC Adv.* **2016**, *6* (109), 107894–107904.
- (186) Zhou, Y.; Boudesocque, S.; Mohamadou, A.; Dupont, L. Extraction of Metal Ions with Task Specific Ionic Liquids: Influence of a Coordinating Anion. *Sep. Sci. Technol.* **2015**, *50* (1), 38–44.
- (187) Vander Hoogerstraete, T.; Wellens, S.; Verachtert, K.; Binnemans, K. Removal of Transition Metals from Rare Earths by Solvent Extraction with an Undiluted Phosphonium



- Ionic Liquid: Separations Relevant to Rare-Earth Magnet Recycling. *Green Chem.* **2013**, *15* (4), 919–927.
- (188) Vander Hoogerstraete, T.; Binnemans, K. Highly Efficient Separation of Rare Earths from Nickel and Cobalt by Solvent Extraction with the Ionic Liquid Trihexyl(Tetradecyl)Phosphonium Nitrate: A Process Relevant to the Recycling of Rare Earths from Permanent Magnets and Nickel Metal Hydride Batteries. *Green Chem* **2014**, *16* (3), 1594–1606.
- (189) Ríos, A. P.; Hernández-Fernández, F. J.; Lozano, L. J.; Sánchez, S.; Moreno, J. I.; Godínez, C. Removal of Metal Ions from Aqueous Solutions by Extraction with Ionic Liquids. *J. Chem. Eng. Data* **2010**, *55* (2), 605–608.
- (190) Rout, A.; Wellens, S.; Binnemans, K. Separation of Rare Earths and Nickel by Solvent Extraction with Two Mutually Immiscible Ionic Liquids. *RSC Adv.* **2014**, *4* (11), 5753–5758.
- (191) Larsson, K.; Binnemans, K. Separation of Rare Earths by Split-Anion Extraction. *Hydrometallurgy* **2015**, *156*, 206–214.
- (192) Kozonoi, N.; Ikeda, Y. Extraction Mechanism of Metal Ion from Aqueous Solution to the Hydrophobic Ionic Liquid, 1-Butyl-3-Methylimidazolium Nonafluorobutanesulfonate. *Monatshefte Für Chem. - Chem. Mon.* **2007**, *138* (11), 1145–1151.
- (193) Albertsson, P. Partition of Proteins in Liquid Polymer-Polymer Two Phase Systems. *Nature* **1958**, *4637*, 709–711.
- (194) Freire, M. G.; Cláudio, A. F. M.; Araújo, J. M. M.; Coutinho, J. A. P.; Marrucho, I. M.; Lopes, J. N. C.; Rebelo, L. P. N. Aqueous Biphasic Systems: A Boost Brought about by Using Ionic Liquids. *Chem. Soc. Rev.* **2012**, *41* (14), 4966–4995.
- (195) Gutowski, K. E.; Broker, G. A.; Willauer, H. D.; Huddleston, J. G.; Swatloski, R. P.; Holbrey, J. D.; Rogers, R. D. Controlling the Aqueous Miscibility of Ionic Liquids: Aqueous Biphasic Systems of Water-Miscible Ionic Liquids and Water-Structuring Salts for Recycle, Metathesis, and Separations. *J. Am. Chem. Soc.* **2003**, *125* (22), 6632–6633.
- (196) Shahriari, S.; Neves, C. M. S. S.; Freire, M. G.; Coutinho, J. A. P. Role of the Hofmeister Series in the Formation of Ionic-Liquid-Based Aqueous Biphasic Systems. *J. Phys. Chem. B* **2012**, *116* (24), 7252–7258.

- (197) Neves, C. M. S. S.; Ventura, S. P. M.; Freire, M. G.; Marrucho, I. M.; Coutinho, J. A. P. Evaluation of Cation Influence on the Formation and Extraction Capability of Ionic-Liquid-Based Aqueous Biphasic Systems. *J. Phys. Chem. B* **2009**, *113* (15), 5194–5199.
- (198) Ventura, S. P. M.; Neves, C. M. S. S.; Freire, M. G.; Marrucho, I. M.; Oliveira, J.; Coutinho, J. A. P. Evaluation of Anion Influence on the Formation and Extraction Capacity of Ionic-Liquid-Based Aqueous Biphasic Systems. *J. Phys. Chem. B* **2009**, *113* (27), 9304–9310.
- (199) Cláudio, A. F. M.; Ferreira, A. M.; Shahriari, S.; Freire, M. G.; Coutinho, J. A. P. Critical Assessment of the Formation of Ionic-Liquid-Based Aqueous Two-Phase Systems in Acidic Media. *J. Phys. Chem. B* **2011**, *115* (38), 11145–11153.
- (200) Mourão, T.; Cláudio, A. F. M.; Boal-Palheiros, I.; Freire, M. G.; Coutinho, J. A. P. Evaluation of the Impact of Phosphate Salts on the Formation of Ionic-Liquid-Based Aqueous Biphasic Systems. *J. Chem. Thermodyn.* **2012**, *54*, 398–405.
- (201) Passos, H.; Ferreira, A. R.; Cláudio, A. F. M.; Coutinho, J. A. P.; Freire, M. G. Characterization of Aqueous Biphasic Systems Composed of Ionic Liquids and a Citrate-Based Biodegradable Salt. *Biochem. Eng. J.* **2012**, *67*, 68–76.
- (202) Vander Hoogerstraete, T.; Onghena, B.; Binnemans, K. Homogeneous Liquid–Liquid Extraction of Metal Ions with a Functionalized Ionic Liquid. *J. Phys. Chem. Lett.* **2013**, *4* (10), 1659–1663.
- (203) Blesic, M.; Gunaratne, H. Q. N.; Jacquemin, J.; Nockemann, P.; Olejarz, S.; Seddon, K. R.; Strauss, C. R. Tunable Thermomorphism and Applications of Ionic Liquid Analogues of Girard’s Reagents. *Green Chem* **2014**, *16* (9), 4115–4121.
- (204) Onghena, B.; Opsomer, T.; Binnemans, K. Separation of Cobalt and Nickel Using a Thermomorphic Ionic-Liquid-Based Aqueous Biphasic System. *Chem Commun* **2015**, *51* (88), 15932–15935.
- (205) Xie, Z.-L.; Taubert, A. Thermomorphic Behavior of the Ionic Liquids [C4mim][FeCl4] and [C12mim][FeCl4]. *ChemPhysChem* **2011**, *12* (2), 364–368.
- (206) Onghena, B.; Binnemans, K. Recovery of Scandium(III) from Aqueous Solutions by Solvent Extraction with the Functionalized Ionic Liquid Betainium Bis(Trifluoromethylsulfonyl)Imide. *Ind. Eng. Chem. Res.* **2015**, *54* (6), 1887–1898.

- (207) Vander Hoogerstraete, T.; Onghena, B.; Binnemans, K. Homogeneous Liquid–Liquid Extraction of Rare Earths with the Betaine—Betainium Bis(Trifluoromethylsulfonyl)Imide Ionic Liquid System. *Int. J. Mol. Sci.* **2013**, *14* (11), 21353–21377.
- (208) Bonnaud, C. Vers Une Méthode de Recyclage et de Valorisation Des Aimants Permanents à Base de Terres Rares Par Électrochimie En Milieux Liquides Ioniques, Université Grenoble Alpes, PhD thesis, 2017.
- (209) Abbott, A. P.; Capper, G.; Davies, D. L.; Rasheed, R. K.; Tambyrajah, V. Novel Ambient Temperature Ionic Liquids for Zinc and Zinc Alloy Electrodeposition. *Trans. IMF* **2001**, *79* (6), 204–206.
- (210) Abbott, A.; Addicoat, M.; Aldous, L.; Bhuin, R. G.; Borisenko, N.; Canongia Lopes, J. N.; Clark, R.; Coles, S.; Costa Gomes, M.; Cross, B.; et al. Ionic Liquids at Interfaces: General Discussion. *Faraday Discuss.* **2018**, *206*, 549–586.
- (211) Bard, A.; Parsons, J.; Jordan, R. *Standard Potentials in Aqueous Solutions*; Marcel Dekker Inc, 1985.
- (212) Abbott, A. P.; McKenzie, K. J. Application of Ionic Liquids to the Electrodeposition of Metals. *Phys. Chem. Chem. Phys.* **2006**, *8* (37), 4265–4279.
- (213) Liu, F.; Deng, Y.; Han, X.; Hu, W.; Zhong, C. Electrodeposition of Metals and Alloys from Ionic Liquids. *J. Alloys Compd.* **2016**, *654*, 163–170.
- (214) Carlin, R. T.; Long, H. .; Fuller, J.; Trulove, P. . Microelectrode Evaluation of Transition Metal-Aluminum Alloy Electrodepositions in Chloroaluminate Ionic Liquids. *J. Electrochem. Soc.* **1998**, *145* (5), 1598–1607.
- (215) Deng, M.-J.; Sun, I.-W.; Chen, P.-Y.; Chang, J.-K.; Tsai, W.-T. Electrodeposition Behavior of Nickel in the Water- and Air-Stable 1-Ethyl-3-Methylimidazolium-Dicyanamide Room-Temperature Ionic Liquid. *Electrochimica Acta* **2008**, *53* (19), 5812–5818.
- (216) Katayama, Y.; Fukui, R.; Miura, T. Electrodeposition of Cobalt from an Imide-Type Room-Temperature Ionic Liquid. *J. Electrochem. Soc.* **2007**, *154* (10), D534–D537.
- (217) Yang, D.; Zhu, J.; Rui, X.; Tan, H.; Cai, R.; Hoster, H. E.; Yu, D. Y. W.; Hng, H. H.; Yan, Q. Synthesis of Cobalt Phosphides and Their Application as Anodes for Lithium Ion Batteries. *ACS Appl. Mater. Interfaces* **2013**, *5* (3), 1093–1099.

- (218) Endres, F.; Bukowski, M.; Hempelmann, R.; Natter, H. Electrodeposition of Nanocrystalline Metals and Alloys from Ionic Liquids. *Angew. Chem. Int. Ed.* **2003**, *42* (29), 3428–3430.
- (219) Deng, M.-J.; Chen, P.-Y.; Sun, I.-W. Electrochemical Study and Electrodeposition of Manganese in the Hydrophobic Butylmethylpyrrolidinium Bis((Trifluoromethyl)Sulfonyl)Imide Room-Temperature Ionic Liquid. *Electrochim Acta* **2007**, *53* (4), 1931–1938.
- (220) Chang, J.-K.; Huang, C.-H.; Tsai, W.-T.; Deng, M.-J.; Sun, I.-W.; Chen, P.-Y. Manganese Films Electrodeposited at Different Potentials and Temperatures in Ionic Liquid and Their Application as Electrode Materials for Supercapacitors. *Electrochim Acta* **2008**, *53* (13), 4447–4453.
- (221) Bhatt, A. I.; May, I.; Volkovich, V. A.; Collison, D.; Helliwell, M.; Polovov, I. B.; Lewin, R. G. Structural Characterization of a Lanthanum Bistriflimide Complex,  $\text{La}(\text{N}(\text{SO}_2\text{CF}_3)_2)_3(\text{H}_2\text{O})_3$ , and an Investigation of La, Sm, and Eu Electrochemistry in a Room-Temperature Ionic Liquid,  $[\text{Me}_3\text{N}^m\text{Bu}][\text{N}(\text{SO}_2\text{CF}_3)_2]$ . *Inorg. Chem.* **2005**, *44* (14), 4934–4940.
- (222) Bourbos, E.; Giannopoulou, I.; Karantonis, A.; Panias, D.; Paspaliaris, I. Electrodeposition of Lanthanum from Ionic Liquids at Room Temperature. *Process. Eur. Metall. Conf. Dusseldorf Ger.* **2015**, *2*, 665–672.
- (223) Hatchett, D. W.; Droessler, J.; Kinyanjui, J. M.; Martinez, B.; Czerwinski, K. R. The Direct Dissolution of  $\text{Ce}_2(\text{CO}_3)_3$  and Electrochemical Deposition of Ce Species Using Ionic Liquid Trimethyl-n-Butylammonium Bis(Trifluoromethanesulfonyl)Imide Containing Bis(Trifluoromethanesulfonyl)Imide. *Electrochim Acta* **2013**, *89*, 144–151.
- (224) Kondo, H.; Matsumiya, M.; Tsunashima, K.; Kodama, S. Investigation of Oxidation State of the Electrodeposited Neodymium Metal Related with the Water Content of Phosphonium Ionic Liquids. *ECS Trans.* **2013**, *50* (11), 529–538.
- (225) Matsumiya, M.; Kikuchi, Y.; Yamada, T.; Kawakami, S. Extraction of Rare Earth Ions by Tri-n-Butylphosphate/Phosphonium Ionic Liquids and the Feasibility of Recovery by Direct Electrodeposition. *Sep. Purif. Technol.* **2014**, *130*, 91–101.
- (226) Bortolini, O.; Chiappe, C.; Ghilardi, T.; Massi, A.; Pomelli, C. S. Dissolution of Metal Salts in Bis(Trifluoromethylsulfonyl)Imide-Based Ionic Liquids: Studying the Affinity of

- Metal Cations Toward a “Weakly Coordinating” Anion. *J. Phys. Chem. A* **2015**, *119* (21), 5078–5087.
- (227) Yang, P.; An, M.; Su, C.; Wang, F. Fabrication of Cobalt Nanowires from Mixture of 1-Ethyl-3-Methylimidazolium Chloride Ionic Liquid and Ethylene Glycol Using Porous Anodic Alumina Template. *Electrochim Acta* **2008**, *54* (2), 763–767.
- (228) MacFarlane, D. R.; Forsyth, S. A.; Golding, J.; Deacon, G. B. Ionic Liquids Based on Imidazolium, Ammonium and Pyrrolidinium Salts of the Dicyanamide Anion. *Green Chem.* **2002**, *4* (5), 444–448.
- (229) Kortly, S.; Sucha, L. *Handbook of Chemical Equilibria in Analytical Chemistry*, Ellis Horwood.; 1985.
- (230) Sillèn, L.; Martell, A. *Stability Constants of Metal-Ion Complexes*, Chemical Society.; London, 1964.
- (231) Zhou, X.; Young, K.; West, J.; Regalado, J.; Cherisol, K. Degradation Mechanisms of High-Energy Bipolar Nickel Metal Hydride Battery with AB<sub>5</sub> and A<sub>2</sub>B<sub>7</sub> Alloys. *J. Alloys Compd.* **2013**, *580*, S373–S377.
- (232) Evans, T. E.; Hart, A. C. Corrosion and Passivation of a Nickel—Silicon-Base Alloy in Sulphuric Acid Solutions. *Electrochim Acta* **1971**, *16* (11), 1955–1970.
- (233) Oudar, J.; Marcus, P. Role of Adsorbed Sulphur in the Dissolution and Passivation of Nickel and Nickel-Sulphur Alloys. *Appl. Surf. Sci.* **1979**, *3* (1), 48–67.
- (234) Larsson, K.; Ekberg, C.; Ødegaard-Jensen, A. Dissolution and Characterization of HEV NiMH Batteries. *Waste Manag.* **2013**, *33* (3), 689–698.
- (235) Lide, D. *Handbook of Chemistry and Physics*, 90th ed.; CRC Press, 1998.
- (236) Högfeltdt, E. *IUPAC Stability Constants of Metal-Ion Complexes Part A: Inorganic Ligands*; IUPAC; Pergamon Press, 1982.
- (237) Pourbaix, M. *Atlas d'Equilibres Electrochimiques*; Gauthier Villars: Paris, 1963.
- (238) Société Chimique de France, Terres Rares, [Http://Www.Societechimiquedefrance.fr](http://www.Societechimiquedefrance.fr) (Accessed May 2018).
- (239) Borges de Lima, I.; Leal Filho, W. *Rare Earths Industry*; Elsevier, 2016.

- (240) Swatloski, R. P.; Holbrey, J. D.; Rogers, R. D. Ionic Liquids Are Not Always Green: Hydrolysis of 1-Butyl-3-Methylimidazolium Hexafluorophosphate. *Green Chem.* **2003**, *5* (4), 361–363.
- (241) Freire, M. G.; Neves, C. M. S. S.; Carvalho, P. J.; Countinho, J. Mutual Solubilities of Water and Hydrophobic Ionic Liquids. *J. Phys. Chem. B* **2007**, *111* (45), 13082–13089.
- (242) Bridget, D.; Stoll, M. E.; Scott, B. L.; Costa, D. A.; Oldham, Jr., W. J. Coordination Chemistry of the Bis(Trifluoromethylsulfonyl)Imide Anion: Molecular Interactions in Room Temperature Ionic Liquids. *Chem. Commun.* **2005**, No. 11, 1438–1440.
- (243) Abdelkader, A. M.; Hyslop, D. J. S.; Cox, A.; Fray, D. J. Electrochemical Synthesis and Characterization of a NdCo<sub>5</sub> Permanent Magnet. *J. Mater. Chem.* **2010**, *20* (29), 6039–6049.
- (244) Charlot, G. *Dosages Colorimétriques Des Éléments Minéraux: Principes et Méthodes*, 2nd ed.; Masson, 1961.
- (245) Chelliah, M.; Rayappan, J. B. B.; Krishnan, U. M. Synthesis and Characterization of Cerium Oxide Nanoparticles by Hydroxide Mediated Approach. *J. Appl. Sci.* **2012**, *12* (16), 1734–1737.
- (246) Som, T.; Karmakar, B. Green and Red Fluorescence Upconversion in Neodymium-Doped Low Phonon Antimony Glasses. *J. Alloys Compd.* **2009**, *476* (1–2), 383–389.
- (247) Zou, D.; Chen, J.; Cui, H.; Liu, Y.; Li, D. Wet Air Oxidation and Kinetics of Cerium(III) of Rare Earth Hydroxides. *Ind. Eng. Chem. Res.* **2014**, *53* (35), 13790–13796.
- (248) Abreu, R. D.; Morais, C. A. Purification of Rare Earth Elements from Monazite Sulphuric Acid Leach Liquor and the Purification of High-Purity Ceric Oxide. *Miner. Eng.* **2010**, *23*, 536–640.
- (249) Panda, R.; Kumari, A.; Jha, M. K.; Hait, J.; Kumar, V.; Rajesh Kumar, J.; Lee, J. Y. Leaching of Rare Earth Metals (REMs) from Korean Monazite Concentrate. *J. Ind. Eng. Chem.* **2014**, *20* (4), 2035–2042.
- (250) Hayes, S. A.; Yu, P.; O’Keefe, T. J.; O’Keefe, M. J.; Stoffer, J. O. The Phase Stability of Cerium Species in Aqueous Systems. *J. Electrochem. Soc.* **2002**, *149* (12), C623.
- (251) Yu, P.; Hayes, S. A.; O’Keefe, T. J.; O’Keefe, M. J.; Stoffer, J. O. The Phase Stability of Cerium Species in Aqueous Systems. *J. Electrochem. Soc.* **2006**, *153* (1), C74.

- (252) Moeller, T.; Kremers, H. E. Observations on the Rare Earths. LI. An Electrometric Study of the Precipitation of Trivalent Hydrous Rare Earth Oxides or Hydroxides. *J. Phys. Chem.* **1944**, *48* (6), 395–406.
- (253) Pasinli, T.; Eroğlu, A. E.; Shahwan, T. Preconcentration and Atomic Spectrometric Determination of Rare Earth Elements (REEs) in Natural Water Samples by Inductively Coupled Plasma Atomic Emission Spectrometry. *Anal. Chim. Acta* **2005**, *547* (1), 42–49.
- (254) Zhang, L.; Chen, J.; Jin, W.; Deng, Y.; Tian, J.; Zhang, Y. Extraction Mechanism of Cerium(IV) in H<sub>2</sub>SO<sub>4</sub>/H<sub>3</sub>PO<sub>4</sub> System Using Bifunctional Ionic Liquid Extractants. *J. Rare Earths* **2013**, *31* (12), 1195–1201.
- (255) Zhang, D.; Wang, W.; Deng, Y.; Zhang, J.; Zhao, H.; Chen, J. Extraction and Recovery of Cerium(IV) and Fluorine(I) from Sulfuric Solutions Using Bifunctional Ionic Liquid Extractants. *Chem. Eng. J.* **2012**, *179*, 19–25.
- (256) Miller, J. .; Irish, D. E. Infrared and Raman Spectra of the Cerium(IV) Ion-Nitrate-Ion Water System. *Can. J. Chem.* **1967**, *45* (147), 149–155.
- (257) Russel; Larsen, D.; Glenn; Brown, J. H. The Structure of Ammonium Hexanitratocerate(IV) in Solution. *J. Phys. Chem.* **1964**, *68* (10), 3060–3062.
- (258) Papaiconomou, N.; Svecova, L.; Bonnaud, C.; Billard, I. Possibilities and Limitations in Separating Pt(IV) from Pd(II) Combining Imidazolium and Phosphonium Ionic Liquids. *Dalton Trans* **2015**, *44* (46), 20131–20138.
- (259) Papaiconomou, N.; Cointeaux, L.; Chainet, E.; Iojoiu, C.; Billard, I. Uncertainty Principle in the Elucidation of the Extraction Mechanism of Ions from Aqueous towards Ionic Liquid Phases. PtCl<sub>6</sub><sup>2-</sup> and [C<sub>1</sub>C<sub>8</sub>IM][NTf<sub>2</sub>] as a Textbook Case. *ChemistrySelect* **2016**, *1* (13), 3892–3900.
- (260) Katsuta, S.; Watanabe, Y.; Araki, Y.; Kudo, Y. Extraction of Gold(III) from Hydrochloric Acid into Various Ionic Liquids: Relationship between Extraction Efficiency and Aqueous Solubility of Ionic Liquids. *ACS Sustain. Chem. Eng.* **2016**, *4* (2), 564–571.
- (261) Chiarizia, R.; Jensen, M. P.; Borkowski, M.; Ferraro, J. R.; Thiyagarajan, P.; Littrell, K. C. Third Phase Formation Revisited: The U(VI), HNO<sub>3</sub>–TBP, N- Dodecane System. *Solvent Extr. Ion Exch.* **2003**, *21* (1), 1–27.

- (262) Rao, P. R. V.; Kolarik, Z. A Review of the Third Phase Formation in Extraction of Actinides by Neutral Organophosphorous Extractants. *Solvent Extr. Ion Exch.* **1996**, *14* (6), 955–993.
- (263) Hua, I.; Hoffmann, M. R. Optimization of Ultrasonic Irradiation as an Advanced Oxidation Technology. *Environ. Sci. Technol.* **1997**, *31* (8), 2237–2243.
- (264) Markevich, E.; Sharabi, R.; Borgel, V.; Gottlieb, H.; Salitra, G.; Aurbach, D.; Semrau, G.; Schmidt, M. A. In Situ FTIR Study of the Decomposition of N-Butyl-N-Methylpyrrolidinium Bis(Trifluoromethanesulfonyl)Amide Ionic Liquid during Cathodic Polarization of Lithium and Graphite Electrodes. *Electrochimica Acta* **2010**, *55* (8), 2687–2696.
- (265) Ternova, D.; Boltoeva, M.; Cointeaux, L.; Gaillard, C.; Kalchenko, V.; Mazan, V.; Miroshnichenko, S.; Mohapatra, P. K.; Ouadi, A.; Papaiconomou, N.; et al. Dramatic Changes in the Solubilities of Ions Induced by Ligand Addition in Biphasic System D<sub>2</sub>O/DNO<sub>3</sub>//[C<sub>1</sub>C<sub>4</sub>Im][Tf<sub>2</sub>N]: A Phenomenological Study. *J. Phys. Chem. B* **2016**, *120* (30), 7502–7510.
- (266) Howlett, P. C.; Izgorodina, E. I.; Forsyth, M.; MacFarlane, D. R. Electrochemistry at Negative Potentials in Bis(Trifluoromethanesulfonyl)Amide Ionic Liquids. *Z. Für Phys. Chem.* **2006**, *220* (10), 1483–1498.
- (267) Brown, D.; Ma, B.-M.; Chen, Z. Developments in the Processing and Properties of NdFeB-Type Permanent Magnets. *J. Magn. Magn. Mater.* **2002**, *9*.
- (268) Brown, C. .; Sherrington, L. . Solvent Extraction Used in Industrial Separation of Rare Earths. *J. Chem. Technol. Biotechnol.* **1979**, *29*, 193–209.
- (269) Wang, Y.; Li, F.; Zhao, Z.; Dong, Y.; Sun, X. The Novel Extraction Process Based on CYANEX® 572 for Separating Heavy Rare Earths from Ion-Adsorbed Deposit. *Sep. Purif. Technol.* **2015**, *151*, 303–308.
- (270) Baba, Y.; Kubota, F.; Kamiya, N.; Goto, M. Recent Advances in Extraction and Separation of Rare-Earth Metals Using Ionic Liquids. *J. Chem. Eng. Jpn.* **2011**, *44* (10), 679–685.
- (271) Yang, F.; Kubota, F.; Baba, Y.; Kamiya, N.; Goto, M. Selective Extraction and Recovery of Rare Earth Metals from Phosphor Powders in Waste Fluorescent Lamps Using an Ionic Liquid System. *J. Hazard. Mater.* **2013**, *254–255*, 79–88.
- (272) Cytec. Cyanex 572 Solvent Extraction Reagent: Product Data Sheet. **2013**.



- (273) Sato, T. Liquid-Liquid Extraction of Rare-Earth Elements from Aqueous Acid Solutions by Acid Organophosphorus Compounds. *Hydrometallurgy* **1989**, *22* (1–2), 121–140.
- (274) Singh, V. P.; Singh, P.; Singh, A. K. Synthesis, Structural and Corrosion Inhibition Studies on Cobalt(II), Nickel(II), Copper(II) and Zinc(II) Complexes with 2-Acetylthiophene Benzoylhydrazone. *Inorganica Chim. Acta* **2011**, *379* (1), 56–63.
- (275) Srivastava, M.; Selvi, E. V.; William, W. V. K.; Rajam, K. S. Corrosion Resistance and Microstructure of Electrodeposited Nickel–Cobalt Alloy Coatings. *Surf. Coat. Technol.* **2006**, *201* (6), 3051–3060.
- (276) Burdo, T. G.; Seitz, W. R. Mechanism of Cobalt Catalysis of Luminol Chemiluminescence. *Anal. Chem.* **1975**, *47* (9), 1639–1643.
- (277) Faber, M. S.; Dziedzic, R.; Lukowski, M. A.; Kaiser, N. S.; Jin, S. High-Performance Electrocatalysis Using Metallic Cobalt Pyrite (CoS<sub>2</sub>) Micro- and Nanostructures. *J. Am. Chem. Soc.* **2014**, *136* (28), 10053–10061.
- (278) Gao, K.; Yoshikai, N. Low-Valent Cobalt Catalysis: New Opportunities for C–H Functionalization. *Acc. Chem. Res.* **2014**, *47* (4), 1208–1219.
- (279) Kazmierski, I.; Bastienne, M.; Gosmini, C.; Paris, J.-M.; Périchon, J. Convenient Processes for the Synthesis of Aromatic Ketones from Aryl Bromides and Carboxylic Anhydrides Using a Cobalt Catalysis. *J. Org. Chem.* **2004**, *69* (3), 936–942.
- (280) Gabay, A. M.; Akdogan, N. G.; Marinescu, M.; Liu, J. F.; Hadjipanayis, G. C. Rare Earth–Cobalt Hard Magnetic Nanoparticles and Nanoflakes by High-Energy Milling. *J. Phys. Condens. Matter* **2010**, *22* (16), 164213.
- (281) Goll, D.; Stadelmaier, H. H.; Kronmüller, H. Samarium–Cobalt 2:17 Magnets: Analysis of the Coercive Field of Sm<sub>2</sub>(CoFeCuZr)<sub>17</sub> High-Temperature Permanent Magnets. *Scr. Mater.* **2010**, *63* (2), 243–245.
- (282) Harris, V. G.; Chen, Y.; Yang, A.; Yoon, S.; Geiler, A. L. High Coercivity Cobalt Carbide Nanoparticles Processed via Polyol Reaction: A New Permanent Magnet Material. *J. Phys. Appl. Phys.* **2010**, *43* (16), 165003.
- (283) Ni, J.; Gao, L.; Lu, L. Carbon Coated Lithium Cobalt Phosphate for Li-Ion Batteries: Comparison of Three Coating Techniques. *J. Power Sources* **2013**, *221*, 35–41.

- (284) Yang, S.; Cui, G.; Pang, S.; Cao, Q.; Müllen, K. Fabrication of Cobalt and Cobalt Oxide/Graphene Composites: Towards High-Performance Anode Materials for Lithium Ion Batteries. *ChemSusChem* **2010**, *3* (2), 236–239.
- (285) Bjerrum, J.; Halonin, A. S.; Skilsted, L. H. Studies on Cobalt (II) Halide Complex Formation. A Spectrophotometric Study of the Chloro Cobalt (II) Complexes in Strong Aqueous Chloride Solution. *Acta Chem. Scand.* **1975**, No. 29, 326–332.
- (286) Pan, P.; Susak, J. Co(LI)-Chloride and -Bromide Complexes in Aqueous Solutions up to 5m NaX and 90°C: Spectrophotometric Study and Geological Implications. *Geochim. Cosmochim.* **1988**, *53*, 327–341.
- (287) Köhlner, V.; Seifert, B. Beiträge Zur Chemie Des Dicyanamid-Und Des Tricyanmethanid-Ions. Kobalt (II)-Dicyanamid-Und-Tricyanmethanid-Komplexe. *Z. Für Anorg. Allg. Chem.* **1966**, *344*.
- (288) Estager, J.; Oliferenko, A. A.; Seddon, K. R.; Swadźba-Kwaśny, M. Chlorometallate(Iii) Ionic Liquids as Lewis Acidic Catalysts – a Quantitative Study of Acceptor Properties. *Dalton Trans.* **2010**, *39* (47), 11375.
- (289) Hardacre, C.; Murphy, R. W.; Seddon, K. R.; Srinivasan, G.; Swadźba-Kwaśny, M. Speciation of Chlorometallate Ionic Liquids Based on Gallium(Iii) and Indium(Iii). *Aust. J. Chem.* **2010**, *63* (5), 845–848.
- (290) Wang, K.; Jian, F.; Zhuang, R. New Ionic Liquid Crystal of N,N'-Dialkylbenzimidazolium Salt Comprising Cobalt (II) Thiocyanate. *Soft Mater.* **2010**, *9* (1), 32–43.
- (291) Messadi, A.; Mohamadou, A.; Boudesocque, S.; Dupont, L.; Guillon, E. Task-Specific Ionic Liquid with Coordinating Anion for Heavy Metal Ion Extraction: Cation Exchange versus Ion-Pair Extraction. *Sep. Purif. Technol.* **2013**, *107*, 172–178.
- (292) Hvastijová, M.; Kohout, J.; Okruhlica, M. Dicyanamide Complexes of Copper(II), Nickel(II) and with Benzimidazole and Its 2-Alkyl-Derivatives. *Transit. Met Chem* **1993**, No. 18, 579–582.
- (293) Manna, S. C.; Ghosh, A. K.; Ribas, J.; Drew, M. G. B.; Ray Chaudhuri, N. Synthesis, Crystal Structure, Magnetic Behavior and Thermal Property of Three Polynuclear Complexes:  $[M(Dca)_2(H_2O)_2]_n \cdot (Hmt)_n$  [M=Mn(II), Co(II)] and  $[Co(Dca)_2(Bpds)]_n$  [Dca, Dicyanamide;

- Hmt, Hexamethylenetetramine; Bpds, 4,4'-Bipyridyl Disulfide]. *Inorganica Chim. Acta* **2006**, *359* (5), 1395–1403.
- (294) Figgis, B. *Introduction to Ligand Fields*; Interscience publishers, 1966.
- (295) Lechat, S.; Khan, M. A.; Bouet, G. Spectrophotometric Study of Cobalt (II) Chloride Complexes in Ethanol and Propan-2-ol. *Inorganica Chim. Acta* **1993**, *211*, 33–36.
- (296) Ballhausen, C. . Studies of Absorption Spectra, the Spectra of Cobalt (II) Complexes. *Acta Chem. Scand.* **1955**, *9*, 397–404.
- (297) Basolo, F.; Ballhausen, C. .; Bjerrum, J. Absorbance Spectra of Geometrical Isomers of Hexacoordinated Complexes. *Acta Chem. Scand.* **1955**, *9* (5), 810–814.
- (298) Osborne, S. J.; Wellens, S.; Ward, C.; Felton, S.; Bowman, R. M.; Binnemans, K.; Swadźba-Kwaśny, M.; Gunaratne, H. Q. N.; Nockemann, P. Thermochromism and Switchable Paramagnetism of Cobalt( II ) in Thiocyanate Ionic Liquids. *Dalton Trans* **2015**, *44* (25), 11286–11289.
- (299) McCourt, É.; Wojnarowska, Z.; Jacquemin, J.; Nockemann, P.; Manyar, H. G.; Hawelek, L.; Paluch, M. Temperature- and Pressure-Induced Structural Changes of Cobalt(II) in a Phosphonium-Based Ionic Liquid. *J. Phys. Chem. C* **2016**, *120* (19), 10156–10161.
- (300) Stojanovic, A.; Keppler, B. K. Ionic Liquids as Extracting Agents for Heavy Metals. *Sep. Sci. Technol.* **2012**, *47* (2), 189–203.
- (301) Boudesocque, S.; Mohamadou, A.; Dupont, L. Efficient Extraction of Gold from Water by Liquid–Liquid Extraction or Precipitation Using Hydrophobic Ionic Liquids. *New J Chem* **2014**, *38* (11), 5573–5581.
- (302) Huddleston, J. G.; Visser, A. E.; Reichert, W. M.; Willauer, H. D.; Broker, G. A.; Rogers, R. D. Characterization and Comparison of Hydrophilic and Hydrophobic Room Temperature Ionic Liquids Incorporating the Imidazolium Cation. *Green Chem.* **2001**, *3* (4), 156–164.
- (303) Coleman, D.; Gathergood, N. Biodegradation Studies of Ionic Liquids. *Chem. Soc. Rev.* **2010**, *39* (2), 600.
- (304) Svecova, L.; Papaiconomou, N.; Billard, I. Quantitative Extraction of Rh( III ) Using Ionic Liquids and Its Simple Separation from Pd( II ). *Dalton Trans* **2016**, *45* (38), 15162–15169.

- (305) Deive, F. J.; Rodríguez, A.; Pereiro, A. B.; Araújo, J. M. M.; Longo, M. A.; Coelho, M. A. Z.; Lopes, J. N. C.; Esperança, J. M. S. S.; Rebelo, L. P. N.; Marrucho, I. M. Ionic Liquid-Based Aqueous Biphasic System for Lipase Extraction. *Green Chem* **2011**, *13* (2), 390–396.
- (306) Ghosh, K.; Maiti, M.; Lahiri, S.; Afzal Hussain, V. Ionic Liquid-Salt Based Aqueous Biphasic System for Separation of  $^{109}\text{Cd}$  from Silver Target. *J. Radioanal. Nucl. Chem.* **2014**, *302* (2), 925–930.
- (307) Mogilireddy, V.; Gras, M.; Schaeffer, N.; Passos, H.; Svecova, L.; Papaiconomou, N.; Coutinho, J. A. P.; Billard, I. Understanding the Fundamentals of Acid-Induced Ionic Liquid-Based Aqueous Biphasic System. *Phys. Chem. Chem. Phys.* **2018**.
- (308) Kanzaki, R.; Uchida, K.; Hara, S.; Umebayashi, Y.; Ishiguro, S.; Nomura, S. Acid–Base Property of Ethylammonium Nitrate Ionic Liquid Directly Obtained Using Ion-Selective Field Effect Transistor Electrode. *Chem. Lett.* **2007**, *36* (5), 684–685.
- (309) Singh, V.; Kaur, S.; Sapehiyia, V.; Singh, J.; Kad, G. Microwave Accelerated Preparation of [Bmim][HSO<sub>4</sub>] Ionic Liquid: An Acid Catalyst for Improved Synthesis of Coumarins. *Catal. Commun.* **2005**, *6* (1), 57–60.
- (310) Saita, S.; Kohno, Y.; Ohno, H. Detection of Small Differences in the Hydrophilicity of Ions Using the LCST-Type Phase Transition of an Ionic Liquid–Water Mixture. *Chem Commun* **2013**, *49* (1), 93–95.
- (311) Wang, R.; Leng, W.; Gao, Y.; Yu, L. Microemulsion-like Aggregation Behaviour of an LCST-Type Ionic Liquid in Water. *RSC Adv.* **2014**, *4* (27), 14055.
- (312) Merchuk, J. C.; Andrews, B. A.; Asenjo, J. A. Aqueous Two-Phase Systems for Protein Separation: Studies on Phase Inversion. *J. Chromatogr. B. Biomed. Sci. App.* **1998**, *711* (1), 285–293.
- (313) Bridges, N. J.; Gutowski, K. E.; Rogers, R. D. Investigation of Aqueous Biphasic Systems Formed from Solutions of Chaotropic Salts with Kosmotropic Salts (Salt–Salt ABS). *Green Chem* **2007**, *9* (2), 177–183.
- (314) Sandler, S. I. *Models for Thermodynamic and Phase Equilibria Calculations*; Dekker, 1994.

- (315) Katsuta, S.; Yoshimoto, Y.; Okai, M.; Takeda, Y.; Bessho, K. Selective Extraction of Palladium and Platinum from Hydrochloric Acid Solutions by Trioctylammonium-Based Mixed Ionic Liquids. *Ind. Eng. Chem. Res.* **2011**, *50* (22), 12735–12740.
- (316) Katsuta, S.; Watanabe, Y.; Araki, Y.; Kudo, Y. Extraction of Gold(III) from Hydrochloric Acid into Various Ionic Liquids: Relationship between Extraction Efficiency and Aqueous Solubility of Ionic Liquids. *ACS Sustain. Chem. Eng.* **2016**, *4* (2), 564–571.
- (317) Tsunashima, K.; Sugiya, M. Physical and Electrochemical Properties of Low-Viscosity Phosphonium Ionic Liquids as Potential Electrolytes. *Electrochem. Commun.* **2007**, *9* (9), 2353–2358.
- (318) Gras, M.; Papaiconomou, N.; Schaeffer, N.; Chainet, E.; Tedjar, F.; Coutinho, J. A. P.; Billard, I. Ionic-Liquid-Based Acidic Aqueous Biphasic Systems for Simultaneous Leaching and Extraction of Metallic Ions. *Angew. Chem.* **2018**, *57* (6), 1563–1566.
- (319) Hsieh, Y.-T.; Lai, M.-C.; Huang, H.-L.; Sun, I.-W. Speciation of Cobalt-Chloride-Based Ionic Liquids and Electrodeposition of Co Wires. *Electrochimica Acta* **2014**, *117*, 217–223.
- (320) Matulis, J.; Sližys, R. On Some Characteristics of Cathodic Processes in Nickel Electrodeposition. *Electrochimica Acta* **1964**, *9* (9), 1177–1188.
- (321) Chassaing, E.; Jousselin, M.; Wiart, R. The Kinetics of Nickel Electrodeposition Inhibition by Adsorbed Hydrogen and Anions. *J Electroanal Chem* **1983**, No. 157, 75–88.
- (322) Piatti, R. C. V.; Arvía, A. J.; Podestá, J. J. The Electrochemical Kinetic Behaviour of Nickel in Acid Aqueous Solutions Containing Chloride and Perchlorate Ions. *Electrochimica Acta* **1969**, *14* (7), 541–560.
- (323) Suryanto, B. H. R.; Lu, X.; Chan, H. M.; Zhao, C. Controlled Electrodeposition of Cobalt Oxides from Protic Ionic Liquids for Electrocatalytic Water Oxidation. *RSC Adv.* **2013**, *3* (43), 20936.
- (324) Qin, W.; Yang, C.; Ma, X.; Lai, S. Selective Synthesis and Characterization of Metallic Cobalt, Cobalt/Platinum, and Platinum Microspheres. *J. Alloys Compd.* **2011**, *509* (2), 338–342.
- (325) Zhang, Q. B.; Hua, Y. X.; Wang, Y. T.; Lu, H. J.; Zhang, X. Y. Effects of Ionic Liquid Additive [BMIM]HSO<sub>4</sub> on Copper Electro-Deposition from Acidic Sulfate Electrolyte. *Hydrometallurgy* **2009**, *98* (3–4), 291–297.

- (326) Atanassov, N.; Mitreva, V. Electrodeposition and Properties of Nickel-Manganese Layers. *Surf. Coat. Technol.* **1996**, *78* (1–3), 144–149.
- (327) STEPHEN, A.; ANANTH, M. V.; RAVICHANDRAN, V.; NARASHIMAN, B. R. V. Magnetic Properties of Electrodeposited Nickel±manganese Alloys: Effect of Ni/Mn Bath Ratio. 4.
- (328) Goods, S. H.; Kelly, J. J.; Yang, N. Y. C. Electrodeposited Nickel/Manganese: An Alloy for Microsystem Applications. *Microsyst. Technol.* **2004**, *10* (6–7), 498–505.
- (329) Lacourcelle, L. *Traité de Galvanotechnique*, Galva-conseils.; 1996.
- (330) Duclos, L.; Svecova, L.; Laforest, V.; Mandil, G.; Thivel, P.-X. Process Development and Optimization for Platinum Recovery from PEM Fuel Cell Catalyst. *Hydrometallurgy* **2016**, *160*, 79–89.
- (331) Glaister, B. J.; Mudd, G. M. The Environmental Costs of Platinum–PGM Mining and Sustainability: Is the Glass Half-Full or Half-Empty? *Miner. Eng.* **2010**, *23* (5), 438–450.
- (332) Serov, A.; Kwak, C. Review of Non-Platinum Anode Catalysts for DMFC and PEMFC Application. *Appl. Catal. B Environ.* **2009**, *90* (3–4), 313–320.



---

---

# ANNEX

## ANNEX 1: Analytical techniques

### 1-A: Scanning electron microscopy (SEM)

In SEM analysis, an electron beam is scanning the surface of a conductive material leading to the emission of various particles such as secondary electrons (SE), backscattered electrons (BSE) or even X-rays. While SE and BSE give topographic and chemical information respectively on the sample, energy dispersive X-ray spectroscopy (EDS) is used to perform a semi-quantification of elements present at the surface of the material.

The SEM used in this work is a ZEISS<sup>®</sup> Ultra-55 FEG. The EDS detector is a Bruker<sup>®</sup> AXS-30mm<sup>2</sup>. The acceleration voltage is close to 3 and 10 kV respectively for imaging and semi-quantification. For experiments carried out in **part IV.3.4**: the apparatus used is a Hitachi<sup>®</sup> S4100 microscope.

### 1-B: X-ray diffraction (XRD)

Based on the diffraction of X-rays on a crystalline material, angles and intensities of the obtained signal can be analysed in order to obtain information on the crystalline structure of a sample.

A Bruker<sup>®</sup> D8 Advance was used within angles  $2\theta$  in the range 0 to 120 ° working at 45 kV 40 mA. The *XRD-commander* software package was used to acquire data. For experiments carried out in **part IV.3.4**: The crystal structure of the deposits was determined by X-ray powder diffraction using a Bruker AXS; the resulting spectra were analysed using the *X'pert Highscore Plus* software package.

### 1-C: Inductively coupled plasma, optical emission spectroscopy (ICP-OES)

ICP-OES is an analytical technique used to determine the concentration of metals in an aqueous solution. Briefly, after injecting the solution in a plasma at approximatively 8000 K through a capillary, species are ionized and emit



photons. The wavelength of the emitted photons is characteristic of the element and can be analysed by an optical detector. The intensity of photons is directly linked to the concentration of the element and can be determined by the preparation of calibration curves.

A 720-ES (Varian®) ICP-OES apparatus was used. Unless specific information is provided in the text, 3 kinds of standard solutions and 5 different concentrations per solution were used and prepared as follows:

	TM	REE	Nd
<b>Metals with their corresponding wavelengths (nm)</b>	Ni(216.6), Co(228.6), Mn(260.6), Fe(238.2)	La(333.7), Ce(446.0), Pr(417.9)	Nd(406.1)
<b>Concentration (ppm)</b>	0.2, 5, 20, 50, 100	0.2, 5, 10, 20, 33	0.2, 5, 10, 20, 40

**Table A.1.** Details for the preparation of ICP standard solution

The solvent used for the dilution of calibration curve was similar to the matrix of the analysed samples. As an example, concentrations of La, Ce, Nd and Pr after liquid-liquid extractions from a nitric acid solution towards  $[C_1C_4Pyrr][NTf_2]$  in **part III.2.3** were analysed by ICP after calibration of standard solution prepared in  $HNO_3$ . Similarly, to analyse the concentration of metals in the leachates using sulfuric or hydrochloric acid in **part II.3.2** calibration solutions were prepared in  $H_2SO_4$  and  $HCl$  respectively. The latter solutions were used as blanks before all analysis.

#### **1-D: UV-visible spectrophotometer**

UV-visible analysis is a method used to identify and quantify the amount of species absorbing photons in a wavelength range comprise between 200 and 800 nm. A light beam hits the sample at a precise wavelength. The ratio between the incident and transmitted beam intensities allows us to measure absorbance. The intensity and wavelength of absorbance gives us information on the concentration and chemical nature of species respectively.

UV-vis spectra were recorded using a Cary 50 (Varian<sup>®</sup>) spectrophotometer with a 1 cm wide quartz cell. All spectra given are measured versus a reference. In other words, absorption of the measured spectra shown is the difference in absorption between the raw spectrum and the reference spectrum. The nature of the reference will always be given in the manuscript.

#### **1-E: Karl Fischer (KF) titration**

KF titration is a coulometric titration defining the concentration of water in a solution by oxidation of sulfur dioxide by iodine in presence of water.

A Titroline<sup>®</sup> 7500 KF Trace was used for all measurements after calibration with a 1000 ppm water standard solution. The given data is the average of 3 consecutive titrations.

#### **1-F: Absorption atomic spectroscopy (AAS)**

AAS can be used to analyse the concentration of transition metals in an aqueous solution. The solution goes through an acetylene flame after being pumped in a capillary. A detector analyse the wavelength and the intensity of absorption rays of the solution characteristic of the nature and the concentration of metals in solution respectively.

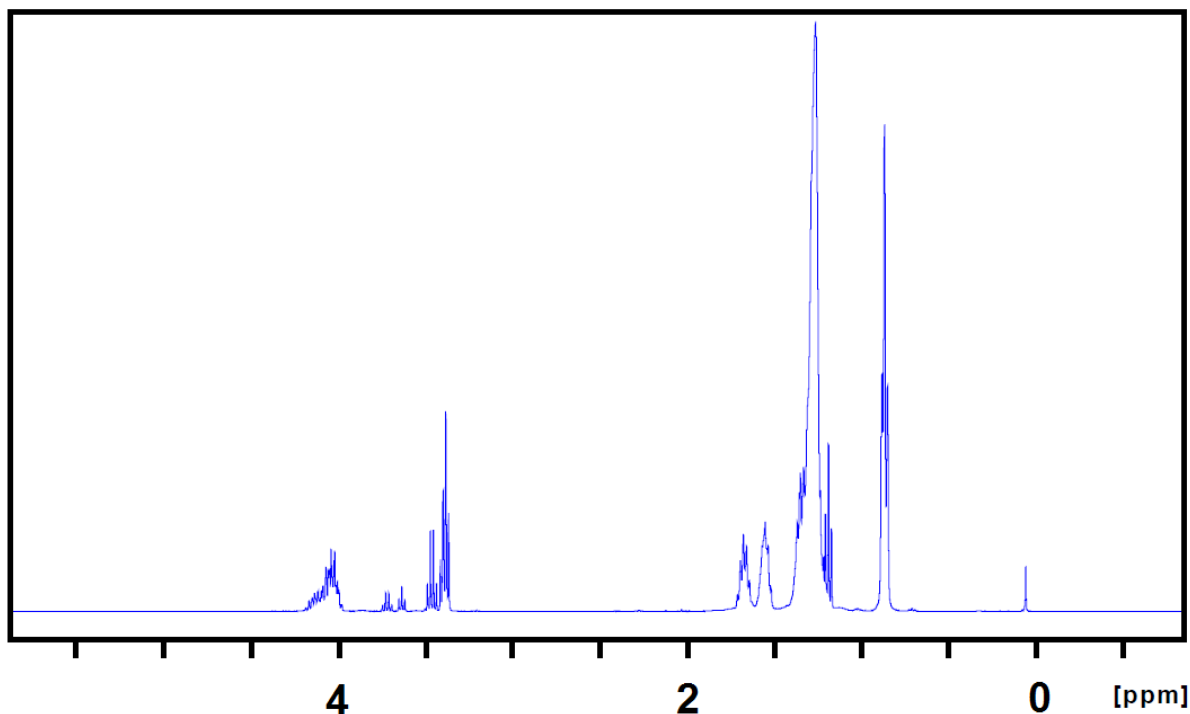
A PinAAcle 900F (Perkin Elmer<sup>®</sup>) was used for all measurments. Similarly to what was done with ICP analysis, all standard curves and blanks were prepared in an appropriate matrix. Unless specific information is provided in the text, all transition metals, namely Ni, Co, Fe and Mn were prepared separately in 4 kinds of solutions and 5 different concentrations as follows:

<b>Metals</b>	<b>Ni</b>	<b>Co</b>	<b>Mn</b>	<b>Fe</b>
<b>wavelengths (nm)</b>	341.5	240.7	279.5	248.3
<b>Concentration (ppm)</b>	1, 5, 20, 50, 75			

**Table A.2.** Details for the preparation of AAS standard solutions

## ANNEX 2: Supplementary materials

### 2-A: $^1\text{H}$ NMR of of $[\text{C}_1\text{C}_8\text{PYR}][\text{C}_8\text{PO}_3\text{H}]$ in deuterated chloroform



Performed with a Bruker<sup>®</sup> Advance III, 400 MHz apparatus

### 2-B: Co-DCA mathematical treatment

According to the law of the conservation of mass, initial concentrations of metal  $M^\circ$  and ligand  $L^\circ$  can be expressed as:

$$[X_0] + [X_1] + [X_2] + [X_3] + [X_4] = M^\circ \quad (\text{S1})$$

$$[L] + [X_1] + 2[X_2] + 3[X_3] + 4[X_4] = L^\circ \quad (\text{S2})$$

By combining equations (4), (S1) and (S2),  $M^\circ$ ,  $L^\circ$  and  $K_n$  can be related in equation (S3):

$$A_0 L^5 + A_1 L^4 + A_2 L^3 + A_3 L^2 + A_4 L - A_5 = 0 \quad (\text{S3})$$

Where  $A_0$ ,  $A_1$ ,  $A_2$ ,  $A_3$ ,  $A_4$  and  $A_5$  are defined by the following equations:

$$K_1 K_2 K_3 K_4 = A_0 \quad (\text{S4})$$

$$K_1 K_2 K_3 + K_1 K_2 K_3 K_4(4M^0 - L^0) = A_1 \quad (\text{S5})$$

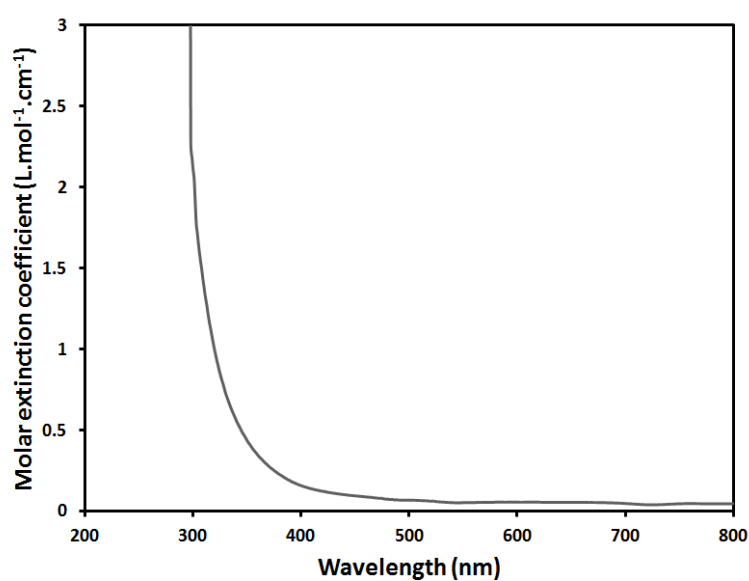
$$K_1 K_2 + K_1 K_2 K_3 (3M^0 - L^0) = A_2 \quad (\text{S6})$$

$$K_1 + K_1 K_2 (2M^0 - L^0) = A_3 \quad (\text{S7})$$

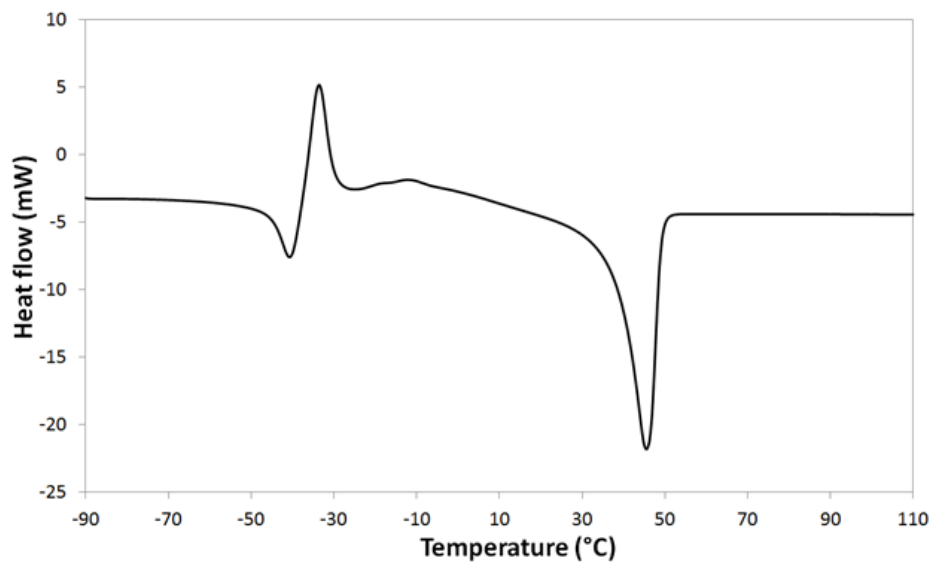
$$1 + K_1 (M^0 - L^0) = A_4 \quad (\text{S8})$$

$$L^0 = A_5 \quad (\text{S9})$$

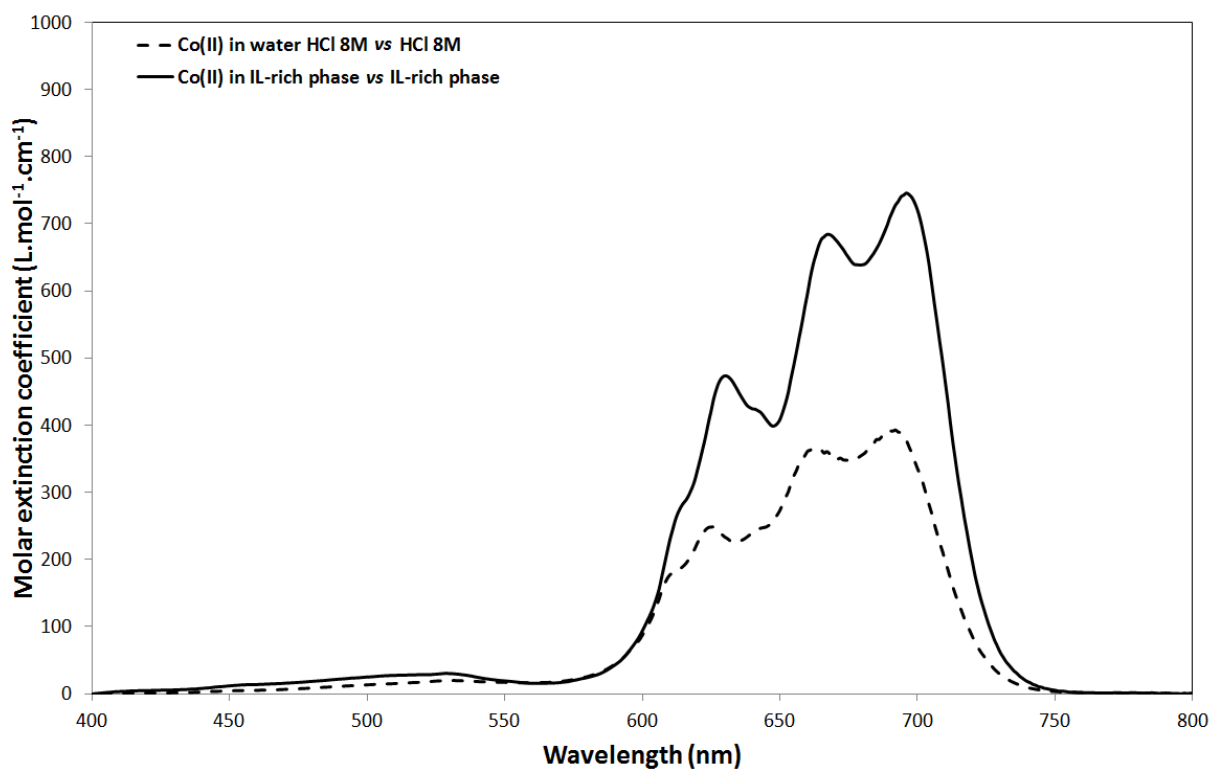
2-C: UV-vis spectrum of 1 mol.L<sup>-1</sup> DCA in water, water was used as reference sample



2-D: Differential scanning calorimetry curve after three scans of [P<sub>44414</sub>][Cl] from -90 °C to 110 °C with a speed of 10°C.min<sup>-1</sup>. The melting point corresponds to the onset of the peak (38.5°C).



2-E: UV-vis measurements of cobalt(II) in an aqueous phase containing 8 mol.L<sup>-1</sup> of HCl and in the IL-rich phase after extraction by the [P<sub>44414</sub>][Cl] / HCl / H<sub>2</sub>O system





## Résumé

Les accumulateurs nickel-hydrure métallique (NiMH) dominent actuellement le marché du stockage de l'énergie pour les véhicules hybrides. On estime à 1 milliard, le nombre de batteries NiMH produites chaque année. En fin de vie, le taux de recyclage de ces déchets électroniques reste faible, bien que la technologie NiMH contienne des quantités importantes de métaux onéreux et stratégiques. Deux grandes familles d'éléments chimiques coexistent sous forme de composés intermétalliques dans l'électrode négative: les métaux de transitions (TM) (Ni, Co, Mn et Fe) ainsi que les terres rares (REE) (La, Ce, Nd et Pr). Parmi les TM, le cobalt présente une criticité accrue. En effet, les minerais issus de réserves naturelles ne permettront pas de couvrir la demande croissante en cobalt liés au développement des technologies émergentes. Les REE produits à plus de 97 % en Chine sont au cœur des préoccupations de l'Union Européenne qui depuis 2010 pointe du doigt des techniques d'extractions dévastatrices pour l'environnement. C'est dans le but de répondre aux problématiques économiques et environnementales que le projet a été construit en associant l'entreprise de recyclage de batteries Recupyl<sup>®</sup> au laboratoire académique LEPMI grâce au financement du Labex CEMAM. L'objectif de ce travail est de proposer un procédé avec un faible impact environnemental pour le recyclage des métaux à partir de véritables accumulateurs NiMH. Pour cela, le remplacement de solvants volatiles organiques par des liquides ioniques, plus respectueux des principes de la 'chimie verte' sera étudié. En s'appuyant sur des procédés innovants d'extraction liquide-liquide et de récupération des éléments par hydrométallurgie et par électrochimie nous proposons une voie de valorisation des métaux présents dans ces batteries.

*Mots clés :* accumulateur NiMH, recyclage, liquide ionique, hydrométallurgie, extraction liquide-liquide, électrochimie.

## Abstract

Nickel-metal hydride (NiMH) batteries are currently dominating the market of energy storage in hybrid electric vehicles. 1 billion cells are estimated to be produced each year. In their end-of-life, these electronical wastes exhibit low recycling rates, despite the fact that NiMH batteries contain high amounts of valuable and strategic metals. Two main metal families coexist as an intermetallic compound in negative electrodes: transition metals (TM) (Ni, Co, Mn and Fe) and rare earth elements (REE) (La, Ce, Nd and Pr). Among TM, cobalt exhibits the highest criticality rate. Indeed, natural ores will not cover the increasing cobalt demand linked to emerging technologies. REE produced at more than 97 % in China are at the centre of European Union's preoccupations. To tackle economic and environmental issues, this project was proposed by associating the company Recupyl<sup>®</sup> and the academic laboratory LEPMI and is supported by the labex CEMAM. It aims at investigating on low environmental impact routes for the recycling of metals present in real spent NiMH batteries. This requires the replacement of volatile organic compounds by ionic liquids, respecting the principles of 'green chemistry'. Based on innovative extraction and recovery processes of elements by hydrometallurgy and electrochemistry, we propose a flowsheet for the valorisation of metals from those batteries.

*Key words:* NiMH batteries, recycling, ionic liquid, hydrometallurgy, liquid-liquid extraction, electrochemistry.

